Molecular and Biochemical Characterization of Cu/Zn Superoxide Dismutase Splice Variants of Rice (*Oryza sativa*)

By

Ravi Prakash Sanyal

LIFE01201404001

Bhabha Atomic Research Centre

Mumbai, India

A thesis submitted to the

Board of Studies in Life Sciences

In partial fulfillment of requirements

for the Degree of

DOCTOR OF PHILOSOPHY

of

HOMI BHABHA NATIONAL INSTITUTE

March, 2021

Homi Bhabha National Institute[1]

Recommendations of the Viva Voce Committee

As members of the Viva Voce Committee, we certify that we have read the dissertation prepared by Ravi Prakash Sanyal entitled 'Molecular and biochemical characterization of Cu/Zn Superoxide dismutase splice variants of rice (*Oryza sativa*)' and recommend that it may be accepted as fulfilling the thesis requirement for the award of Degree of Doctor of Philosophy.

Chairman - **Dr. Thumballi R. Ganapathi**		**Date:** 6-4-21
Guide / Convener - **Dr. Ajay Saini**	Ajay Saini	**Date:** 06-04-2021
Co-guide -		**Date:**
Examiner - **Prof. Prabodh K. Trivedi**		**Date:** 01.04.2021
Member 1- **Dr. Hema Rajaram**	HemaRajaram	**Date:** 6/4/2021
Member 2- **Dr. P. K. Mukherjee**		**Date:** 6.4.21
Member 3- **Dr. Santosh K. Sandur**		**Date:** 6/4/21

Final approval and acceptance of this thesis is contingent upon the candidate's submission of the final copies of the thesis to HBNI.

I/We hereby certify that I/we have read this thesis prepared under my/our direction and recommend that it may be accepted as fulfilling the thesis requirement.

Date: 06-04-2021

Place: BARC, MUMBAI

Signature
Co-guide (if any)

Ajay Saini 06/04/2021

Signature
Guide

[1] This page is to be included only for final submission after successful completion of viva voce.

STATEMENT BY AUTHOR

This dissertation has been submitted in partial fulfillment of requirements for an advanced degree at Homi Bhabha National Institute (HBNI) and is deposited in the Library to be made available to borrowers under rules of the HBNI.

Brief quotations from this dissertation are allowable without special permission, provided that accurate acknowledgement of source is made. Requests for permission for extended quotation from or reproduction of this manuscript in whole or in part may be granted by the Competent Authority of HBNI when in his or her judgment the proposed use of the material is in the interests of scholarship. In all other instances, however, permission must be obtained from the author.

Ravi Sanyal

Ravi Prakash Sanyal

DECLARATION

I, hereby declare that the investigation presented in the thesis has been carried out by me. The work is original and has not been submitted earlier as a whole or in part for a degree / diploma at this or any other Institution / University.

Ravi Sanyal

Ravi Prakash Sanyal

List of publications arising from the thesis

Journals

1. "Biochemical and functional characterization of OsCSD3, a novel Cu/Zn superoxide dismutase from rice" **Sanyal RP,** Samant A, Prashar V, Misra HS and Saini A, *Biochemical Journal*, **2018**, 475, 3105-3121. DOI: 10.1042/BCJ20180516.

Conferences

1. Comparative Analysis of Two Cu/Zn Superoxide Dismutase Isoforms of Rice (*Oryza sativa).* **Sanyal RP,** Saini A and Misra HS. In Proceedings/ Abstracts of 86th SBC(I) annual meeting: Emerging discoveries in health and agricultural sciences. 2017 at JNU, New Delhi, India.
2. Molecular and biochemical analysis of a putative Cu/Zn superoxide dismutase from Rice. **Sanyal RP,** Samant A, Saini A, and Jawali N. In proceedings of "International conference on scenario of biotechnology in 21st century".2016 at DAU, Indore, India.

Other publications

1. "Heat-stress priming and alternative splicing-linked memory", **Sanyal RP**, Misra HS and Saini A, *Journal of Experimental Botany* **2018**,11; 475(19):3105-3121. DOI: 10.1093/jxb/ery111.
2. "GLADS: A gel-less approach for detection of STMS markers in wheat and rice", Vishwakarma G, **Sanyal RP***, Saini A, Sahu PK, Patel RRS, Sharma D and Das BK et al., *PLoS One*, **2019**, 14(11): e0224572. DOI: 10.1371/journal.pone.0224572.
3. "Validation and Marker Assisted Selection of stem rust resistance gene *Sr2* in Indian wheat using gel-based and gel-free methods", Vishwakarma G, **Sanyal RP**, Shitre A, Gadekar D A, Saini A and Das BK, *Journal of Crop Science and Biotechnology,* **2019**, 22(9): 309- 315. DOI No. 10.1007/s12892-017-0083-0.

Submission to GenBank

Nine, full-length and partial cDNAs of rice Cu/Zn SODs, **Sanyal RP** and Saini A. (2013-2020), Accession numbers: KF953542 (OsCSD3), KF953543 (OsCSD3), MW091043 (OsCSD1), MW091044 (OsCSD4), MW091045 (OsCSD2), MW091046 (OsCSD2), MW091047 (OsCSD3), MW091048 (OsCSD3), MW091049 (OsCSD3).

Ravi Sanyal

Ravi Prakash Sanyal

ACKNOWLEGEMENTS

At the very outset, I would like to express my heartfelt gratitude to my supervisor Dr. Ajay Saini, Group leader, Plant Molecular Biology Group, Molecular Biology Division, BARC for his guidance, support, and encouragement throughout my Ph. D. I found him learned, motivating and patient. I personally learnt a lot from him and still a lot more to go.

I would like to express my sincere thanks to Doctoral Committee members: Dr. Thumballi R. Ganapathi (Chairperson), NA & BTD, Dr. Prasun K. Mukherjee, NA & BTD, Dr. Hema Rajaram, MBD, Dr. Santosh K. Sandur, RB & HSD for their constructive criticism and valuable suggestions.

I express my gratitude to Dr. Hema Rajaram, Dean (Academic), Life Sciences, Homi Bhabha National Institute for coordinating in documentation related to Ph. D.

I sincerely thank Dr. H. S. Misra, Head, MBD for the encouragement, suggestions and support. I am obliged to Dr. Narendra Jawali, Ex-Head, MBD for his guidance, suggestions during the course of study.

I am thankful to Dr. Vishal Prashar, RB & HSD for suggestions and help in biophysical and *in silico* analysis. I thank Gamma-field facility in-charge to allow me to use the facility and his team for help in routine maintenance of rice germplasm.

I thank to my fellow lab mates Dr. Amol Samant, Ms. Dharitree Joshi-Bapat, Ms. Sabiha Perween, Ms. Neeta Prasad, for motivation, discussions and help during the study. I express my sincere thanks to my MBD colleagues for their suggestions, discussions and help throughout my research work.

I thankfully acknowledge International Rice Research Institute (IRRI) for providing the rice germplasm and Bhabha Atomic Research Centre, Mumbai and Homi Bhabha National Institute, Mumbai for granting fund, facilities utilized for my study.

Any word would be less to express thankfulness for my family. I thank my parents for their blessings, my companion Sucharitra for her consistent moral support, encouragement and pains endured. A very special thanks to my beloved daughter Pratishtha, for relieving my stress with her innocent activities.

Last but not the least, I acknowledge my thanks to all those who directly or indirectly helped me any way in completion of my Ph. D.

Ravi Prakash Sanyal

CHAPTER 5

CONCLUSIONS

AND

FUTURE DIRECTIONS

Conclusions:

Plants are generally more susceptible to adverse environmental conditions, which perturbs the physiological balance and results into elevated ROS levels leading to 'oxidative stress'. Plants contain diverse mechanisms operating in a well-coordinated manner to modulate gene expression as per the intrinsic factors and environment fluctuations. Genes are regulated at multiple levels, and in addition to the transcription/translation controls, post-transcriptional mechanisms have also been found to be important for modulation of RNA/protein levels. Alternative splicing (AS), affecting >60% intron-containing genes in plants, is central to rapid and dynamic regulation of gene expression in diverse cellular processes, and to generate structurally and functionally diverse isoforms. Despite several high-throughput studies to unveil the impact of AS on whole transcriptome, insights into its impact on individual genes is rather limited and such information is increasing gradually.

Antioxidant machinery in plants is comprised of enzymatic and non-enzymatic antioxidant components, to contain ROS induced damage. Superoxide dismutases (SODs) are essential for maintenance of cellular ROS levels for signaling, and to minimize elevated levels under stress conditions. SODs undergo AS in plants, however barring few studies its significance in functioning of SODs in plants in not completely understood. This thesis is focused on understanding the impact of AS in rice SODs on both RNA and protein level.

Rice (*Oryza sativa*) contains seven SOD genes that generate 14 splice variants (SVs) with maximum number of nine from four Cu/Zn SODs (CSDs). The objective of the present work was to study the characteristics of OsCSD SV transcripts, and the encoded protein isoforms to understand their role in regulation and functioning of

CSDs. All the nine SVs (4 constitutive and 5 alternative) from 4 OsCSDs (2 cytosolic, 1 chloroplastic and 1 peroxisomal) were analyzed at transcript level, while eight were cloned, expressed, purified and analyzed at protein level.

Transcript analysis carried out by qRT-PCR using SV specific primers, compared the basal levels of SVs in rice seedlings and different tissues. SVs were also compared for stability and responsiveness to salinity, PEG and oxidative stress conditions. Variations in basal transcript levels of SVs in different tissues and their stress-specific modulation were observed, and certain AS events affecting the stability of SVs were identified. Results indicate that the AS mechanism *per se* is modulated in tissue- and stress-specific manner, and is capable of modification of transcript properties.

The second and more important aspect was to clone, express and purify protein isoforms encoded by constitutive and alternative SVs of four rice CSDs. All cDNAs were amplified and cloned into expression vectors for heterologous expression in *E. coli*. For SVs of OsCSD3 different approaches were utilized for the expression of four OsCSD3-SVs for various experimental objectives, and to enhance the solubility of alternative isoforms. OsCSD3-SV1 (constitutive isoform) showed SOD function with some remarkable properties (tolerance to pH changes, thermostability, and tolerance to H_2O_2). This isoform also enhanced the oxidative stress tolerance of the *E. coli* wild type and *sodA sodB* double mutant cells. The alternative isoforms, OsCSD3-SV2 (different C-terminal region due to alternative exon), OsCSD3-SV3 (lacks all Zn^{2+} binding site, and few active site residues) and OsCSD3-SV4 (lacks considerable region at C-terminal) showed no SOD function. This was attributed to AS mediated loss of major regions containing essential structural and functional features. The possibility of these isoforms to perform alternate functions associated with the

domains present may not be completely ruled out, and will need more thorough analysis.

The two chloroplastic CSD isoforms, OsCSD2-SV1 (constitutive) and OsCSD2-SV2 (alternative), showed difference of four amino acids (GPTT, missing in SV2). The two CSD2 isoforms exists as homodimer, and were enzymatically active. However, AS-mediated loss of four amino acids in OsCSD2-SV2 resulted in its substantially low specific activity, thermostability, and higher susceptibility to pH changes.

Overall, the analysis of OsCSD SVs at the transcript and protein level showed that AS modulates the transcript levels of rice CSDs in tissue- and stress-specific manner. In addition, AS generated SVs can form alternative protein isoforms with altered/no SOD activity with some other properties. These changes at RNA and/or protein level may be important for control of SOD level/activity in different conditions.

An important aspect of two cytosolic CSDs (OsCSD1 and OsCSD4) in rice was investigated. An inconsistency was observed in the RGAP-MSU predicted gene structure of OsCSD1, which was also supported by *in silico* analysis and experimental results. Both genes showed differential response to abiotic stresses suggesting variation in their up-stream regulatory elements. The two cytosolic CSDs originated from a block duplication event (Chr3 and Chr7), and have accumulated differences in promoter and coding regions. Promoter region analysis revealed differences in the length, number and sequence of the CpG islands, and variation in the presence and copy number of *cis*-regulatory elements. The two proteins also showed amino acid changes at 18 positions. Both CSDs were cloned, expressed and purified and analyzed for different protein characteristics. OsCSD4 showed high specific activity, pH

stability, structural stability than OsCSD1. This analysis suggested that post-duplication divergence has affected the regulatory and structural-functional characteristics of the two CSDs that may be useful for plant in certain conditions.

The findings from this study highlighted the importance of alternative splicing in modulating the levels and/or characteristics of the rice CSD transcripts/protein isoforms, likely to be important for regulation and functioning of CSDs in rice. Furthermore, a block duplication event was also found to be important with differential regulation and protein properties of the two cytosolic CSDs in rice.

Future directions:

The present study was focused on understanding the significance of alternative splicing at RNA and protein level in regulation and functioning of CSDs. It further assessed the impact divergence after the gene duplication event on the regulation and properties of two rice cytosolic CSDs. Based on the results, several new and interesting queries have been raised, which will be worth investigating. Several examples of alternative isoforms with altered properties have been reported that modulates the gene function. Rice CSDs exists as homodimer in native form and may also form heteromeric complexes with the alternative isoforms. Although such isoforms have no/reduced SOD function, they can form heterodimers with reduced SOD function, thereby regulating the protein function. Similarly, alternative isoforms of which contains metal binding domains can possibly play role metal homeostasis. These interesting aspects of the alternative CSD isoforms are worth investigating to understand the true impact of AS in functioning of the SODs. It will be also interesting to investigate how variation introduced through gene duplication events

influence the regulation and properties of SODs across the plant genomes. Additionally, as no information is available on the variant isoforms in the structural databases, it will important to solve structures of some of these isoforms to better insights into structure-function relationships. Together these studies will enhance our understanding of complete picture of different mechanisms in regulation and functioning of SODs in plants.

CHAPTER 5

CONCLUSIONS

AND

FUTURE DIRECTIONS

Conclusions:

Plants are generally more susceptible to adverse environmental conditions, which perturbs the physiological balance and results into elevated ROS levels leading to 'oxidative stress'. Plants contain diverse mechanisms operating in a well-coordinated manner to modulate gene expression as per the intrinsic factors and environment fluctuations. Genes are regulated at multiple levels, and in addition to the transcription/translation controls, post-transcriptional mechanisms have also been found to be important for modulation of RNA/protein levels. Alternative splicing (AS), affecting >60% intron-containing genes in plants, is central to rapid and dynamic regulation of gene expression in diverse cellular processes, and to generate structurally and functionally diverse isoforms. Despite several high-throughput studies to unveil the impact of AS on whole transcriptome, insights into its impact on individual genes is rather limited and such information is increasing gradually.

Antioxidant machinery in plants is comprised of enzymatic and non-enzymatic antioxidant components, to contain ROS induced damage. Superoxide dismutases (SODs) are essential for maintenance of cellular ROS levels for signaling, and to minimize elevated levels under stress conditions. SODs undergo AS in plants, however barring few studies its significance in functioning of SODs in plants in not completely understood. This thesis is focused on understanding the impact of AS in rice SODs on both RNA and protein level.

Rice (*Oryza sativa*) contains seven SOD genes that generate 15 splice variants (SVs) with maximum number of nine from four Cu/Zn SODs (CSDs). The objective of the present work was to study the characteristics of OsCSD SV transcripts, and the encoded protein isoforms to understand their role in regulation and functioning of

CSDs. All the nine SVs (4 constitutive and 5 alternative) from 4 OsCSDs (2 cytosolic, 1 chloroplastic and 1 peroxisomal) were analyzed at transcript level, while eight were cloned, expressed, purified and analyzed at protein level.

Transcript analysis carried out by qRT-PCR using SV specific primers, compared the basal levels of SVs in rice seedlings and different tissues. SVs were also compared for stability and responsiveness to salinity, PEG and oxidative stress conditions. Variations in basal transcript levels of SVs in different tissues and their stress-specific modulation were observed, and certain AS events affecting the stability of SVs were identified. Results indicate that the AS mechanism *per se* is modulated in tissue- and stress-specific manner, and is capable of modification of transcript properties.

The second and more important aspect was to clone, express and purify protein isoforms encoded by constitutive and alternative SVs of four rice CSDs. All cDNAs were amplified and cloned into expression vectors for heterologous expression in *E. coli*. For SVs of OsCSD3 different approaches were utilized for the expression of four OsCSD3-SVs for various experimental objectives, and to enhance the solubility of alternative isoforms. OsCSD3-SV1 (constitutive isoform) showed SOD function with some remarkable properties (tolerance to pH changes, thermostability, and tolerance to H_2O_2). This isoform also enhanced the oxidative stress tolerance of the *E. coli* wild type and *sodA sodB* double mutant cells. The alternative isoforms, OsCSD3-SV2 (different C-terminal region due to alternative exon), OsCSD3-SV3 (lacks all Zn^{2+} binding site, and few active site residues) and OsCSD3-SV4 (lacks considerable region at C-terminal) showed no SOD function. This was attributed to AS mediated loss of major regions containing essential structural and functional features. The possibility of these isoforms to perform alternate functions associated with the

domains present may not be completely ruled out, and will need more thorough analysis.

The two chloroplastic CSD isoforms, OsCSD2-SV1 (constitutive) and OsCSD2-SV2 (alternative), showed difference of four amino acids (GPTT, missing in SV2). The two CSD2 isoforms exists as homodimer, and were enzymatically active. However, AS-mediated loss of four amino acids in OsCSD2-SV2 resulted in its substantially low specific activity, thermostability, and higher susceptibility to pH changes.

Overall, the analysis of OsCSD SVs at the transcript and protein level showed that AS modulates the transcript levels of rice CSDs in tissue- and stress-specific manner. In addition, AS generated SVs can form alternative protein isoforms with altered/no SOD activity with some other properties. These changes at RNA and/or protein level may be important for control of SOD level/activity in different conditions.

An important aspect of two cytosolic CSDs (OsCSD1 and OsCSD4) in rice was investigated. An inconsistency was observed in the RGAP-MSU predicted gene structure of OsCSD1, which was also supported by *in silico* analysis and experimental results. Both genes showed differential response to abiotic stresses suggesting variation in their up-stream regulatory elements. The two cytosolic CSDs originated from a block duplication event (Chr3 and Chr7), and have accumulated differences in promoter and coding regions. Promoter region analysis revealed differences in the length, number and sequence of the CpG islands, and variation in the presence and copy number of *cis*-regulatory elements. The two proteins also showed amino acid changes at 18 positions. Both CSDs were cloned, expressed and purified and analyzed for different protein characteristics. OsCSD4 showed high specific activity, pH

stability, structural stability than OsCSD1. This analysis suggested that post-duplication divergence has affected the regulatory and structural-functional characteristics of the two CSDs that may be useful for plant in certain conditions.

The findings from this study highlighted the importance of alternative splicing in modulating the levels and/or characteristics of the rice CSD transcripts/protein isoforms, likely to be important for regulation and functioning of CSDs in rice. Furthermore, a block duplication event was also found to be important with differential regulation and protein properties of the two cytosolic CSDs in rice.

Future directions:

The present study was focused on understanding the significance of alternative splicing at RNA and protein level in regulation and functioning of CSDs. It further assessed the impact divergence after the gene duplication event on the regulation and properties of two rice cytosolic CSDs. Based on the results, several new and interesting queries have been raised, which will be worth investigating. Several examples of alternative isoforms with altered properties have been reported that modulates the gene function. Rice CSDs exists as homodimer in native form and may also form heteromeric complexes with the alternative isoforms. Although such isoforms have no/reduced SOD function, they can form heterodimers with reduced SOD function, thereby regulating the protein function. Similarly, alternative isoforms of which contains metal binding domains can possibly play role metal homeostasis. These interesting aspects of the alternative CSD isoforms are worth investigating to understand the true impact of AS in functioning of the SODs. It will be also interesting to investigate how variation introduced through gene duplication events

influence the regulation and properties of SODs across the plant genomes. Additionally, as no information is available on the variant isoforms in the structural databases, it will important to solve structures of some of these isoforms to better insights into structure-function relationships. Together these studies will enhance our understanding of complete picture of different mechanisms in regulation and functioning of SODs in plants.

CHAPTER 1

INTRODUCTION

AND

LITERATURE REVIEW

1.1. Abiotic stress in plants

Abiotic factors (light, temperature, water, air, soil etc.) are integral components of environment and essential for proper growth, development and survival of all living beings. Optimum level of the abiotic components often deviate due to various natural and man-made factors leading to stress to organisms [1]. Organisms can adapt to minor environmental fluctuations, however, if variation exceeds the tolerable limit it can be detrimental. Changes in global climate has resulted into more frequent episodes of drought, floods, soil erosion, temperature variation (heat and cold wave) [2,3]. Additionally, due to depletion of ozone layer exposure to harmful UV-radiation has also increased [4]. Plants being sessile faces various stresses that have detrimental effect on growth development and productivity [1]. Conditions like drought, salinity, extreme temperatures (alone or in combination) can reduce crop productivity of most crops by more than 40-50 %, including wheat, rice, maize which collectively account for 50 % global crop production [5–7]. It has also been predicted that global warming will lead to the increase in the temperature rise per decade to ~0.2 °C from the past average value of ~0.13 °C [8], which may further decline the crop production by 4-7 % [9]. The situation can further aggravate due to additional factors viz., increase in global population, industrialization, scarcity of agricultural land, and may impose great threat to food security [10–12]. Furthermore, for increasing global population it is necessary to double the crop production by 2050, however, in view of the above-mentioned factors the situation is really challenging [12].

Rice (*Oryza sativa* L., Family: Poaceae), an important staple crop and a rich source of carbohydrates and several micronutrients [13], provides more than 20 % of

daily energy need to more than half of the world population [14]. With a considerably small genome size (389 Mb, packed into 12 chromosomes) than other cereals such as maize (2.7 Gb) and wheat (17 Gb), it also serves as an important monocot model plant. With advancements in biotechnological tools and tissue cultures techniques, experimental studies in rice will enhance our knowledge which may be utilized to develop improved varieties and stress management in other crop plants [15–17].

Rice is a 'kharif' season crop and scarcity/unavailability of water makes it sensitive to drought, however like many other crops it is also sensitive to most abiotic stresses [7,18,19]. Among different abiotic stresses, drought, salinity and temperature are the major constraints for almost all crops [6,18,20]. These conditions affect plant growth and development through morphological, physiological and biochemical alterations [21].

Drought: Drought is major global concern, which limits crop productivity of almost every crop [6]. In India, most of the agriculture is rainfed and dependent on 'monsoon'. A delayed/ insufficient monsoon resulting into a dry spell season, negatively affects crop productivity and may even lead to complete failure of the crop [22]. Drought causes increase in water potential inside roots, making it difficult for plant to absorb water and soluble minerals [23], resulting in loss of cell turgor and metabolic disturbances [24]. As a physiological response, plants induce closure of stomata to reduce transpiration-mediated water loss [25]. Closure of stomata affects it's roles in thermo-regulation and gaseous exchange in plants [25]. Elevated cellular temperature leads to dehydration, denaturation/inactivation of proteins, and hampered cellular activities [22]. Furthermore, restricted CO_2 entry (and ongoing photosynthesis) leads to reduced CO_2 fixation (Calvin Benson cycle, dark cycle) and causes

oversaturation of photosystem PSI and PSII [26]. In these conditions, leakage of high energy electrons (produced from photolysis of water) from the ETC to O_2 results in generation of ROS ($^1O_2$ and $O_2^{\cdot -}$) in chloroplast [27] that causes damage to membranes, proteins and DNA [28]. Increased O_2 levels in chloroplast also leads to 'photorespiration' resulting into production of H_2O_2 in peroxisomes from the action of glycolate oxidase [29].

Salt-stress: Salts (minerals), in optimum concentration, are important for normal plant physiology and development, however, soil with higher concentration of salts (electrical conductivity; EC $\geq$ 4 dS m^{-1}, referred to as salinity) is detrimental for growth and development of plants [19]. Saline soils are mostly rich in chloride and sulfate salts of Na^+. Globally, around ~400 Million hectares (Mha) land area is saline and increasing further [7]. In India, around ~3-4 Mha land is estimated to be affected by salinity [2]. Salinity affects the physiology of plants in multiple ways [30,31]. It imposes osmotic stress, ionic stress, and oxidative stress. Osmotic stress is experienced in the initial phase and is marked with plants inability to absorb water from soil due to net negative water potential in the rhizosphere. Ionic stress occurs relatively late and causes ion toxicity due to accumulation of salts and resulting in injury to cells/tissues. Both osmotic stress and ionic stress also led to elevated ROS levels, resulting in oxidative damage to cellular components [32].

Temperature: Temperature is another abiotic factor that is important for plant growth, and deviations from the optimum conditions (high temperature: heat; low temperature: chilling stress) are detrimental for survival [33,34]. With increase in the emission of greenhouse gases global temperature is increasing. This will have a positive effect on colder regions whereas some other regions may be drastically affected by rise in

temperature. It has been suggested that every 1 °C increase in temperature can reduce the productivity of major crops (wheat, rice, maize, soybean etc.) by 3-7 % [9]. Crops are most sensitive to heat stress at reproductive stage, where it affects pollen viability and grain filling, and ultimately yield [35]. Heat stress is often associated with drought and/or salinity. It affects metabolic activities, damages membranes, inactivate enzymes and affects electron transport chain (ETC) efficiency, resulting in enhanced ROS levels [36]. Low temperature (or cold stress) also affect every stage of plant. Tropical and subtropical region plants such as rice, maize are most affected by low temperature stress [37,38]. Cold stress causes slowdown of the metabolism, affects cellular membranes and cause reduction in activities of enzymes [39]. It also affects photosynthesis efficiency and elevate cellular ROS levels [33,40].

Metal toxicity: Industrialization and other human activities (mining, improper waste disposal, irrigation with poor quality water etc.) often give rise to heavy metal (Cadmium; Cd, Aluminum; Al, Lead; Pb, Arsenic; As and Chromium; Cr) pollution leading to hazardous environment for human health and plants [41,42]. Metal toxicity not only hampers plant development and crop productivity, but the contaminated produce may also cause health complications [43,44]. Accumulation of heavy metals displaces essential metal cofactors and inhibits activity of enzymes [45]. Heavy metals also interact with proteins containing thiol (–SH) groups and alter signaling pathways [44,46,47]. Heavy metals (e.g., Cr, Ni) may also leads to enhanced ROS generation, and affect the redox status of the cell [41,44,46].

Ultra-violet (UV)-radiation: UV-radiation is a high energy radiation, harmful to living organisms. Human activities (e.g. industrialization and release of gases like chlorofluorocarbons, CFCs) have caused extensive damage to protective ozone (O_3)

layer, leading to increased penetration of UV to earth's surface [48]. Plant are continuously exposed to harmful UV-radiation which causes damage to DNA molecules [49]. The UV-mediated damage to photosynthetic machinery also results in photoinhibition [50]. UV-radiation also induces ROS generation, and can produce $^{\cdot}OH$ from H_2O_2 *via* photolysis affecting integrity of chloroplast membrane [50].

The above-mentioned stresses and many other adverse environmental conditions affect physiology of plants in multiple ways viz. metabolic disturbances, membrane damage, negative impact on photosynthesis, nutrient imbalance etc. Most stress conditions are also associated with some common secondary stress components, such as reactive oxygen species or ROS (**Fig.1.1**) [51,52]. At lower levels, ROS are important signaling molecules and essential for plant's adaptive response to diverse environmental cues [53]. However, prolonged stress conditions, alter the physiologically relevant ROS levels, and results into elevated or toxic levels that causes 'oxidative stress' to the cell [51,54]. Thus ROS plays dual role (harmful and beneficial) which depends upon their cellular level [55].

1.2. Reactive oxygen species (ROS)

1.2.1. Origin of ROS

Approx. 2.4 billion years ago ancient organisms like cyanobacteria acquired ability to harness the energy of sunlight and produce oxygen through the process of photosynthetic. This event referred to as 'The Great Oxidation Event' changed the nature of earth's atmosphere from reducing to oxidizing [57]. This marked the era of aerobic life forms that utilize 'O_2 as electron acceptor' during respiration which gave higher energy gain to aerobes compared to anaerobes [57]. It has been suggested that

ROS also appeared as an inevitable byproduct of oxidative metabolic reactions and being highly reactive, these are damaging to cellular macromolecules [55]. This leads

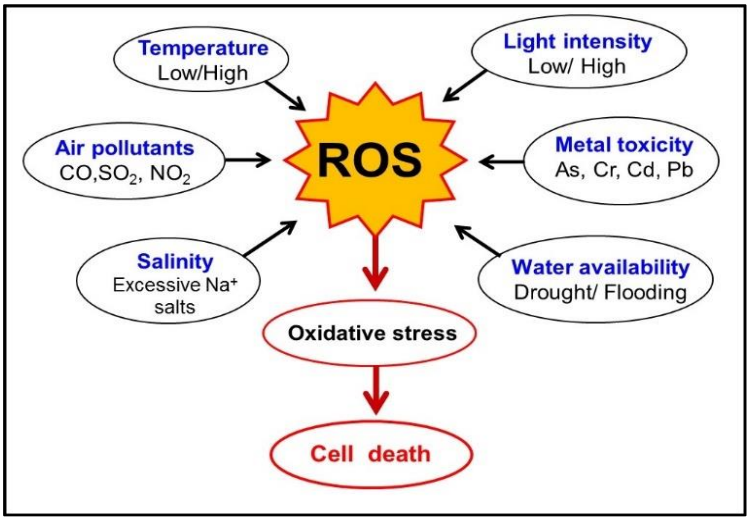

Fig. 1.1. Abiotic stress induced generation of reactive oxygen species (ROS). Adapted from Das et al. 2014 [56]

to evolution of various defense mechanisms like non-enzymatic/enzymatic antioxidants and repair systems to regulate the ROS levels, and repair the associated oxidative damage [58]. Over the time, organisms also managed to overcome the ROS associated toxicity by different means like containment at site of production, neutralization, regulation of production, and utilization for certain advantages [58,59].

1.2.2. ROS in biological systems

Reactive oxygen species (ROS) are group of highly reactive radical ($O_2^{\cdot -}$, $^{\cdot}OH$) and non-radical ($^1O_2$, H_2O_2) species of oxygen. Molecular oxygen (O_2) at ground state (triplet state) is paramagnetic biradical (two unpaired parallel electrons in outer orbitals) and is relatively stable [58]. This results into spin restrictions and limited reactivity of oxygen, which can be activated by two ways: (1) absorption of sufficient

energy to flip the electron spin for formation of singlet oxygen ($^1O_2$) and (2) sequential single electron reduction to H_2O and formation of superoxide ($O_2^{\cdot -}$), peroxide (H_2O_2) and $^{\cdot}OH$ radicals as reaction intermediates [58].

1.2.3. Sites of ROS generation in plants

ROS are continuously generated as a metabolic byproduct in various oxidative reactions as well as a primary product in some enzymatic reactions, occurring in cellular compartments like chloroplast, mitochondria, peroxisomes etc., which collectively constitute the major ROS generation sites [60,61] (**Fig. 1.2**).

Chloroplast: ROS are generated in chloroplast during photosynthesis at photosystems, PS I and PS II [62]. Chloroplasts are the main site of $^1O_2$ generation in the cell [63]. Absorption of high energy radiation by chlorophyll (Chl) molecules results in the formation of chlorophyll triplet state (^{3}Chl), that transfers the energy to molecular oxygen leading to the formation of $^1O_2$ [63]. Chloroplast is also a potential site for the generation of $O_2^{\cdot -}$, where it is produced from the leakage of electrons during electron transfer in the PS I and II to oxygen. The $O_2^{\cdot -}$ is converted into H_2O_2 spontaneously or efficiently by the action of superoxide dismutases localized in chloroplasts [64]. In presence of transition metals (e.g. Fe), $O_2^{\cdot -}$ and H_2O_2 form highly reactive and damaging $^{\cdot}OH$ [27].

Mitochondria: Mitochondria (power-house of cell) is a metabolically active organelle and an important site of ROS generation [56]. Electrons generated from oxidative metabolic reactions are transferred to mitochondrial membrane localized electron transport system (ETC) comprised of multi-protein complexes (complex I-IV). Complex I (NADH ubiquinone oxidoreductase) and Complex III (cytochrome bc_1

complex) are sites of $O_2^{\cdot -}$ generation, which is converted (spontaneously or by mitochondrial superoxide dismutases) into H_2O_2 [64].

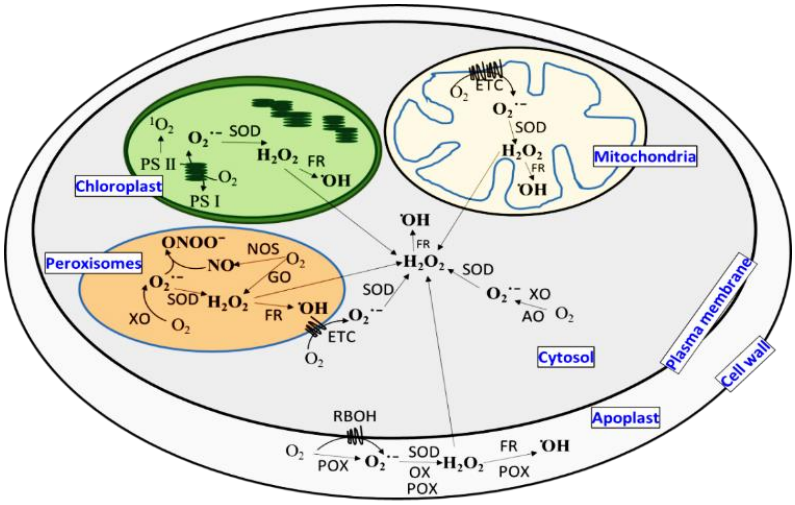

Fig. 1.2. ROS generation in different cellular compartments of plant cell. Adapted from Janku et al. 2019 [61]

Peroxisomes: Peroxisomes are involved in the photo-respiration and oxidative metabolism of lipids and other metabolites [65]. Peroxisome localized Xanthine oxidase (XO) generate $O_2^{\cdot -}$ during the oxidation of Xanthine. Also membrane localized NAD(P)H-dependent ETC comprised of three peroxisomal integral membranes polypeptides (PMPs) also generate $O_2^{\cdot -}$ from the oxidation of NAD(P)H [65]. Peroxisomal SOD, oxidase enzymes (Glycolate oxidase, GO) and Amine oxidase (AO) produce H_2O_2 from oxidation of various metabolites [66]. Apart from ROS production, peroxisome is also involved in the generation of reactive nitrogen species (RNS) such as NO, mediated by Nitrate synthase (NOS), which combines with $O_2^{\cdot -}$ and produces powerful oxidant peroxynitrite ($ONOO^-$) [67].

Plasma membrane and apoplast: Plasma membranes produces $O_2^{\cdot -}$ in the apoplast region from the membrane bound respiratory burst oxidases homolog (RBOH), using

NADPH as electron donor. It is subsequently converted to H_2O_2 by apoplastic SODs and oxalate oxidase (OX) [68]. Class III peroxidases (POXs) localized in the apoplast also produces $O_2^{\cdot -}$, H_2O_2 and $^{\bullet}OH$ [69,70].

Endoplasmic reticulum: Endoplasmic reticulum (ER) contains membrane bound NADPH dependent cytochrome P450 system that is responsible for generation of $O_2^{\cdot -}$ in the ER lumen, which is spontaneously converted to H_2O_2 and then to $^{\bullet}OH$ *via* Fenton reaction [61].

Cytoplasm: Several metabolic reactions contribute to the generation of ROS in the cytosol. For example, xanthine oxidase (XO) generates $O_2^{\cdot -}$ during catalytic conversion of xanthine into uric acid. Similarly, aldehyde oxidase (AO) catalyzed oxidation of various aldehydes to acids and produces $O_2^{\cdot -}$ [71]. Additionally, ROS produced in other cellular compartments (chloroplast, mitochondria, peroxisome etc.) may also diffuse into cytosol. For example, H_2O_2 produced in different organelles can diffuse through membrane or aquaporin like channels [72]. Similarly, in cardiomyocytes and endothelial cells $O_2^{\cdot -}$ is generated extracellularly and in mitochondria, it can diffuse into cytosol *via* chloride intracellular ion channel (CLIC) proteins [73,74].

1.2.4. Reactivity and targets of ROS

Reactive oxygen species are produced in several cellular compartments (**Fig. 1.2**). Under normal physiological conditions, ROS homeostasis in the cell is delicately maintained by interplay of ROS generation and scavenging systems [55,75]. Unfavourable conditions elevates ROS to toxic levels resulting in damage to several cellular biomolecules (lipids, proteins, DNA), and posing a threat to integrity and survival of the cell [56,76]. However, ROS showed differential attributes, in terms of

reactivity to biomolecules and ability to diffuse across membranes [77] (**Table 1.1**).

Table No. 1.1. An overview of different ROS types, their cellular targets and types of damage. Adapted from Das et al. 2014 and Mittler R. 2017 [55,56]

Type of ROS	**Half-life and Diffusion range**	**Cellular targets/damage**
Singlet oxygen ($^1O_2$)	1-4 µs, 30 nm	Highly reactive, limited diffusion, oxidizes lipids (PUFA), protein (aromatic and sulfur containing amino acids) and DNA.
Superoxide ($O_2^{\cdot -}$)	1-4 µs, 30 nm	Moderately reactive, inactivates iron-sulfur (Fe-S) centre proteins, limited diffusion, participate in Haber-Weiss reaction.
Hydrogen peroxide (H_2O_2)	>1 ms, > 1 µm	Moderately reactive, diffusion through membrane and aquaporin like channels, Proteins with sulphydryl (-SH) groups and aromatic amino acids, causes reversible and irreversible modifications. Damage DNA via production of ˙OH.
Hydroxyl radical (˙OH)	1 µs, 1 nm	Extremely reactive, interacts with DNA, proteins, lipids. causes membrane damages, mutagenesis, inactivation of proteins.

1.3. ROS: Small molecules with big impact

Reactive oxygen species were initially considered as harmful species with their association in aging and senescence [78,79]. However, several recent developments in redox biology unveiled the beneficial roles of ROS in regulating diverse biological processes such as controlling the plant physiology, development and in the stress

adaptation at normal physiological levels [55] (**Fig. 1.3**).

1.3.1. ROS as signaling molecule

Reactive oxygen species serve as important redox-signaling molecules in cell [75].The characteristics like specificity to interact with biomolecules, ability to diffuse, and shorter half-life makes ROS important secondary (2°) messengers [67,80]. Role of H_2O_2 as signaling molecule has been extensively studied, however recently studies have highlighted the significance of $^1O_2$ and $O_2^{\cdot -}$ signaling in plant development and stress response [52,59]. Different environmental cues leads to the generation of a ROS wave, which propagates intracellularly as well as extracellularly, and activates systemic defense responses [53]. Post-translational modifications (PTMs) of redox-sensitive transcription factors (TFs) by H_2O_2 is known to regulate signaling networks [81]. H_2O_2-mediated inactivation of redox-sensitive protein tyrosine phosphatase PTP1 results in the activation of the MAPK6 signaling in *Arabidopsis* [82].

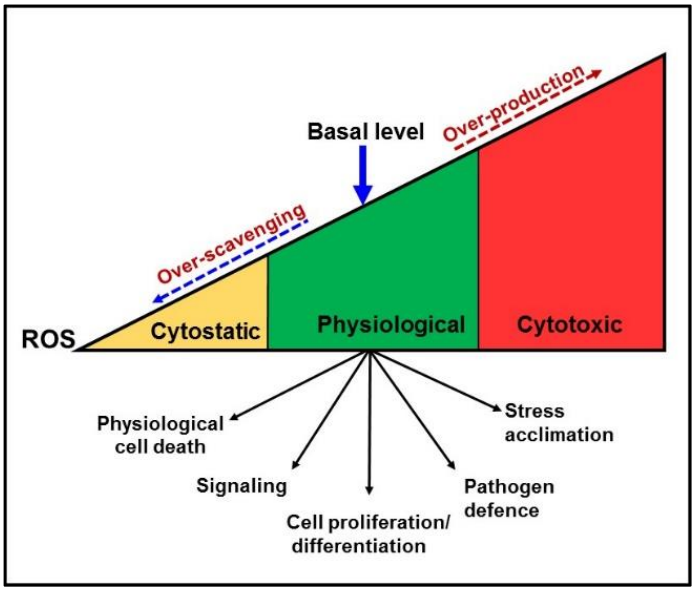

Fig. 1.3. Beneficial and harmful effect of ROS. Adapted from Mittler R. 2017 [55]

Understanding the role of $^1O_2$ role in signaling was limited due to its high reactivity and short-life. Role of $^1O_2$, however, in cell death and stress acclimation has been demonstrated in *Arabidopsis* [83]. *Arabidopsis* FLU gene (negative regulator of chlorophyll biosynthesis) and CHO gene (chlorophyll-a oxygenase) mutants (*flu* and *ch-1*) have been reported to accumulate higher $^1O_2$ under dark/light cycles [54]. The *flu* and *ch-1* mutants showed Executer (Ex1 and Ex2) proteins dependent and independent cell death mediated by $^1O_2$ [54]. Lipid soluble antioxidants (β-carotenes, tocopherols etc.) in chloroplastic membranes quench the photo-oxidative damage mediated of $^1O_2$. The oxidation product of β-carotenes (β-cyclocitral) also acts as chloroplastic retrograde signal in plant stress acclimation [83]. *Arabidopsis*, Zinc finger protein LSD1 (negative regulator of the cell death signaling) mutant showed uncontrolled cell death mediated by $O_2^{\cdot -}$ [84]. In another example, inactivation of chloroplastic SAL1 phosphatase by H_2O_2 leads to accumulation of PAP (phosphoadenosine 5′- phosphate), that regulate miRNA biogenesis by inhibiting nuclear exonuclease XRN activity [85].

1.3.2. ROS as plant growth regulators

Phytohormones that are important for regulation of plant growth and development, also influence cellular ROS levels. ROS involved in seed germination are governed by an interplay of abscisic acid (ABA) and GA (gibberellic acid) [86]. It is also known that methyl viologen treatment is helpful in breaking seed dormancy [87]. Similarly, auxin regulated cell expansion is mediated by apoplastic ROS [88,89]. A co-ordinated action of plasma membrane localized RBOH, apoplastic class III peroxidases and SODs generate $O_2^{\cdot -}$, H_2O_2 and $^{\cdot}OH$, that alters the stiffness and loosening of the cell wall [88]. Recent reports have shown that auxin controls pollen

tube growth by regulating the activity of RBOH [90]. In *Arabidopsis*, shoot and root apical meristems (SAM and RAM) maintain gradient of $O_2^{\cdot -}$ and H_2O_2. While, high $O_2^{\cdot -}$ levels promotes cell proliferation and are important for maintenance of stem cell niche, high H_2O_2 promotes cell differentiation in the elongation zone [91]. The two ROS works antagonistically and their gradient levels regulate cell differentiation/proliferation [91].

1.3.3. ROS in programmed cell death (PCD)

ROS also regulate the PCD in plants [92]. ROS induces PCD in various plant tissues such as tapetum, seed coat, endosperm etc. [92]. PCD of tapetum is important for microspore development [93]. In rice, *dtc1* (defective in tapetal cell death mutant1) showed delayed PCD of tapetal tissue and results in male sterile plants [75,93].

1.3.4. ROS in stromules formation

Stromules, tubular like projections from plastids, filled with stroma have been demonstrated to be involved in physical interactions with other organelles [94,95]. Function of these specialized structures is not fully understood, however, few studies suggest role in plant innate immunity [95]. Elevated ROS levels induces the formation of stromules from chloroplast [96]. Subcellular imaging of organelles suggest that many biomolecules can flow through these stromules [97].

1.3.5. ROS in plant in stress response

ROS also play an important role in plant abiotic and biotic responses. ROS are involved in the activation of stress adaptive responses in plant, such as regulation of stomatal aperture in coordination with phytohormones (e.g., ABA) to control water loss and induction of systemic response [32,53]. In wounding, alternation in ROS level in the injured tissues is shown to induce systemic response in other part of the plants

[98]. However, with prolonged stress conditions, elevated ROS level acts as danger signal [55]. Being highly reactive, ROS serve as useful and potent weapon against pathogens. Several reports show a rapid release of ROS referred to as 'oxidative burst' or 'hypersensitive response', often used to restrict/kill pathogens [99,100]. In *Arabidopsis*, membrane localized NAPDH oxidases (in apoplast or organelles) are important for oxidative burst [101,102].

Studies in *Arabidopsis* mutants lacking *rbohD* and *rbohF* showed altered ROS level and increased susceptibility to *P. syringe* suggesting involvement of $O_2^{\cdot -}$ (and its derivatives) in plant immunity [103,104]. In a similar manner ROS generation by class III peroxidases (apoplastic) in *Arabidopsis* are important for resistance to *Fusarium oxysporium* [99]. Oxidative burst is also modulated by phytohormones, Jasmonic acid and Salicylic acid [105], and is important for systemic acquired resistance [105,106].

1.4. Antioxidant systems

Plants use different strategies (neutralization, sequestration, modification etc.) to contain the excess ROS levels and to maintain ROS homeostasis [107,108]. Antioxidant (ANTs) systems regulate the cellular ROS levels by neutralization and/or transformation into less reactive species. Such antioxidants function by donating electrons to ROS, and prevent/reduce the damage to cellular components. Under normal circumstances, ANTs maintain the basal ROS level, however their levels are elevated under stress conditions to minimize ROS mediated toxicity [32,76]. ANTs are ubiquitous in the cell and protect the cellular environment from any harmful effects of ROS. Antioxidants are classified into two major groups, non-enzymatic and enzymatic antioxidants.

1.4.1. Non-enzymatic antioxidants

Non-enzymatic antioxidant metabolites are essential part of antioxidant system and are grouped into two types, water soluble (ascorbic acid, glutathione) and lipid soluble (tocopherols, carotenoids) [56]. Ascorbic acid (AsA) is highly abundant and widely distributed in the cell. It reacts with most of the ROS ($^1O_2$, $O_2^{\cdot -}$, H_2O_2 and $^{\cdot}OH$) generated in the cell and also regenerates α- tocopherol damaged by free radicals. Glutathione (GSH) is an antioxidant tripeptide (γ-glutamyl-cysteinyl-glycine) that reacts with the ROS ($^1O_2$, $O_2^{\cdot -}$, H_2O_2, $^{\cdot}OH$), and is oxidized to form GSSG. It also regulates activity of proteins by glutathionylation, regenerates AsA, and is involved in maintenance of cellular redox status [56,109]. Tocopherols are lipid soluble metabolites synthesized by the photosynthetic organisms. Tocopherols exists as four isomers (α, β, γ and δ), among them α-tocopherols are most potent antioxidant. These maintain the membrane integrity and protect it from the damaging effect of ROS. Tocopherols reacts with $^1O_2$ and lipid radicals ($RO^{\cdot}$, $ROO^{\cdot}$) and terminates the chain propagation reaction of lipid peroxidation cycle [110]. Carotenoids are another type of lipophilic antioxidants vital for protection of integrity of cellular membranes from damaging effects of $^1O_2$. In plants, these also protect the photosynthetic machinery from the photo-oxidative damage. Flavonoids play diverse roles in plants like defense against pathogens and protect the membrane from damaging effect of $^1O_2$ [56].

1.4.2. Enzymatic antioxidants

Plant possesses a complex enzymatic antioxidant network comprised of several enzymes viz. superoxide dismutases (SODs), Catalases (CATs), Ascorbate peroxidases (APXs), Glutathione peroxidases (GPXs), actively involved in the scavenging of ROS generated in different cellular compartments [26,111,112].

Superoxide dismutases:

Superoxide dismutases (SODs) (EC 1.15.1.1) are important group of ubiquitous antioxidant metalloenzymes. SODs catalyzes dismutation of $O_2^{\cdot -}$ into H_2O_2 and O_2 [60]. SOD catalyzed reaction is highly efficient (near diffusion limit) and is ~10^4 times faster than the spontaneous dismutation of $O_2^{\cdot -}$ [113]. SOD catalyzed dismutation of $O_2^{\cdot -}$ occurs via two-step ping-pong mechanism: 1) oxidation of $O_2^{\cdot -}$ to O_2 and 2) reduction of $O_2^{\cdot -}$ to H_2O_2 (**Fig. 1.4**).

Step I (Oxidation): $O_2^{\bullet -} + M^{n+1} \longrightarrow O_2 + M^n$

Step II (Reduction): $O_2^{\bullet -} + M^n + 2H^+ \longrightarrow H_2O_2 + M^{n+1}$

[n= 2 (Fe, Mn and Ni SOD), n =1 (CuZn and Cu SOD)]

Fig. 1.4. Reaction of Superoxide dismutases

Catalases:

Catalases (CATs) are heme-containing enzymes and the first discovered antioxidant enzymes [60]. In plants, CATs are localized in peroxisomes and cytosol [114]. CATs are highly efficient enzymes, do not require any external reducing agent, and converts H_2O_2 into water and oxygen [56].

Ascorbate peroxidases (APX) and Glutathione peroxidases (GPX):

Ascorbate peroxidases (APX) and Glutathione peroxidases (GPX) are present at multiple cellular locations like cytosol, mitochondria, and chloroplast. Both, APX and GPX catalyzes H_2O_2 into H_2O and O_2, however unlike catalase these requires ascorbate and glutathione as external reducing agents. APX and GPX are important

constituent of plant water-water cycle and Ascorbate-Glutathione cycle to mitigate ROS toxicity [64,115].

1.5. Superoxide dismutases (SODs)

Superoxide dismutase (SODs) are present in all aerobic organisms [116]. Among the different antioxidant enzymes, SODs forms the first line of defense against ROS toxicity [112]. It was first isolated from bovine erythrocytes as 'erythrocuprin' (a copper containing protein) and later demonstrated to perform dismutation of $O_2^{\cdot -}$ [117]. Subsequently, other SOD isozymes were identified in different organisms.

1.5.1. Evolution of SODs

Multiple isozymes of SODs are present in organisms, and based on metal ion cofactor present, these proteins are classified as Fe SOD, Mn SOD, Ni SOD and Cu/Zn SOD [116]. It has been suggested that availability of metal ions with change in the primordial earth environment from reducing to oxidizing lead to the evolution of multiple SOD types [113].

Iron SOD (Fe SOD): Fe SODs are most primitive among the different SODs, and found in both prokaryotes and eukaryotes [118]. In primitive earth, under highly reducing environmental conditions Fe, Mn and Ni were present as soluble ions (M^{2+} state), however due to high abundance Fe was readily available as cofactor for the SODs [113]. Fe SODs exists as homo-dimeric and homo-tetrameric form, is sensitive to H_2O_2 and insensitive to cyanide [116]. In plants, Fe SODs are nuclear encoded and localized to chloroplast. The absence of Fe SOD in animals suggests that it has evolved in primitive photosynthetic microorganisms (e.g. cyanobacteria), followed by gene transfer to eukaryotic nuclear genome during endosymbiosis with the eukaryotic

cell [116,119].

Cambialistic SOD: These SOD types are capable of using Fe or Mn as the metal cofactor, based on availability [120]. During evolution, with the increase in atmospheric oxygen levels soluble Fe(II) form was less available due to its oxidation to insoluble Fe(III) [113]. Mn(II), with more availability/abundance and characteristics similar to Fe(II), was accommodated in the protein structure leading to the evolution of Fe/Mn-SOD (cambialistic SOD) [118]. Cambialistic SOD are reported in bacteria and fungi, however, these isoforms have not been reported in higher eukaryotes [118,121].

Manganese SOD (Mn SOD): Mn SOD is present in both prokaryotes and eukaryotes. In eukaryotes, MnSOD are localized mostly in mitochondria but also reported in peroxisomes [116,122] and chloroplast [123]. When primitive atmosphere became oxidizing, due to less availability of the soluble Fe(II) form it was replaced with Mn(II). The cofactor replacement and some minor changes in the protein leads to the evolution of Mn SOD. Unlike cambialistic SODs, these enzymes are divergent from Fe SOD and show strict dependency on Mn cofactor [113,124]. Incorporation of Fe in human Mn SOD (SOD3) results into little/no SOD activity. However, the protein loses metal specificity and behave as cambialistic SOD with a single amino acid mutation (H142Q), suggesting that similar changes at crucial positions may have contributed towards the evolution of Mn SOD [125].

Nickel SOD (Ni SOD): Ni SOD are cytosolic SODs, which exists as hexameric protein. Ni SOD was first isolated from *Streptomyces* [113]. Compared to other SOD isoforms, Ni SOD had different active site ligands formed from cysteine and histidine residues and is structurally diverse. Ni SODs were identified among certain groups of

green algae, however it is not present in higher eukaryotes, suggesting its independent evolution in certain group of organisms [118,126].

Copper/Zinc SODs: Copper/Zinc SODs (designated as Cu/Zn SODs, CuZn SODs, Cu-Zn SODs, CSDs) have evolved much later after 'the Great Oxidation Event', when the oxidation of Cu(I) to Cu(II) enhanced this metal ion availability [121,127]. However, Cu(II) showed larger differences in the properties compared to Fe/Mn, which indicates it cannot be accommodated in the protein without major structural changes, and hence this isoforms is likely to have evolved independently [113]. Initially, it was thought that Cu/Zn SODs are exclusive to eukaryotes, however, subsequently this isoform was also reported in prokaryotes [116].

Cu-only SOD: Cu-only SOD is a new addition to SOD group of isozymes, which lack of zinc (Zn) cofactor. Cu-only SOD was first identified in *Mycobacterium tuberculosis* [128] and later in *Candida albicans* [129]. Mycobacterial Cu-only SOD (*sodC*) lacks amino acid residues involved in Zn binding, whereas in *C. albicans* the isoform also lack residues of electrostatic loop (ESL) that guide the $O_2^{\cdot -}$ to the catalytic Cu cofactor [129]. Cu-only SOD are localized in extracellular spaces and are involved in the pathogenesis as it protects the pathogen from oxidative burst of host immune system [130]. Despite the absence of ESL and missing Zn, Cu-only SODs are still able to detoxify the $O_2^{\cdot -}$ and exhibit pH sensitivity [131,132]. Interestingly, an unexpected organization in zebrafish was identified, where in place of single Cu-only SOD, four tandem repeats of Cu-only SOD domain were present. These were referred to as Cu-only SOD repeat proteins (CSRPs) with unknown function. However Cu-only SOD and CSRPs type proteins were not reported in plants [131].

1.6. Superoxide dismutases in plants

All five SOD types viz. Fe, Mn, Ni, Cu/Zn and Cu-only SOD, are present in eukaryotes [116,133] whereas in plants, only three SOD types; Fe, Mn and Cu/Zn SODs are reported and localized to diverse subcellular compartments [116]. Fe SOD are mostly localized in chloroplast, and Mn SOD in mitochondria, and Cu/Zn SOD at multiple locations (cytosol, chloroplast, peroxisomes, apoplast etc.) [56,64]. Unlike most organisms, plants generally have multiple forms of each SOD class encoded by more than one gene [134].

Structural features of SODs:

Superoxide dismutases (SODs; Fe, Mn and Cu/Zn) in plants are reported to exist in different oligomeric forms; monomer, dimer, tetramer and sometimes also as an equilibrium of mono- and dimeric forms [134]. Cu/Zn SODs in eukaryotes are mostly dimeric, and also reported to be present in an equilibrium of mono- and dimeric forms [135,136]. Moreover, only monomeric and tetrameric forms are also reported in eukaryotes [137,138]. Cu/Zn SODs are structurally diverse than Fe SOD and Mn SODs. Secondary structure analysis showed Mn SOD and Fe SOD are rich in α-helices content whereas, Cu/Zn SODs are rich in β-pleated sheets and folded into highly stable Greek-key topology [139]. The Cu/Zn SOD has an intra-molecular di-sulfide bond and in some cases inter-subunit also, which is involved in the Cu/Zn stability/activity of the protein. Some of these structural features contribute towards the Cu/Zn SODs tolerance to chemical denaturants, pH change and temperature [140,141]. An important structural feature of the SOD is an electrostatic loop (ESL) that guide the negatively charged $O_2^{\cdot -}$ to the active site centre for catalysis [113].

1.7. Importance of SODs in plants

1.7.1. SOD in plant development and stress tolerance

Superoxide ($O_2^{\cdot -}$) being charged molecule do not diffuse across membranes, however few evidences indicate possibility of limited diffusion [73,142]. Thus presence of SODs in metabolically active cellular organelles/compartments is important for localized scavenging and protection from damaging effect of $O_2^{\cdot -}$ [116,134]. SOD expression is upregulated under various stress conditions like salinity, drought, heat, etc. [143–148]. Analysis of plant *sod* mutants and overexpression experiments have provided insights into role of individual SODs in physiological and developmental processes [149,150]. *Arabidopsis* chloroplastic Fe SOD mutants (*fsd*2 and *fsd3*) show impaired photosynthetic function with pale green phenotype and enhanced photo-oxidative stress [149]. Analysis of *Arabidopsis* chloroplastic Cu/Zn SOD *AtCSD2* knockdown mutant showed increased sensitivity to high light and negative impact on growth and development [115]. Overexpression of AtCSD2 in *Arabidopsis* and OsCSD2 in rice showed increased protection to multiple abiotic stresses [150,151]. Likewise, overexpression of SODs in different plants showed enhanced tolerance to abiotic stresses [123,151–156].

1.7.2. SOD as modulator of ROS signaling

SOD play crucial role in regulation of ROS signaling [157]. Cellular $O_2^{\cdot -}$ serve as a precursor for generation of other potent ROS viz. H_2O_2, $HO_2^{\cdot}$ and $^{\cdot}OH$. H_2O_2 generated by SOD serve as signaling molecule for communication among organelles and nucleus, resulting in modulation of gene expression in response to environmental cues [52,53,158]. Studies on human and yeast cytosolic CSD (SOD1) also indicated its novel function as a redox sensitive transcription factor [159]. $O_2^{\cdot -}$

also combines with NO to generate peroxynitrite ($ONOO^-$) and modulates activity/function of proteins through post-translational modification or PTMs [160]. SODs by managing the cellular $O_2^{\cdot -}$ pool, also control the levels of other ROS/RNS. Thus, SODs play a dual role in maintaining a fine balance of physiologically relevant ROS levels for beneficial outcomes, and to prevent detrimental effects [157]. Hence, regulation of SODs is an important component and central to maintenance of ROS homeostasis. In plants, differential expression of SOD and H_2O_2 degrading enzymes in apical meristem has been shown to be important for establishment of gradient of $O_2^{\cdot -}$/ H_2O_2 and to regulate cell proliferation and differentiation [91]. The stem cells residing in the central zone showed low SODs and high H_2O_2 degrading enzyme levels, to maintain elevated $O_2^{\cdot -}$ levels. On the contrary, cells in periphery and elongation zone show contrasting expression pattern of SOD and H_2O_2 degrading enzymes to maintain higher H_2O_2 levels [91,92]. Hence, differential cell-/tissue-specific expression of SODs is important for modulation of ROS signaling and regulation of growth and development.

1.8. Gene expression and regulation

Regulation of expression of genes is necessary for optimal response to intrinsic physiological perturbations as well as to extrinsic factors (e.g. stresses), for growth, development and adaptation to environmental conditions [161,162]. All the cells in an organism have the same genomic information, however, the functional components varies in different cells/tissues and conditions due to differential expression [161]. In eukaryotes, gene expression is regulated at multiple levels (transcription, post-transcription, translation, post-translation etc.), however, cross talk between different regulatory mechanisms have also been reported [161,163,164].

1.8.1. Transcriptional gene regulation

Gene expression at transcriptional level is controlled by promoter and multiple regulatory elements (*cis*-response elements, enhancers, suppressors etc.) present in the gene to regulates its response to various stimuli [162]. The presence/absence of stress-responsive elements in gene that make it responsive/unresponsive to particular stress conditions has been observed in different plants [165,166]. In eukaryotes, DNA is wrapped around the histone proteins and offer advantages in terms of a) compaction of the genome and b) regulation of transcription of genes by epigenetic modifications [163,167]. Epigenetics that refers to heritable alterations without any change in the nucleotide sequences, is crucial for genomic stability, adaptability and transgenerational memory [163,168]. These alterations include post-translational modification of histones (methylation, acetylation) and methylation of cytosine bases in DNA [169]. Post-translation modifications of histones influence the compactness of chromatin (euchromatin: open state; heterochromatin: close state), re-positions nucleosomes by chromatin remodeling complexes (e.g. SWR1 remodeling complex), and alters the accessibility of a gene for transcription (switch on/off for expression) [170]. Analysis of CpG island distribution in rice and *Arabidopsis* showed that most of the these are associated with genes [171]. Differential methylation pattern of the CpG islands can tune the gene expression in response to environmental signals [169,171]. Generally, methylation of DNA/histones lead to repression/silencing of genes and acetylation results in activation. Alterations in the methylation pattern have also been shown to have pleiotropic effects on plant development [172,173].

1.8.2. Post-transcriptional regulation

Several post-transcriptional mechanisms are known that act on pre-existing

transcripts for various outcomes including regulation of gene expression and enhanced transcriptome/proteome diversity. Some of these mechanisms such as RNA interference (RNAi), alternative splicing, non-sense mediated decay (NMD) are important players for regulation of gene expression under diverse environmental cues [174,175].

1.8.3. Translation/ post-translational mechanisms

Post-translation regulatory mechanisms covalently modify the amino acid residues of the proteins to modulate its function/activity. Some prominent post-translational mechanisms include phosphorylation, acetylation, ubiquitination, methylation etc. [176]. Post-translational modifications generate another layer of complexity in regulation of gene expression. For example, addition of ubiquitin moieties mark proteins for proteasome mediated degradation [177], and phosphorylation affects protein properties like cellular localization, interactions, activity etc.[178,179]

1.9. Significance of post-transcriptional regulation mechanisms

Plant genes are regulated at multiple levels, however, in recent years post-transcriptional mechanisms like miRNA and alternative splicing have emerged as important players. Both the mechanisms act on pre-existing transcripts and dynamically regulate expression of genes in normal and stress conditions [180,181]

1.9.1. MicroRNAs (miRNAs)

Eukaryotic cells contain a diverse array of non-protein coding RNAs (referred to as non-coding RNAs or ncRNAs) [180]. One of the type, known as microRNA (miRNA), function as regulatory RNA at post-transcription level. MicroRNAs are 21-

25 nt long ncRNAs involved in regulation of a target gene by mediating the transcript cleavage or translation suppression [182]. Several studies in plants have shown involvement of miRNAs in regulating diverse cellular processes including development, nutrient homeostasis, abiotic and biotic stress responses [182,183]. Although, binding of miRNAs to its target is governed by 'seed rule', where 10-11 nt are important for target recognition [184], involvement of non-canonical binding sites is also reported, that diversify the targets and functions of miRNAs [185,186].

1.9.2. Splicing

1.9.2.1. Splicing or constitutive splicing (CS)

The eukaryotic gene structure is very different from prokaryotes. The 'discontinuous gene structure' was first reported in adenovirus 2 (subsequently seen in other eukaryotes), where the coding regions (exons) are interrupted with non-coding sequences (introns) [187,188]. This gene organization was also referred to as 'interrupted genes' or 'split genes' [187]. After transcription, precursor messenger RNA (pre-mRNA, contains both exons and introns) undergoes a complex process of excision of introns and joining of exons to generate mature mRNA through a process known as 'splicing' [188,189]. There are three types of introns, group I, II and III having differences in the processing of introns. Among them, group I and II are self-splicing introns (spliceosome independent) whereas processing of group III type introns are spliceosome dependent. It was speculated that group III introns were evolved from the self-splicing group II introns (spliceosome independent) [188]. Splicing is performed by ribonucleoprotein (RNP) complex 'spliceosome' that consists of hundreds of proteins [190]. Two types of spliceosomes, U2 type (canonical or major) and U12 type (non-canonical or minor) are reported and having differences

in the core spliceosome components. [191,192]. In U2 type snRNPs, U1, U2, U4, U5 and U6 forms the core of spliceosome, whereas in U12 type, U11, U12, U4atac, U5 and U6atac, snRNAs are the major RNA components [193]. The splicing requires consensus sequences in the introns, conserved dinucleotide donor (5′ GU) and acceptor (3′ AG) sites, branch point adenosine, and polypyrimidine tract near 3′ end [194] (**Fig. 1.5**). The splicing of most of the intron containing genes is governed by GU-AG rule (for U12 type; A/GU- AC/G), and involves two trans-esterification reactions [193].

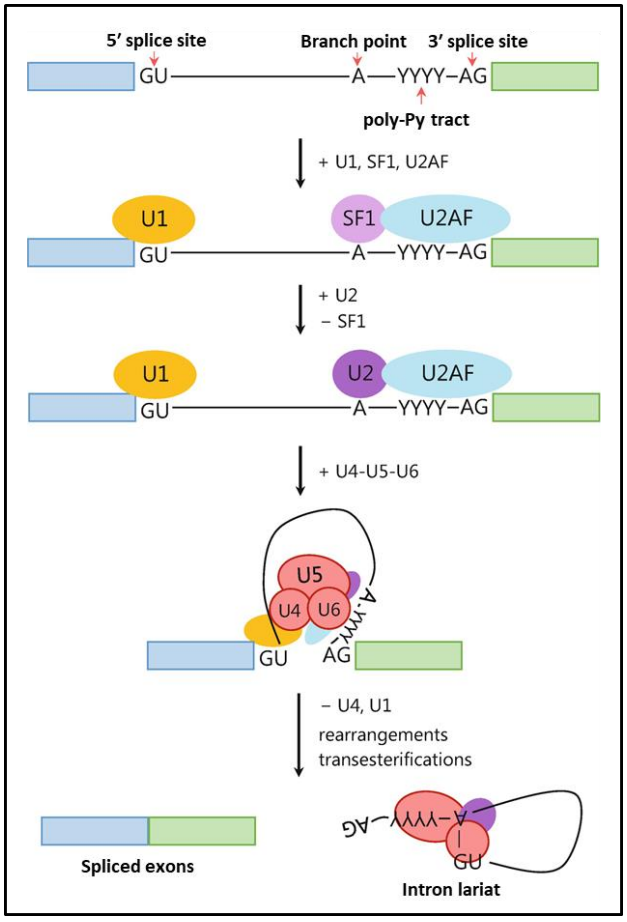

Fig. 1.5. Schematic model of splicing of a eukaryotic gene. Adapted from Staiger et al. 2013 [194]

1.9.2.2. Alternative splicing (AS)

According to ‘one gene one polypeptide’ hypothesis, one gene codes for one polypeptide. However in eukaryotes, intron-containing genes may also undergo ‘alternative splicing’ that involve different combination of UTRs/exons resulting in generation of more than one RNA/protein isoform from a single gene [188] (**Fig. 1.6**). AS was first discovered in adenovirus 2 and later AS of immunoglobulin IgM gene was reported from human [192].

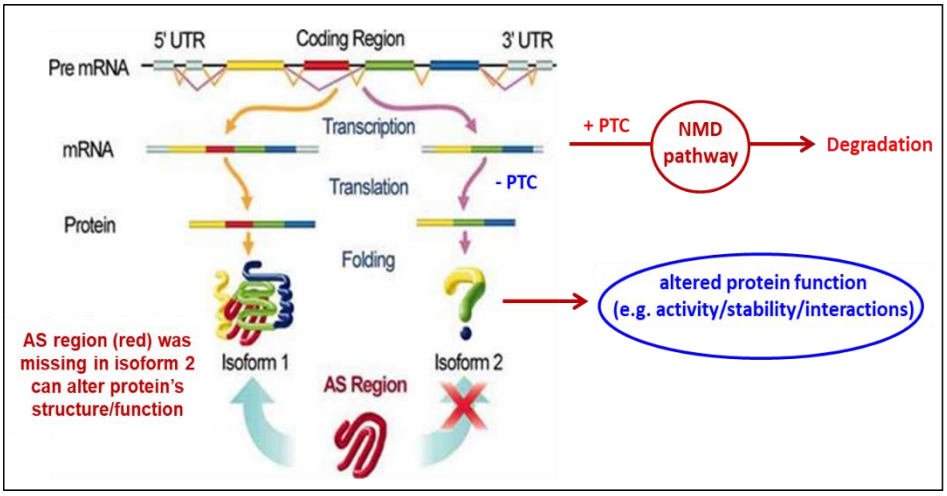

Fig. 1.6. Gene expression and alternative splicing. Adapted from Romero et al. 2006 [195].

Alternative splicing of genes can occur by multiple ways such as, exon skipping (ES), intron retention (IR), 5′ alternative splice site (5′ASS) and 3′ alternative splice site (3′ ASS) and mutual exclusive events (MEE) (**Fig. 1.7**). However, the predominance of these events may varies in different organisms, for example IR events are more prevalent in plants, whereas ES type events are predominant in humans [196].

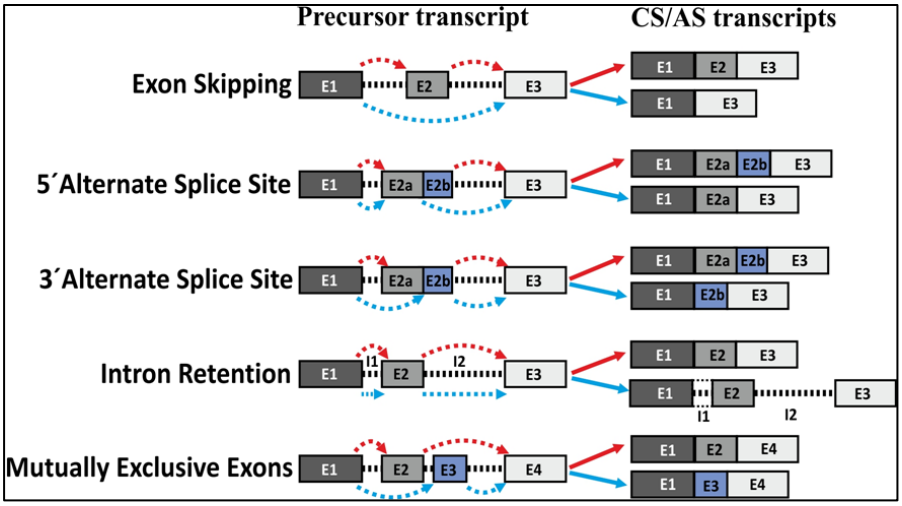

Fig. 1.7. Different types of alternative splicing events. Adapted from Sanyal et al. 2018 [197].

1.9.2.3. Splice sites recognition

Recognition of splice sites is very crucial step for correct constitutive/alternative splicing of the primary transcripts. Selection of splice sites by spliceosome is reported to be influenced by *cis*-elements and *trans*-regulatory factors [192,198]. Certain *cis*-elements such as exon splice site enhancers (ESE)/silencers (ESS) and intron splice site enhancers (ISE)/silencers (ISS) on pre-mRNA interact with trans-regulatory factors (serine-arginine rich (SR) proteins, heterogeneous nuclear ribonucleoproteins (hnRNPs), other auxiliary factors to influence the binding to a particular site [192]. SR proteins contain RRM motifs (RNA recognition motifs) for RNA binding, and RS domain for protein-protein interaction. In plants, *Arabidopsis* and rice contain 18 and 22 SR genes, respectively [198,199]. Analysis of SR genes in plant tissues, development stages and stress conditions showed expression differences suggesting tissue-and stress-specific regulation [199]. Interestingly, SR genes are also reported to be extensively alternatively spliced which further increases the complexity of AS [192].

1.9.2.4. Alternative splicing as gene function diversification mechanism

Alternative splicing diverts the primary transcript pool towards multiple alternative RNAs, and affects the levels of constitutive transcript/protein isoform. The alternatively spliced transcripts/variants (splice variants, SVs) may have variations in the non-coding, untranslated regions (UTRs) at 5′- or 3′- ends, and/or coding (exons) regions, resulting in altered transcript properties like stability, translation efficiency etc. [174,200]. The SVs with variation in the coding region may have altered characteristics of encoded proteins like activity, stability, localization, and interaction [174,201]. It is also reported that some of the SVs are under the scrutiny of RNA surveillance system like 'non-sense mediated decay' (NMD) pathway, which channelize transcripts with pre-mature termination codon (PTC) towards degradation [202]. Thus, AS is a multi-dimensional gene regulation mechanism, which can regulate transcript and protein levels, but can also diversify the gene/protein function (**Fig 1.6**) [174,196].

Studies based on high-throughput transcriptome analysis have revealed widespread impact of AS on human transcriptome/proteome with >95 % intron-containing genes subjected to alternative splicing. Similarly, the mechanism is equally prevalent in plants with >60 % genes now known to undergo AS [174]. Plant genes affected by AS is likely to be increase further with more high-throughput studies on developmental/tissues/stress conditions [196,203]. Studies have also shown differences in predominant splicing events in human and plants. Exon skipping (ES) is more prevalent in humans while intron retention (IR) is more predominant in plants [196]. A vast amount of transcriptomic data analysis from animals and plants has shown that AS play important roles in diverse cellular processes ranging from growth,

development and differentiation to different types of stress responses [174,204].

1.10. Significance of AS in plants

Alternative splicing serves as a dynamic master regulator of eukaryotic transcriptome/proteome affecting a diverse array of cellular processes viz. growth, development, differentiation, and adaptive responses to various environmental perturbations and stress conditions [174,181,205].

1.10.1. Role of AS in regulation of hormone signaling

Plant hormones are important growth regulators and regulates overall plant physiology, growth, development, and adaptation to stresses [206]. AS mediated control of hormone signaling, is involved in regulation of plant response to different stimuli. In *Arabidopsis*, AS of JAZ (negative regulator of Jasmonic acid signaling) generates an alternative isoform lacking regulatory phosphorylation site (crucial for E3-ligase mediated proteasomal degradation). *Arabidopsis* plants overexpressing alterative isoform showed male sterile phenotype suggesting role of AS in anther development [207,208]. Similarly, AS affects the localization of YUCCA4 gene (Flavin-dependent monooxygenase; FMO, involved in auxin biosynthesis) by generating two alternative isoforms localized to endoplasmic reticulum (ER) and cytosol in a tissue-specific manner [209,210]. In another example, AS of HAB1 produced splice isoforms with antagonist function and modulates ABA signaling by regulating kinase activity of SnRK2 [182].

1.10.2. Role of AS in flowering

Alternative splicing is also known to play important role in regulation of flowering in *Arabidopsis*. *Arabidopsis* FLM (Flowering locus M) that code for a

MADS-box transcription factor controls flowering in temperature-dependent manner, and act as repressor of flowering [211]. FLM undergo AS to generate two splice variants, β and δ. Both isoforms interact with SVP (short vegetative phase) protein but only FLM β is able to interact with DNA. At low temperature, FLM β is the predominant form, which binds to the promoter elements of its target genes and suppress flowering. However at ambient conditions, AS shift towards FLM δ isoform but it fails to bind to DNA and thus activates flowering [212,213] (**Fig. 1.8**).

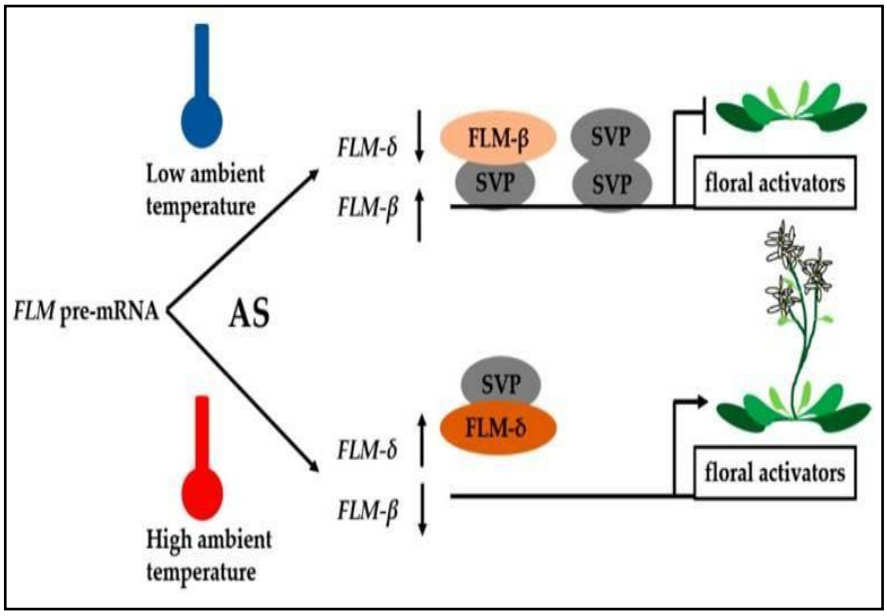

Fig. 1.8. Temperature dependent alternative splicing of FLM and regulation of flowering. Adapted from Shang et al. 2017 [181]

1.10.3. Role of AS in plant defense

Alternative splicing play important role in plant defense response against pathogens and affects host-pathogen interaction [192,214]. Alternative splicing of 'N' gene in tobacco that codes for Toll like/interleukin 1 receptor generates two isoforms, large; N_L and small; N_S. Both N_L and N_S isoforms are needed for full resistance against TMV, while expression of either isoform confers little/no protection [214].

Similarly, *Arabidopsis* RPS4 gene (TIR-NBS-LRR family) also undergo AS and both the isoforms are required for resistance against *P. syringe* [215].

1.10.4. Alternative splicing in abiotic stress tolerance

Alternative splicing modulates the expression level or function of genes in response to abiotic stress conditions. In *Arabidopsis*, heat stress induces AS of HSFA2 (heat shock transcription factor) and generates both full-length and truncated isoforms, of which truncated one bind to its own promoter to enhance transcription [181]. A dehydration response element binding protein (DREB) undergo AS in rice. Under normal conditions, DREB2B (non-functional isoform) is produced, whereas functional form is induced under abiotic stress conditions for the activation of adaptive response [181].

Apart from AS mediated modulation of individual genes, spliceosome machinery components are also implicated in modulating the response in certain conditions. For example, hypersensitivity of *Arabidopsis SR34b* mutant to Cd toxicity due to mis-splicing of IRT1 (an iron transporter) suggests direct role of splicing components in controlling adaptive response to stress conditions [216]. Similarly, U1A protein of spliceosome is found to be involved in salt tolerance in *Arabidopsis* [217]. In another example, many of the DNA repair genes are also reported to undergo alternative splicing indicating the possibility of role of AS in modulating plant DDR (DNA damage response) [205].

1.10.5. Stress-priming and AS-linked memory

Studies have shown that plants exposed to sub-lethal doses (priming dose) of stress perform better than the plants directly exposed to lethal doses [218]. This suggests that priming of plants generates a stress-memory for subsequent episodes

[219], however, underlying mechanisms are not fully understood. A recent study has shown that AS is involved in heat stress-memory establishment [218]. *Arabidopsis* plants primed with sub-lethal heat stress showed protection from subsequent exposure to lethal heat stress [218], that was shown to be due to accumulation of non-spliced, intron retention (IR) transcripts resulting in establishment of splicing memory. Subsequent exposure to lethal heat stress activated the correct splicing pattern and ensured survival of the plants [218,220].

1.10.6. Cross-talk of regulatory mechanisms

Alternative splicing also interacts/ cross talks with other regulatory mechanism to influence gene expression and function [221,222]. For example, many miRNAs in plants are localized in the intronic region of other genes and substrate for both AS and RNAi machinery [223]. Recently, miR400 (localized in the intronic region) was shown to be regulated by heat stress-induced AS of the host gene that affected miR400 levels [221]. Likewise, the non-coding RNA and post-translation modifications of SR proteins also modulates the splicing patterns of genes [196,224].

1.11. Regulation of plant SODs

The regulation of SODs in plants is controlled by multiple modes and is indicative of importance of intricate balance of ROS levels required for cellular functioning.

1.11.1. Transcription regulation of SODs

Superoxide dismutases as stress-responsive genes are differentially induced under stress conditions [165,225]. Rice expression database showed variation in expression pattern of seven SODs in different tissues suggesting cell/tissue-specific

regulation of the antioxidant enzymes [226]. In *Arabidopsis* apical meristems, central and peripheral zone cells showed contrasting expression of SODs, necessary for maintenance of proliferation/differentiation, and highlights the importance of SOD regulation [88,91]. The two rice cytosolic SODs are also differentially regulated under certain abiotic stresses suggesting regulation at promoter level [148,227,228]. Similarly, *Arabidopsis* chloroplastic SODs are shown to be positively regulated by MKK5 signaling [229,230].

1.11.2. Post-translational regulation of SOD

1.11.2.1. Copper (Cu) chaperone for SOD (CCS) mediated activation of SOD

In eukaryotes, Cu/Zn SOD is also regulated by a metallo-chaperone CCS [231]. CCS is important for activation and maturation of Cu/Zn SODs [232,233]. CCS has N-terminal ATX-1 like domain and C-terminal domains for oxidoreductase activity and interaction with SOD [234]. CCS is multi-function protein that delivers Cu cofactor to the active site of apo-protein and is important in managing the levels of active Cu/Zn SOD [231]. Both CCS-dependent and independent pathways of SOD activation exists in eukaryotes [235,236]. In humans SOD1 is completely dependent on CCS, whereas in *C. elegans*, it is not required [237]. In *Arabidopsis*, both CCS-dependent and independent pathways exists for activation of Cu/Zn SOD [238] (**Fig. 1.9).**

1.11.2.2. Peroxynitrite mediated nitration of SOD

SOD are also found to be regulated by PTMs mediated by peroxynitrite ($ONOO^-$) [160]. Nitration of SODs in *Arabidopsis* has been shown to inhibit the activities of all SODs specific to different cellular compartments, and MnSOD isoform was found to be most-sensitive to NO-mediated inhibition [160].

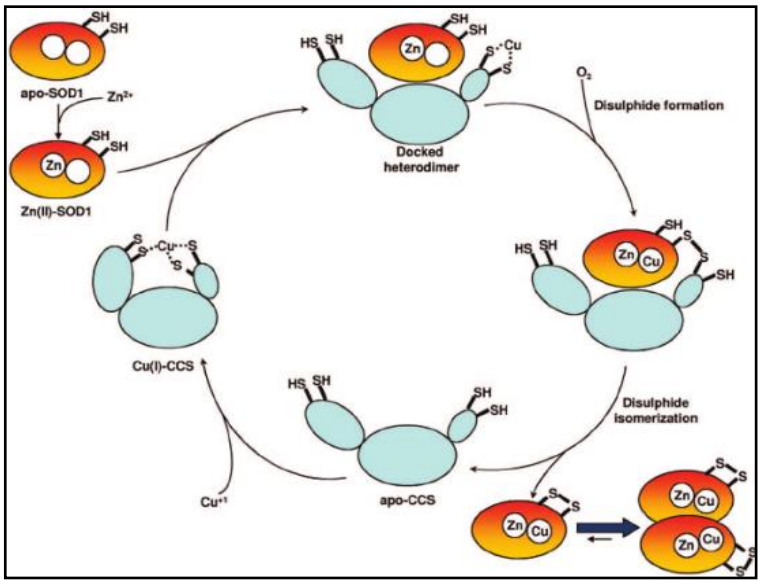

Fig 1.9. Cu chaperone for SOD (CCS) mediated activation and maturation of Cu/Zn SOD. Adapted from Banci et al. 2009 [233]

1.11.2.3. SOD as transcription factor

In human and yeast, a novel function of cytosolic Cu/Zn SOD (SOD1) as a redox sensitive transcription factor has been demonstrated [159]. Phosphorylation of SOD1 by ATM dependent Dun1 is important for nuclear translocation and activation of oxidative stress response genes [159].

1.11.3. Post-transcriptional regulation of SOD

1.11.3.1 MicroRNA 398 (miR398) mediated regulation

Cu/Zn SODs in rice and *Arabidopsis* are negatively regulated by miR398, at post-transcriptional level [150,239–241]. Interestingly, miR398 also regulates some other transcripts including Cu chaperone for SOD (CCS) and COX5B-1 (subunit of mitochondrial cytochrome b oxidase). In *Arabidopsis*, miR398 is known to regulate blue copper binding protein (BCBP) [185]. These cognate target genes are Cu containing proteins. Regulation of these targets by miR398 in important for

maintenance of Cu homeostasis in the cell [242]. Studies in plants show that down regulation of miR398 levels resulted in upregulation of Cu/Zn SODs, which is important to control ROS toxicity [242,243], as shown below (**Fig.1.10**). In *Arabidopsis*, SPL7 gene (Squamosa Promoter binding protein like gene 7) also regulates SOD levels via modulating the levels of miR398 under Cu deficiency condition [244].

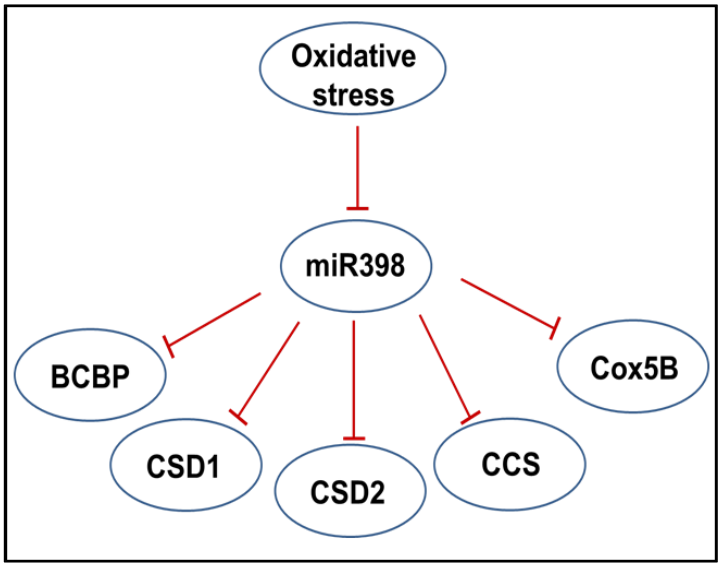

Fig. 1.10. Post-transcriptional regulation of Cu/Zn SOD and other target genes by miR398.

1.11.3.2. Alternative splicing mediated regulation of SODs

RNAseq studies show evidence of AS events in large number of genes in different plants that also include antioxidant genes, however, there are few studies on detailed investigations. Involvement of AS in regulation and functioning of SODs have also been reported in *Oryza sativa* (Fe SOD), *Glycine max* (Cu/Zn SOD), *Arabidopsis thaliana* (Fe SOD), and *Populus trichocarpa* (Cu/Zn SOD) [245–248]. Two AS isoforms of rice Fe SOD (chloroplastic) were responsive to certain stresses, and were functionally active [245], whereas *Arabidopsis* Fe SOD splice variant isoforms show

differential involvement in chloroplast development [248]. AS isoforms of soybean Cu/Zn SOD showed tissue specificity and response to copper content, and suggested to perform metal sink function in excess copper conditions [246]. AS isoforms of *Populus* Cu/Zn SOD showed distinct tissue specificity but alternative isoform was enzymatically inactive [247]. These evidences indicate that AS is involved in regulation of SOD expression, tissue specificity and functional diversification of isoforms in different plants.

It is interesting to see that number and type of AS events predicted/identified in SOD types differ in plants such as rice (http://rice.plantbiology.msu.edu/) and *Arabidopsis* (https://www.Arabidopsis.org/). This suggests that mode/impact of AS involvement in SOD functioning may differ in different plants. Hence, unlike in transcription level regulation (driven by specific *cis*-elements) it is not possible to draw parallels between significance of isoforms (of a gene) from different plants. In view of emerging important role of alternative splicing in diverse array of cellular processes (including stress responses), a thorough analysis is required to understand its precise role in functioning of a gene at both RNA and protein level.

1.12. Rationale of the thesis:

Rice genome has seven SOD genes that code for four Cu/Zn SODs (CSDs), two Fe SODs (FSDs) and one Mn SOD (MSD). Rice Genome Annotation Project (RGAP-MSU) database show that these seven SOD generate 14 splice variants (SVs) by AS. The SVs showed heterogeneity in the non-coding 5′- and/or 3′- UTRs and exons. Among various SODs, CSDs are most abundant and localized to multiple sub-cellular compartments like cytosol, chloroplast and peroxisomes. The rice CSDs also generates maximum number of splice variants (4 constitutive SVs and 5 alternative

SVs), and the nature of events in rice are more diverse than *Arabidopsis*. Detailed characteristics of these SV isoforms and their impact on functioning of rice SODs is unknown. In view of this, the present study proposed a detailed molecular and biochemical analysis of the constitutive and alternative SVs of rice CSDs at RNA and protein level to understand the role of AS in regulation and functioning of these genes.

1.13. Objectives of the thesis:

1) Expression analysis of predicted splice variants of four Cu/Zn superoxide dismutases for tissue specificity and relative abundance.
2) Effect of salinity stress on alternative splicing of Cu/Zn SODs.
3) Cloning, expression and comparative biochemical characterization of the proteins encoded by a major and one alternative splice variant transcripts of two Cu/Zn SODs.

CHAPTER 2

MATERIALS

AND

METHODS

2.1. Materials

2.1.1. Plant material

Rice genotype; *Oryza sativa* L. ssp. *indica* var. NSICRc106 used in the study, was obtained from International Rice Research Institute (IRRI, Philippines). NSICRc106 is a salt-tolerant rice variety developed from *IR32429-47-3-2 / Wagwag*.

2.1.2. Plant growth media, abiotic stress media and transcription inhibition solution

Hoagland media was used as growth media for rice. Hoagland media (1 X) was prepared by dissolving 1.63 g of Hoagland No. 2 basal salt mixture (HiMedia, India) into 1 L of distilled water. Constituents of 1 X Hoagland No. 2 Basal salt mixture (1.63 g) for 1 L media are as follows: Potassium nitrate (606.60 mg), Calcium nitrate (656.40 mg), Magnesium sulfate (240.76 mg), Ammonium phosphate monobasic (115.03 mg), Manganese chloride tetrahydrate (1.81 mg), Boric acid (2.86 mg), Molybdenum trioxide (0.016 mg), Zinc sulfate heptahydrate (0.22 mg), Copper sulfate pentahydrate (0.08 mg) and Ferric tartrate (5.00 mg). All abiotic stress media solutions for rice were prepared in 1 X Hoagland media.

Salt stress media: 150 mM Sodium chloride (NaCl) solution was prepared by dissolving 8.77 g in 1 L of 1 X Hoagland media. Drought stress media: 15 % Polyethylene Glycol (PEG) was prepared by dissolving 150.00 g of PEG-8000 in 1 X Hoagland media and made up volume to 1 L with distilled water. Oxidative stress media: Dissolved 2.57 mg of Methyl viologen dichloride hydrate in 1 L of 1 X Hoagland media to prepare 10 μM Methyl viologen (MV) solution.

Transcription inhibitor solution: All the stock reagents were sterilized by autoclaving.

0.1 M PIPES-KOH pH 5.6: Dissolved 0.151 g of PIPES in MilliQ water and pH was adjusted to 5.6 with 4 M KOH and volume was made up to 50 ml with MilliQ water.

0.1 M Potassium chloride (KCl): Dissolved 0.74 g of potassium chloride in 100 ml of MilliQ water.

0.15 M Sucrose: Dissolved 0.51 g of sucrose in 10 ml of MilliQ water.

0.1 M Sodium citrate: Dissolved 0.294 g of sodium citrate dihydrate in 10 ml of MilliQ water.

Incubation buffer containing 1 mM PIPES, 1 mM KCl, 15 mM sucrose and 1 mM sodium citrate, pH 5.6 was prepared by dilution of the stock reagents.

Transcription inhibitor solution was prepared by dissolving 5 mg of α-amanitin in 50 ml of incubation buffer solution to prepare effective concentration of 0.1 mg ml^{-1}.

2.1.3. Bacterial strains and growth conditions

Strains of *E. coli* used during the course of this study are listed in the **Table 2.1.**

E. coli growth conditions

E. coli strains Top 10, BW25113 and BL-21(DE3) were grown at temperature 37 °C and for SHuffle strains 30 °C was used as optimal temperature condition unless specified.

2.1.4. Bacterial growth media

Luria Bertani (LB) media was used as *E. coli* growth media.

Composition of LB media (1 L): Peptone – 10.0 g, Yeast extract- 5.0 g, NaCl- 10.0 g were dissolved in distilled water, pH adjusted to 7.2-7.5 with 4 M hydroxide (NaOH) solution and volume was made up to 1 L with distilled water and sterilized by autoclaving. For LB-agar (LBA), 1.6 % agar was added in LB-media and autoclaved.

Table 2.1: List of *E. coli* strains

Strain	Genotype	Source/ Reference
Top 10	*F^- mcrA Δ(mrr-hsdRMS-mcrBC) φ80lacZΔM15 ΔlacX74 recA1 araD139 Δ(araleu)7697 galU galK rpsL (StrR) endA1 nupG*	Novagen (Germany)
BL-21 (DE3)	*F^- ompT gal dcm lon hsdSB(rB^-mB^-) λ(DE3)*	Novagen (Germany)
SHuffle T7 Express	*fhuA2 lacZ:T7 lon dcm ompT endA1 ahpC λ(DE3)pNE3-r1-cDsbC ΔtrxB Δgor*	NEB (USA)
SHuffle Express	*fhuA2 lon dcm ompT endA1 ahpC pNE3-r1-cDsbC ΔtrxB Δgor*	NEB (USA)
BW25113	*F^- DE(araD-araB)567lacZ4787(del)::rrnB-3 LAM^- rph-1 DE(rhaD-rhaB)568 hsdR514*	Keio collection library, Japan
BW25113 *ΔsodA*	*BW25113 ΔsodA* (Kan^R)	Keio collection library, Japan
BW25113 *ΔsodB*	*BW25113 ΔsodB* (Kan^R)	Keio collection library, Japan
BW25113 *ΔsodA ΔsodB*	*BW25113 ΔsodAΔsodB* (Kan^R)	Generated in this study

Kan^R; Kanamycin resistance gene

2.1.5. Antibiotics and additives

Details of the preparation and usage of solutions of antibiotics and additives used is listed below in **Table 2.2**. All solutions were filter (0.22µm) sterilized.

Table 2.2: List of antibiotics and additives

Antibiotic/ additives	**Stock conc. (mg ml^{-1})**	**Solvent**	***E. coli* strain**	**Working conc. (µg ml^{-1})**
Ampicillin (Amp)	100	distilled water	All strains	100
			BW25113	50
Kanamycin (Kan)	50	distilled water	BL-21 (DE3)	50
			All strains	25
Chloramphenicol (Cm)	34	100 % Ethanol	BL-21 (DE3)	34
			All strains	17
IPTG-Isopropyl β-d-1-thiogalactopyranoside (IPTG)	1 M	distilled water	0-1 mM	
L-Arabinose	0.2 M	distilled water	0-0.2 mM	
Methyl viologen (MV)	0.1 M	distilled water	0-1mM	
Tetracycline	0.01 M	Methanol	0-10 nM	

2.1.6. Bacteriophage P1 mediated transduction

0.1 M Calcium chloride ($CaCl_2$): Dissolved 1.47 g of $CaCl_2$ in 10 ml of water.

0.1 M Magnesium chloride ($MgCl_2$): Dissolved 0.095 g of $MgCl_2$ in 10 ml of water.

1 M Sodium citrate: Dissolved 2.94 g of sodium citrate in 10 ml of water.

10 % Glucose: Dissolved 1 g of glucose in 10 ml of water.

The solutions were sterilized by autoclaving.

2.1.7. Plasmids vectors

Plasmid vectors used in the study are listed below in **Table 2.3**.

Table 2.3: List of plasmid vectors

Plasmid	Important Features	Source/ Reference
pET28a (+)	Kan^R, N-terminus 6 X Histidine purification tag, T7 RNA polymerase dependent protein expression	Novagen (Germany)
pMAL-c5x	Amp^R, N-terminus MBP purification tag, T7 RNA polymerase independent protein expression	NEB (USA)
pMAL-HIS	Modified pMAL-c5x vector (MBP gene was replaced with 8X Histidine residues), Amp^R, T7 RNA polymerase independent protein expression	Generated in this study
pTwin1	Amp^R, N-terminus Intein purification tag, T7 RNA polymerase dependent expression, pH dependent self-cleavable Tag, Tag-less protein purification	NEB (USA)
pCP20	Amp^R, Cm^R, contained the temperature sensitive origin of replication and temperature inducible yeast FLP recombinase gene,	Coli genetic stock center (CGSC), Yale [249]
pGro7, pTF16, pGTF-2, pKJE7 and pG-KJE8	Cm^R, L-arabinose and or Tetracycline inducible chaperone gene.	TaKaRa (USA)

Amp^R- ampicillin resistance gene, Cm^R- chloramphenicol resistance gene, MBP- Maltose binding protein

2.1.8. Enzymes

DNA polymerases, *Pwo* DNA polymerase was procured from Roche Diagnostics (Germany) and *Taq* DNA polymerase was procured from New England Biolabs (USA); Ligases, T4 Polynucleotide kinase and restriction endonucleases were

procured from NEB (USA). Nucleases, Restriction enzymes were procured from New England Biolabs (USA). SuperScript II Reverse Transcriptase was procured from Invitrogen (USA).

2.1.9. DNA and protein molecular size standards

DNA molecular size standards (Lambda phage DNA-HindIII digest, Phi X 174 DNA-HaeIII digest, 100 bp DNA size ladder) and colour pre-stained protein ladder were procured from New England Biolabs (USA). Gel filtration protein standard was procured from GE healthcare (USA).

2.1.10. Molecular biology kits

Kits for Rapid DNA ligation, plasmid DNA isolation and PCR product purification were procured from Roche Diagnostics (Germany). SYBR Green Jumpstart *Taq* Ready mix was procured from Sigma-Aldrich (USA). Pierce BCA Protein estimation kit from Thermo Fisher Scientific (USA) and Braford Reagent was procured from Sigma-Aldrich (USA)

2.1.11. Chemicals

Molecular biology grade and electrophoresis grade chemicals were procured from Sigma-Aldrich (USA) and HiMedia (India). Other chemical such as inorganic salts and organic solvent of AR/LR grade were procured from either Qualigens (India) or Himedia (India).

2.1.12. Buffers

Reagents for preparation of buffers such as Trizma base **(**2-Amino-2-(hydroxymethyl)-1,3-propanediol), PIPES (Piperazine-N, N′-bis (2-ethanesulfonic acid), Sodium phosphate monobasic, Sodium phosphate dibasic, Potassium phosphate

monobasic, Potassium phosphate dibasic, Sodium carbonate and Sodium bicarbonate were procured from Sigma Aldrich (USA).

2.1.13. Resins, columns and membranes

Amylose and chitin resins were from New England Biolabs (USA) and Ni-NTA resin were procured from Roche Diagnostics (Germany). Gel filtration column from GE healthcare (USA), empty columns from Bio-Rad (USA) and dialysis membranes from Sigma-Aldrich (USA) were procured. Protein concentrator column was procured from Corning (USA).

2.1.14. Disposable plastic material and glassware

Nuclease and pyrogen free polypropylene microfuge tubes, PCR tubes and sterile polypropylene tubes of 15 ml, 50 ml capacity were procured from Axygen (USA). Disposable sterile plastic petri plates were procured from Genexy (India), sterile disposable syringe filters (0.22 μm and 0.45 μm) were procured from Corning (USA). Real-time PCR plates/strips, optical clear films/ strip caps were procured from Roche Diagnostics (Germany), sterile multi-well plates were from Corning (USA). Electroporation cuvettes were procured from Eppendorf (Germany). All the glassware was procured from Schott Duran (Germany).

2.1.15. Miscellaneous chemicals

Sodium dodecyl sulfate (SDS), Acrylamide, N,N′-Methylenebisacrylamide, Ammonium persulfate, Tetramethylethylenediamine, Agarose, Riboflavin, Ethylenediaminetetraacetic acid (EDTA), Diethylenetriaminepentaacetic acid, Nitro blue tetrazolium chloride, Nicotinamide adenine dinucleotide reduced (NADH), Sodium diethyldithiocarbamate trihydrate, Supra pure Nitric acid, 2-Thiobarbituric acid, Trichloroacetic acid, Glycerol, Diethyl pyrocarbonate (DEPC),

Phenylmethylsulfonyl fluoride (PMSF), equilibrated phenol, 1,1,3,3-tetramethoxypropane were procured from Sigma Aldrich (USA). Acetone, Methanol, Isopropanol, and Chloroform were procured from USB (USA). Phenazine methosulfate (PMS), Polyethylene glycol (PEG) 8000 and Absolute Ethanol was procured from Himedia (India). TRIzol reagent was procured from Invitrogen (USA) and Hydrogen peroxide was from Merck-millipore (USA). Oligonucleotide primers were custom synthesized from Integrative DNA technologies (IDT), (USA).

Solution preparation:

All the solutions were prepared in MilliQ water unless specified.

2.1.16. Reagents for total RNA isolation

RNase free water: Added 1 ml of DEPC (0.1 % v/v) into 1 L of water, mixed vigorously and autoclaved.

Other reagents: TRIzol reagent**,** Chloroform, Isopropanol, β-mercaptoethanol (β-ME).

2.1.17. Reagents for gel electrophoresis

2.1.17.1. Reagents for polyacrylamide gel electrophoresis (PAGE)

30 % Acrylamide: Dissolved 290.0 g of Acrylamide and 10.0 g of N, N′-methylenebisacrylamide in 600 ml of water. Adjusted the volume to 1 L with water and solution was filtrated through 0.45 μm pore size filter. Solution was kept in dark coloured bottle and stored at 4 °C.

10 % Sodium dodecyl sulfate (SDS): 10.0 g of SDS was dissolved in water with gentle stirring and made the volume to 100 ml with water and stored at room temperature.

10 X Tris-Glycine buffer: Dissolved 30.0 g of Trizma base, 144.0 g of Glycine in water, made up the volume to 1 L with water and autoclaved. 1 X Tris-Glycine buffer was prepared by ten-times dilution of the 10 X Tris-Glycine buffer. 1 X Tris-Glycine-SDS was prepared by dissolving 100 ml of 10 X Tris-Glycine buffer, 10 ml of 10 % SDS and made up volume to 1 L with water.

1.0 M Tris-HCl pH 6.8; Dissolved 12.11 g of Trizma base in water and pH of the solution was adjust to 6.8 with 4 M Hydrochloric acid (HCl) and volume made up to 100 ml with water.

1.5 M Tris-HCl; pH 8.8; Dissolved 18.17 g of Trizma base in water and pH of the solution was adjust to 8.8 with 4 M HCl and volume made up to 100 ml with water.

10 % Ammonium persulfate (APS): APS (25 mg) was dissolved in 0.25 ml of water and was prepared fresh every time before use.

2 X Native sample buffer: Native sample buffer (2 X) was prepared by mixing the reagents to the final concentrations (62.5 mM Tris-Cl, pH 6.8, 40 % glycerol, 0.01 % (w/v) bromophenol blue).

4 X Laemmli sample buffer: Laemmli sample buffer (4 X) prepared by mixing the reagents to the final concentrations (200 mM Tris-Cl, pH 6.8, 8 % (w/v) SDS**,** 40 % (v/v) glycerol, 0.2 % (w/v) bromophenol blue and 20 % of β-mercaptoethanol).

Coomassie Brilliant Blue R-250 staining solution: Dissolved 10.0 g of Coomassie Brilliant Blue R-250 (CBB) in 500 ml methanol, 100 ml glacial acetic acid and 400 ml distilled water, mixed thoroughly and filtered through Whatman filter paper No. 1 and stored in dark coloured bottle at room temperature.

Destaining solution: Prepared by mixing 400 ml Methanol, 100 ml glacial acetic acid and 500 ml of distilled water and stored at room temperature.

Preparation of polyacrylamide gel:

Non-denaturing PAGE gel (10 %): Non-denaturing PAGE gel (10 %) was prepared by mixing 1.5 M Tris-HCl pH-8.8 (2.5 ml), 30 % acrylamide solution (3.33 ml), 10 % APS (0.1 ml), water (4.07 ml) and 4 µl of TEMED. TEMED was added in last, just before pouring. Gel was kept at room temperature till polymerization. Prior to use, wells were washed thoroughly with 1 X Tris-Glycine buffer and pre-run for 30 min.

Denaturing PAGE (SDS-PAGE) gel: It has two component system: Resolving and Stacking gel. Resolving gel (12 %, 10 ml) was prepared by mixing 1.5 M Tris-Cl pH 8.8 (2.5 ml), 30 % acrylamide solution (4 .0 ml), 10 % APS (0.1 ml), 10 % SDS (0.1 ml), water (3.3 ml) and 4 TEMED (4 µl). Stacking gel (4%, 4 ml) was prepared by mixing 1 M Tris-Cl pH 6.8 (0.5 ml), 30 % Acrylamide solution (0.68 ml), 10 % APS (0.04 ml), 10 % SDS (0.04 ml), water (2.72 ml) and TEMED (4 µl). TEMED was added just before pouring the gel. Resolving gel was poured between the plates followed by overlaying of isopropanol (0.2 ml) and allowed to polymerize. After polymerization, isopropanol layer was removed, stacking gel was poured and kept for polymerization. Before use wells were washed with 1 X Tris-Glycine-SDS buffer.

2.1.17.2. Reagents for agarose gel electrophoresis

5 X Tris-Borate EDTA (5X TBE) buffer: 5 X stock solution of TBE buffer was prepared by dissolving 54.0 g of Trizma base, 27.5 g of Boric acid in water and mixing 20 ml of EDTA (0.5 M, pH 8.0) solution to a final volume of 1 L and sterilized by autoclaving. Working buffer solution (1X TBE buffer) was prepared by five-fold dilution of 5 X TBE buffer stock in water and used for preparation of agarose gels and as electrophoresis buffer.

6 X sample loading buffer: The sample loading dye was prepared by mixing the

components to the final concentrations; Bromophenol blue dye (0.25 % w/v), Xylene Cyanol FF dye (0.25 % w/v) and 30 % (v/v) Glycerol and stored at 4 °C.

Ethidium bromide (EtBr) staining solution: EtBr stock solution (10 mg ml^{-1}) was prepared by dissolving 0.1 g EtBr in 10 ml water with gentle stirring. The container was wrapped in aluminum foil and stored at room temperature. Working staining solution (0.5 µg ml^{-1}) was prepared by adding 10 µl of EtBr stock solution into 200 ml of water.

All electrophoresis reagents for RNA work were prepared and diluted in autoclaved DEPC treated water.

Preparation of agarose gel:

Agarose gel (1-2 %) was prepared by adding appropriate amount of agarose in 40 ml of 1 X TBE buffer, heated in micro-oven with gentle stirring, poured on gel-casting tray and allowed to solidify. Wells were flushed with electrophoresis buffer prior to use.

2.1.18. Reagents for biochemical analysis

Acetate buffer:

Solution A; (0.2 M Sodium acetate; CH_3COONa): Dissolved 2.72 g of Sodium acetate trihydrate ($CH_3COONa.3H_2O$) in 100 ml of water.

Solution B;(0.2 M acetic acid; CH_3COOH): Prepared 100 ml of 0.2 M glacial acetic acid solution by diluting 1.15 ml of the stock (17.4 M) in water.

0.2 M acetic acid buffer solution (50 ml) for pH 4.0 and 5.0 was prepared by mixing solution A and B as below mentioned.

For pH 4.0 (Solution A; 9 ml and solution B; 41 ml), for pH 5.0 (solution A; 35 ml and solution B; 15 ml) was mixed.

Sodium phosphate buffer:

Solution A; (1 M Sodium phosphate dibasic; Na_2HPO_4): Dissolved 14.2 g of Na_2HPO_4 in 100 ml of water.

Solution B; (1 M Sodium phosphate monobasic monohydrate; $NaH_2PO_4.H_2O$): Dissolved 13.8 g of $NaH_2PO_4.H_2O$ in 100 ml of water.

0.2 M Sodium phosphate buffer solution (50 ml) for pH (6.0-8.0) was prepared by mixing different proportion of solution A and B as below mentioned.

For pH 6.0 (solution A; 1.2 ml and solution B; 8.8 ml), pH 7.0 (solution A; 5.77 ml and solution B; 4.23 ml), pH 7.8 (solution A; 8.96 ml and solution B; 1.04 ml) and pH 8.0 (solution A; 9.32 ml and solution B; 0.68 ml) and made up the volume to 50 ml with water.

Potassium phosphate buffer:

Solution A; (1 M Potassium phosphate dibasic; K_2HPO_4): Dissolved 17.42 g of K_2HPO_4 in 100 ml of water.

Solution B; (1 M Potassium phosphate monobasic; KH_2PO_4): Dissolved 13.6 g of KH_2PO_4 in 100 ml of water.

0.2 M Potassium phosphate buffer solution (50 ml) for pH (6.0-8.0) was prepared by mixing different proportions of solution A and B as below mentioned.

For pH 6.0 (solution A; 1.32 ml and solution B; 8.68 ml), pH 7.0 (solution A; 6.15 ml and solution B; 3.85 ml), pH 7.8 (solution A; 9.08 ml and solution B; 0.92 ml) and pH 8.0 (solution A; 9.40 ml and solution B; 0.60 ml) and made up the volume to 50 ml with water.

Bicarbonate buffer:

Solution A (0.2 M Sodium carbonate; Na_2CO_3): Dissolved 4.4 g Na_2CO_3 in 200 ml

water.

Solution B (0.2 M Sodium bicarbonate; $NaHCO_3$): Dissolved 3.36 g of $NaHCO_3$ in 200 ml of water.

0.2 M Sodium bicarbonate buffer solution (50 ml) for pH (9.2-10.8) was prepared by mixing different proportions of solution A and B as below mentioned.

For pH 9.2 (solution A; 5.0 ml and solution B; 45.0 ml), pH 10.0 (solution A; 30.0 ml and solution B; 20.0 ml), pH 10.5 (solution A; 40.0 ml and solution B; 10.0 ml) and pH 10.8 (solution A; 45.0 ml and solution B; 5.0 ml) was mixed.

Tris-HCl buffer:

1 M Tris-HCl; pH 7.0, 8.0 and 9.0 was prepared by dissolving 12.11 g of Trizma base in water, pH was adjusted to respective pH 7.0, 8.0 and 9.0 with 4 M HCl and made up the volume to 100 ml with water.

0.5 M Ethylenediaminetetraacetic acid (EDTA) pH 8.0: Disodium salt of EDTA (18.6 g) was added to 80 ml of water and vigorously stirred. The pH of solution was adjusted to 8.0 with 4 M NaOH solution and volume made to 100 ml with water and was sterilized by autoclaving.

4 M NaCl: Dissolved 23.4 g of NaCl in 100 ml of water.

4 M Imidazole: Dissolved 27.23 g of imidazole in 100 ml of water.

0.1 M Maltose: Maltose stock solution (0.1 M) was prepared by dissolving 1.71 g of maltose in 50 ml of water.

0.2 M Phenylmethylsulfonyl fluoride (PMSF): Dissolved 0.348 g of PMSF in 10 ml of absolute ethanol and stored at 4 °C.

2.1.19. Reagents for SOD activity assay

0.2 M phosphate buffer, pH 7.8

10 mM EDTA: Diluted 0.1 ml of 0.5 M EDTA solution in 4.9 ml water.

7.8 mM Nicotinamide adenine dinucleotide reduced (NADH): NADH disodium salt (11.06 mg) was dissolved in 2 ml water.

5 mM Nitro Blue Tetrazolium (NBT): 5 mM solution was prepared by dissolving 8.16 mg NBT in a final volume of 2 ml water.

16.5 mM Phenazine methosulphate (PMS): PMS stock solution (16.5 mM) was prepared by dissolving 10.1 mg of PMS in 2 ml of water. Stock solution was diluted to prepare PMS working stock solution (8.25 µM). PMS stock was prepared fresh every time before use.

SOD assay mix: Stock reagents were mixed to prepare SOD assay mix (50 mM Buffer, 0.1 mM EDTA, 78 µM NADH, 50 µM NBT).

0.1 M Hydrogen peroxide (H_2O_2) solution: H_2O_2 stock concentration was estimated spectrophotometrically at absorbance ($A_{240\ nm}$) and using molar extinction coefficient of 43.6 M^{-1} cm^{-1}. H_2O_2 stock was diluted accordingly to prepare 0.1 M H_2O_2 working stock solution.

0.1 M sodium azide (NaN_3): Dissolved 13 mg of sodium azide in 2 ml of water.

0.1 M Diethyldithiocarbamate (DDC): Dissolved 17.13 mg of DDC in 1 ml of water.

2.1.20. Reagents for peroxidase activity assay

0.1 M Diethylene triamine pentaacetic acid (DTPA): Dissolved 39.34 mg of DTPA in 1 ml of water.

10 mM 2', 7' dichlorodihydrofluroscein- diacetate (DCFH-DA): DCFH-DA (4.87 mg) was dissolved in 1 ml of methanol.

5 mM 2', 7' dichlorodihydrofluroscein (DCFH): DCFH (5 mM) was prepared by hydrolyzing 0.2 ml of 10 mM DCFH-DA with 0.2 ml of 10 mM NaOH for 30 min in

dark at room temperature and kept in ice during the experiment.

2.1.21. Reagents for lipid peroxidation assay

1 X Phosphate buffer saline (PBS): Dissolved 0.144 g Na_2HPO_4, 24.0 mg of KH_2PO_4, 20.0 mg KCl and 0.8 g NaCl in 100 ml of water.

1 % 2-Thiobarbituric acid (TBA): TBA, 1 % (w/v) was prepared by dissolving 0.1 g of TBA in 10 ml of water.

2.5 M HCl: Concentrated HCl (11.5 M) was diluted to prepare working stock (2.5 M).

30 % Trichloroacetic acid (TCA): Dissolved 3.0 g TCA in 10 ml of water.

Thiobarbituric acid (TBA) reagent: TBA reagent was prepared by mixing the stocks to final concentration: 0.375% TBA, 0.25 M HCl, 15% TCA and 6 mM EDTA.

1, 1, 3, 3-Tetramethoxypropane (TMP): TMP used as MDA equivalent standard (0-10 µM) and prepared by diluting the TMP in water.

2.1.22. Reagents for Polymerase Chain Reaction (PCR)

dNTP solution (10 mM): The 100 mM dNTPs stock solutions of each of the four deoxynucleotide triphosphates (dATP, dGTP, dCTP and dTTP) were mixed, diluted to 10 mM using autoclaved MilliQ water, and stored at -20 °C.

Oligonucleotide primers: Oligonucleotide primers were designed and custom synthesized.

Primer designing: OsCSDs DNA sequences were retrieved from Rice genome annotation project (RGAP-MSU) database for designing primers for cDNA amplification and cloning for heterologous expression in *E. coli*. While for quantitative RT-PCR (qRT-PCR) analysis primers already available in the laboratory were used.

2.1.22.1. Oligonucleotide primers for qRT-PCR analysis

Spliced variants specific primers used for qRT-PCR analysis are listed in **Table 2.4**.

Table 2.4: List of gene specific and splice variant specific qRT-PCR primers.

List of gene specific qRT-PCR primers				
Locus/ Gene name	**Primer Name**	**Primer sequence (5′-3′)**	**Length (nt)**	**% GC**
LOC_Os03g22810 (OsCSD1)	OsCSD1-TS-F	GCATGTCAACTGGGCCACACTACA	24	54.17
	OsCSD1-TS-R	CATGGATATTAGCAACACCATCTTC	25	40
LOC_Os08g44770 (OsCSD2)	OsCSD2-TS-F	TGGGTGCATATCAACAGGACCACA	24	50
	OsCSD2-TS-R	GGTTGCCTCAGCTACACCTTCAGC	24	58.33
LOC_Os03g11960 (OsCSD3)	OsCSD3-TS-F	CAACGGCTGCAACTCTACCGGGCC	24	66.67
	OsCSD3-TS-R	GGTCCTTTATGAAGATATCTGCAACAC	27	40.74
LOC_Os07g46990 (OsCSD4)	OsCSD3-TS-F	CATGTCAACTGGACCACACTTCAA	24	45.83
	OsCSD3-TS-R	ATTGACATTAGCAACACCATCTGC	24	41.67
List of splice variant specific qRT-PCR primers				
LOC_Os03g22810 (OsCSD1)	OsCSD1-F	GCATGTCAACTGGGCCACACTACA	24	54.2
	OsCSD1-R	CATGGATATTAGCAACACCATCTTC	25	40.0
LOC_Os08g44770 (OsCSD2)	OsCSD2-Com-F	AAGAAGGCCGTCGCCGTGCTCA	22	63.6
	OsCSD2-SV1-R	CACGGACATTCACTGTTGTAGGAC	24	50.0

	OsCSD2-SV2-R	GTCCCGTCACACGGACATTCACTT	24	54.2
LOC_Os03g11960 (OsCSD3)	OsCSD3-SV1-F	GTAGCCAACAAAGATGGTGTTGC	23	47.8
	OsCSD3-SV1/3-R	TGTTTTACTGAGTTCATGACCACC	24	41.7
	OsCSD3-SV2-F	GATGACCTAGGAAGGGCTATGGT	23	52.2
	OsCSD3-SV2-R	AGTTCATGACCACCTGTCTTATGA	24	41.7
	OsCSD3-SV3-F	TGCAACTCTACCGGTGTTGCAG	22	54.5
	OsCSD3-SV4-F	ACGGCTGCAACTCTACCGGGCC	22	68.2
	OsCSD3-SV4-R	ATATTTTACATATTTCAAGACAATGGA	27	22.2
LOC_Os07g46990 (OsCSD4)	OsCSD4-SV1-F	CATGTCAACTGGACCACACTTCAA	24	45.8
	OsCSD4-SV1-R	ATTGACATTAGCAACACCATCTGC	24	41.7
	OsCSD4-SV2-F	CCTTCTGGAGTCTTCCTCATCAGAA	25	48
	OsCSD4-SV2-R	AGCAACAGCCTTCACCATCTCA	22	58.29
LOC_Os10g36650 (Actin-2)	Actin-2-F	CTAGTGGACGTACTACTGGTATTG	24	45.8
	Actin-2-R	GATCCCTACCAGCAAGATCAAGAC	24	50.0
LOC_Os08g03290 (GAPDH)	GAPDH-F	GTGACAGCAGGTCGAGCATCTTCG	24	58.3
	GAPDH-R	GTCGATGACACGGTTGCTGTAACC	24	54.2

F- Forward primer, R- Reverse primer, Com- Common primer, nt- nucleotide

2.1.21.2. Oligonucleotide primers for cloning

Primers were designed to amplify the full-length OsCSDs-cDNA for cloning, expression and characterization of proteins encoded by constitutive and alternative splice variants. Restriction digestion pattern of the CDS were analyzed using NEB cutter tool (http://nc2.neb.com/NEBcutter2/). Few restriction enzymes were found suitable for cloning, of which NdeI site was incorporated in the sequence of forward primers and EcoRI site was introduced in the reverse primers.

For cloning OsCSDs-cDNA at multiple cloning sites (MCS) of pET28a(+) and pMAL-c5x plasmid expression vectors NdeI and EcoRI restriction sites were used and for cloning into pTwin1 expression vector EcoRI restriction sites in both forward and reverse primers were used. Few non-specific bases were also added prior to restriction sites for efficient digestion.

Details of primers used for OsCSDs amplification are given in **Table 2.5**. Restriction enzyme sites NdeI and EcoRI were underlined and italicized respectively in the primer sequence.

Table 2.5: List of primers used for cloning of OsCSDs and splice variants

Gene Name	**Primer Name**	**Primer sequence (5′- 3′)**	**Length (nt)**	**% GC**
OsCSD1	OsCSD1-F	ATCGGGATCCCCATATGGTGAAG GCTGTTGTTGTGCTTGGTAGCAG	46	52.2
	OSCSD1-R	CG*GAATTC*TCAGCCTTGAAGTCC GATGATC	30	50.0
OsCSD2	OsCSD2-SV1-F	CGGCAGCCATATGGCCGACGCC ACCAAGAAGGCCGTC	37	67.6
	OsCSD2-SV2-F	CGATCGGGATCCCCATATGGCCG ACGCCACCAAGAAGGCCGTCGC CGTGCTCAAGGGCACCTCCCAGG	136	61.8

		TTGAGGGAGTCGTCACCCTCACC CAGGATGACCAAGTGAATGTCC GTGTGACGGGACTTACTCCTGGA		
	OsCSD2-Com-R	CG*GAATTC*CTACAACGGGGTCAG CCCAAC	29	58.6
OsCSD3	OsCSD3-Com-F	GG*GAATTC*CATATGATGGCAGGG AAAGCCGGCGGCC	36	61.1
	OsCSD3-SV1/3-R	CG*GAATTC*TTAAACTGCAGATCG AAGTCCAATGATAC	37	40.5
	OsCSD3-SV2-R	CG*GAATTC*CTAGTAGTTACACTC AAGGTTGAAGAGC	36	44.4
	OsCSD3-SV-3a-F	GTGTTGCAGATATCTTCATAAAG GACCTACAG	32	40.6
	OsCSD3-SV-3b-R	CGGTAGAGTTGCAGCCGTTGGTG GTGTC	28	60.7
	OsCSD3-SV4-R	CG*GAATTC*TCAAGACAATGGAAC	23	43.5
	OsCSD3-SV4a-R	TCA*GAATTC*TCAAGACAATGGAA CCTGTAGGTCCTTTATGAAG	43	39.5
OsCSD4	OsCSD4-F	GG*GAATTC*CATATGATGGTGAAG GCTGTTGCTGTGC	36	50
	OsCSD4-R	CG*GAATTC*CTAACCCTGGAGTCC GATG	27	55.6

F-Forward, R- Reverse, Com-Common

2.1.22.3. Oligonucleotide primers for OsCSD1 exon mapping

Exon-specific primers were designed for mapping of OsCSD1 cDNA region was mentioned in **Table 2.6**.

Table 2.6: List of OsCSD1 exon specific primers

Primer name	Primer sequence (5′-3′)	Length (nt)	% GC
$E1_F$	ATGGTTCAGGTCATCAGTGATGAGC	25	48
$E2_F$	AACACGGGGCAAAGGAGGATATATC	25	48
$E2a_R$	CTTGGCGCTAGATCCGGTGTCCA	23	60.9
$E2_R$	CTTGCGCCCAAGGTCACGGACTGC	24	66.7
$E3a_F$	GGCCCTCAATGTTGGCTGGTG	21	61.9
$E3_R$	CTCAGGCGACCCCCGCGGCGACG	23	82.6
$E4_F$	ATCACATTAACAATGGTGAAGGCTG	25	40
$E10_R$	TCAGCCTTGAAGTCCGATGATC	22	50
$E3b_F$	GGTGGCTGCAACTGCAAGCTGCCA	24	63
$E3c_F$	CTGCCAGTTTGACTACAAATACCACCGCA	29	48
$E3d_F$	ACCGCACACCGCTGGAGGGAGGGGAACCTTC	31	68
$E3e_F$	CCTTCCAGAAGCTCCAGATTCCAAACCAG	29	52
$E3f_F$	ACCAGCAGGAGTCGCCTCGCCTCCTC	26	69
$E3g_F$	CTCCTCCTTCATCCTCCTCGTCGTC	25	60
$E3h_F$	TCGTCGCCGCGGGGGTCGCCTGAG	24	79

Tris-EDTA (TE) buffer: Tris-EDTA buffer (Tris-HCl: 10 mM, EDTA; 1 mM, pH 8.0) was prepared, autoclaved and used for dissolving lyophilized primers (100 pmol μl^{-1}) and stored at −20 °C. The working concentration of primers (10 pmol μl^{-1}) was prepared by diluting in nuclease free water.

2.1.23. Miscellaneous reagents

100 X SYPRO orange: SYPRO orange (100 X) was prepared from 50-fold dilution of SYPRO orange stock (5,000 X) in MilliQ water and final concentration (5 X) was

used for Differential Scanning Fluorimetry (DSF) analysis of protein.

Methyl viologen (MV): MV (0.1 M) was prepared by dissolving 25.7 mg of methyl viologen dichloride hydrate in 1 ml of water.

0.85 % Saline: Dissolved 1.7 g NaCl in 200 ml of distilled water and autoclaved.

2.1.24. Offline and online computational tools

a) Rice Genome Annotation Project database at Michigan State University (RGAP-MSU) (http://rice.plantbiology.msu.edu/)
b) Rice Annotation Project Database (RAP-DB) (https://rapdb.dna.affrc.go.jp/)
c) Rice Expression Database (RED) (http://expression.ic4r.org/)
d) The Arabidopsis Information Resource (TAIR) (https://www.arabidopsis.org/)
e) Conserved domain database of NCBI (http://www.ncbi.nlm.nih.gov/structure/cdd/wrpsb.cgi)
f) NCBI website (http://www.ncbi.nlm.nih.gov)
g) Primer BLAST (http://www.ncbi.nlm.nih.gov/tools/primer-blast/)
h) ChloroP (http://www.cbs.dtu.dk/services/chloroP/)
i) ExPASy Compute pI/Mw tool (https://web.expasy.org/compute_pi/)
j) NEB cutter (http://nc2.neb.com/NEBcutter2/)
k) Clustal X [250]
l) BioEdit [251]
m) MEGA 4.0 [252]
n) Plaza monocot and dicot resource (https://bioinformatics.psb.ugent.be/plaza/)
o) PlantPAN 3.0 (http://plantpan.itps.ncku.edu.tw/)
p) PlantCARE (http://bioinformatics.psb.ugent.be/webtools/plantcare/html/)
q) SWISS-MODEL work space (http://swissmodel.expasy.org/workspace)

r) PyMOL (https://pymol.org/2/)

s) IBS tool [253]

t) Chou and Fasman Secondary Structure Prediction server (CFSSP) (http://www.biogem.org/tool/chou-fasman/index.php)

2.1.25. List of common instruments

Plant Growth Chamber (Sanyo, Japan), Thermal cycler (Eppendorf, Germany), Real time PCR instrument (Roche Diagnostics, Germany), Centrifuge (Hermle, Germany), Shaker incubator (Orbitek, India), Circular Dichroism Polarimeter (JASCO 815, USA), Gel-Documentation system (Syngene, England), Spectrophotometer (Shimadzu, Japan), Multi-well plate reader (Tecan, UK), Electroporator (Eppendorf, Germany), AKTA Start protein purification instrument (GE Healthcare, USA), FPLC-chromatography system (Bio-Rad, USA) and cell sonicator (Branson, CT, USA) were used for various experiments**.**

2.2. Methods

2.2.1. Rice seedling growth conditions and abiotic stress treatment

Rice genotype NSICRc106 seeds were surface sterilized by 0.1 % $HgCl_2$ solution for 10 min and rinsed several times with distilled water. Seeds were imbibed in distilled water for 1 day and kept for germination in sterile moist filter paper in dark for 2 days. Two-day after germination, (plumule length: ~1 cm) seedlings were transferred to perforated 96-well plates and grown hydroponically in Hoagland media in plant growth chamber (Sanyo, Japan). The following chamber conditions for growth of seedlings were used: 14 h light/ 10 h dark, light intensity: 150 µmol m^{-2} s^{-1} (photon flux density), temperature: 28 ± 1 °C (light period) and 26 ± 1 °C (dark period)

and humidity: 65 %. For stress treatment, the six-day old rice seedlings were subjected to salt stress (150 mM NaCl), drought (15 % PEG), and oxidative stress (10 µM MV). Shoot tissues were collected at different time-points from control and stressed seedlings. Some 15-day olds seedlings were also transferred to pots and grown under field conditions and used for collection of rice tissues viz. mature leaf, panicle, stem and flag leaf. Tissues collected were immediately frozen in liquid nitrogen, and stored at − 70°C until further use.

2.2.2. Transcription inhibitor treatment

Rice shoot tissues were treated with transcription inhibitor (α- amanitin) as per [254], with minor modifications. Six-days old rice shoot tissues were cut into small pieces (approx. 0.5 cm in length), transferred to transcription inhibitor solution containing α- amanitin (0.1 mg ml^{-1}) and vacuum infiltrated for 5 min, thrice. Samples were collected at different time-points and stored at − 70°C until further use.

2.2.3. Electrophoresis of nucleic acids and proteins

2.2.3.1. Separation of nucleic acids

Nucleic acids (DNA and RNA) samples were mixed with 6 X sample loading buffer and loaded on agarose gel along with appropriate molecular size markers. Samples were resolved electrophoretically on agarose gel (0.8- 2.0 %) in 1 X TBE running buffer at 80-100 V. Gel was stained in ethidium bromide solution and photographed on gel documentation system.

2.2.3.2. Separation of proteins

For non-denaturing/native PAGE, protein samples were mixed with 2 X native sample buffer. Tris-Glycine buffer (1 X) was used as electrophoresis buffer. Protein samples were loaded on 10 % PAGE gel and electrophoresed at 100-120 V at 4 °C.

Gel was activity stained (Zymogram analysis)/ CBB stained for visualization of proteins.

For denaturing PAGE (SDS-PAGE), 1 X Tris-Glycine-SDS buffer was used as electrophoresis buffer. Protein samples were mixed with 4 X Laemmli sample buffer. The samples were heated in boiling water bath for 10 min and subjected to centrifugation at 13680 x g for 10 min. Samples (along with protein standard molecular markers) were resolved by electrophoresis. The gels were stained with CBB-staining solution for 10-15 min and washed with destaining solution for 15 min, twice. Gel was photographed on gel documentation system.

2.2.4. Plant total RNA isolation

Total RNA from rice tissues was isolated using TRIzol method. Tissue samples were fine grounded with liquid N_2 in mortar and pestle. TRIzol (1 ml) was added to ~100 mg of tissue, mixed and incubated at room temperature for 5 min. Samples were mixed with 0.2 ml of chloroform and incubated at room temperature for 15 min followed by centrifugation at 13680 x g for 15 min at 4 °C. Aqueous phase was collected, mixed with 0.5 ml isopropanol. Sample was incubated for 10 min at room temperature and centrifuged at 13680 x g for 10 min at 4 °C. The pellet obtained was washed with 1 ml 70 % ethanol. Pellet was air dried, dissolved in 0.1 ml RNase free water and stored at −70 °C until further use. RNA integrity was accessed by electrophoresis on 1 % agarose gel. RNA samples were resolved by electrophoresis at 80 V, EtBr stained and photographed on gel documentation system. RNA was quantified by spectrophotometrically as mentioned in **Section 2.2.7**.

2.2.5. DNase I treatment

Total RNA (10 µg) in a volume of 20 µl with reaction mixture consists of 1.0

µl of 25 mM $MgCl_2$, 10 U DNase I (RNase free) and nuclease free water was incubated at 37 °C for 1 h. The DNase activity was terminated by addition of 2.5 mM EDTA (1.0 µl) followed by incubation at 70 °C for 20 min.

2.2.6. First-strand cDNA synthesis

RNA was reverse transcribed into complementary DNA strand (cDNA) by reverse transcriptase (RT) enzyme. First-strand cDNA was synthesized using SuperScript II (SS II) RT, random nonamers (N_9) and anchored oligo$(dT)_{23}$ primer. DNase I treated RNA (5µg) was incubated at 70 °C for 5 min and snap-chilled on ice for 5 min. A reaction mix (20 µl), consists of with/without 10 U μl^{-1} SuperScript II RT, 1 X first-strand buffer, 10 mM DTT, 0.5 mM dNTPs, 25 ng μl^{-1} anchored oligo$(dT)_{23}$ and 12.5 ng μl^{-1} random primers was set up. The following program used for cDNA synthesis: annealing at 25 °C (10 min); extension at 42 °C (60 min) and inactivation at 70 °C (15 min). Samples were stored at −20 °C until further use. Reaction without RT served as minus (−)RT control. Synthesized cDNA was quantified spectrophotometrically as described in **Section 2.2.7**.

2.2.7. Estimation of nucleic acids

Spectrophotometric estimation of RNA and DNA

Quantification of DNA and RNA samples was carried out spectrophotometrically by measuring the optical density (OD) at absorbance ($A_{260\ nm}$) and using the following standard calculations:

1 OD at $A_{260\ nm}$ for RNA = 40 µg ml^{-1}

1 OD at $A_{260\ nm}$ for single strand DNA (ssDNA) = 33 µg ml^{-1}

1 OD at $A_{260\ nm}$ for double strand DNA (dsDNA) = 50 µg ml^{-1}

2.2.8. Quantitative Reverse Transcription-Polymerase Chain Reaction (qRT-PCR)

Quantitative RT-PCR (qRT-PCR) is very sensitive and high-throughput technique for detection, quantification and analysis of gene expression under different conditions. OsCSD splice variants in different rice tissues and treatment conditions were analyzed by qRT-PCR using specific primers listed in **Table 2.4**. Assay conditions were optimized for annealing temperature, amount of template, primer etc. using SYBR-Green JumpStart *Taq* ready mix and qRT-PCR primers on a Real-time PCR machine. Specificity of the reaction was assessed by melt curve analysis of the reaction products as well as analyzing the sample on 2 % agarose gel.

The assay mix contained cDNA (10- 50 ng μl^{-1}), primers (FP and RP; 0.5 pmol μl^{-1} each), 1 X SYBR-Green jumpstart *Taq* ready mix, total volume of the reaction adjusted to 10 µl with DNase free water. The RT-PCR program used with following settings: initial denaturation; 95 °C- 2 min, 45 repetition of cycling step (95 °C- 15 sec; 65 °C-20 sec; 68 °C-25 sec) followed by melting-curve analysis using a linear temperature ramp from 60 °C- 94 °C in 20 min. Rice Actin-2 was used as reference gene and validation was also done using a second reference gene, Glyceraldehyde 3-phosphate dehydrogenase (GAPDH). No template control (NTC) and minus RT control (-RT control) were also included, and data analysis was carried out using delta-delta Ct [$2^{(-\Delta\Delta Ct)}$] method [255]. All PCR samples were run in triplicates and with two biological replicates.

2.2.9. *E. coli* competent cells preparation

2.2.9.1. Electrocompetent cells

E. coli strain Top10 was streaked on LBA and incubated at 37 °C for 16 h. A

single isolated colony was inoculated in LB media and grown at 37 °C, 150 rpm for 16 h. Culture was 100-fold diluted (1 ml in 100 ml) in fresh LB media and grown up to absorbance ($A_{600\ nm}$) of 0.4-0.6. Cells were harvested by centrifugation at 4430 x g for 10 min at 4 °C. Cell pellet was gently resuspended in 50 ml of sterile ice-chilled MilliQ water followed by centrifugation at 4430 x g for 10 min at 4 °C. This washing step was repeated twice and finally the cells were resuspended in 1 ml of 10 % glycerol. Cells were aliquoted (50µl); snap-freezed in liquid N_2 and stored at −70 °C till further use.

2.2.9.2. Chemical competent cells

E. coli expression host strain BL-21 (DE3) was streaked onto LBA plate and grown at 37 °C. A single isolated colony was inoculated in LB-media and grown for 16 h at 37 °C. Culture was 100-fold diluted in 100 ml (1 ml in 100 ml) of LB media and grown at 37 °C till absorbance (A_{600nm}) reached to ~0.4. Culture was kept on ice for 30 min and cells were harvested by centrifugation at 1970 x g for 10 min at 4 °C. Cell pellet was gently resuspended in 25 ml sterile ice-chilled 0.1 M $CaCl_2$ and kept again on ice (15 min). This step was repeated twice with gradually decreasing the volume of $CaCl_2$. Finally, cell pellet was resuspended in 0.5 ml of 0.1 M $CaCl_2$ with 10 % glycerol and aliquoted (50 µl). Cells were snap-freezed with liquid N_2 and stored at − 70 °C till further use.

Competent cells of other *E. coli* strains (SHuffle, Top 10, BW25113) were also prepared in a similar manner using recommended growth conditions mentioned in **Section 2.1.3**.

2.2.10. Plasmid DNA isolation

Top 10 *E. coli* cells carrying plasmid of interest e.g. pET28a (+) was cultured

in 4 ml of LB media containing kanamycin (LB-Kan$^+$) and grown at 37 °C for 16 h at 150 rpm. Cells were harvested by centrifugation at 4430 x g for 10 min at 4 °C. Plasmid DNA was isolated using High Pure Plasmid isolation kit. Cell pellet was resuspended in 250 µl of resuspension buffer followed by gently mixing in 250 µl of lysis buffer and incubated for 5 min at room temperature. Chilled binding buffer (350 µl) was added to the sample, gently mixed and incubated for 10 min on ice, followed by centrifugation at 13680 x g for 10 min at room temperature. Supernatant was transferred to filter column and centrifuged at 13680 x g for 1 min and flow through was discarded. Column was washed with 500 µl of washing buffer I, subsequently washed with 700 µl of washing buffer II and flow through was discarded. Column was centrifuged for additional 1 min and placed on to a fresh 1.5 ml microfuge tube. Plasmid DNA was eluted from column with addition of 100 µl MilliQ water by centrifugation. Plasmid DNA was analyzed on 1 % Agarose gel.

2.2.11. Purification of DNA

PCR amplified, restriction digested and DNA products of ligation reaction were purified by High Pure PCR product purification kit. DNA products (100 µl) were mixed with 500 µl of binding buffer, loaded on filter column and centrifuged at 13680 x g for 1 min, flow through was discarded. Subsequently, filter column was washed twice with 500 µl and 200 µl of wash buffer. Filter column was placed onto fresh 1.5 ml microfuge tube, MilliQ water (50 µl) was added. DNA was eluted from column by centrifugation. Purified DNA was analyzed on 1-2 % agarose gel.

2.2.12. Isolation and cloning of rice CSDs (OsCSDs) and splice variants

2.2.12.1. Isolation of cDNA of OsCSD splice variants and genomic DNA fragments

OsCSD splice variant (SV) sequences were PCR amplified from cDNA of rice genotype NSICRc106 using *Pwo* DNA polymerase and specific primers listed in **Table 2.5 and 2.6**. PCR reaction (volume: 50 µl) contained following components: cDNA (100-200 ng), primers (FP and RP, 0.5 pm μl^{-1}), dNTPs (0.4 mM), $MgSO_4$ (2 mM), 1 X *Pwo* DNA polymerase buffer, *Pwo* DNA polymerase (2.5 U) in a reaction volume of 50 µl. PCR program used was as follows: 95 °C- 5 min, 35 cycles of 95 °C- 1 min; 65 °C- 1-5 min (based on the amplicon length); 72 °C- 1.5 min and 72 °C- 5 min.

2.2.12.2. Inverse Polymerase Chain Reaction (Inverse PCR)

Inverse PCR was performed to generate pET28a-OsCSD3-SV3 (lacking exon3) from pET28a-OsCSD3-SV1 as template DNA and *Pwo* DNA polymerase (**Fig. 2.1**). Primers, OsCSD3-SV3a-F and OsCSD3-SV3b-R were used for inverse PCR assay. PCR reaction (volume: 50 µl) contained plasmid DNA (pET28a-OsCSD3-SV1; 0.1 ng μl^{-1}), primers (FP and RP, 0.5 pm μl^{-1}), dNTPs (0.4mM) $MgSO_4$ (2 mM), 1 X *Pwo* DNA polymerase buffer, and *Pwo* DNA polymerase (2.5 U). PCR program settings: 95 °C- 5 min, 35 cycles of 95 °C- 1 min; 60 °C- 1 min; 72 °C- 6 min and 72 °C- 10 min. Amplified PCR product was analyzed on 1 % agarose gel with λ DNA-HindIII digest as DNA size standard. The PCR amplified pET28-OsCSD3-SV3 linear plasmid was purified as described in **Section 2.2.11** and subsequently, phosphorylated at 5′-end by T4 polynucleotide kinase and ligated as detailed in **Section 2.2.12.4** and **2.2.12.5**.

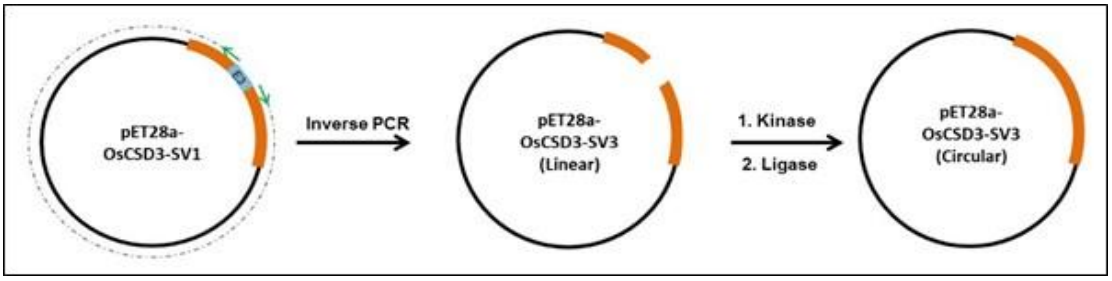

Fig. 2.1. Schematic representation of Inverse PCR strategy for pET28a-OsCSD3-SV3 generation. Recombinant plasmid pET28a-OsCSD3-SV3 was generated by inverse PCR using pET28a-OsCSD3-SV1 plasmid as template. Blue box highlights the Exon 3 (E3) of the cloned OsCSD3-SV1 in pET28a (+) whereas green arrow indicates showed primer positions.

2.2.12.3. Restriction digestion

Required amount of appropriate plasmid DNA and purified PCR products of OsCSDs and splice variants were restriction digested with specified restriction enzymes (NdeI and EcoRI for cloning into pET28a (+)/ pMAL-c5x and with EcoRI for cloning into pTwin1) as per manufacturer's instruction. Reaction mix (50 µl) contained DNA (5.0 µg), 1 X Cut-Smart buffer and restriction enzymes; NdeI and EcoRI (20 U each) or only EcoRI (20 U). Samples were incubated at 37 °C for 16 h. Restriction digestion was confirmed on 1 % agarose gel along with λ DNA-HindIII digest as DNA marker. Restriction digested products were purified as mentioned in **Section 2.2.11**.

2.2.12.4. Phosphorylation of DNA

DNA was phosphorylated at 5′-termini using T4 polynucleotide kinase. The reaction mix (20 µl) containing DNA (0.2 µg), 1 X T4 polynucleotide buffer and T4

polynucleotide kinase (10 U), was incubated at 37 °C for 30 min followed by inactivation at 65 °C for 30 min.

2.2.12.5. Ligation

Ligation was performed using Rapid DNA ligation kit as per the recommended protocol. Restriction digested plasmid vector and insert DNA (OsCSD-cDNA) was quantified on spectrophotometer method as mentioned in **Section 2.2.7**. Vector and insert were taken in a molar ratio (1:5) and added to ligation mix consists of 1 X ligation buffer and T4 DNA ligase (2 U) in a total volume of 20 µl, and incubated at room temperature for 1 h. Ligation mix was purified as mentioned in **Section 2.2.11**.

2.2.13. Transformation of *E. coli*

2.2.13.1. Transformation by electroporation

Approximately, 20-50 ng (DNA equivalent) of purified ligation mix was added to Top10 *E. coli* electro-competent cells. The sample was transferred to an ice-chilled electroporation cuvette, placed in an electroporator and subjected to an electric pulse of field strength 18 kV cm^{-1} (time constant: 5.5-6.0 ms). After electroporation, 1 ml of LB- media was added to the cuvette and sample was transferred to a sterile tube. Sample was kept in shaker at 37 °C for 1 h. Transformants were selected on LBA-Kan^{+} plates incubated at 37 °C for 16 h.

2.2.13.2. Transformation by heat-shock

E. coli BL-21(DE3) competent cells were thawed on ice, plasmid DNA (5 ng) was added, gently mixed and incubated in ice for 10 min. Sample was given heat-shock (42 °C, 60 s) immediately shifted to ice and incubated for 15 min. LB- media (1 ml) was added in the sample and grown at 37 °C for 1 h. Cells were selected on LBA plates containing appropriate antibiotics as mentioned in **Table 2.2** and

incubated at 37 °C for 16 h. Similarly, other *E. coli* strains were transformed with plasmid DNA and grown at optimal growth conditions and selected on appropriate antibiotics as per **Section 2.1.3** and **Table 2.2**.

2.2.13.3. Characterization of positive recombinant clones

Transformants obtained were screened for presence of desired insert DNA by colony PCR and restriction analysis of the plasmids. Colony PCR was carried out using gene or splice variant specific/ vector specific primers or a combination of these. *E. coli* cells were directly added in the assay for template plasmid DNA in colony PCR, while all other reagents were same as detailed previously. The following colony PCR conditions were used: 95°C- 10 min, 35 cycles of (95 °C- 1 min, 60 °C- 45 s, 72 °C-1.5 min (35 cycles) and 72 °C- 5 min (final extension). Plasmids were isolated from PCR positive clones as described in **Section 2.2.10**. Isolated plasmids were verified by restriction digestion for presence of desired DNA fragment. DNA sequences of the restriction digestion positive clones were further confirmed by sequencing.

2.2.14. Heterologous expression of rice CSD proteins in *E. coli*

2.2.14.1. Overexpression of recombinant rice CSD proteins

Recombinant pET28a(+) plasmids containing OsCSD-cDNA inserts were transformed into *E. coli* BL-21(DE3) expression host as described in **Section 2.2.13.2**. Transformants were selected on LBA-Kan^+ plates and incubated at 37°C for 16 h. An isolated colony was inoculated into LB-Kan^+ and grown at 37 °C for 16 h. The culture was diluted 100-fold in fresh LB–Kan^+ media containing 0.2 mM $CuCl_2$ and $ZnCl_2$ and grown further at 37 °C till absorbance (A_{600nm}) reached to ~ 0.4. At this cell density, 0.1 mM IPTG was added and cells were grown further at 20 °C- 37 °C for 16

h. An aliquot of induced (+IPTG) culture was withdrawn and centrifuged at 4430 x g for 10 min at 4 °C. Cells from rest of the culture were harvested by centrifugation. Cell pellet was resuspended in resuspension buffer (20 mM Tris-HCl, 200 mM NaCl, 1 mM PMSF; pH 8.0) and lysed by sonication (total time: 5 min, Pulse On/Off: 2 s each and amplitude at 35 %, repeated twice and samples were kept in ice during the sonication). Cell lysate was centrifuged at 4430 × g for 15 min at 4 °C to remove cell debris, followed by another centrifugation at 13680 x g at 4 °C for 20 min to isolate soluble and insoluble fraction of cell lysate. Uninduced (-IPTG) culture used as expression control, was also processed in a similar manner. Total protein samples isolated from different fractions, were analyzed on denaturing PAGE as described in **Section 2.2.3.2**. Similarly, expression conditions of other OsCSD proteins were optimized for different *E. coli* strains.

2.2.14.2. Chaperone assisted folding of recombinant OsCSD proteins

Recombinant plasmids (pET28a-OsCSDs) were transformed in BL-21(DE3) carrying different chaperone plasmids (**Table 2.6**). Transformants were selected on LBA-$Kan^{+}Cm^{+}$ plate. A saturated culture of BL-21(DE3) cells containing both plasmids, were diluted 100-fold in LB-$Kan^{+}Cm^{+}$ containing 0.2 mM $CuCl_2$ and $ZnCl_2$ and induced with chaperone inducers (**Table 2.7**) for 1 h at 30 °C. Subsequently, 0.1 mM IPTG was added in the culture and grown further at 20 °C for 16 h for expression of recombinant OsCSD protein. Cells were harvested; lysed and soluble fraction of the cell lysate was isolated as mentioned in **Section 2.2.14.1**, and amount of protein in soluble fraction was analyzed on denaturing PAGE.

Table 2.7: List of chaperones and inducers

S. No.	Plasmid	Chaperone	Inducer	Inducer concentration
1.	pGro7	GroELS	L-Arabinose	0.2 mg ml $^{-1}$
2.	pG-Tf2	groEL-groES-tig	L-Arabinose	0.2 mg ml $^{-1}$
3.	pTf16	Tig	Tetracycline	10 ng ml $^{-1}$
4.	pKJE7	dnaK,dnaJ, grpE	L-Arabinose	0.2 mg ml $^{-1}$
5.	pG-KJE8	groEL-groES,dnaK-dnaJ-grpE	L-Arabinose, Tetracycline	0.2 mg ml $^{-1}$, 10 ng ml $^{-1}$

The details of the OsCSDs expression conditions attempted for are listed in **Table 2.8**.

2.2.14.3. Overexpression and purification of Histidine tagged OsCSDs

E. coli strains containing recombinant expression vectors e.g. pET28a-OsCSD or pMAL-His-OsCSD were induced at optimized expression conditions. Cells were harvested, resuspended in resuspension buffer containing 5 mM imidazole and lysed by sonication (total time: 15 min, Pulse On/Off: 2 s each and amplitude at 35 % and repeated twice, samples were kept in ice during the sonication). Soluble cell lysate was isolated and recombinant protein was loaded on to a Ni-NTA affinity column/matrices pre-equilibrated with resuspension buffer and kept for binding for 2 h at 4°C in tube rotator. Protein was purified using AKTA Start protein purification system. The column was washed thoroughly with resuspension buffer and bound protein was eluted using linear gradient of imidazole (5-200 mM) in the elution buffer A (resuspension buffer containing 200 mM imidazole). Eluted protein fraction was analyzed on denaturing PAGE.

Table 2.8: Expression conditions attempted for OsCSD and its splice variants

Protein	*E. coli* strain	Plasmid	Splice variant	IPTG (mM)	Temperature (°C)
OsCSD1	SHuffle T7 express	pET28a-OsCSD1	-	0.25	25
OsCSD4	SHuffle T7 express	pET28a-OsCSD4	-	0.25	25
OsCSD2	SHuffle Express	pMAL-HIS-OsCSD2	SV1	0.1-0.25	20, 25
			SV2	0.1-0.25	20, 25
OsCSD3	BL-21 (DE3)	pET28a-OsCSD3	SV1	0.1-1	20, 37
	SHuffle T7 Express			0.1-1	25
	BW25113 Δ*sodA* Δ*sodB*	pMAL-c5x-OsCSD3	SV1	0.5	25
	BL-21 (DE3)	pET28-OsCSD3	SV2, 3, 4	0.1-1	20
	SHuffle T7 Express				
	BL-21 (DE3)	pET28a-OsCSD3 + chaperone plasmid	SV2, 3, 4	0.1 mM IPTG + specific chaperone inducer	20
	SHuffle Express	pTwin1-OsCSD3	SV1, 2, 3, 4	0.1	20
	SHuffle Express	pMAL-c5x-OsCSD3	SV1, 2, 3, 4	0.1	25

2.2.14.4. Overexpression and purification of Intein tagged OsCSD proteins

Recombinant plasmid pTwin1 carrying OsCSDs were transformed in SHuffle

T7 Express *E. coli* strain and culture was induced at optimized conditions (0.1 mM IPTG at 20 °C for 16 h). Cells were harvested, pellet was resuspended in resuspension buffer and lysed by sonication as mentioned in **Section 2.2.14.3**. Soluble cell lysate was isolated and loaded on chitin column/matrices (pre-equilibrated with resuspension buffer) and kept for 2 h at 4° C on tube rotator for binding. Column was washed with resuspension buffer followed by gradient washing with wash buffer (20 mM Tris-HCl and 500 mM NaCl and 1 mM PMSF; pH 8.0). Protein was eluted by incubation of column in elution buffer B (20 mM Tris-HCl, 200 mM NaCl and 1 mM PMSF; pH 7.0) at 4 °C for 16 h, and fractions were collected and analyzed on denaturing PAGE.

2.2.14.5. Overexpression and purification of Maltose binding protein (MBP) tagged-OsCSDs

SHuffle Express cells containing pMAL-c5x-OsCSDs, was induced under optimized conditions (IPTG: 0.1 mM, temperature: 25 °C) for 16 h. Cell were harvested, resuspended in resuspension buffer and lysed by sonication as mentioned in **Section 2.2.14.3**. Soluble fraction was isolated and loaded on amylose column/matrices (pre-equilibrated with resuspension buffer) and incubated at 4 °C for 2 h on tube rotator for binding. Column was washed thoroughly with wash buffer (20 mM Tris-HCl and 500 mM NaCl, 1 mM PMSF, pH 8.0) and eluted with elution buffer C (resuspension buffer containing 10 mM Maltose).

2.2.15. Dialysis

Affinity-purified recombinant proteins were dialyzed against dialysis buffer (20 mM Tris-HCl, 200 mM NaCl; pH 8.0) using 12 kDa molecular weight cut-off (MWCO) dialysis membrane and concentrated using 10 kDa MWCO protein concentrator columns.

2.2.16. Estimation of protein concentration/amount

Protein concentration was determined calorimetrically by Bradford method [256] using Bradford reagent kit and also carried out by BCA method [257] using Pierce BCA protein estimation kit. Bovine Serum albumin (BSA) protein standards (0-1 mg ml^{-1}) were prepared. Reaction was performed in a multi-well plate (reaction volume: 200 µl) and absorbance was recorded on multi-well plate reader. For Bradford method-based protein estimation, plate was incubated for 15 min at 25 °C and absorbance (A_{595nm}) was measured. For BCA based protein estimation, multi-well plate was covered with aluminum foil and incubated at 37 °C for 30 min and absorbance (A_{560nm}) was measured.

2.2.17. Biophysical characterization of proteins

2.2.17.1. Gel filtration chromatography and molecular weight determination of proteins

Affinity purified, dialyzed and concentrated recombinant OsCSD protein samples were further subjected to gel-filtration chromatography using Superdex 75 10/300 GL chromatography column on FPLC system. Gel filtration column was pre-equilibrated with gel-filtration column buffer (20 mM Tris-HCl, 200 mM NaCl; pH 8.0). Purified protein was injected, absorbance (A_{230nm}) was monitored and fraction corresponding to peaks were collected and analyzed on denaturing PAGE. Gel filtration purified OsCSD proteins were used for further biochemical and biophysical characterization.

For native molecular weight determination of the proteins, gel-filtration chromatographic column was pre-calibrated with following standard proteins, BSA (66.5 kDa), chicken egg albumin (45 kDa), carbonic anhydrase (29 kDa), and

cytochrome C (12.4 kDa). The native molecular weight was estimated by plotting a calibration curve of the molecular weight of the standard proteins versus their respective V_e/V_o values (V_e: elution volume, V_o: void volume). Purified OsCSD proteins were injected in the column, absorbance ($A_{230\ nm}$) was monitored and absorbance peaks were collected. The eluted protein fractions were analyzed on denaturing PAGE and molecular weight of the monomeric subunit was determined.

2.2.17.2. Metal content analysis

Copper and zinc content of the protein was estimated on a VG PQExCell Inductively Coupled Plasma-Mass Spectrometer (ICP-MS) instrument. Recombinant protein (1 mg) was dialyzed against MilliQ water using 2 kDa MWCO dialysis tubing. The protein sample (in a silica crucible) was charred at 500 °C in a blast furnace and the inorganic ash was resuspended with 1% supra-pure nitric acid solution for ICP-MS analysis. The metal content was expressed as the number of Cu^{2+} and Zn^{2+} ions per protein subunit.

2.2.17.3. Spectrophotometric analysis of OsCSD

Spectrophotometric characteristics (UV and visible) of the rice OsCSD proteins were analyzed at room temperature (25 °C) on spectrophotometer. Absorbance spectra of protein (1 mg ml^{-1}) in potassium phosphate buffer (10 mM, pH 8.0) containing KCl (10 mM) were recorded between wavelengths of 200 and 800 nm, using a quartz cuvette (path length: 1.0 cm).

2.2.17.4. Circular Dichroism (CD) analysis

Circular dichroism (CD) analysis was carried out on a CD spectropolarimeter at 20 °C, using protein sample (0.15 mg ml^{-1}) in potassium phosphate buffer (10 mM, pH 8.0) containing KCl (10 mM). CD spectra was recorded between wavelengths

190–260 nm using a quartz cuvette (path length: 0.2 cm) with the following settings: scan speed: 20 nm min^{-1}, data integration time: 2 s, data pitch: 0.1 nm, and band width: 1.0 nm. The measurements from five scans were averaged and corrected for the sample buffer. Protein concentration estimated by the Bradford method was used to determine the molar ellipticity.

2.2.17.5. Differential Scanning Fluorimetry (DSF) analysis

DSF analysis was carried to estimate melting temperature/unfolding temperature of the rice proteins on real-time PCR instrument with excitation and emission wavelength settings at: 465 nm and 580 nm. The assay volume of 20 µl included purified protein (0.5 mg ml^{-1} in 50 mM Tris-HCl; pH 8.0) and SYPRO orange at final concentration of 5 X. DSF analysis was carried out in continuous data recording mode using the following settings: initial incubation: 25 °C for 10 min, gradual increase in the temperature to 95 °C (ramp rate: 0.04 °C sec^{-1}) with 10 data acquisitions $°C^{-1}$). The melting/unfolding temperature of the proteins was obtained as maxima of the first derivatives of the melting curves.

2.2.18. Biochemical characterization of OsCSD proteins

2.2.18.1. Superoxide dismutase activity assay

SOD activity was carried out in two ways; (i) In-gel activity assay (Zymogram) and (ii) Spectrophotometer based assay analysis.

(i) In-gel SOD activity assay/Zymogram analysis

In-gel SOD activity assay was carried out on both non-denaturing as well denaturing polyacrylamide gel as per Chen et al. [258], with minor modifications. Protein samples were resolved on PAGE gels (10% for non-denaturing and 15 % for denaturing PAGE). Denaturing PAGE (after washing in distilled water for 15 min;

thrice) and non-denaturing PAGE gel were incubated in 'solution A' (50 mM sodium phosphate buffer, pH 8.0 + 28 μM riboflavin + 28 mM TEMED for 30 min. Then, 'solution B' (50 mM sodium phosphate buffer, pH 8.0 + 1 mM NBT) was added and the gel was exposed to light (20 min, for color development) and photographed on the gel-documentation system.

(ii) Spectrophotometric method for determination of SOD activity

In solution, SOD activity of rice CSDs was determined as per Ewing et al. [259], based on the nitro blue tetrazolium (NBT) reduction in a multi-well-plate. Increasing concentration (0-5 μg ml^{-1}) of the purified protein was added to 200 μl assay volume containing sodium phosphate buffer (50 mM, pH 7.8), NADH (78 μM), NBT (50 μM), and EDTA (0.1 mM). Reaction was initiated by PMS (final concentration: 3.3 μM; for sodium phosphate buffer and 1.65 μM; for Tris-HCl), and absorbance ($A_{560\ nm}$) was monitored for 5 min on a multi-well plate reader. Rate of superoxide generation was kept at 0.05- 0.06 min^{-1} throughout the assay. One unit (1 U) of SOD activity is defined as the amount of protein required to inhibit the NBT reduction by 50% [136]. Enzyme activity and specific activity of the protein was calculated using following formula:

$$\text{Inhibition rate of NBT reduction (\%)} = \frac{[\Delta A560\ \text{nm (control)} - \Delta A560\ \text{nm(sample)}]}{\Delta A560\ \text{nm (control)}} \text{ x } 100$$

For analysis of other biochemical properties, 1 U equivalent of protein was used for assay reaction.

2.2.18.2. Effect of pH on OsCSD stability and activity

The effect of pH on OsCSD protein (i) stability and (ii) activity was analyzed by

incubating the protein in buffers (50 mM) of different pH range (sodium phosphate: pH 7.0-8.0; Tris-HCl: pH 7.0-9.0 and sodium bicarbonate: pH 9.1- 10.8) for different time points (0-48 h) at 25 °C, followed by estimation of SOD activity.

(i) Effect of pH on stability of OsCSD proteins was assayed using standard SOD assay mentioned in **Section 2.2.18.1** and activity at 0 h time point was considered as 100 %.

(ii) Effect of pH on SOD activity was assayed in respective pH buffers after 1 h incubation. Rate of superoxide generation was kept similar to 0.05-0.06 min^{-1} during the assay. Activity at 0 h time point was considered as 100 %.

2.2.18.3. Effect of temperature on activity

Effect of temperature on the rice CSDs was evaluated as per [260], with minor modifications. The recombinant protein was incubated in 50 mM sodium phosphate buffer (pH 7.8) at different temperatures (25 °C, 37 °C, 45 °C, 50 °C, 60 °C, and 70 °C). Aliquot of protein sample were taken at different time-points, kept on ice for 10 min and relative SOD activity was analyzed as per **Section 2.2.18.1**. Temperature at which maximum activity obtained was considered 100 %.

2.2.18.4. Effect of SOD inhibitors

Effect of inhibitors on the SOD activity of OsCSDs was investigated in an activity based assay. For measuring the effect of diethyldithiocarbamate (DDC), sodium azide (NaN_3), and hydrogen peroxide (H_2O_2), the protein was pre-incubated with increasing concentration of DDC (0.0–2.0 mM), NaN_3 (0.0–10.0 mM) and H_2O_2, (0.0–10.0 mM) for 30-60 min. Relative enzyme activity was measured as described in **Section 2.2.18.1**. Activity at 0 mM inhibitor concentration was considered as 100 %.

2.2.18.5. Peroxidase activity assay

Superoxide dismutases are also known to exhibit bicarbonate-dependent peroxidase activity. Bicarbonate-dependent peroxidase activity of rice CSDs was determined as per Zhang et al. [261], by monitoring oxidation of dichlorodihydrofluorescein (DCFH) to 2', 7'-dichlorofluorescein (DCF). The assay was carried out at 25 °C in potassium phosphate buffer (100 mM, pH 7.4) containing 0.1 mM DTPA, 50 μM DCFH, 25 mM sodium bicarbonate ($NaHCO_3$), and increasing amount (0-250 nM) of protein. The reaction was initiated by the addition of H_2O_2 (0.3 mM) and fluorescence signal (excitation: 480 nm; emission: 524 nm) of the product DCF was monitored for 5 min. Data is expressed as rate of change in DCF fluorescence. The analysis was carried out on a multi-well plate reader instrument.

2.2.19. Construction of *E. coli* sod double-knockout (*ΔsodA ΔsodB*) mutant strain

Single-gene *sodA* and *sodB* knockout of *E. coli* (BW25113) were obtained from Keio collection [262]. *E. coli* sod double-knockout (*ΔsodA ΔsodB*) strain was generated using the FLP-FRT recombination system described in [263], with minor modifications. Briefly, *E. coli sod*A mutant was transformed with pCP20 plasmid and selected on LBA-Amp^+ plates at 30 °C. Few positive cells were grown at 43 °C in LB media, serially diluted in 0.85 % saline, plated on LBA plates and incubated at 30 °C. Loss of Kan^R and Amp^R was confirmed by simultaneously patching clones on LBA-Kan^+, LBA-Amp^+ and LBA plates. These *sodA* cells with sensitivity to kanamycin were designated as *sodA*-Kan^S (S: sensitive). *E. coli sodB* mutant culture was transduced with P1 phage, and the phage lysate was prepared and was used for transduction of *E. coli sodA*-Kan^S cells as per Thomason et al. [264]. The transformed cells were selected on LBA-Kan^+ plates to identify *sodA sodB* double-knockout

mutants. Generated *E. coli* BW25113 *sodA sodB* double mutant was also verified for loss of SOD activity by zymogram analysis as described in **Section 2.2.18.1**.

2.2.20. Oxidative stress tolerance in *E. coli* wild-type and mutant strains

Effect of MV-induced oxidative stress on growth of *E. coli* wild-type BL-21(DE3) and BW25113 *sod* double-knockout mutant (*ΔsodA ΔsodB*) was carried out as per Goulielmos et al. [265], with minor modifications. Oxidative stress tolerance was analyzed in wild-type *E. coli* BL-21(DE3) cells containing either pET28a(+) (control vector) or pET28a-OsCSD. Transformed *E. coli* cells were induced at optimized expression conditions: 0.1 mM IPTG, 20 °C, 16 h. The induced cultures were normalized to absorbance (A_{600nm} to ~0.2), the cells were treated with different MV concentrations (0.0–0.2 mM) in presence of IPTG and absorbance ($A_{600\ nm}$) was measured at regular intervals. Additionally, the cultures were serially diluted in 0.85 % saline and analyzed by spot test (10 µl of respective dilutions were spotted) on LBA-Kan^+ plates.

Oxidative stress tolerance was also analyzed in *E. coli* BW25113 *sod* double-knockout mutant cells containing either pMAL-c5x (control vector) or pMAL-c5x-OsCSD3-SV1 were grown and induced as per optimized conditions mentioned in **Table 2.8**. The induced cultures were normalized to absorbance (A_{600nm}~0.2) and treated with different MV concentrations (0.0– 25 µM) in the presence of IPTG. Growth of cells was monitored by measuring absorbance ($A_{600\ nm}$) at regular intervals. Cultures were serially diluted in saline and different dilutions were spotted on LBA-Amp^+Kan^+ plates. The experiments were repeated three times in triplicates. Statistical analysis was carried out by Student's t-test and the differences were considered significant only when $P < 0.05$.

2.2.21. Lipid peroxidation analysis

Lipid peroxidation level is used as measure of membrane damage induced by oxidative stress. Lipid peroxidation of *E. coli* cells subjected to MV stress was determined as per Panat et al. [266], with minor modifications. The assay is based on quantification of malondialdehyde (MDA), an end product of lipid peroxidation that reacts with 2-thiobarbituric acid (TBA) to produce a red-colored adduct. Briefly, *E. coli* cells were harvested, washed (twice) with phosphate buffer saline (PBS, pH 7.4), resuspended in 300 µl of PBS and lysed by sonication as mentioned in **Section 2.2.14.1**. Sample volume of 300 µl was mixed with 900 µl of TBA reagent and incubated at 95°C for 30 min. Samples were cooled to room temperature and centrifuged at 13680 x g for 20 min at 4 °C. MDA equivalents were estimated in the supernatant by measuring the fluorescence signal (excitation/emission: 530/590 nm) on a multi-well-plate reader. The experiment was repeated three times in triplicates. The lipid peroxidation was expressed as µmoles of MDA equivalents mg^{-1} protein using 1, 1, 3, 3-tetramethoxypropane (TMP) (0-10 µM) as a standard for MDA.

2.2.22. Statistical analysis

All the experiments were done in triplicates with two or more independent biological replicates, and data is expressed as mean ± SD. Student's t-test was performed and statistical significant differences are indicated by '*' (*p <0.05, **p < 0.01 and ***p < 0.001).

CHAPTER 3

RESULTS

Section 3.1

Transcript analysis of rice Cu/Zn Superoxide dismutase (OsCSD) splice variants

3.1.1. Introduction

Plant are susceptible to environmental stress conditions, which negatively affect their growth, development and survival [267]. Plant harbour multiple mechanisms for adaptation from normal environmental fluctuations and adverse environmental conditions, and involve dynamic modulation of gene expression [268]. In eukaryotes, a gene may be regulated at multiple levels, transcription, post-transcription, translation and post-translation by different regulatory mechanisms and affect the gene function in diverse array of conditions [162,201,269]. Regulation of gene expression at transcription level is influenced by presence/absence of *cis*-regulatory elements, trans-regulatory factors, and by chromatin modifications that modulates the accessibility of the gene for transcription [270,271]. The generated transcripts may further be regulated post-transcriptionally by RNA interference and alternative splicing mechanisms, which alter the levels or properties (stability, accessibility for translation etc.) transcript [183,272]. Further, the gene function is also controlled at translational/post-translational levels by protein degradation or modifications mechanisms [268,273]. Post-transcriptional regulatory mechanisms can act rapidly on the pre-existing transcripts to dynamically regulate the gene function [242,274]. Alternative splicing (AS), a eukaryotic mechanism, generates multiple transcripts from same precursor transcript, and regulate level of transcript (or protein) and diversify gene function [174,196]. Recent studies in plants have shown the impact of AS on plant physiology, development, stress responses and establishment of stress memory [204,205,218]. Studies also suggest that AS regulates genes differentially, in cell- /tissue-type specific, condition specific and species/genotype specific manner [275–277]. In recent years, several studies have shown the role and

impact of AS in diverse array of cellular processes, advocating more thorough analysis of this mechanism [181]. Few studies have shown that SODs in plants has been reported to be regulated by alternative splicing [245–247]. However, in most studies the analysis is mainly focused at RNA level. A preliminary search at Rice Genome Annotation Project (RGAP-MSU) database revealed that seven rice SODs produces fourteen splice variants, of which nine are from four Cu/Zn SOD genes. In this section, impact of AS on four rice Cu/Zn SODs (cytosolic, chloroplastic and peroxisomal) of NSICRc106 rice genotype was investigated, with focus on basal transcript levels, different tissues and abiotic stress conditions.

Results

3.1.2. Phylogenetic analysis showed sequence divergence among SODs specific to different subcellular compartments

Rice genome encode four Cu/Zn SODs (CSDs), two on chromosome 3 (LOC_Os03g11960 and LOC_Os03g22810) and one each on chromosome 7 (LOC_Os07g46990) and chromosome 8 (LOC_Os08g44770). The four rice CSDs (OsCSDs), showed considerable heterogeneity in gene structure with gene length (2.119-5.422 kbp), coding region sequence (459-813 bp) and encoded proteins (152-270 aa) predicted at RGAP-MSU rice genome database. Amino acid sequences of four rice CSDs were aligned with CSDs from 9 monocots and 12 dicots using Clustal X sand phylogenetic tree was constructed by neighbour-joining (NJ) method using MEGA 4.0 (**Fig. 3.1.1**). All the plant CSDs showed distinct divergence and were grouped into three clusters: cluster I (cytosolic); II (chloroplastic), and III

(peroxisomal). Furthermore, in each cluster monocot and dicot CSDs were placed into separate sub-clusters. The three CSDs of *Arabidopsis*, AtCSD1, AtCSD2 and AtCSD3

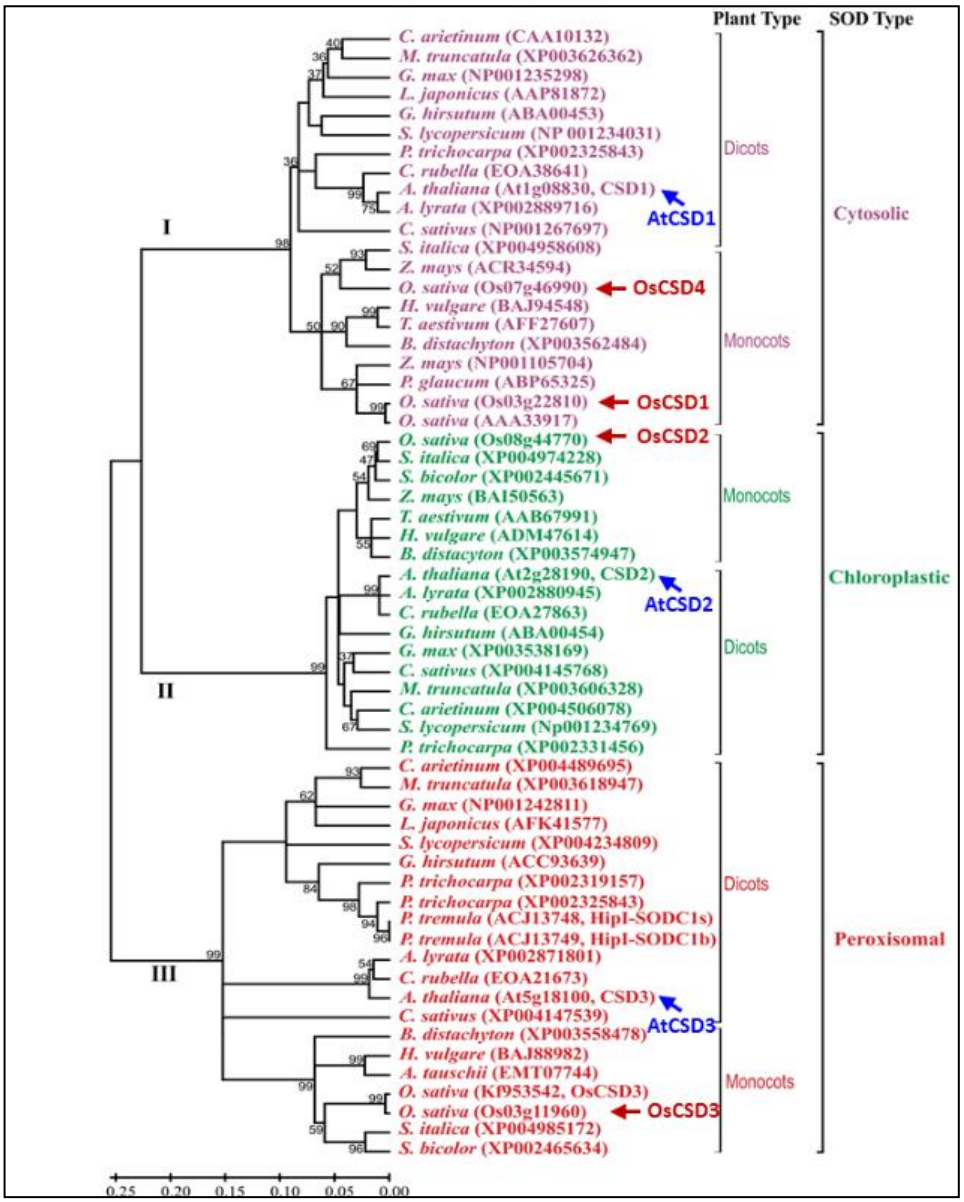

Fig. 3.1.1. Phylogenetic analysis of Cu/Zn SODs. CSDs from 09 monocot and 12 dicot plant species was carried out by Neighbor-joining (NJ) method using MEGA 4 software. Clusters specific to cytosolic (I), chloroplastic (II) and peroxisomal (III) type SOD isozymes are indicated. The numbers at the nodes represents bootstrap values (in %) for a 500-replicate analysis.

were placed into dicot specific cytosolic, chloroplastic and peroxisomal sub-clusters. Of the four rice CSDs, one each was placed in chloroplastic and peroxisomal and two were placed in cytosolic sub-clusters (monocot specific). The designation used for the four rice CSDs were as per the clustering and in accordance to similarity with *Arabidopsis* CSDs types; LOC_Os03g22810 as OsCSD1 (cytosolic), LOC_Os08g44770 as OsCSD2 (chloroplastic) and LOC_Os03g11960 as OsCSD3 (peroxisomal). One extra cytosolic CSD in rice (LOC_Os07g46990) was referred to as OsCSD4. The OsCSD1 and OsCSD4, although cytosolic, showed substantial divergence and clustered with different neighbouring species.

3.1.3. Heterogeneity in the organization/structure of the OsCSDs and splice variant transcripts

The CSDs gene structure/organization was compared using the sequences available at the Rice Genome Annotation Project (RGAP-MSU) database. The four genes shows considerable length and sequence heterogeneity. In addition, three of the four rice CSDs undergo alternative splicing (AS) to generate multiple transcripts (referred to as splice variants, SVs). Four CSD genes generate nine transcripts, four constitutive (referred to as SV1) and five alternative transcripts (referred to as SV2, SV3, SV4). Gene and cDNA sequences of respective OsCSD were retrieved from the RGAP-MSU database, aligned (using ClustalX and edited using BioEdit software). For each of the four CSD genes, the variation in the organization of UTRs, exons and introns in the variant transcripts vis-à-vis gene was compared using IBS tool and is shown in a schematic representation below (**Fig. 3.1.2**).

3.1.3.1. LOC_Os03g22810 (OsCSD1gene) generates a single constitutive transcript

Rice locus LOC_Os03g22810 on chromosome 3 codes for cytosolic Cu/Zn SOD (OsCSD1). The gene is 5.422 kb long and is predicted to code for 813 bp coding region with 10 exons, 9 introns and a single 3′-UTR. OsCSD1 codes for a single constitutive transcript referred to as OsCSD1-SV1 (**Fig. 3.1.2A**).

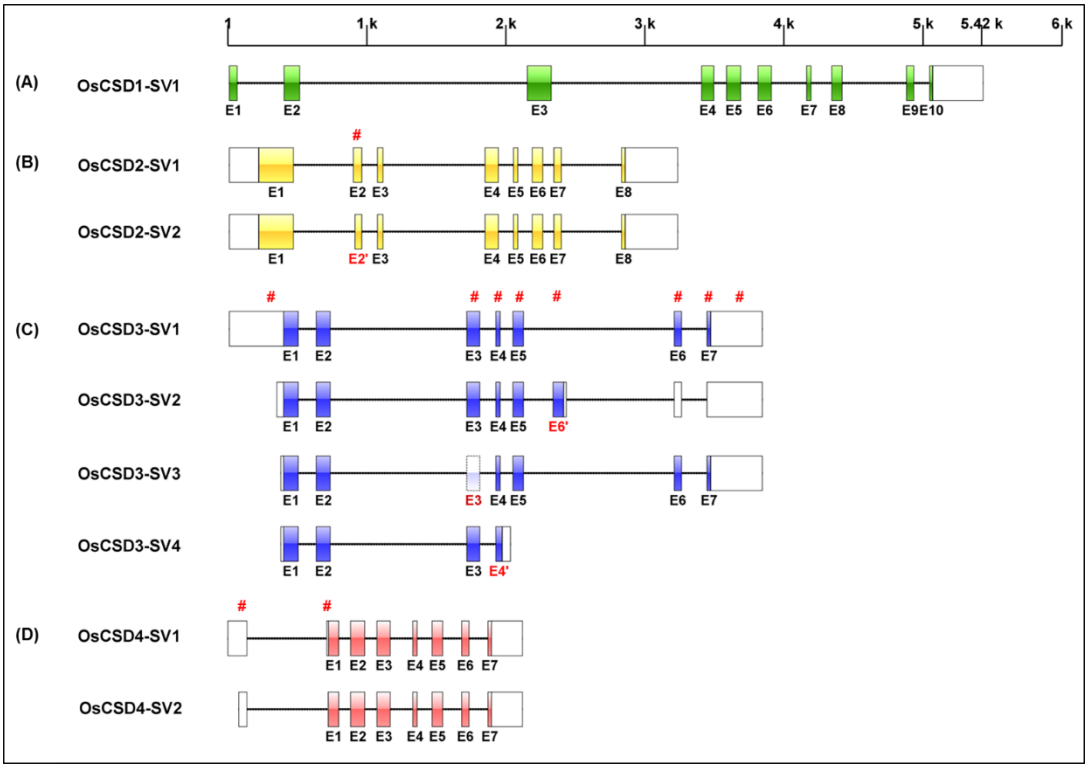

Fig. 3.1.2. Schematic overview of structure and organization (UTR, exon and introns) of constitutive and alternative splice variants of rice CSDs as per RGAP-MSU database. The scheme was designed using IBS tool. (A) LOC_Os03g22810 (OsCSD1), **(B)** LOC_Os08g44770 (OsCSD2), **(C)** LOC_Os03g11960 (OsCSD3), and **(D)** LOC_Os07g46990 (OsCSD4). UTRs (white box), exons (coloured boxes) and introns (solid lines), and variable regions (#) are indicated. Certain important differences in AS-events are indicated with red font colour.

3.1.3.2. LOC_Os08g44770 (OsCSD2 gene) generates one constitutive and one alternative splice variant

Rice locus LOC_Os08g44770 codes for a chloroplastic Cu/Zn SOD (OsCSD2). OsCSD2 gene (3.226 kbp) is smaller than OsCSD1, codes for two UTRs (5′-UTR and 3′-UTR), 8 exons and 7 introns and generates two splice variants, OsCSD2-SV1 and OsCSD2-SV2. The two variants differ in 12 bp coding region (missing in exon2 of SV2) due to a 3′-ASS (3′ alternative splice site) event. Hence, the two SVs differ in the length of coding region (OsCSD2-SV2: 636 bp; OsCSD2-SV2: 624 bp) (**Fig. 3.1.2B**).

3.1.3.3. LOC_Os03g11960 (OsCSD3 gene) generates one constitutive and three alternative splice variants

LOC_Os03g11960 codes for a peroxisomal Cu/Zn SOD (OsCSD3). The 3.834 kbp long gene generates one constitutive SV (OsCSD3-SV1) and three alternative SVs (OsCSD3-SV2, OsCSD3-SV3, OsCSD3-SV4) due to AS-mediated variations in UTRs and/or exon regions (**Fig. 3.1.2C**). OsCSD3-SV1 consists of 7 exons, 6 introns and a relatively long 5′-UTR region compared to other SVs. OsCSD3-SV2 contain 6 exons (E1-E5 + alternative exon E6′), 7 introns and a small 5′- and longer 3′-UTR regions. The alternative exon (E6′) is generated through a AS-intron retention (IR) event. Organization of OsCSD3-SV3 is similar to OsCSD3-SV1 in most aspects except lack of exon3 (E3), due to AS-exon skipping (ES) event and contains a short 5′-UTR. OsCSD3-SV4 (smallest SV of all) contains a slightly long (15 bp) exon4 (E4′) due to partial AS-IR event and very small 3′-UTR. All exons/3′-UTRs downstream to E-4, but seen in other variants, were not present in OsCSD3-SV4 (**Fig. 3.1.2C**).

3.1.3.4. LOC_Os07g46990 (OsCSD4 gene) generates one constitutive and one alternative splice variant

LOC_Os07g46990 in rice genome codes for a second cytosolic Cu/Zn SOD (OsCSD4). This additional gene present on chromosome 7 is 2.119 kbp long (smaller than OsCSD1 cytosolic CSD gene) and generates two splice variants (OsCSD4-SV1 and OsCSD4-SV2) which contain minor variation in the 5′-UTR (OsCSD4-SV2 has smaller UTR). The remaining exons, introns and 3′-UTR show similar organization (**Fig. 3.1.2D**). The heterogeneity in the non-coding regions of rice OsCSD SVs might affect the properties of alternative transcripts.

3.1.4. Rice CSD splice variants showed tissue specific expression pattern

Alternative splicing alters the levels of transcripts in response to different conditions. This aspect of AS in modulation of OsCSD transcripts was investigated by qRT-PCR using gene-specific or SV-specific primers (**Table 2.4**). Analysis was carried out for OsCSD transcript levels in different tissues viz. shoot, mature leaf, panicle, stem and flag leaf. All the four OsCSDs were detected in the tissues analyzed, however difference in relative abundance was observed. In shoot, the transcript levels of OsCSD1 and OsCSD2 were comparable and each contributed to ~35 % of the total CSD transcript, compared to OsCSD3 and OsCSD4 (contributed to ~15 % each) (**Fig. 3.1.3**).

Further analysis revealed tissue-specific differences in the transcript levels of four OsCSDs. As an example, **Fig. 3.1.4A and 3.1.4B** show the relative transcript levels of OsCSD1 and OsCSD4, in mature leaf, flag leaf, stem, and panicle tissue. OsCSD1 transcript levels were highest in mature leaf and lowest in stem (**Fig. 3.1.4A)**. OsCSD4 showed a similar tissue-specific trend but its levels were lower than OsCSD1

(**Fig. 3.1.4B**). Similarly, OsCSD2 showed highest transcript levels in shoot tissue and OsCSD3 showed highest abundance in flag leaf followed by panicle and comparable expression in mature leaf and stem.

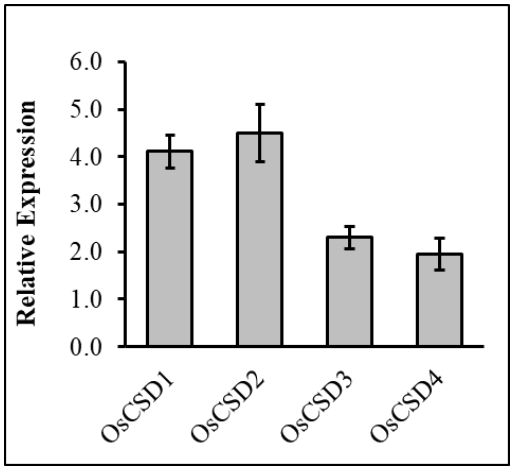

Fig. 3.1.3. Quantitative RT-PCR analysis of OsCSDs in rice seedlings. Relative The experiment was carried out with two independent biological and three technical replicates. Data are represented as normalized transcript level ±SD.

Tissue-specific qRT-PCR analysis was extended to estimate the OsCSD SV levels, using splice variant-specific primers in the assays. For OsCSD1, there was only constitutive transcript (no alternative variant) and the expression pattern is shown in **Fig. 3.1.4A**. For OsCSD4, the abundance of alternative SV (OsCSD4-SV2) was very low and it could not be analyzed. Tissue-specific expression trend of constitutive OsCSD4-SV1 is shown in **Fig. 3.1.4B**.

The two splice variants of OsCSD2 showed differential transcript abundance in rice tissues. High transcript levels were detected in shoot tissue and the overall trend for two SVs was similar but OsCSD2-SV2 levels were generally lower than OsCSD2-SV1 (**Fig. 3.1.5A and 3.1.5B**).

Among the four OsCSDs, OsCSD3 generates maximum number of four SVs and showed differential expression among rice tissues. Highest transcript levels were

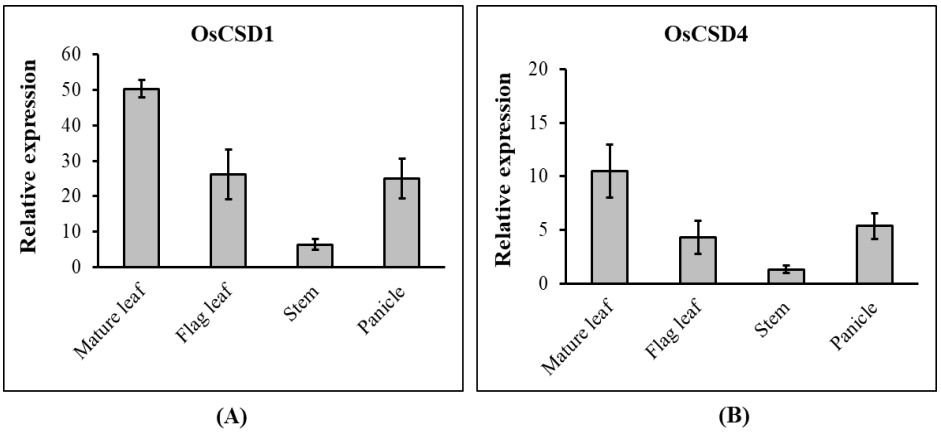

Fig. 3.1.4. Analysis of transcript levels of cytosolic CSDs in different rice tissues. (A) OsCSD1 and **(B)** OsCSD4. Transcript analysis in rice tissues (mature leaf, flag leaf, stem and panicle) was carried out by qRT-PCR using actin as a reference gene. The experiment was carried out with two independent biological replicates and three technical replicates. Data are represented as normalized transcript level ±SD.

present in flag leaf followed by panicle and lowest expression in shoot tissue. As an example, OsCSD3-SV1 and OsCSD3-SV2 transcript levels in rice tissues are shown in **Fig. 3.1.5C and 3.1.5D**. The levels of OsCSD3-SV3 were low, while that of OsCSD3-SV4 were extremely low and hence could not be analyzed.

3.1.5. Stability of OsCSDs transcript and splice variants

Since AS creates variation in UTRs and/or exons, its effect on the stability of transcript was investigated. Rice shoot tissue treated with α-amanitin (inhibits transcript synthesis) was used for RNA isolation and stability (in terms of relative abundance due to differential degradation rates) of OsCSDs and splice variants was evaluated by qRT-PCR analysis. Among the OsCSDs, OsCSD3 transcript was most

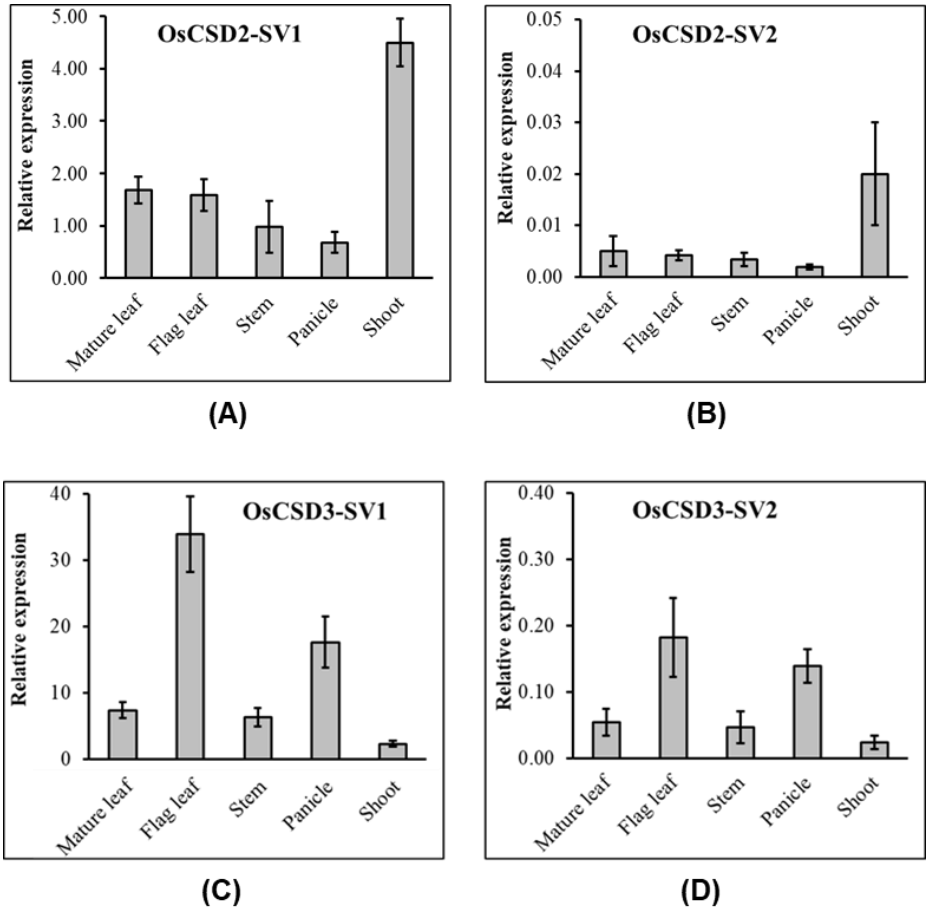

Fig. 3.1.5. Analysis of transcript levels of OsCSD2 and OsCSD3 SVs in rice tissues. (A) OsCSD2-SV1, **(B)** OsCSD2-SV2, **(C)** OsCSD3-SV1 **(D)** OsCSD3-SV2. Transcript analysis in rice tissues was carried out by qRT-PCR using actin as a reference gene. The experiment was carried out with two independent biological replicates and three technical replicates. Data are represented as normalized transcript level ± SD.

stable, showed similar levels till 4 h and half- life ($t_{1/2}$, time of reduction of 50 % transcript) of ~15.2 h. Of the two cytosolic OsCSDs, OsCSD4 was slightly more stable than OsCSD1 (OsCSD4 $t_{1/2}$: 4.2 h; OsCSD1 $t_{1/2}$: and 3.0 h). OsCSD2 showed slightly higher stability ($t_{1/2}$; 5.6 h) than cytosolic CSDs (**Fig. 3.1.6A**). Analysis of relative stability of CSD SVs was also carried. The two SVs of OsCSD2 showed

similar transcript stability pattern (**Fig. 3.1.6B**). Among the OsCSD3 SVs difference in transcript stability was observed (**Fig. 3.1.6B**). OsCSD3-SV2 transcript was comparatively more stable ($t_{1/2}$: 18.7 h) than OsCSD3-SV1 (Give $t_{1/2}$: 14.5 h) and OsCSD3-SV3 ($t_{1/2}$: 12 h), with no significant difference in levels till 8 h (**Fig. 3.1.6B**). Due to lower levels, the stability pattern of OsCSD3-SV4 could not be analyzed. Collectively these results show that AS mediated changes affect transcript stability of certain CSD splice variants.

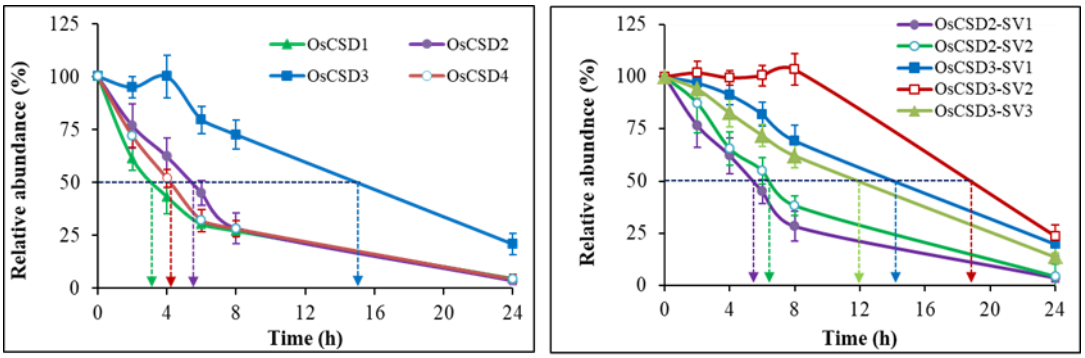

Fig. 3.1.6. Analysis of transcript stability of OsCSDs and its splice variants. (A) Analysis of relative transcript stability of the four OsCSDs, OsCSD1, OsCSD2, OsCSD3 and OsCSD4. **(B)** Analysis of relative transcript stability of splice variants of OsCSD2 and OsCSD3. Transcript stability was measured in term of relative abundance considering transcript level at 0 h time point as 100 %. Arrow indicates the half- life values ($t_{1/2}$) of the transcript. The experiment was carried out with two independent biological replicates and three technical replicates. Data are represented as normalized transcript level ± SD.

3.1.6. Abiotic stress responsiveness of OsCSDs and splice variants

Abiotic stress responsiveness of the four OsCSDs and the splice variants was analyzed in rice seedlings by qRT-PCR. Transcript analysis was carried out in the rice

seedlings subjected to three abiotic stress conditions, salinity (150 mM NaCl), drought (15 % PEG), and oxidative stress (10 µM methyl viologen).

3.1.6.1. OsCSDs showed differential response to abiotic stress

Transcript analysis of OsCSDs showed differential response to abiotic stress conditions. Among the two cytosolic OsCSDs, OsCSD4 was strongly upregulated in response to Salinity (2.5-3.5 fold) and drought (3-4 fold) compared to OsCSD1 (~1.5-1.75 fold) (**Fig. 3.1.7A and 3.1.7B**). In response to oxidative stress, both the cytosolic OsCSDs showed delayed upregulation, with OsCSD1 showing slightly higher levels (**Fig. 3.1.7A and 3.1.7B**). The chloroplastic OsCSD2 showed early induction (~3 fold) in salinity and drought (>1.5 fold), while under oxidative stress it shows ~2-2.5-fold upregulation (**Fig. 3.1.7C**). OsCSD3 also showed upregulation (~1.5-1.8-fold) in response to salinity and drought, and upto >2.5 fold under oxidative stress (**Fig. 3.1.7D**).

3.1.6.2. Abiotic stress modulates the splicing pattern of OsCSDs

Responsiveness of OsCSD splice variants to stress conditions was also analyzed. Results showed that abiotic stress treatments modulate the splicing pattern of certain OsCSDs. The two OsCSD2 SVs (OsCSD2-SV1 and OsCSD2-SV2) were up-regulated in response to abiotic stress conditions however no significant differences were observed in their relative levels (**Fig. 3.1.8A, 3.1.8B and 3.1.8C**). OsCSD3 SVs showed variation in expression levels in response to stress conditions. Under drought stress OsCSD3-SV2 showed slightly higher levels than OsCSD3-SV1and OsCSD3-SV3 (**Fig. 3.1.9A**). On the contrary, under salinity and oxidative stress reverse abundance pattern was observed, with OsCSD3-SV1 and OsCSD3-SV3 higher than

OsCSD3-SV2 (**Fig. 3.1.9B and 3.1.9C**). As the OsCSD4-SV2 and OsCSD3-SV4 showed low levels, their expression pattern could not be analyzed.

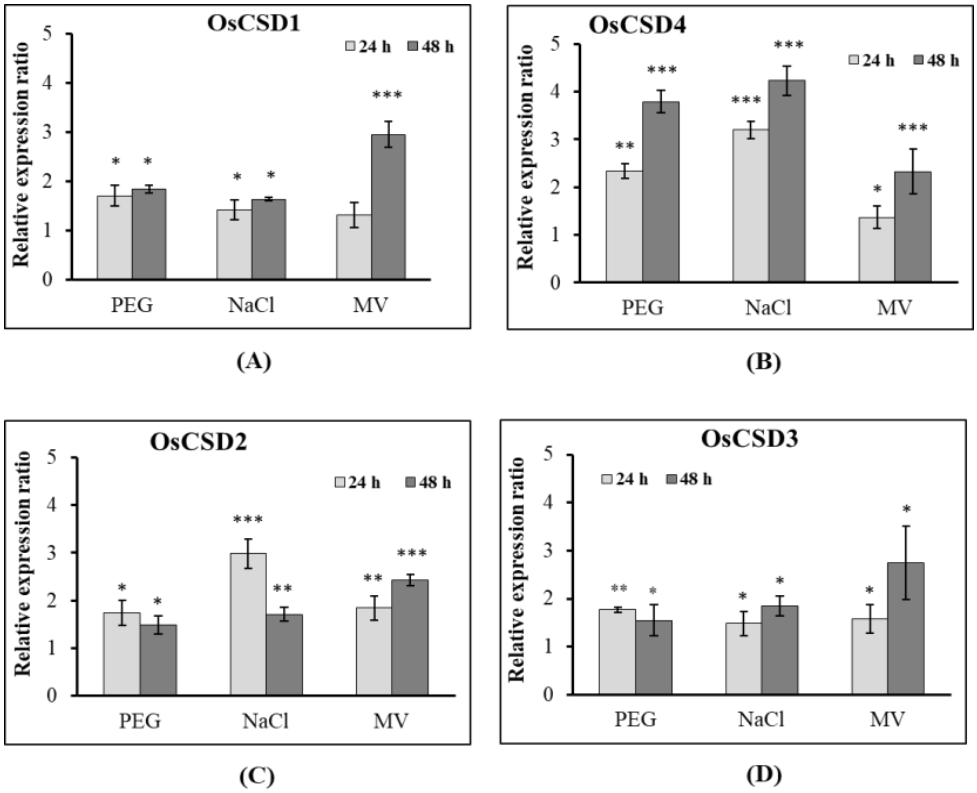

Fig. 3.1.7. Transcript analysis of OsCSDs under abiotic stress conditions. Rice seedling were subjected to 15 % PEG, 150 mM NaCl and 10 µM MV. Relative transcript levels of OsCSD1 **(A)**, OsCSD4 **(B)**, OsCSD2 **(C)**, and OsCSD3 **(D)** were analysed by qRT-PCR. The experiment was carried out using two independent biological replicates, and three technical replicates. Data is represented as relative expression ratio ±SD. Statistical analysis was carried out by Student's t-test and significance was shown (* $p < 0.05$, ** $p < 0.01$, *** $p < 0.001$).

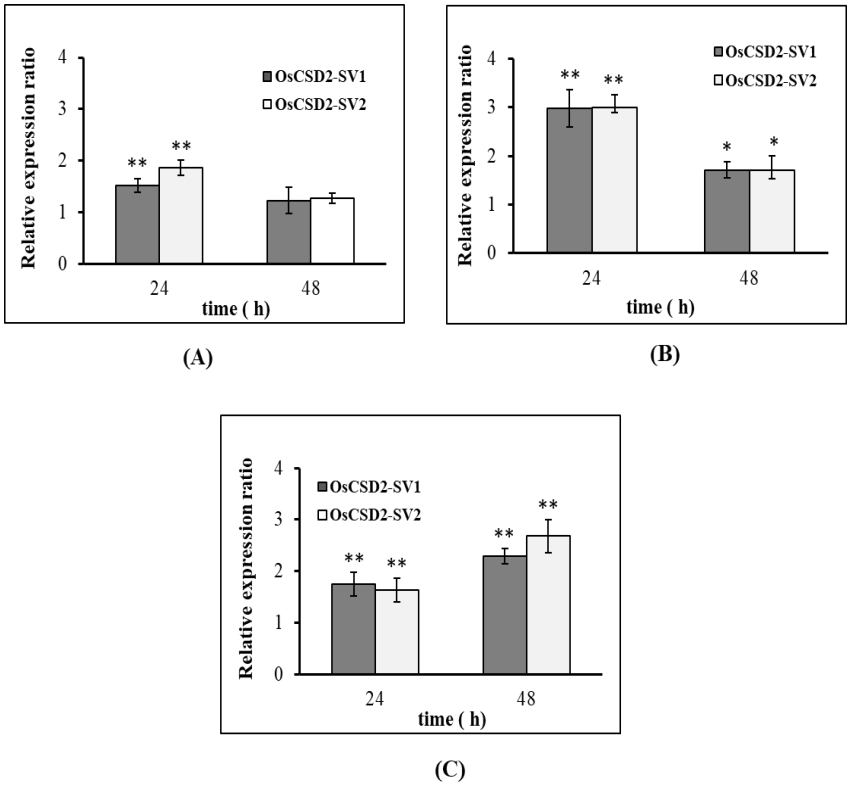

Fig. 3.1.8. Expression analysis of OsCSD2 splice variants under abiotic stress. (A) 15 % PEG; **(B)** 150 mM NaCl and **(C)** 10 µM MV. Relative transcript levels of OsCSD2-SV1 and OsCSD2-SV2 were analyzed by qRT-PCR. The experiment was carried out using two independent biological replicates, and three technical replicates. Data is represented as relative expression ratio ±SD. Statistical analysis was carried out by Student's t-test and significance was shown (** $p < 0.01$, * $p < 0.05$).

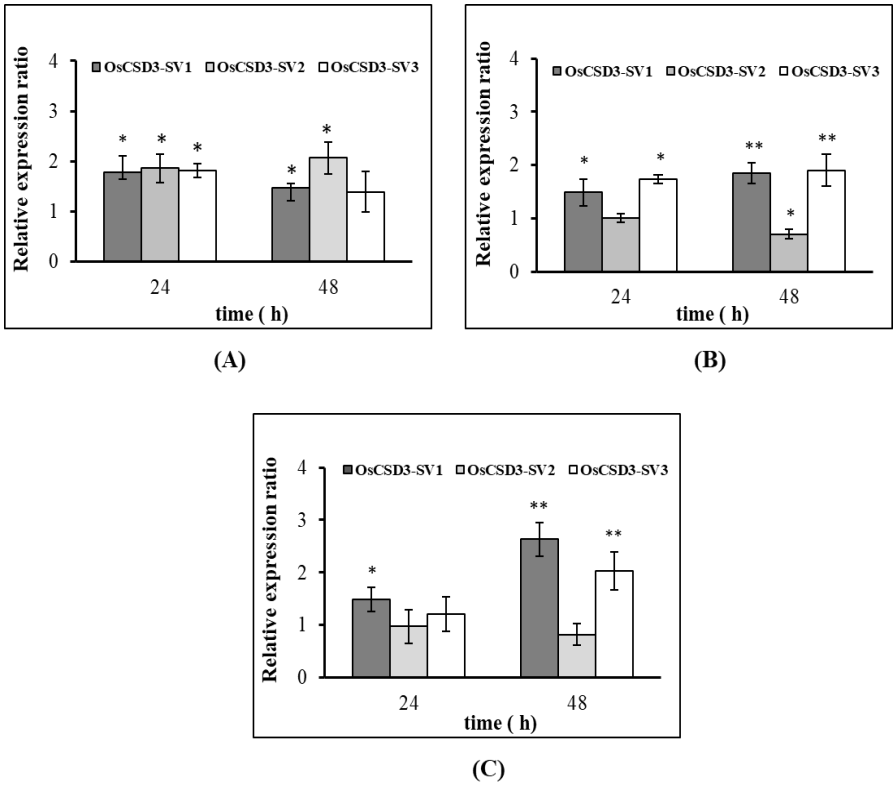

Fig. 3.1.9. Transcript analysis of rice peroxisomal CSD (OsCSD3) splice variants under abiotic stress conditions: (A) PEG, **(B)** NaCl, and **(C)** MV. Relative transcript levels of OsCSD3-SVs (OsCSD3-SV1, -SV2 and -SV3) were analyzed by qRT-PCR. The experiment was carried out using two independent biological replicates, and three technical replicates. Data is represented as relative expression ratio ±SD. Statistical analysis was carried out by Student's t-test and significance was shown (* $p < 0.05$, ** $p < 0.01$).

These results showed that the abiotic stress conditions modulate the splicing pattern of the rice CSDs, and the extent of modulation seems specific to different CSDs as well to the nature of abiotic stress conditions.

3.1.7. Discussion

Most stress conditions are known to elevate cellular ROS levels, causing oxidative damage [32]. SODs, like other antioxidants, maintain cellular ROS

homeostasis and also provide tolerance to stress conditions [134]. The response to stress conditions is regulated by several mechanisms that rapidly and dynamically modulate gene expression [268]. Alternative splicing (AS), a post-transcriptional mechanism, is important for several cellular processes. In this section, expression pattern of nine OsCSD SVs (four constitutive and five alternative SVs) were analyzed for tissue specificity, transcript stability, and stress-response, to understand the role of AS in modulation of CSD transcript levels under different conditions.

Differential abundance pattern of four rice CSDs in different tissues indicates tissue-specific regulation. Such, tissue-specific abundance of CSDs have also been reported in different plants [226,278,279]. Unlike plants (e.g. *Arabidopsis*) that contain single cytosolic CSD, rice contain two (OsCSD1 and OsCSD4) with differences in tissue-specific patterns. OsCSD1 transcript remained at higher levels than OsCSD4 in the tissues analyzed in the present study. However, OsCSD4 is also more abundant in other tissues (e.g. at germination stage) [143]. Higher levels of OsCSD2 (chloroplastic) observed in photosynthetically active tissue was consistent with its involvement in $O_2^{\cdot -}$ scavenging in chloroplast, and similar with tissue-specific expression pattern in plants [143,279]. Higher OsCSD3 (peroxisomal) levels may be important for maintenance of ROS level in flag leaf, as it is important for development of reproductive organs as well as grain filling [280].

AS in plants has emerged as versatile mechanism with impact on diverse array of physiological, development, and stress responses [181,272,281]. Like several other genes, rice Cu/Zn SOD genes also undergo AS to produces nine splice variants (http://rice.plantbiology.msu.edu/). Their differential splicing pattern in rice tissues suggest that in addition to the other regulatory mechanisms, AS is also involved in

tissue-specific expression pattern of CSDs as also observed in previously published reports in Soybean and Populus [246,247]. Comparison of the AS events in CSDs of *Arabidopsis* in TAIR database (https://www.*Arabidopsis*.org/index.jsp), Rice from RGAP-MSU (http://rice.plantbiology.msu.edu/), and published reports of Soybean and Populus showed differences (type and number of AS events) that might be important for plant specific fate of transcripts [246,247]. Moreover, AS event in different regions (UTR/exon/introns) of precursor transcripts affect different characteristics of the mature transcript like [282,283] and encoded protein length/sequence [245–248]. Analysis of stability of OsCSDs and SV transcripts showed that OsCSD3 transcript was most stable (OsCSD1 least stable), where sequence/structural variations among different OsCSD transcripts could also be an important contributing factor. For example, CSDs are negatively regulated by miR398 in control conditions and stress conditions [150,239,284]. Heterogeneity in miR398 target site among rice CSDs might affect the miR398 mediated cleavage. Similarly, higher stability of OsCSD3-SV2 than OsCSD3-SV1 might be associated intron derived alternative exon (in OsCSD2-SV2) as such intronic region in transcripts have been linked to higher transcript stability [283].

Plants SODs are induced under different abiotic stresses [134,143,225], and it is associated with reduced damage and enhanced tolerance under stress [150,260,285]. AS is also involved in modulation of stress responsiveness of genes in plants [286,287]. Stress responsiveness of four OsCSDs and their SVs was investigated in NSICRc106 genotype. All four OsCSDs were differentially responsive to abiotic stresses including the two cytosolic OsCSDs (OsCSD1 and OsCSD4), as also observed in previous reports on stress and phytohormone (ABA) treatment

[143,148,227,228]. Such patterns are indicative of *cis*-element differences in rice cytosolic CSD genes, as also reported for cytosolic localized APX [288]. Stress specific *cis*-elements are associated with induction of specific genes under different stress conditions leading to efficient ROS detoxification. Stress-specific up-regulation of chloroplastic OsCSD2 and peroxisomal OsCSD3 mitigates the stress induced ROS toxicity and protects the two organelles that are important sites for ROS generation in plants. Similar, differential responses of these two isoforms have been reported in rice, *Arabidopsis* and *Nicotiana* plants exposed to abiotic stresses [143,225,289].

In addition to the *cis*-element driven transcript induction, AS events are also important contributors to the stress-responsiveness of variety of genes including SODs [194,286,287]. Analysis of splice variants of OsCSDs under difference stress conditions indicates that the alternative splicing *per se* is differentially modulated, leading to stress-specific differences in expression pattern. Furthermore, AS of certain variants was more responsive to stress conditions than others. While OsCSD2 showed similar trend of splicing patterns, OsCSD3 showed contrasting splicing pattern of SVs different abiotic stresses. Here, OsCSD3-SV2 was down-regulated resulting in up-regulation of other SVs (OsCSD3-SV1 and OsCSD3-SV3) suggesting AS mediated fine tuning of level of transcripts to dynamically modulate the OsCSD3 transcript/protein levels under stress conditions. Transcript analysis showed that OsCSD SVs exhibit tissue- and stress-specific abundance patterns, which may influence CSD protein/activity in a tissue under normal and stress conditions. OsCSD SVs with heterogeneity in coding region could produce alternative protein isoforms, which may have altered SOD properties or different functions which is addressed in subsequent sections.

Section 3.2

Analysis of rice peroxisomal Cu/Zn SOD and its alternative isoforms

3.2.1. Introduction

Peroxisomes are ubiquitous, single-membrane-bound organelles present in eukaryotic cells. It was first discovered in mouse kidney (isolated first from rat liver) and named 'peroxisomes' due to presence of H_2O_2 generating (oxidases) and degrading (catalase) enzymes [290]. Plant peroxisomes exhibit substantial functional versatility and are involved in diverse metabolic processes such as, lipid metabolism, photo-respiration and phytohormones synthesis and other oxidative reactions [85,291]. Peroxisomes are dynamic structures that multiply/disintegrate in response to cellular metabolic needs and environmental perturbations [292]. Peroxisomes are also site for synthesis/detoxification of various reactive oxygen species (ROS; e.g. $O_2^{\cdot -}$ and H_2O_2) and reactive nitrogen species (RNS; e.g. NO) that serve as important signaling molecules in cellular/sub-cellular communications, and stress acclimation [66,293]. Peroxisome also contain sites of $O_2^{\cdot -}$ generation such as, matrix located xanthine oxidase (XO) and membrane localized NAD(P)H dependent peroxisomal integral membrane polypeptides (PMPs, PMP18, PMP29 and PMP32) [65,294]. Peroxynitrite radical ($ONOO^-$, formed in peroxisomes) mediated modifications (N-nitrosylation and S-nitroglutathionylation) alter the activities of proteins and regulate signaling pathways and developmental processes [295,296].

On the other hand, higher accumulation of the ROS and RNS in unfavourable conditions causes oxidative and nitrosative stress [297]. Peroxisomes contain various non-enzymatic (ascorbate, glutathione etc.) and enzymatic (superoxide dismutases, catalases etc.) antioxidants to control the level of ROS and RNS under different conditions [298].

Despite importance of peroxisomes in ROS/RNS management and cellular functioning, studies on peroxisomal SODs are relatively less compared to cytosolic, chloroplastic and mitochondrial isoforms. Presence of a SOD (Mn SOD) in peroxisomes was first reported in *Pisum sativum* [299,300], followed by identification of other SODs in different plants [65]. Presence of Cu/Zn SOD in peroxisomes has been reported in oilseed plants, sunflower and cotton [301]. Interestingly, *Dianthus caryophyllus* and *Citrullus* sp. peroxisomes were found to contain two SOD isoforms, Mn SOD along with Fe SOD in *D. caryophyllus* and with Cu/Zn SOD in *Citrullus* sp. [122,302–304]. Presence of peroxisomal isoforms contributes to the diversity of SOD isozymes in dicots, compared to the monocots [65].

This section investigates a relatively less studied locus in rice that codes for a putative peroxisomal Cu/Zn SOD (CSD). The rice locus LOC_Os03g11960 (OsCSD3) has been analyzed at transcript level in very few studies [225]. As per the RGAP-MSU database OsCSD3 undergoes AS and generates four splice variants (SVs) differing in organization of UTRs, coding region or both. Analysis of expression pattern of NSICSRc106 OsCSD3-SVs at RNA level showed tissue- and stress specific responses (**Section 3.1**). However, the characteristics of the SV encoded protein isoforms vis-à-vis other isoforms are not known. This section deals with the analysis of the protein characteristics of OsCSD3-SV1 and its alternative splice isoforms.

Results

3.2.2. Rice OsCSD3 contains conserved features of Cu/Zn SODs

Rice locus LOC_Os03g11960 codes for OsCSD3, a Cu/Zn SOD highly similar to peroxisomal isoforms (**Fig. 3.1.1**). Multiple sequence alignment of peroxisomal CSDs from monocot and dicot species identified conserved and variable regions. The

CSD sequences showed substantial conservation, while length variation was observed at N- and C-terminal of the proteins (**Fig. 3.2.1**). Amino acid residues involved in coordination with Cu^{2+} (His-55, -57, -72 and -129) and Zn^{2+} (His-72, -80, -89, Aps-92), disulfide bond formation (Cys-66 and Cys-155) and surface interactions were highly conserved (**Fig. 3.2.1**). The OsCSD3 when compared with other rice Cu/Zn SODs (OsCSD1, OsCSD2 and OsCSD4) showed length variation and sequence heterogeneity at ~37 % sites. Despite similarity to peroxisomal CSDs, *in silico* analysis could not predict/identify canonical peroxisome specific targeting signals in OsCSD3.

3.2.3. Exon-intron organization of OsCSD3 splice variants

As per RGAP-MSU database, OsCSD3 generates four splice variants (OsCSD3-SV1, -SV2, -SV3 and -SV4) with considerable length heterogeneity (351-495 bp) (**Fig. 3.1.2**). The four SVs were transcriptionally active, showed tissue- and stress-specific response (**Fig. 3.1.5C, 3.1.5D and section 3.1.4**). Comparison of OsCSD3-SVs showed the differences in exon organization affecting the encoded amino acids sequences (**Fig. 3.1.2**). Hence, to investigate the properties of the OsCSD3 SV encoded protein isoforms, CDS sequence were analyzed using NEB Cutter 2.0 and PCR primers containing NdeI and EcoRI restriction sites were designed for full-length cDNA amplification and cloning into plasmid vector for heterologous expression in *E. coli* (**Table 2.5**).

3.2.4. Alternative splicing-mediated effects on domain organization of OsCSD3 isoforms

The impact of the missing/alternative exons on four OsCSD3 SV isoforms was

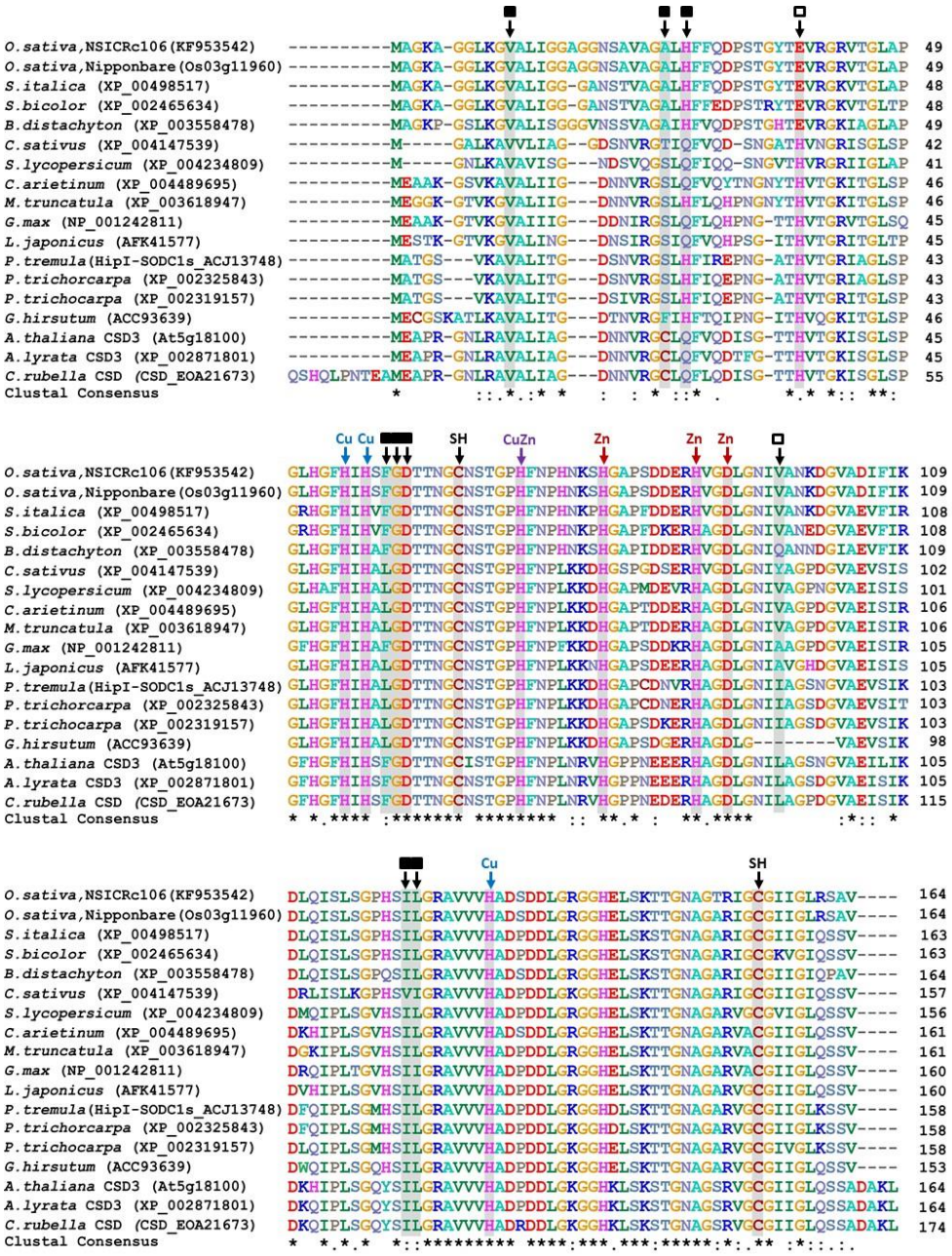

Fig. 3.2.1. Multiple sequence alignment of peroxisomal Cu/Zn SODs from monocot and dicot plants. The sequences were aligned by ClustalX software. Conserved residues are indicated by symbols below each block of the alignment. Residues that are part of active site, involved in coordination with Cu^{2+} (Cu) and Zn^{2+} (Zn), disulfide (SH) and surface interactions (E-class '■'; and P-class '□' dimer interface) are also indicated.

first investigated by *in silico* analysis. Conserved domain analysis indicated that AS affected certain regions important for SOD function and properties (**Fig. 3.2.2**). OsCSD3-SV1 isoform (length: 164 aa) contained all characteristic features of a typical plant Cu/Zn SODs with conserved residues for Cu^{2+} and Zn^{2+} binding, disulfide bond formation, and subunit interactions (**Fig. 3.2.2**).

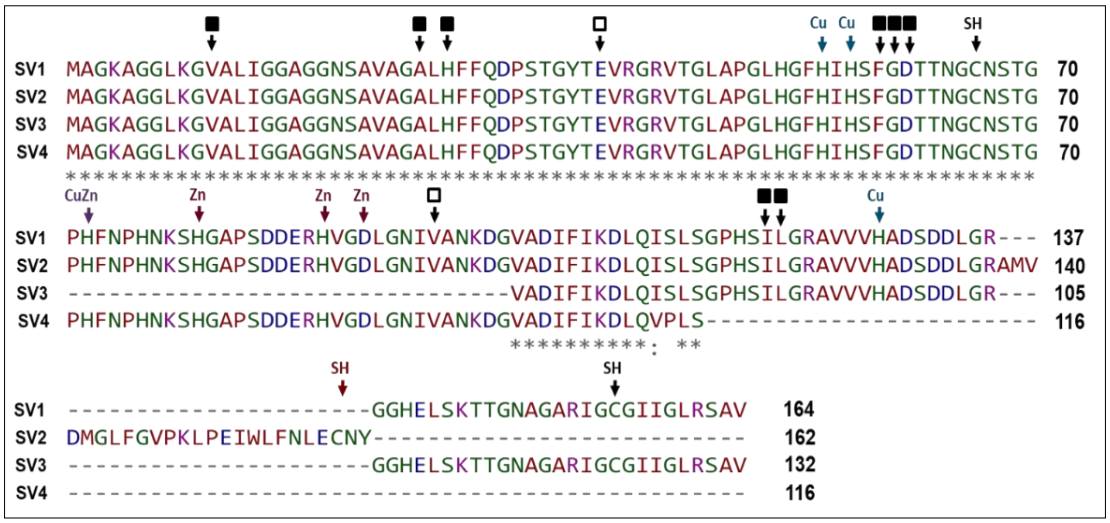

Fig. 3.2.2. Sequence and domain analysis of OsCSD3 SV protein isoforms. Sequence alignment of OsCSD3 isoforms was carried using ClustalX, while domain analysis was carried out at Conserved Domain Database (CDD-NCBI) at NCBI web server. Conserved residues are indicated with '*', while structurally and functionally important residues are shown with arrows and appropriate symbols; Cu^{2+} and Zn^{2+} ion coordination (Cu and Zn), subunit interaction residues (E-class '■' and P-Class '□' interaction), and cysteine residues (SH).

In the OsCSD3-SV2 isoform (length: 161aa), C-terminal 27 aa residues (as in SV1) were replaced with 24 aa encoded by an alternative exon. This also resulted in change in the position of 2nd cysteine residue (Cys-160) compared to Cys-155 (as in OsCSD3-SV1), while the residues for Cu^{2+} and Zn^{2+} binding and dimeric interactions

remained unaffected (**Fig. 3.2.2**). OsCSD3-SV3 isoform lacked region corresponding to 71-102 aa position (as in SV1) due to skipping of exon3 (E3), resulting in loss of residues involved in Zn^{2+} coordination, and a bridging histidine residue (His-72) for Cu^{2+} and Zn^{2+} metal ions (**Fig. 3.2.2**). OsCSD3-SV4 isoform is smallest alternative isoform (length: 116 aa) that lacked 112-164 residues corresponding to the SV1, but contained four-amino acid (^{113}VPLS^{116}) due to partial intron retention event at C-terminal. It also lacked His-129 (Cu^{2+} co-ordination), two surface interaction residues, and one cysteine (Cys-155) involved in the intra-molecular disulfide bond (**Fig. 3.2.2**).

3.2.5. PCR amplification and cloning of full-length cDNAs of OsCSD3 SVs

To study the characteristics of OsCSD3 isoforms, full-length cDNAs (FL-cDNAs) were PCR amplified using *Pwo* DNA polymerase and cloned into plasmid vectors for heterologous expression in *E. coli*. As the basal transcript levels of OsCSD3 SVs was low, a different strategy was used. Using first-strand cDNA of NSICRc106 genotype, FL-cDNAs of OsCSD3-SV1 and OsCSD3-SV2 were successfully PCR amplified, using specific primers (OsCSD3-SV1: OsCSD3-Cm-F + OsCSD3-SV1/3-R; OsCSD3-SV2: OsCSD3-Cm-F + OsCSD3-SV2-R) (**Fig. 3.2.3, Table 2.5**). The FL-cDNAs were cloned into different *E. coli* expression vectors such as pET28a(+), pMAL-c5x and pTwin1. As direct amplification of OsCSD3-SV3 FL-cDNA using SV3 specific primers (OsCSD3-Cm-F + OsCSD3-SV1/3-R) was not successful, inverse PCR approach was used. Plasmid pET28a-OsCSD3-SV1 was used as template along with two outward primers (OsCSD3-SV3-Fa + OsCSD3-SV3-Rb), to create deletion of exon3 (**Fig. 2.1**). The linear PCR product was then self-ligated to generate pET28a-OsCSD3-SV3. This plasmid was subsequently used for cloning of

FL-cDNA of OsCSD3-SV3 into other expression plasmids (**Fig. 3.2.3**). Similarly, due to lower transcript levels, FL-cDNA of OsCSD3-SV4 also was not directly PCR amplified from total cDNA, and a variant specific reverse transcription reaction was carried using OsCSD3-SV4b-R primer, and subsequently FL-cDNA was successfully PCR amplified using SV4 specific primers **(Fig. 3.2.3).**

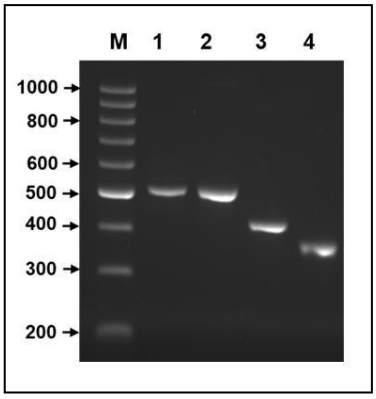

Fig. 3.2.3. Analysis of the PCR amplified FL-cDNAs of OsCSD3 SVs. PCR amplified products were analyzed on 2 % agarose gel. Lane 1: OsCSD3-SV1, lane 2: OsCSD3-SV2, lane 3: OsCSD3-SV3 and lane 4: OsCSD3-SV4. Lane M; 100 bp DNA ladder marker.

The OsCSD3-SV3 and OsCSD3-SV4 cDNAs were also cloned into *E. coli* expression vectors pET28a(+), pMAL-c5x and pTwin1. The four recombinant plasmids were transformed into *E. coli* TOP10 cells and positive clones were identified by colony PCR and confirmed by restriction analysis of plasmids. The sequence of the clones was verified by sequencing and submitted to the GenBank (Accession No.: OsCSD3-SV1; KF953542 and KF953543, OsCSD3-SV2; MW091047; OsCSD3-SV3: MW091048; OsCSD3-SV4: MW091049). The recombinant pET28a(+) plasmid containing OsCSD3 splice variant cDNAs were designated as pET28a-OsCSD3-SV1/SV2/SV3/SV4 and a similar scheme was

followed for expression plasmids pMAL-c5x and pTwin1.

3.2.6. Sequence analysis of NSICRc106 OsCSD3 splice variants

The of NSICRc106 OsCSD3-SV1 cDNA sequence showed two variations (270^{th} and 451^{th} positions) compared to Nipponbare sequence (RGAP-MSU). A single variation was present in other three SVs; SV3 (355^{th} position) and in SV2 and SV4 (270^{th} position). This resulted in minor sequence heterogeneity in OsCSD3-SVs of the two genotypes (% identity: SV1; 99.59 %, SV2; 99.79 %, SV3; 99.74 % and SV4; 99.71 %). Variation at 270^{th} position is a silent mutation, whereas change at 451^{th} in OsCSD3-SV1 (and 355^{th} in OsCSD3-SV3) position changed alanine to threonine. Hence, OsCSD3-SV1 (A151T) and OsCSD3-SV3 (A119T) showed 99.39 % and 99.24 % identity to Nipponbare sequences, while OsCSD3-SV2 and OsCSD3-SV4 showed 100% identity. The OsCSD3-SVs showed variation in length (116-164 aa) and predicted molecular weight (11.8-16.5 kDa) of the encoded protein isoforms.

3.2.7. Overexpression and purification of OsCSD3 splice variant protein isoforms

The recombinant pET28a(+) plasmids containing OsCSD3-SV cDNAs were transformed into *E. coli* BL-21(DE3) for overexpression of recombinant proteins, as described in material and methods (**Section 2.2.13.2**). Overexpression of rice proteins was optimized by varying the induction temperature (20-37 °C) and IPTG concentration (0.1-1 mM IPTG). Under optimized conditions (temperature: 20 ºC, 0.1 mM IPTG, time: 16 h) all the four OsCSD3 SV isoforms were successfully overexpressed and showed expected sized proteins (OsCSD3-SV1: ~18.7 kDa, OsCSD3-SV2: ~18.9 kDa, OsCSD3-SV3: ~15.3 kDa and OsCSD3-SV4: ~14 kDa)

(**Fig. 3.2.4A**). For comparative analysis, initially purification and characterization of the OsCSD3-SV1 (constitutive isoform, not characterized previously) was carried out. The OsCSD3-SV1 isoform was purified to near homogeneity from the soluble fraction of cell lysate using Ni-NTA affinity chromatography (**Fig. 3.2.4B**). The protein was further purified by gel-filtration chromatography and used for analysis.

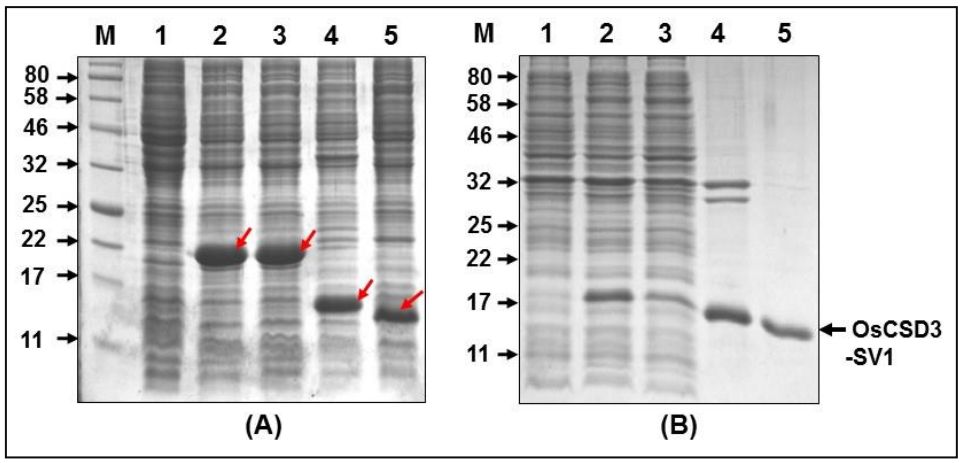

Fig. 3.2.4. Heterologous expression of OsCSD3 SV isoforms in *E. coli* BL-21 (DE3). BL-21(DE3) cells containing pET28a(+) or pET28a-OsCSD3-SVs (SV1/SV2/SV3/SV4 cDNAs) were induced and total protein isolated and analyzed on 15 % denaturing polyacrylamide gel. **(A)** Expression of OsCSD3 SV isoforms. Lane 1; pET28a (+), lane 2; pET28a-OsCSD3-SV1, lane 3; pET28a-OsCSD3-SV2, lane 4; pET28a-OsCSD3-SV3, lane5; pET28a-OsCSD3-SV4. Lane M: Protein molecular weight standards in kilodaltons (kDa). Red arrows indicate the overexpressed OsCSD3 isoform bands. **(B)** Expression and purification of OsCSD3-SV1 isoform. Lane 1 and 2; uninduced and induced total cell lysate of BL-21(DE3) containing pET28a-OsCSD3-SV1, Lane 3 and 4; soluble and pellet fraction of induced BL-21(DE3) pET28a-OsCSD3-SV1, lane 5; Ni-NTA affinity purified OsCSD3-SV1. Lane M: Protein molecular weight standards in kilodaltons (kDa).

3.2.8. Biophysical characterization of OsCSD3 SV1 isoform

3.2.8.1. OsCSD3-SV1 isoform exists as a homodimer in native state

On gel-filtration, the OsCSD3-SV1 isoform was eluted as single peak and corresponding to ~36 kDa native molecular weight (**Fig. 3.2.5A and 3.2.5B**). Analysis on denaturing PAGE showed a single band corresponding to subunit size of ~18 kDa **(Fig. 3.2.5C)**. These results show that the protein exists as homodimer.

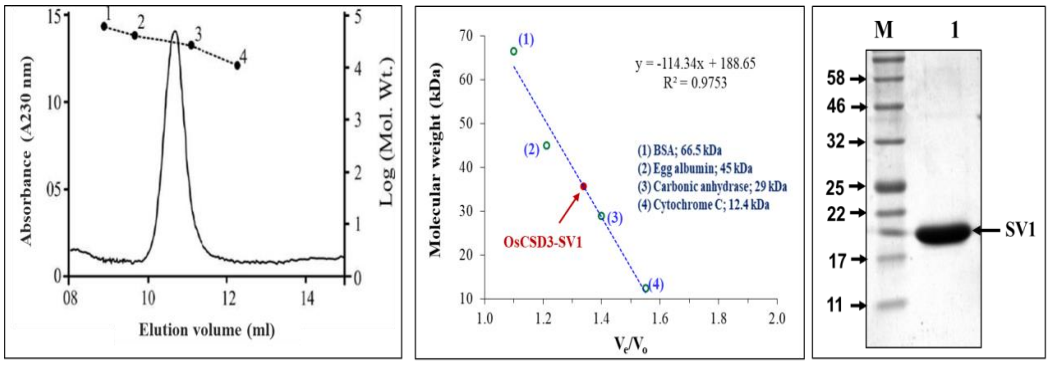

Fig. 3.2.5. Determination of native and subunit molecular weight of OsCSD3-SV1 isoform. (A) Recombinant OsCSD3-SV1 was subjected to gel-filtration chromatography on Superdex 75 10/300 GL column. **(B)** A calibration plot of molecular weight of the standard proteins versus their respective V_e /V_o values (V_e: elution volume, V_o: void volume) was plotted. Positions of the protein standards used and OsCSD3-SV1 are indicated in the figure. **(C)** Analysis of gel filtration fraction on 15 % denaturing PAGE. Lane 1; gel-filtration purified fraction of OsCSD3-SV1. Lane M: Protein molecular weight standards in kilodaltons (kDa).

3.2.8.2. OsCSD3-SV1 isoforms shows spectral features similar to Cu/Zn SODs

The spectrum characteristic of OsCSD3-SV1 isoform were analyzed in UV and visible wavelength range. The protein contained a single tyrosine (Tyr-37),

phenylalanine residues at six positions (Phe: 29, 30, 54, 59, 73, and 107), but no tryptophan (Trp). Spectral analysis range showed specific peaks (between 250-270 nm) associated with the aromatic amino acids (**Fig. 3.2.6A**), and evidence of electronic transitions around ~620-680 nm (indicative of *d-d* electronic transition for Cu^{2+} coordination) and ~380-410 nm (ligand-to-metal interaction between imidazole ring of the His-62 and Cu^{2+}) (**Fig. 3.2.6B**). Circular Dichroism (CD) analysis indicated high β-sheet content and low α-helix content in the SV1 isoform (**Fig. 3.2.6C**).

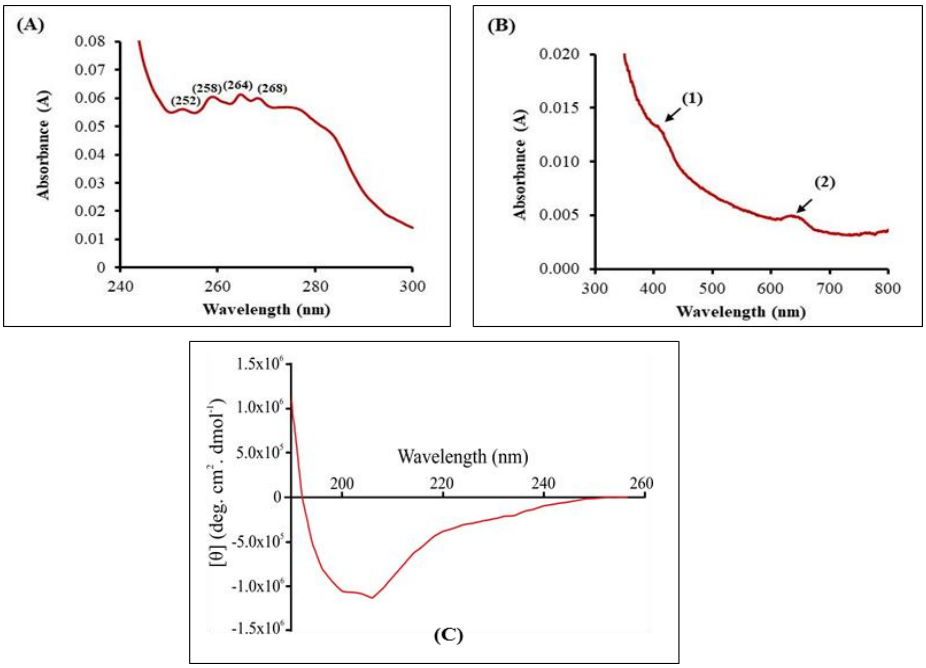

Fig. 3.2.6. UV and Visible spectroscopic analysis of OsCSD3-SV1 isoform. (A) UV absorption spectra of OsCSD3-SV1 from wavelength 240 nm to 300 nm. Peaks associated with aromatic amino acids (Phe and Tyr) are indicated. **(B)** Absorption spectra of OsCSD3-SV1 in from wavelength 300 nm to 800 nm. Peaks indicative of electronic transitions are indicated with arrows: 1) indicates ligand-to-metal transition and 2) indicates *d-d* electronic transition for Cu^{2+} coordination. (**C**) Circular Dichroism (CD) spectra of OsCSD3-SV1 isoform (wavelength range: 190–260 nm).

3.2.8.3. Structural thermostability analysis by Differential Scanning Fluorimetry (DSF)

The OsCSD3-SV1 isoform was analyzed for structural stability by DSF analysis that monitors increase in binding of SYPRO Orange dye, as a function of temperature, and is reflected in terms of unfolding /melting temperature of the protein (Tm). DSF revealed that the OsCSD3-SV1 is thermostable with the Tm value of 75.5 °C **(Fig. 3.2.7).**

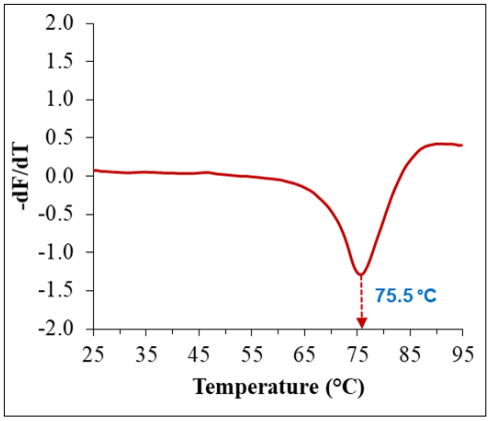

Fig. 3.2.7. Effect of temperature on structural stability of OsCSD3-SV1 isoform. Structural unfolding of the protein was measured by continuous acquisition of SYPRO Orange fluorescence (Excitation: 465 nm, Emission: 580 nm) with increasing temperature (25- 95 °C, ramp rate; 0.04 °C s^{-1}). The data was transformed into first derivative to estimate the unfolding/melting temperature (Tm) of the protein (indicated by vertical arrow).

3.2.9. Biochemical characterization of OsCSD3-SV1 isoform

3.2.9.1. OsCSD3-SV1 isoform is enzymatically active

The OsCSD3-SV1 isoform was analyzed for biochemical characteristics using NBT reduction based SOD activity assays, as detailed in **section 2.2.18.1**.

Zymogram analysis on native PAGE showed that OsCSD3-SV1 is enzymatically active. Spectrophotometric analysis showed that OsCSD3-SV1 has specific activity 1030 ± 90 U mg^{-1} ml^{-1} (**Fig. 3.2.8A**). Analysis on denaturing PAGE showed that protein is tolerant to SDS, but is sensitive to β-merceptoethanol treatment that suggest importance of disulfide bond in functional conformation of protein (**Fig. 3.2.8B**).

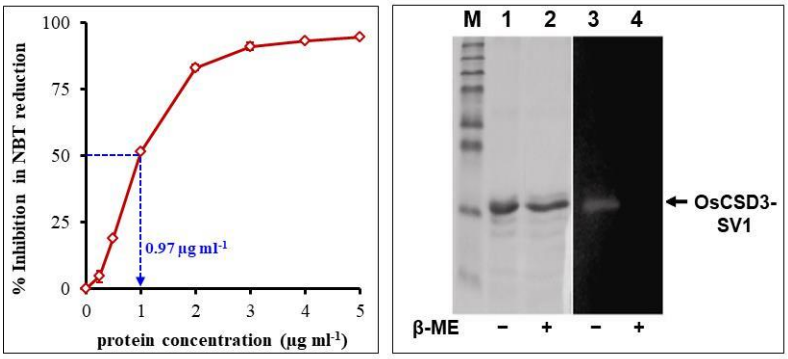

Fig. 3.2.8. Spectrophotometric and in-gel SOD activity analysis of OsCSD3-SV1 by NBT reduction assay. (A) SOD activity was measured spectrophotometrically by taking the increasing concentration (0-5.0 µg ml^{-1}) of protein in the assay. Vertical arrow indicates the protein concentration for inhibition of NBT reduction by 50 % (equivalent to 1 U SOD). **(B)** In-gel SOD activity assay of OsCSD3-SV1 isoform in the absence/presence of β-mercaptoethanol (β-ME). Lanes 1, 3 contained control protein (no β-ME treatment), lanes 2, 4 treated with β-ME, and lane M: protein Mw standards (kDa). Arrow indicates the position of the OsCSD3-SV1 isoform.

3.2.9.2. OsCSD3-SV1 isoform showed SOD inhibitor profiles like Cu/Zn SODs

Effect of SOD inhibitors on activity of OsCSD3-SV1 isoform was investigated using NBT-reduction assay described in **section 2.2.18.1**. The OsCSD3-SV1 isoform showed differential response to inhibitors. DDC inhibited the SOD activity of OsCSD3-SV1 in a concentration dependent manner, with complete inhibition at 2 mM

DDC (IC_{50}: 0.4 mM), which is typical of a Cu/Zn type SOD. The OsCSD3-SV1 was relatively insensitive to H_2O_2 (IC_{50} ~7.6 mM) as it retained >20 % activity even at 10 mM H_2O_2. The protein remained unaffected by NaN_3 up to 10 mM. Collectively these results showed that the OsCSD3-SV1 is a Cu/Zn type SOD (**Fig. 3.2.9**). The ICP-MS analysis confirmed that protein in indeed a Cu/Zn SOD with single Cu^{2+} and Zn^{2+} metal ion per subunit (Cu^{2+} ion; 0.905 ± 0.18 and Zn^{2+} ion; 0.945 ± 0.16 per subunit).

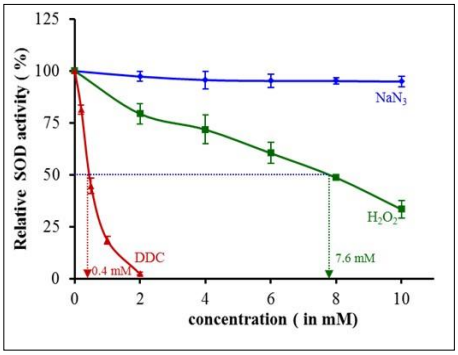

Fig. 3.2.9. Analysis of effect of SOD inhibitors on activity of OsSCD3-SV1 isoform. OsCSD3-SV1 isoform (1U equivalent) was treated with DDC (0.0–2.0 mM), H_2O_2 (0.0–10.0 mM) and NaN_3 (0.0–10.0 mM) for 30 min at 25 °C. Relative SOD activity was estimated by considering activity at 0 mM inhibitor concentration as 100 %. Vertical arrows indicate IC_{50} values for DDC and H_2O_2. Data are represented as mean ± SD of three independent replicates.

3.2.9.3. Effect of pH on activity and stability of OsCSD3-SV1 isoform

Analysis of SOD activity of the OsCSD3-SV1 isoform in different buffers showed that the optimum pH of the enzyme is 9.0, however it showed 60-80 % of activity from pH 7.0-10.8 **(Fig. 3.2.10A).** Effect of pH on the stability of OsCSD3-SV1 isoform showed that the protein was relatively stable and loss of activity as a function of time was comparable from pH 7.0-10.0. However, beyond pH 10.0, loss of

activity was high and the protein retained < 40 % activity after pre-incubation of 24 h (**Fig. 3.2.10B**).

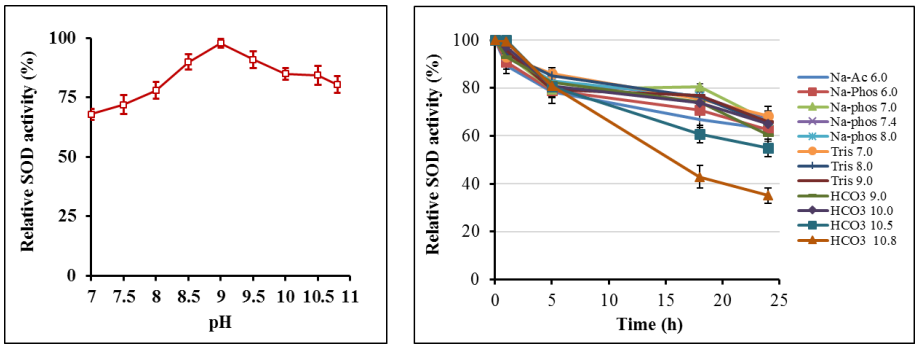

Fig. 3.2.10. Effect of pH on SOD activity and stability of OsCSD3-SV1 isoform. One unit (1 U) equivalent of purified protein was used for analysis **(A)** Effect of pH on the activity: SOD activity of the protein was assayed in different pH buffers (50 mM; pH 7-10.8). Relative SOD activity was estimated by considering maximum activity as 100 %. **(B)** Effect of pH on stability: Protein was pre-incubated in different buffers (pH range, 7.0-10.8) for 0-24 h. Activity was assayed using standard SOD assay. Relative SOD activity was measured considering activity at 0 h (before pre-incubation) as 100 %. Data are represented as mean ± SD of three independent replicates.

3.2.9.4. Rice OsCSD3-SV1 isoform showed higher thermostability

The effect of temperature on thermal inactivation of OsCSD3-SV1 was evaluated in term of residual SOD activity remains after pre-incubation at different temperatures (20- 80 °C). When pre-incubated for 1 h, OsCSD3-SV1 isoform showed tolerance to thermal inactivation with no substantial loss of activity up to 50 ºC and complete loss at 70 ºC, with a $T_{1/2}$ value (temperature at which 50 % activity was lost)

of 62 ºC. However, at lower pre-incubation time (20 min or 40 min) the rice protein retained 20 % activity even at 80 ºC (**Fig. 3.2.11A**).

3.2.9.5. OsCSD3-SV1 exhibits bicarbonate dependent peroxidase activity

Superoxide dismutases are also reported to harbor bicarbonate dependent peroxidase activity. For OsCSD3-SV1 isoform, the peroxidase activity was assessed by monitoring enzyme-mediated oxidation of dichlorodihydrofluorescein (DCFH) to dichlorofluorescein (DCF) as detailed in **section 2.2.18.5**. Results showed that OsCSD3-SV1 harbor bicarbonate dependent peroxidase activity (**Fig. 3.2.11B**).

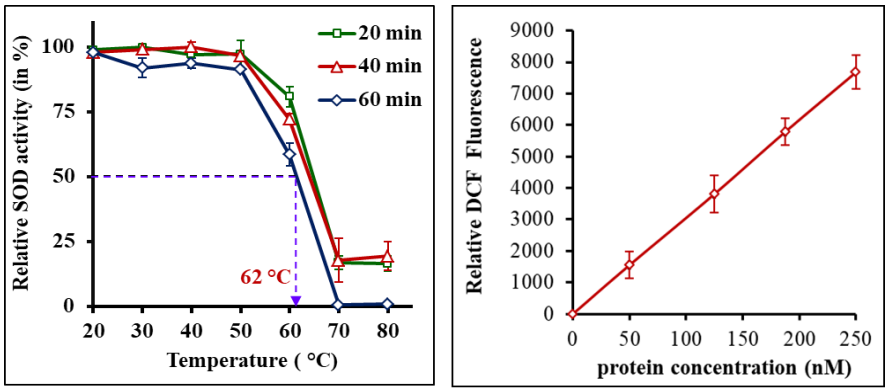

Fig. 3.2.11. Analysis of thermostability and peroxidase activity of OsCSD3-SV1 isoform. (A) Analysis of thermostability of OsCSD3-SV1: Protein (1 U equivalent) was incubated at different temperatures (20–80°C). Aliquots were removed at 20, 40 and 60 min and assayed for SOD activity. Relative SOD activity was estimated by considering activity at 0 h time-point as 100 %. Vertical arrow the indicates $T_{1/2}$ value. Data are represented as mean ± SD of three independent replicates. **(B)** Bicarbonate dependent peroxidase activity of OsCSD3-SV1: Peroxidase activity of protein was measured by estimation of DCF (excitation/emission wavelength: 524/ 480 nm) formation in presence of bicarbonate and H_2O_2. Data are represented as mean ± SD of three independent replicates.

3.2.10. OsCSD3-SV1 isoform enhanced oxidative stress tolerance of wild type and *sod* double mutant *E. coli* cells

SODs confer protection to the cellular components against oxidative damage. The ability of rice OsCSD3-SV1 isoform to protect *E. coli* cells from methyl viologen (MV) mediated oxidative stress was investigated. Growth of *E. coli* BL-21(DE3) cells containing pET28a(+) (empty vector) or pET28a-OsCSD3-SV1 was evaluated in the presence increasing MV concentration (0-0.2 mM) by spot assay and measuring the culture OD at absorbance ($A_{600\ nm}$). Analysis showed that over-expression of OsCSD3-SV1 considerably enhanced the oxidative stress tolerance of BL-21(DE3) cells till 0.2 mM MV (**Fig. 3.2.12A and B**).

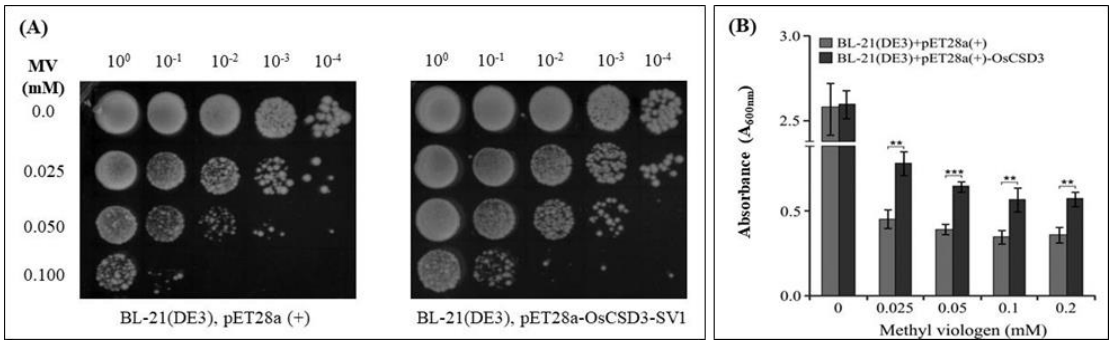

Fig. 3.2.12. Analysis of oxidative stress tolerance in wild type *E. coli* BL-21 (DE3) expressing OsCSD3-SV1 isoform. Growth of BL-21(DE3) cells containing pET28a(+) or pET28a-OsCSD3-SV1 in presence of MV was monitored by **(A)** Spot assay and **(B)** Spectrophotometrically by measuring absorbance ($A_{600\ nm}$). The experiment was repeated three times and data are represented as mean absorbance ($A_{600\ nm}$) ± SD of three replicates. Statistical analysis was carried out by Student's t-test, and significant differences are indicated by **P < 0.01, ***P < 0.001.

As wild type *E. coli* cells contain inherent SODs (e.g. SOD-A and SOD-B contributes ~98% of total SOD activity) (**Fig. 3.2.13A**), the analysis was also extended to *E. coli sod* double knockout (*ΔsodA ΔsodB*) mutant generated as per protocol detailed in **section 2.2.20**. Loss of inherent SOD-A and SOD-B activities in the *E. coli sodA sodB* double mutant was confirmed by in-gel SOD assay (**Fig. 3.2.13A**). Growth analysis of the double mutant in presence of MV (0-0.5 mM) confirmed that it is highly sensitive to MV treatment (**Fig. 3.2.13B**). Direct analysis

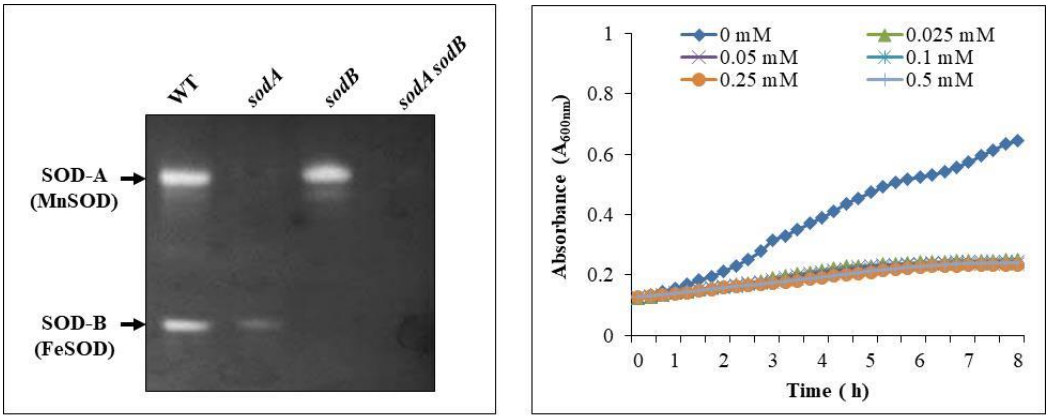

Fig. 3.2.13. Validation of loss of SOD activities in *sodA sodB* double mutant and analysis of sensitivity to MV treatment. (A) Zymogram analysis of total protein isolated from *E. coli* BW25113 wild type and *sod* mutant cultures were performed as described in **section 2.2.18.1**. Lane WT denotes BW25113 wild type, lane *sodA*, *sodB* and *sodA sodB* denotes corresponding BW25113 *sod* mutants. **(B)** *E. coli* BW25113 *sod* double mutant (*sodA sodB*) culture (OD_{600} ~0.15) was grown with increasing concentration of MV (0- 0.5 mM) at 25 °C. Culture growth was monitored by measuring absorbance ($A_{600\ nm}$). Data are represented as mean ± SD of three independent replicates.

of the *sod* double mutant using the plasmid construct used for stress tolerance of BL-21(DE3) was not feasible. The pET28a-OsCSD3-SV1 construct is compatible for heterologous expression in *E. coli* BL-21(DE3) expression host, but not for *E. coli sod* double mutant as it lacked T7 RNA polymerase dependent overexpression and contains selection marker (kanamycin) similar to pET28a(+). Hence, plasmid vector pMAL-c5x (containing MBP tag) that was suitable for T7 RNA polymerase independent expression and contained ampicillin selection marker was used. Also, N-terminal MBP tag enhances the solubility of the recombinant OsCSD3-SV1. Plasmid pMAL-c5x (empty plasmid) or pMAL-c5x-OsCSD3-SV1 were transformed into *sod* double mutant cells, induced with 0.5 mM IPTG and the activity of the MBP-OsCSD3-SV1 fusion protein was confirmed by Zymogram (**Fig. 3.2.14A**). Growth of *sod* double mutant cells containing pMAL-c5x and pMAL-c5x-OsCSD3-SV1 was monitored in the presence of increasing MV concentration (0-0.025 mM). The double mutant showed enhanced tolerance at 0.01 mM MV (**Fig. 3.2.14B and C**).

The *sod* double mutant was also evaluated for oxidative stress induced lipid peroxidation. Methyl viologen treatment resulted in increased lipid peroxidation in the *sod* double mutant. However, the cells expressing MBP-OsCSD3-SV1 protein showed substantial reduction in lipid peroxidation (**Fig. 3.2.15**).

These results show that the OsCSD3-SV1 isoform is able to protect the *E. coli* cells from the MV-mediated oxidative damage.

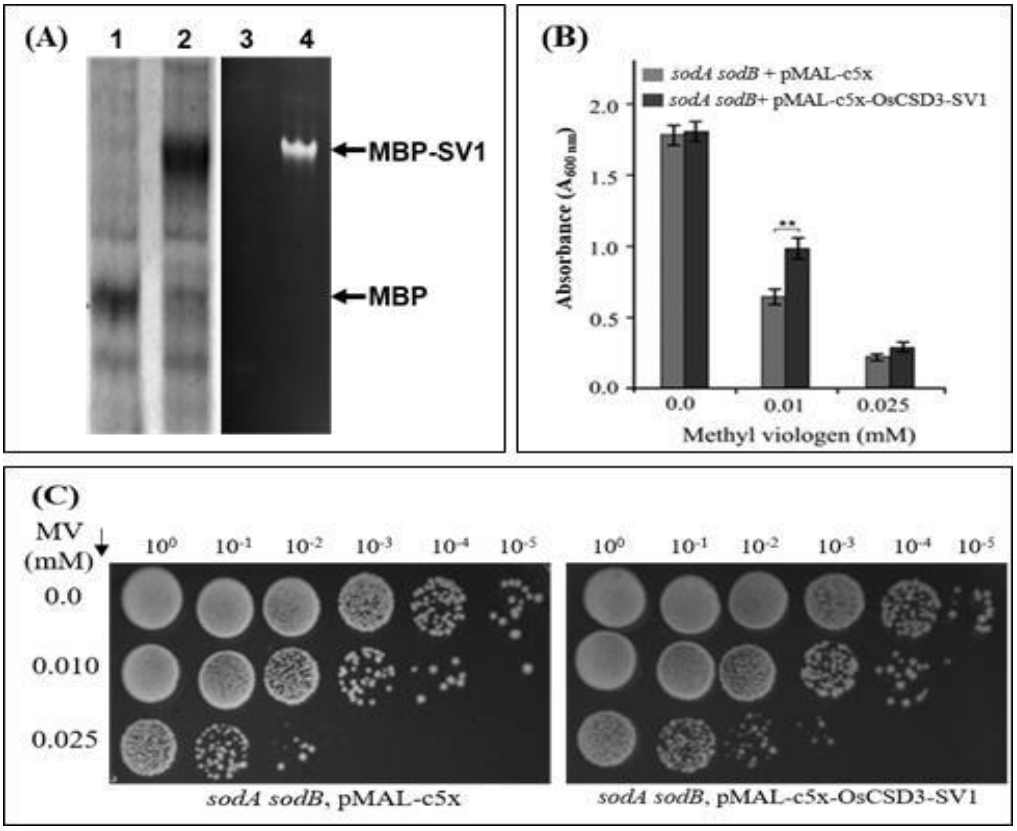

Fig. 3.2.14. Analysis of oxidative stress tolerance of *E. coli* BW25113 *sodA sodB* double mutant expressing OsCSD3-SV1 isoform as MBP fusion. (A) Zymogram analysis of total protein isolated from IPTG induced *sodA sodB* double mutant cells carrying pMAL-c5x (vector control) or pMAL-c5x-OsCSD3-SV1. Lane 1 and 3; correspond to *sodA sodB* pMAL-c5x (vector control), lane 2 and 4; *sodA sodB* pMAL-c5x-OsCSD3-SV1. Position of MBP and MBP-OsCSD3-SV1 isoform are indicated by arrows. **(B) and (C)** Comparison of growth of IPTG induced *E. coli sod* double-mutant cells containing pMAL-c5x (empty vector) or pMAL-c5x-OsCSD3-SV1 treated with MV at 25 °C, by measuring absorbance ($A_{600\ nm}$) and Spot assay respectively. Data are represented as mean absorbance ($A_{600\ nm}$) ± SD of three independent replicates. Statistical significant values are indicated by '*' (**P < 0.01).

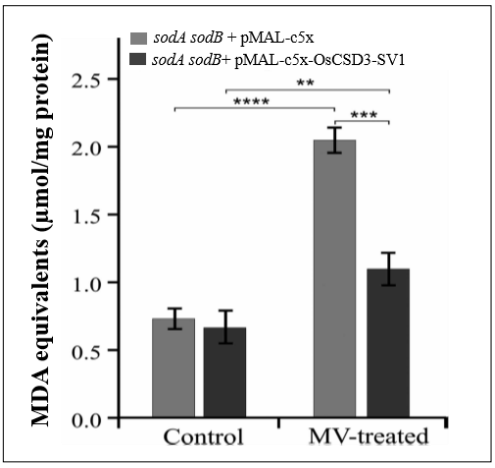

Fig. 3.2.15. Lipid peroxidation analysis in *E. coli sodA sodB* mutant cells. *E. coli sodA sodB* mutant cells carrying either pMAL-c5x or pMAL-c5x-OsCSD-SV1 in absence/presence to MV. Data are represented as mean MDA equivalents ± SD of three independent replicates. Statistical significant differences are indicated by '*' (**P < 0.01, ***P < 0.001 and ****P < 0.0001).

3.2.11. Homology model show conserved structural features in OsCSD3-SV1

The homology model of OsCSD3-SV1 was generated using *Solanum lycopersicum* Cu/Zn SOD crystal structure (PDB ID: 3PU7) as template. The two sequences showed 64 % identity. The template structure, refined to 1.8 Å resolution, included both Cu and Zn co-factors. OsCSD3-SV1 homology model was a homodimer covering the residue range 19-160 (QMEANscore4: 0.782; QMEAN4-Z-score: -0.21), and showed the Greek-key β-barrel structural core typical of Cu/Zn SODs. The alpha carbons (residues 19-31, 37-160) of both the chains of the model were superposed onto the corresponding residues of the template, thus omitting a beta turn where there is an insertion of a proline residue in case of rice model (**Fig. 3.2.16A**). Structural superposition showed that the positions of active site residues

(His55, His57, His72, His129, His 80, His89 and Asp92), involved in coordination with the metal co-factors (Cu and Zn), two cysteine (Cys66 and Cys155, involved in intra-subunit disulfide bond) and catalytically important second-sphere residues (Asp133 and Arg152) were highly conserved. The two structures superposed to a *root-mean square deviation (RMSD)* of 0.08 Å. After the superposition, active site of the model could very well accommodate both the metal cofactors (Cu and Zn) from the template (**Fig. 3.2.16B**).

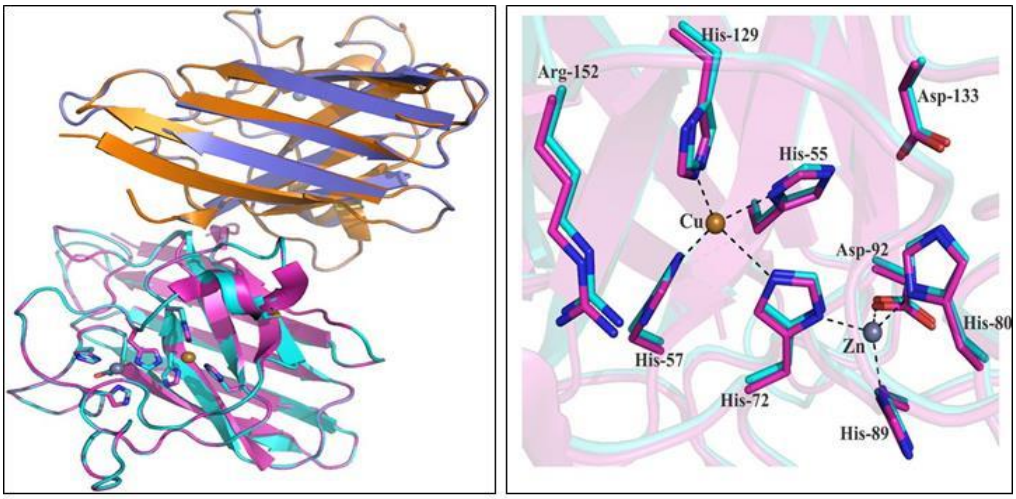

Fig. 3.2.16. Homology model of OsCSD3-SV1 isoform generated using SWISS-MODEL work-space. (A) Predicted homology model (shown as homodimer) of rice OsCSD3-SV1 isoform superimposed with the template Cu/Zn SOD structure (PDB ID: 3PU7) from *S. lycopersicum*. Figures of the molecular models was made using PyMOL program. Two chains of the dimer are shown in cyan and slate color in case of the rice model while those are shown in magenta and orange color in case of the template. **(B)** Enlarged view of the active site region showing histidine and aspartate residues involved in the Cu and Zn coordination. Rice protein residues are shown in cyan carbons, whereas template residues are shown in magenta carbons.

The rice OsCSD3-SV1 isoform was enzymatically active, homodimeric protein that showed thermostability and tolerant to H_2O_2 and could protect the *E. coli* cells from oxidative stress. Properties of other three alternative isoforms (SV2, SV3 and SV4) having large variations were investigated to know the significance in functioning of OsCSD3.

3.2.12. Strategies for enhancing solubility of OsCSD3 alternative isoforms

Over-expression of OsCSD3 alternative isoforms (OsCSD3-SV2, OsCSD3-SV3 and OsCSD3-SV4) with optimized expression conditions (used in OsCSD3-SV1) in BL-21(DE3):pET28a(+) system was not successful and the three isoforms were always present in the inclusion bodies. As an example, results of OsCSD3-SV2 are shown in **Fig. 3.2.17**. Other two alternative isoforms (OsCSD3-SV3 and OsCSD3-SV4) were also present in the inclusion bodies. Different strategies (variation in expression conditions, different *E. coli* expression hosts, fusion tags, chaperone assisted folding etc.) were attempted to enhance the solubility of the three OsCSD3 alternative isoforms (**Table 2.8**). The OsCSD3-SV1 isoform was also expressed using similar conditions and purified for comparative analysis with alternative isoforms.

3.2.12.1. OsCSD3 alternative protein isoform expression as intein fusion

Second approach involved use of expression vector pTwin1 (contain an intein tag), which has pH-dependent self-cleavage property, and also helps in enhancing solubility of fusion protein. At optimized expression conditions, the OsCSD3 alternative isoforms (OsCSD3-SV2, OsCSD3-SV3 and OsCSD3-SV4), were successfully expressed as soluble fusion proteins. However, subsequent pH-dependent

cleavage of intein tag showed issues related to incomplete cleavage and protein aggregation during purification.

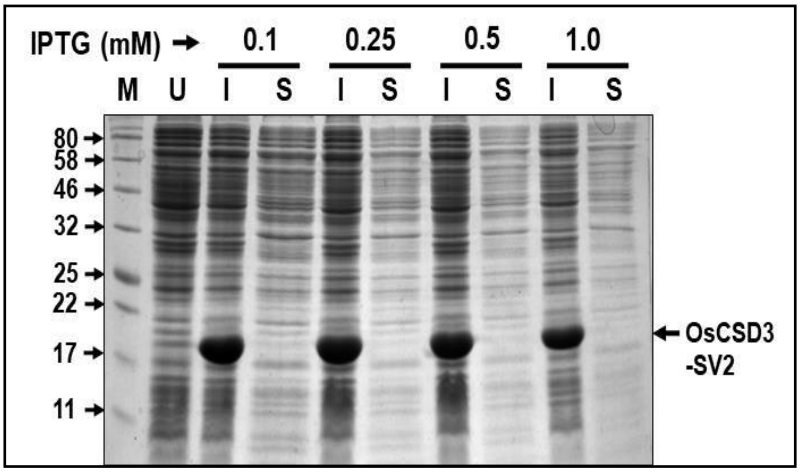

Fig. 3.2.17. Overexpression of OsCSD3-SV2 isoform. Expression of BL-21(DE3) cells carrying pET28a-OsCSD3-SV2 with different IPTG (0.1-1.0 mM) concentration at 20 °C**.** Total protein from different fractions was isolated. Lane U; uninduced, I; induced; and S; soluble fraction. Lane M denotes the protein Mw standards (kDa). Arrow indicates the position of the OsCSD3-SV2 protein.

3.2.12.2. Co-expression of OsCSD3 isoforms with chaperones

Chaperone co-expression based approach was also attempted for *in vivo* folding of OsCSD3 alternative isoforms. Co-expression of individual pET28a-OsCSD3-SVs with five different chaperone containing plasmids (pGro7, pTf16, pG-Tf2, pKJE7 and pG-KJE8) was carried out in BL-21(DE3) *E. coli* cells as detailed in **section 2.2.14.2** and **Table 2.7**. In case of OsCSD3-SV2 isoform, analysis of different fractions of cell lysate showed an appreciable amount of protein in soluble fraction when co-expressed along with pKJE7, pG-KJE8, pTf16, pG-Tf2 (**Fig. 3.2.18A and 3.2.18B**). The three isoforms, OsCSD3-SV2, OsCSD3-SV3 and OsCSD3-SV4, were

overexpressed at optimized conditions and affinity purified. However, denaturing PAGE analysis showed that OsCSD3-SV2 isoforms co-eluted with chaperone DNaseJ (40 kDa) (**Fig. 3.2.19A**). Gel-filtration analysis showed a single absorbance peak, which on further confirmation showed that the chaperone was associated with OsCSD3-SV2 (**Fig. 3.2.19B**). Similar results were observed for other two alternative isoforms (SV3, SV4) of OsCSD3.

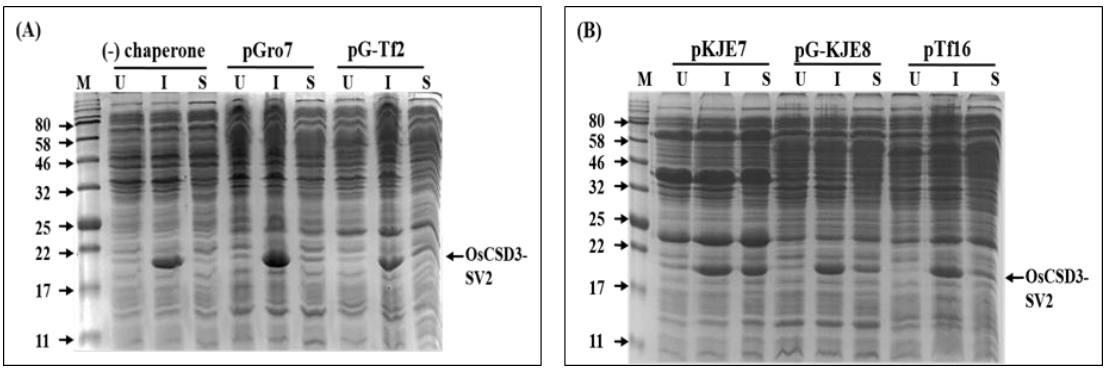

Fig. 3.2.18. Chaperone assisted folding of OsCSD3-SV2 isoform in BL-21 (DE3). BL-21 (DE3) cells carrying pET28a-OsCSD3-SV2 were co-expressed with five different chaperones **(A)** and **(B)** and the total protein from insoluble and soluble fractions was analyzed by denaturing PAGE. Lane U, I and S corresponds to total isolated protein from uninduced, induced culture and soluble fraction respectively. The names of the chaperone plasmids used are indicated on top of the lanes. Arrow indicates the position of OsCSD3-SV2 isoform.

3.2.12.3. Overexpression of OsCSD3 alternative isoforms as maltose binding protein (MBP) fusion

Overexpression of OsCSD3-SV1 isoform as MBP-fusion yielded soluble protein that was also enzymatically active (**Fig. 3.2.14A**). Hence, other three

alternative isoforms (OsCSD3-SV2, OsCSD3-SV3 and OsCSD3-SV4) were also cloned in pMAL-c5x expression vector and overexpressed as MBP-fusion in SHuffle Express *E. coli* strain. All the three OsCSD3 alternative isoforms (as MBP-fusion) were present in the soluble fraction (**Fig. 3.2.20**). All spliced isoforms were successfully purified to near homogeneity and were used for further analysis **(Fig. 3.2.21A and 3.2.21B).**

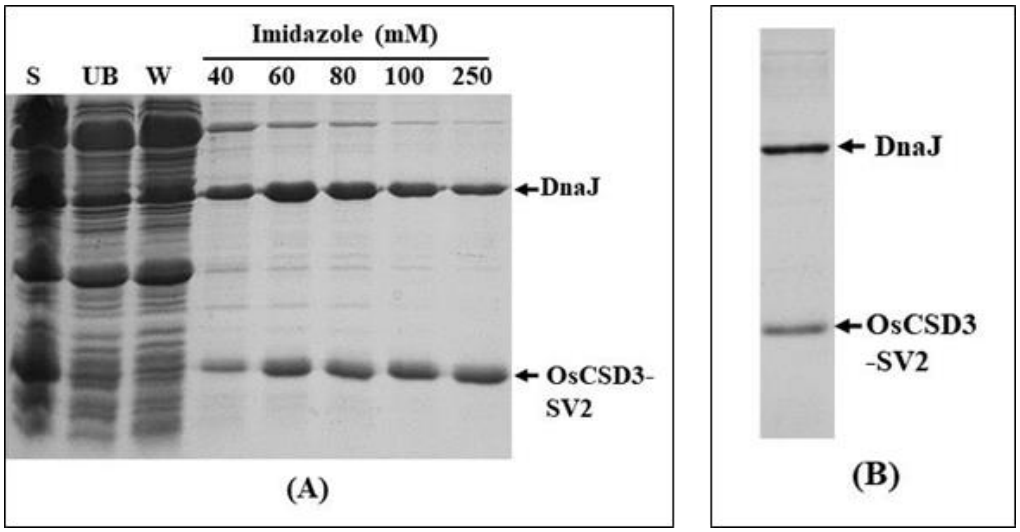

Fig. 3.2.19. Expression and purification of OsCSD3-SV2 isoform. (A) BL-21(DE3) cells carrying pET28a-OsCSD3-SV2 with chaperone plasmid pKJE7 were induced. Soluble fraction was isolated and protein was purified using Ni-NTA chromatography. Lane S, UB and W correspond to soluble fraction, unbound and washing flow through fraction respectively. Lane 40-250; corresponds to the protein fraction eluted with mentioned imidazole concentration (mM). Arrow indicates the position of OsCSD3-SV2 and DnaJ chaperone. **(B)** Denaturing PAGE analysis of gel filtration purified protein fraction of OsCSD3-SV2 overexpressed in the presence of DnaJ chaperone. Arrow indicates the position of OsCSD3-SV2 and chaperone protein (DnaJ).

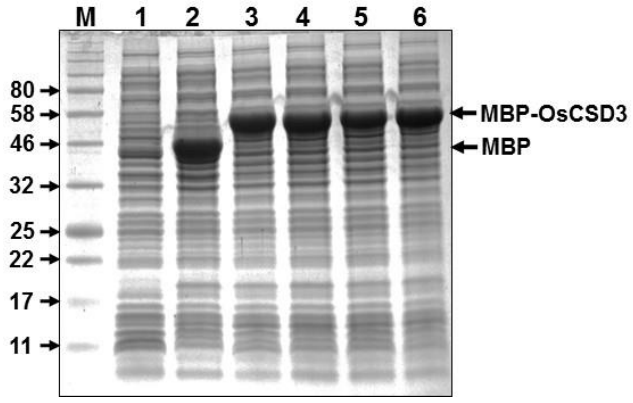

Fig. 3.2.20. Expression of OsCSD3 isoforms as Maltose binding protein (MBP) fusion. SHuffle Express cells carrying pMAL-c5x (empty vector) or pMAL-c5x-OsCSD3-SVs were expressed and total protein from different cultures was isolated. Lane 1; Uninduced and lane 2; soluble fraction of induced SHuffle Express containing pMAL-c5x, lane 3-6, soluble fraction isolated from induced culture of SHuffle Express pMAL-c5x-OsCSD3-SV1, -SV2, -SV3 and -SV4. Lane M indicates protein Mw standards (in kDa). Arrow indicates the position of MBP and MBP-OsCSD3 splice isoforms.

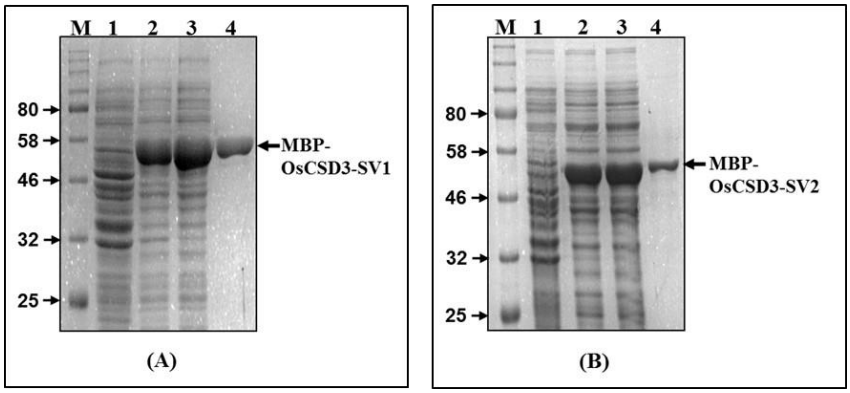

Fig. 3.2.21. Expression, purification of MBP-OsCSD3-SV1 and MBP-OsCSD3-SV2 isoform. Expression and purification of **(A)** MBP-OsCSD3-SV1 isoform and **(B)** MBP-OsCSD3-SV2 isoform. Lane 1 and 2; uninduced and induced. Lane 3; soluble fraction and lane 4; amylose affinity chromatography purified fraction. Lane M denotes the protein Mw standards (in kDa). Arrow indicates the position of the MBP-OsCSD3-SV1/-SV2 isoforms.

3.2.12.4. Analysis of SOD activity of MBP-OsCSD3-SV protein isoforms

All the four purified MBP-OsCSD3-SV isoforms were analyzed for SOD activity. Results showed that only MBP-OsCSD3-SV1 harbor SOD activity, whereas no SOD activity was observed in alternative OsCSD3-SV isoforms (**Fig. 3.2.22**). This could be attributed to lack of important residues/regions due to AS-mediated major differences in the exon organization (**Fig.3.2.2**).

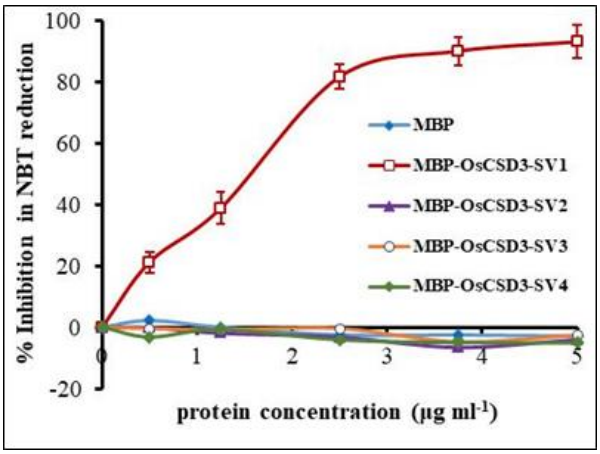

Fig. 3.2.22. Analysis of SOD activity of MBP-OsCSD3 isoforms. Increasing protein concentration (0-5 µg ml^{-1}) was taken and SOD activity of the OsCSD3 isoforms was measured by NBT reduction assay. Maltose binding protein (MBP) was used as negative control in the assay. Data represents the mean ± SD of three independent replicates.

3.2.13. Discussion

Peroxisomes are important for different cellular functions, however there are relatively few reports of characterization of peroxisomal CSDs compared to chloroplastic and cytosolic isoforms. In rice locus LOC_ Os03g11960, that codes for OsCSD3 and generates four splice variants (SVs) with major variations in UTRs, exons or both. Sequence and protein characteristics showed that OsCSD3 is similar to

plant peroxisomal SODs. Initially, OsCSD3-SV1 isoform was characterized for comparative analysis with other isoforms.

OsCSD3-SV1 showed conserved residues at structurally and functionally important sites, with N-terminal length variations and sequence variations across the protein. Such amino acid variations are known to affects several characteristics CSDs viz. stability, oligomerization dynamics, enzyme activity [136,260,305]. Although, OsCSD3-SV1 was found to be a homodimeric protein with spectral signatures typical of a functional Cu/Zn SODs, it showed certain remarkable properties (stability to wide pH range, thermal stability and high H_2O_2 tolerance). Peroxisomal CSD isoforms are generally more thermostable [304,306], as also observed for OsCSD3-SV1and was attributed to the presence of higher β-sheet content, which was confirmed by the CD analysis. Homology model confirmed that β- pleated sheets forms a highly stable Greek-key fold, generally seen in CSDs [260,305]. The protein also exhibited bicarbonate dependent peroxidase activity, as seen in CSDs from some other plants [136,260].

High H_2O_2 tolerance of OsCSD3-SV1 further suggested its peroxisomal nature as the peroxisomal proteins are generally adapted for higher H_2O_2 levels [304]. The isoform was substantially active at alkaline pH and tolerant to pH induced changes, which generally affect stability/activity [136,306,307]. These characteristics makes OsCSD3 suitable for functioning in the alkaline environment of plant peroxisomes [308]. However, despite overall sequence similarity to peroxisomal SODs, the canonical C-terminal peroxisomal targeting signal 1 (PTS1) was not predicted in OsCSD3-SV1. Typical C-terminal tripeptide PTS1 signals (AKL, SKL, SSV etc.) also show heterogeneity in terms of sequence [309] and position from C-terminus

[114,310]. Hence, of C-terminal SAV as a PTS1 signal in rice may not be ruled out completely, but needs more analysis. Furthermore, N-terminal region of OsCSD3-SV1 could not be homology modeled, the possibility of its involvement in an alternative non-canonical peroxisomal signal sequence cannot be ruled out.

Being an antioxidant enzyme, SOD overexpression minimize the stress induced oxidative damage by scavenging the $O_2^{\cdot -}$ [311]. Rice OsCSD3-SV1 performed *in vivo* $O_2^{\cdot -}$ scavenging function and enhanced tolerance of wild-type and *sod* double-mutant *E. coli* cells against oxidative stress-mediated damage including lipid peroxidation. [265,305].

The OsCSD3 gene undergoes AS to generate three alternative SVs. These SV isoforms lacked important regions of the protein required to perform SOD function. Comparative activity analysis of isoforms showed that except OsCSD3-SV1 all three isoforms lack SOD function. Several mutation studies in CSDs targeting subunit interaction residues, cysteine residues and other sites has been shown to affect the protein characteristics of the mutant proteins [135,140,260,312].

In case of OsCSD3 alternative isoforms, removal of large regions mediated by AS, deleted several important resulting in loss of SOD activity. Loss of activity of OsCSD3-SV1 due to disruption of disulfide bond also indicates that it may be important in the loss of SOD function of OsCSD2-SV2. In comparison to OsCSD3-SV1, SV2 has heterogeneity in the C-terminal region (138-163) due to an AS event and different position cysteine residue (SV2; Cys-160 in place of Cys-155 in case of SV1). These changes can affect the overall confirmation of the protein leading to loss of SOD activity. Similar finding was reported in *Populus* where PtHipCSD1 (homologous to OsCSD3) produced two SVs with no SOD activity in the alternative

isoform [247]. Isoform OsCSD3-SV3 lack bridging His-72 residue and Zn^{2+} binding sites due to skipping of exon3. As both Zn^{2+} ion and His-72 are important for protein stability and pH independent behaviour of SODs, their absence may be responsible for no SOD activity in SV3 [313,314]. OsCSD3-SV4, which have lost major region of the protein due to AS, lacked one of Cu^{2+} metal ion coordination residue (His-129) and a Cys-155. Analysis of *P. atrosanguinea* Cu/Zn SOD mutant proteins have shown that active site flanking residues and cysteine residues are involved structural stability and biochemical activity of the protein [140]. Hence the OsCSD3-SV4 lacking many features is not able to retain the SOD function.

Analysis of alternative SV isoforms of OsCSD3 suggested that deletion of the active site residues, residues involved in structural stabilization of protein, are responsible for loss of SOD function of alternative isoforms. However, despite variations at different regions, which had affected the SOD function some of these splice isoforms had intact Cu^{2+} or Zn^{2+} binding residues, and dimer interface residues. Thus, these SV isoforms could perform other functions (like metal binding heteromeric interactions etc.), however, it will need further investigation.

Section 3.3

Comparative analysis of rice chloroplastic Cu/Zn SOD and its alternative isoform

3.3.1. Introduction

Chloroplasts are important cellular organelle in plant cells that perform a vital life process known as 'photosynthesis'.

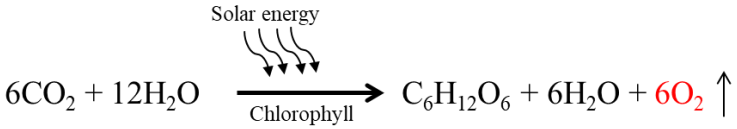

$$6CO_2 + 12H_2O \xrightarrow[\text{Chlorophyll}]{\text{Solar energy}} C_6H_{12}O_6 + 6H_2O + 6O_2 \uparrow$$

Fig. 3.3.1. Reaction of oxygenic photosynthesis

Around 2.4 billion years ago (Bya), this process originated in the primitive microbe cyanobacteria and transformed the earth's atmosphere from reducing to oxidizing [54]. Chloroplasts had originated as a result of endosymbiotic relationship between free-living photosynthetic microbes and an ancient eukaryotic host cell [119]. In plant cells, chloroplasts are one of the major sites of $O_2^{\cdot -}$ and $^1O_2$ generation [58]. Reactive oxygen species (ROS) are generated (as a byproduct) during photosynthesis due to leakage of electrons from electron transport system (ETS) to molecular oxygen, and from the overexcited chlorophyll molecules [60]. Chloroplast through ROS, relay its redox status through retrograde signaling and co-ordinate with the nucleus and other cellular organelles and regulate physiological processes and stress responses [68,315]. Environmental stress conditions (high light intensity, salinity, drought and temperature, radiation etc.) perturb the physiological ROS balance, and their excessive accumulation damage several cellular biomolecules, and also affect photosynthesis [32,60]. $O_2^{\cdot -}$ cause damage to Fe-S clusters of proteins and inhibit photosynthesis, while $^1O_2$ damage essential chlorophyll molecules and D1 protein of photosystem leading to photoinhibition [54,316]. Free iron released from damaged Fe-S proteins further participates in generation of highly reactive $^{\cdot}OH$ through Haber-Weiss/Fenton reaction and further enhance the oxidative damage [317,318]. Chloroplastic DNA is

more prone to ROS mediated damage than nuclear DNA due to its vicinity to the site of generation, and being unprotected unlike nuclear DNA [60]. Both non-enzymatic (e.g. carotenoids, Ascorbate etc.) and enzymatic (e.g. SODs, peroxidases etc.) antioxidants are present in chloroplasts to minimize ROS damage [56]. Plant chloroplasts contain multiple SODs for protection against ROS toxicity [116]. *Arabidopsis* contain two Fe-SODs (FSD2 and FSD3) and one Cu/Zn SOD (CSD2) localized to chloroplast [133,319]. Recently, a Mn SOD has also been reported to be present along with two Fe SODs and one Cu/Zn SOD, in rice chloroplasts [123]. The chloroplastic SODs exhibit some functional diversity [149,319], where CSD localized in stroma (associated with outer surface of thylakoid) prevent $O_2^{\cdot -}$ mediated damage to photosystems [319]. Genetic studies in *Arabidopsis* suggest that chloroplastic FSD and CSD have specific roles in chloroplast development and plant stress response [149]. Chloroplastic CSD levels are also regulated post-transcriptionally by miR398 to modulate responses to abiotic and biotic stress conditions [150,239]. The CSD2 knockdown lines show growth retardation, reduced chlorophyll content, and photosynthetic activity [115]. Transgenic plants overexpressing chloroplastic CSD or/and in combination with other antioxidant enzymes enhance tolerance to multiple abiotic stresses [134,150,151,320]. Furthermore, few reports have also shown role of AS in regulation/functioning of chloroplastic SODs Fe SOD in *O. sativa* [244], *Glycine max* Cu/Zn SOD [245] and *A. thaliana* Fe SOD3, [247]. Information at RGAP-MSU rice database show two splice variants of chloroplastic CSD gene, with small variation in the coding region. Although, transcript response of rice CSDs based on some RNAseq data studies is available (http://expression.ic4r.org/), the impact of AS generated coding region variation on protein function is generally lacking. This

chapter presents the results of cloning, expression, purification and biochemical and biophysical analysis of the two OsCSD2 isoforms to understand the role of AS in its regulation and functioning.

Results

3.3.2. *In silico* analysis of OsCSD2 splice variants

Rice locus LOC_Os08g44770 codes for a chloroplastic CSD (OsCSD2), and the RGAP-MSU database predicts generation of two splice variants (SVs), OsCSD2-SV1 (constitutive) and OsCSD2-SV2 (alternative), with coding regions of 636 bp and 624 bp. Multiple sequence alignment of OsCSD2 gene and coding region of two predicted SVs was carried by ClustalX. Presence of a 3′-alternate splice site (3′-ASS) in exon-2 (E2) resulted in generation of OsCSD2-SV2. Consequently, 12 bp region (position: 250-262) is absent in E2′ (alternative exon) of OsCSD2-SV2 (**Fig. 3.3.2**).

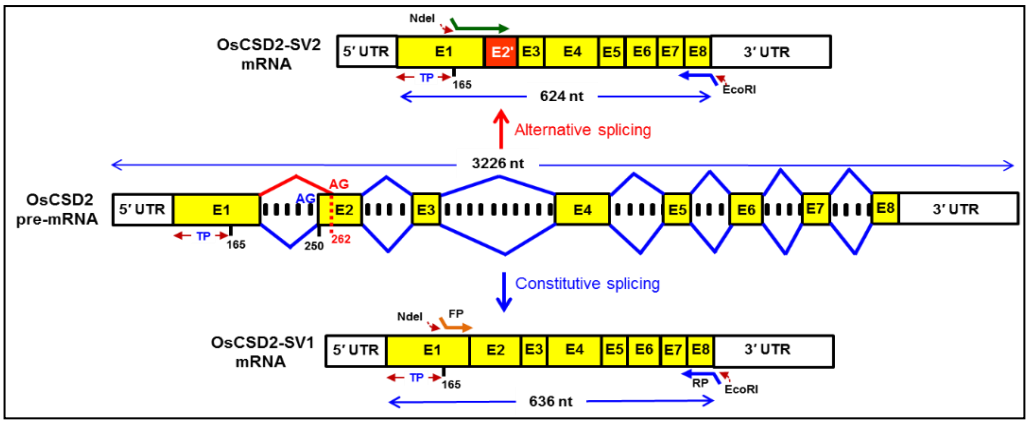

Fig. 3.3.2. Schematic representation of constitutive and alternative splicing of rice chloroplastic CSD (OsCSD2) pre-mRNA. Untranslated regions (UTRs, white box), exons (E, yellow box), introns (dashed line), truncated exon in SV2 (orange box), region coding for transit peptide (TP) and primer (Forward primer; FP and Reverse primers; RP) binding are indicated in the figure.

These 12 missing bases corresponds to four amino acid residues ^{84}GPTT^{87} (**Fig. 3.3.3)**. OsCSD2-SV1 code for a 211 aa long polypeptide (inclusive of the chloroplast localization signal/transit peptide, TP) with theoretical molecular weight (Mw) of 21.3 kDa, while the OsCSD2-SV2 codes for a 207 aa polypeptide with Mw of 20.9 kDa. The two proteins showed similar isoelectric point (pI; 5.79). Analysis of conserved domains at CDD-NCBI webserver predicted involvement of Thr-87 in subunit interactions and loss of this amino acid might affect the subunit interaction in OsCSD2-SV2 (**Fig. 3.3.3**).

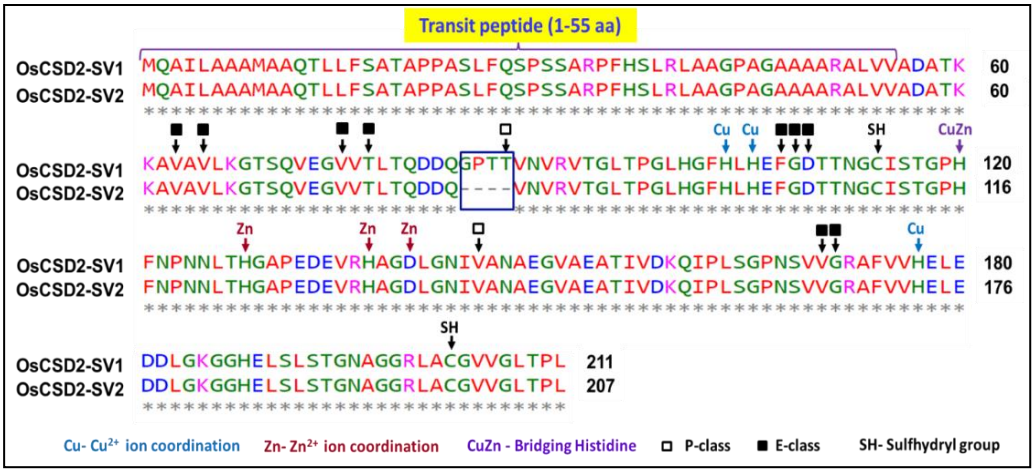

Fig. 3.3.3. Multiple sequence alignment and domain analysis of rice OsCSD2-SV1 and OsCSD2-SV2 protein sequences. Multiple sequence alignment carried out by ClustalX shows the positions of structurally and functionally important sites as identified by analysis at Conserved Domain Database (CDD). '*' indicates conserved sites while arrows indicate other important residues involved in Cu^{2+} and Zn^{2+} coordination (Cu and Zn), subunit interaction (E-class '■' and P-Class '□' interaction) and intra-subunit disulfide bond formation (SH). Transit peptide region (1-55 aa residues) predicted using ChloroP online tool is also highlighted. Deletions of four amino acids is indicated with '-' and highlighted with blue rectangle.

The OsCSD2 sequence was also analyzed for the presence of transit peptide using ChloroP tool at ExPASy. Analysis predicted that amino acid positions 1-55 at N- terminal region of protein serve as the transit peptide (TP, corresponds to 1-165 bp region in the cDNA). Subsequent to the localization to the chloroplast the TP gets cleaved and functional OsCSD protein lack this region.

The OsCSD2 isoforms were cloned and overexpressed without the TP region to avoid any effect of this region on the biochemical/biophysical characteristics of the proteins. Two cDNAs lacking the TP, ΔTP-OsCSD2-SV1 (length: 471 nt) and ΔTP-OsCSD2-SV2 (length: 459 nt), were coding for polypeptides of 156 aa (Mw: 15.9 kDa) and 152 aa (Mw: 15.5 kDa) with similar pI value (5.17). From here onwards, ΔTP-OsCSD2-SV1 and ΔTP-OsCSD2-SV2 are referred to as OsCSD2-SV1 and OsCSD2-SV2, respectively. PCR primers were designed to amplify the cDNAs lacking TP (**Table 2.5**) and for cloning and overexpression of two isoforms in *E. coli*.

3.3.3. PCR amplification and cloning of OsCSD2 splice variants

The OsCSD2-SV1 and OsCSD2-SV2 cDNAs (lacking TP region) were successfully PCR amplified from rice NSICRc106 cDNA using *Pwo* DNA polymerase and variant specific primers (OsCSD2-SV1: OsCSD2-SV1-F + OsCSD2-Com-R; OsCSD2-SV2: OsCSD2-SV2-F + OsCSD2-Com-R, **Table 2.5**). PCR amplification yielded products of expected length (inclusive of primer sequences) of 489 and 483 bp, respectively (**Fig. 3.3.4**). Subsequently, the two cDNAs were purified, double digested with NdeI and EcoRI restriction enzymes, ligated to the linearized (NdeI and EcoRI digested) pMAL-HIS vector, and transformed into *E. coli* TOP10 strain as detailed in the materials and methods (**Section 2.2.9.1**). Positive clones were confirmed by colony PCR and restriction analysis of the isolated plasmids. The

OsCSD2-SV cDNA cloned fragments were sequenced and submitted to the GenBank (Accession no: OsCSD2-SV1: MW091045 and OsCSD2-SV2: MW091046). The NSICRc106 OsCSD2 sequences showed 100 % identity with the corresponding Nipponbare sequence at the RGAP-MSU database.

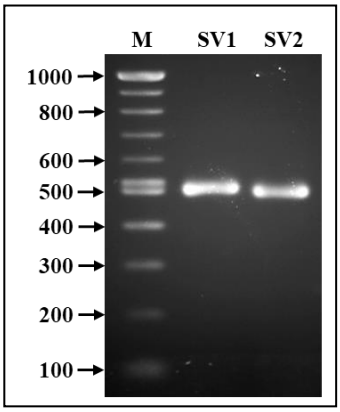

Fig. 3.3.4. PCR amplification of cDNAs (lacking transit peptide region) of OsCSD2 splice variants. PCR amplified rice OsCSD2-SV1 (lane SV1) and OsCSD2-SV2 (lane SV2) cDNAs were from rice NSICRc106 genotype. Lane M; denotes 100 bp DNA ladder marker.

3.3.4. Expression and purification of OsCSD2 SV isoforms

For heterologous expression of rice OsCSD2 SVs, recombinant plasmids pMAL-HIS-OsCSD2-SV1 and pMAL-HIS-OsCSD2-SV2 were transformed in *E. coli* SHuffle Express strain. The conditions for overexpression of the recombinant OsCSD2 proteins were optimized by varying the IPTG concentration (range: 0.1-0.5 mM IPTG) and growth temperature 25 °C. At 0.25 mM IPTG concentration and induction temperature of 25 °C both the OsCSD2 isoforms were successfully overexpressed with expected sizes of ~18 kDa (inclusive of 2.2 kDa His-tag). At induction temperature of 25 °C, OsCSD2-SV1 was present in the soluble fraction, while OsCSD2-SV2 present in the insoluble fraction. On reducing the temperature to

20 °C, both the SV protein isoforms were present in soluble fraction, however, yield of CSD2-SV1 was substantially higher than the CSD2-SV2 (**Figure 3.3.5A and 3.3.5B**). Both the protein isoforms were overexpressed at optimized conditions (temperature: 20 °C, IPTG: 0.1 mM) and purified using Ni-NTA affinity purification column **(Fig. 3.3.5A and 3.3.5B)**. The proteins were further purified by gel filtration chromatography (detailed in **section 2.2.17.1**) and used for further analysis.

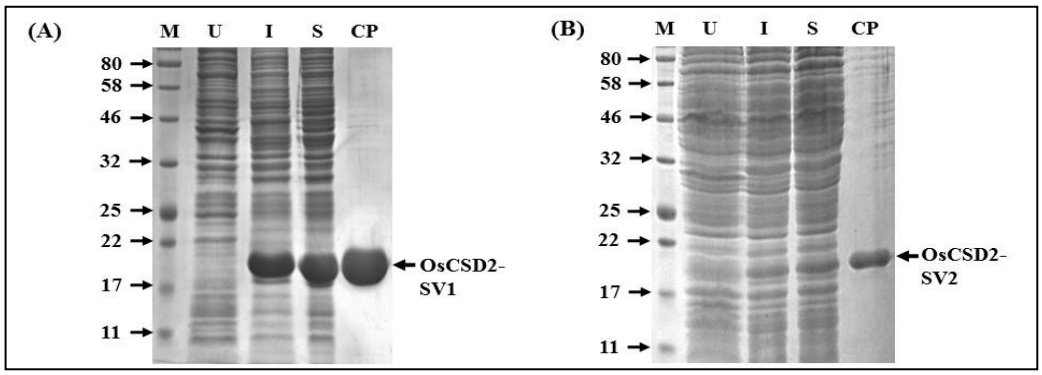

Fig. 3.3.5. Expression and purification of OsCSD2 SV isoforms from *E. coli* SHuffle Express cells. Total protein isolated from different fractions was analyzed on 15 % denaturing polyacrylamide gel. Protein **(A)** OsCSD2-SV1 and (**B**) OsCSD2-SV2; was overexpression and purified. Lane U; uninduced sample, Lane I; induced sample, Lane S; soluble protein fraction, Lane CP; Ni-NTA affinity chromatography purified protein. Lane M; indicates the position of protein Mw standards in kilodaltons (kDa). Arrow indicates the position of OsCSD2 isoforms.

3.3.5. Biophysical and biochemical analysis of OsCSD2 SV isoforms

3.3.5.1. The OsCSD2-SV1 and -SV2 protein isoforms exist as homodimers

In silico analysis of OsCSD2 isoforms indicated that the AS-mediated loss of four amino acids (^{84}GPTT^{87}) might affect oligomeric status of OsCSD2-SV2 isoform. Gel-filtration analysis of OsCSD2-SV1 and OsCSD2-SV2 isoforms was carried out to

assess the oligomeric status of two protein isoforms. Analysis showed a single absorbance peak for both OsCSD2-SV1 and OsCSD2-SV2 corresponding to native molecular weight of ~40 kDa and ~43 kDa respectively **(Fig. 3.3.6A and 3.3.6B)**. Denaturing PAGE analysis of fraction showed single expected sized bands indicating that both the isoforms exists as homodimer **(Fig. 3.3.6C)**. Hence, AS-mediated loss of the four amino acids did not affected the homo-dimeric interactions in OsCSD2-SV2 isoform.

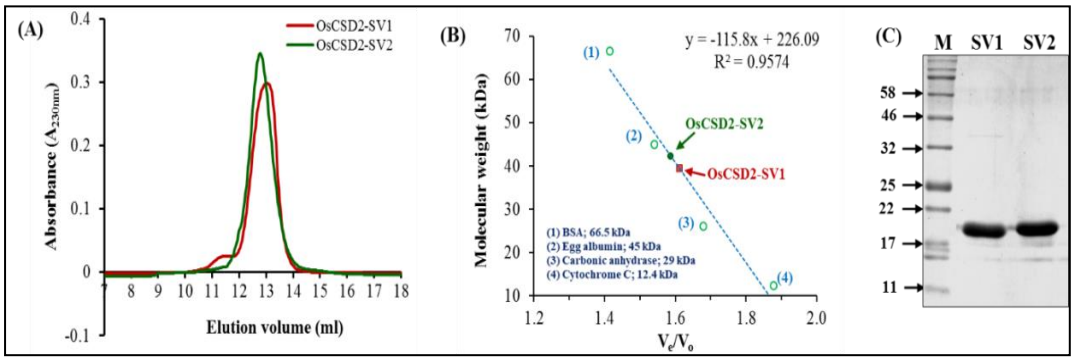

Fig. 3.3.6. Determination of oligomeric status of OsCSD2 splice isoforms by Gel-filtration chromatography: (A) Gel filtration profile of recombinant OsCSD2-SV1 and OsCSD2-SV2 isoform. Proteins were subjected to gel-filtration chromatography as described in **section 2.2.17.1**. **(B)** The gel-filtration column was pre-calibrated with standard proteins. A calibration curve of molecular weight of the standard proteins (kDa) versus their respective V_e /V_o values (V_e: elution volume, V_o: void volume) was plotted and used for estimation of native molecular weight of the recombinant OsCSD2 isoforms. **(C)** Denaturing PAGE analysis of gel-filtration fraction of OsCSD2-SV1 (lane SV1) and OsCSD2-SV2 (lane SV2). Lane M indicates the position of protein molecular weight standards in kilodaltons (kDa).

3.3.5.2. The two OsCSD2-SV isoforms are enzymatically active

In the previous chapter, the alternative isoforms of OsCSD3 were found to contain no SOD activity, which was attributed to large missing regions/alternative domains (**Fig. 3.2.2**). On the contrary, the two OsCSD2 isoforms differed in presence/absence of only four amino acid region (**Fig. 3.3.3**). The SOD activity of the isoforms was analyzed by both in-gel activity assay (Zymogram) and spectrophotometric method detailed in **section 2.2.18.1**. Zymogram analysis revealed that the two OsCSD2 isoforms are enzymatically active, but showed substantial difference in the SOD activity (**Fig. 3.3.7A**). Spectrophotometric analysis of SOD activity carried out with increasing concentration (0-2.5 μg ml^{-1}) of proteins further confirmed that the isoforms are enzymatically active, and differ substantially in the specific activity. The OsCSD2-SV1 showed almost 5-fold more activity than the OsCSD2-SV2 as evident in the in-gel activity analysis using different ratios (1:1 and 1:5) of the two proteins (**Fig. 3.3.7A**). Spectrophotometric analysis by NBT-reduction assay confirmed > 4-fold higher specific activity of OsCSD2-SV1 isoform (4360 ± 686 U $mg^{-1}ml^{-1}$) than OsCSD2-SV2 (946 ± 34 U $mg^{-1}ml^{-1}$) (**Fig. 3.3.7B**).

3.3.5.3. The OsCSD2 isoforms showed similar sensitivity to SOD inhibitors

OsCSD2 isoforms were treated with SOD inhibitors (diethyldithiocarbamate, DDC; hydrogen peroxide, H_2O_2; sodium azide, NaN_3) to compare their relative sensitivity. DDC inhibited both the OsCSD2 isoforms in concentration dependent manner (OsCSD3-SV1; IC_{50}: 0.35 mM and OsCSD2-SV2; IC_{50}: 0.43 mM), however beyond 1 mM concentration the two proteins showed differential sensitivity. At 1.5 mM DDC concentration OsCSD2-SV1 retained 20 % SOD activity while OsCSD2-SV2 was inactive.

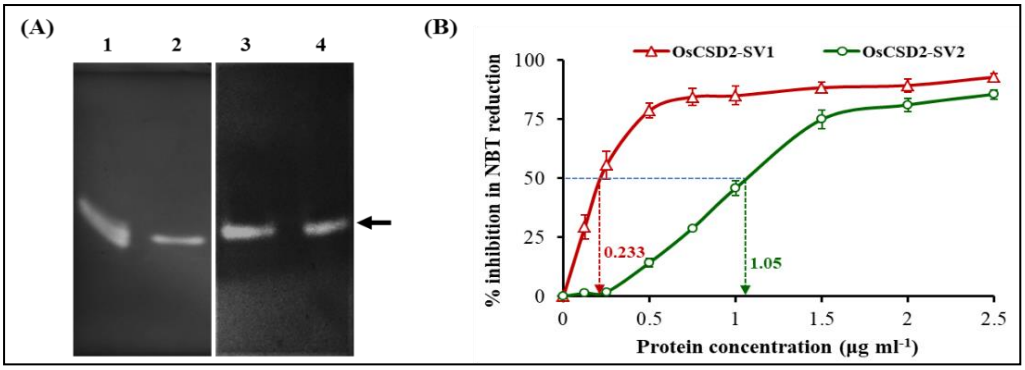

Fig. 3.3.7. Estimation of SOD activity of OsCSD2 splice isoforms by NBT reduction assay. (A) In-gel SOD activity assay of OsCSD2-SV1 and OsCSD2-SV2 was performed. Protein amount (20 ng) of OsCSD2-SV1 and OsCSD2-SV2 protein was loaded in lane 1 and lane 3 (OsCSD2-SV1) and lane 2 (OsCSD2-SV2). Lane 4 contained 5-times higher amount (100 ng) of OsCSD2-SV2. Arrow shows the achromatic zone indicative of SOD activity. **(B)** Increasing concentrations of OsCSD2 protein isoforms were taken and SOD activity was measured spectrophotometrically. Vertical arrows indicate protein concentration equivalent to 1 U of SOD. Data are represented as mean ± SD of three independent replicates.

At 2 mM DDC, SV1 also lost complete SOD activity **(Fig. 3.3.8A)**. The two isoforms showed concentration dependent decrease in activity on H_2O_2 treatment, however they showed differential sensitivity beyond 0.2 mM H_2O_2 concentration. OsCSD2-SV2 showed relatively higher tolerance to H_2O_2 than OsCSD2-SV1 (IC_{50}: OsCSD2-SV1, 0.3 mM; OsCSD2-SV2, 0.52 mM), with OsCSD2-SV2 retaining 15 % SOD activity even at 1 mM H_2O_2 concentration **(Fig. 3.3.8B)**. Both OsCSD2-SV1 and OsCSD2-SV2 remained unaffected by NaN_3 treatment up to 10 mM concentration **(Fig. 3.3.8C)**. Collectively, SOD inhibitor analysis showed both OsCSD2-SV1 and OsCSD2-SV2 are Cu/Zn type SOD.

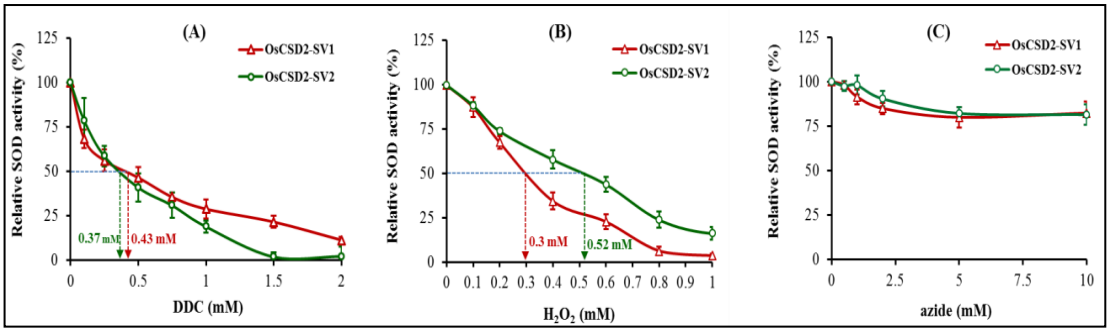

Fig. 3.3.8. Effect of SOD inhibitors on activity of OsCSD2 isoforms. One unit (1 U) equivalent protein amount of OsCSD2-SV1 and OsCSD2-SV2 was treated with **(A)** diethyldithiocarbamate (DDC; 0.0- 2.0 mM), **(B)** hydrogen peroxide (H_2O_2; 0.0- 10.0 mM) and **(C)** sodium azide (NaN_3; 0.0- 10.0 mM) for 1 h at 25 °C and SOD activity was measured. Relative SOD activity was estimated by considering activity at 0 mM inhibitor concentration as 100 %. Vertical arrow indicates IC_{50} values (in mM). Data are represented as mean ± SD of three independent replicates.

3.3.5.4. OsCSD2 protein isoforms showed similar pH optima but differential stability

The two OsCSD2 isoforms were further investigated for effect of pH on SOD activity and stability of the proteins. The proteins were pre-incubated in different buffers (pH range: 7–10.8) and analyzed for activity and stability. Both the isoforms showed similar pH optima (pH: 8.0) and with further increase (beyond pH 8.0) the two isoforms showed reduction in the SOD activity, with more pronounced effect in OsCSD2-SV2 **(Fig. 3.3.9A)**. On comparison of stability of proteins pre-incubated (4 h) in different buffers. OsCSD2-SV1 showed no appreciable change in SOD activity whereas OsCSD2-SV2 remained stable till pH 9.0 and showed substantial loss of SOD activity at pH 10 and pH 10.8. **(Fig. 3.3.9B).**

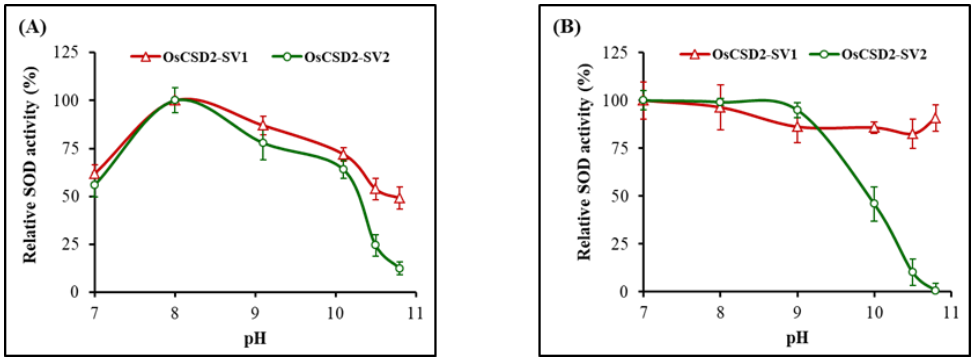

Fig. 3.3.9. Effect of pH on OsCSD2 isoforms. One unit (1 U) equivalent amount of OsCSD2-SV1 and OsCSD2-SV2 was used for analysis. **(A)** Effect of pH on activity: SOD activity of the protein was assayed in different buffers (50 mM); phosphate (pH 7.0–8.0), Tris–Cl (pH 7.0–9.0), and bicarbonate (pH 9.0–10.8) after pre-incubation for 1 h at 25 °C. Relative SOD activity was estimated by considering maximum activity as 100 %. **(B)** Effect of pH on stability: Protein was incubated in different buffers (pH range, 7.0-10.8) and aliquots were removed 4 h after incubation and SOD activity was assayed. Relative SOD activity was measured considering activity at 0 h as 100 %. Data are represented as mean ± SD of three independent replicates.

3.3.5.5. OsCSD2 isoforms showed differential response to temperature

The two OsCSD2 isoforms, differing in four amino acids, showed differences in characteristics, as detailed above. The proteins, were further investigated for thermostability. Both the isoforms were pre-incubated (1 h) at different temperatures and analyzed for residual SOD activity. OsCSD2-SV1 showed no significant loss of SOD activity up to 55 °C, retained >75 % activity at 60 °C and completely lost the activity at 65 °C ($T_{1/2:}$ 62 °C). The OsCSD2-SV2 exhibited more sensitivity towards thermal inactivation. This isoform was stable only up to 40 °C and lost complete SOD activity at 50 °C ($T_{1/2}$: 43 °C) **(Fig. 3.3.10A)**. The impact of temperature was also

investigated by SYPRO Orange-based DSF analysis. Initially, the optimum DSF assay conditions were identified by varying the protein (0.25-0.5 mg ml^{-1} in 50 mM Tris-Cl pH 8.0) and SYPRO Orange dye concentration (5 to 7.5X). Using 0.5 mg ml^{-1} protein and 5 X SYPRO Orange unfolding of the OsCSD2 isoforms was monitored as function of temperature (range: 25 °C to 95 °C, ramp rate: 0.04 °C s^{-1}). The two OsCSD2 isoforms exhibited differential thermostability as evident from substantial difference in their protein unfolding temperature (OsCSD2-SV1: Tm; 70.5 °C and OsCSD2-SV2: Tm; 51.8 °C) **(Fig. 3.3.10B)**.

These results show that AS mediated loss of four amino acids has enhanced the sensitivity of OsCSD2-SV2 towards thermal inactivation.

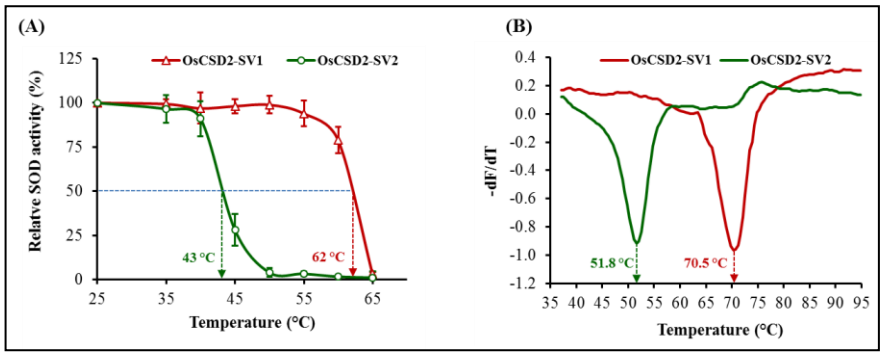

Fig. 3.3.10. Effect of temperature on stability of OsCSD2 splice isoforms. (A) OsCSD2 splice isoforms (1 U equivalent protein) was pre-incubated (1 h) at different temperatures (25–80°C) and assayed for SOD activity. Relative SOD activity was estimated by considering activity at 0 h time-point as 100 %. Vertical arrow indicates half-life temperature $T_{1/2}$ (°C) of isoform. **(B)** Differential Scanning Fluorimetry (DSF) analysis of OsCSD2-SV1 and -SV2 isoforms. Effect of temperature on unfolding of the protein was measured by DSF by continuous acquisition of SYPRO Orange fluorescence (Excitation: 465 nm Emission: 580 nm). Protein unfolding/melting temperature (Tm) was obtained from the first derivatives of the melting curves. Vertical arrow indicates the Tm (°C) values of isoform. Data are represented as mean ± SD of three independent replicates.

3.3.6. Discussion

Chloroplastic CSDs are important regulators of ROS levels, and are involved in localized scavenging of $O_2^{\cdot -}$ generated during photosynthesis [133]. Several overexpression studies have shown protective role of chloroplastic CSDs against abiotic stress conditions in plants [150,151,321]. In rice, as per RGAP-MSU database locus LOC_Os08g44770 coding for a chloroplastic CSD (OsCSD2) undergoes alternative splicing to generate two splice variants (OsCSD2-SV1 and OsCSD2-SV2). The encoded proteins showed difference of only four amino acids, missing specifically in OsCSD-SV2. For comparative analysis, the transit peptide region was excluded during cloning, and the protein isoforms were analyzed to understand the impact of AS-mediated removal of small region on the protein characteristics.

Most of the characterized chloroplastic CSDs are known to be dimeric, however monomeric form has also been reported [136,137]. OsCSD2-SV1 isoform was found to be homodimeric in native state. The OsCSD2-SV2 isoform lack four residues including Thr-87 that is predicted to be important for subunit interactions. Some previous studies on mutations targeting subunit interaction residues in CSDs impacted the oligomeric status of the protein [135,260,322]. On the contrary, OsCSD2-SV2 homodimer remained unaffected suggesting involvement of some other residues in protein dimerization, and that the missing region is not solely essential for subunit interaction. However, it will be interesting to see the relative strength of subunit interactions of the two isoforms, and if it has any implications on functioning of rice OsCSD2. Site directed mutagenesis studies have highlighted the involvement of residues important for protein function, stability and other properties of CSDs [135,260,307,312]. However, such studies generally involve substitutions and reports

on effect of deletions are relatively less, and have shown diverse outcomes in different plants [140,246]. AS-mediated C-terminal truncation generated an active Fe SOD isoform in rice [245] but resulted in an isoform with effect on chloroplast development in *Arabidopsis* [248]. An alternative chloroplastic CSD isoform containing deletion was found to be functionally active in Soybean [246]. Whereas, deletion in CSD active site region has affected the activity and stability of the mutant proteins [140]. In the present study, OsCSD2-SV2 lacked four amino acid region including Thr-87 (involved in subunit interactions) and showed differences in biochemical and biophysical characteristics. The two OsCSD2 isoforms showed substantial difference in specific activity. OsCSD2-SV1 isoform exhibited higher thermostability and tolerance to pH changes as previously reported for chloroplastic and other CSD isoforms [136,137,305,306,323]. Alteration in subunit interaction regions have been shown to impact few other characteristics [135,260]. Compared to OsCSD2-SV1, specific activity, thermal-stability and pH stability of the OsCSD2-SV2 was drastically reduced, however, the isoform was relatively more tolerant to H_2O_2. Higher sensitivity of OsCSD2-SV2 to DDC, indicates that the catalytic active site is more accessible for chelation of Cu^{2+}, resulted in reduced activity.

Overall analysis suggests that deletion had a profound impact on biophysical and biochemical properties of chloroplastic CSD of rice.

Section 3.4

Comparative analysis of two rice cytosolic Cu/Zn SODs

3.4.1. Introduction

Superoxide dismutases (SODs) are important component of enzymatic antioxidant defense system to provide protection against oxidative stress in different cellular compartments [116,134]. In plants, cytosol also contain Cu/Zn SODs (CSDs) for ROS detoxification, however few other isoforms are also reported [116,324]. These isoforms scavenge $O_2^{\cdot -}$ generated in cytosol from metabolic reactions such as, oxidation of xanthine and aldehydes respectively [61], and also contributed by peroxisomes, through production from membrane localized NAD(P)H dependent PMPs [65]. Overexpression of cytosolic CSD alone [156,325,326] or in combination with other antioxidant enzymes (catalase, CAT; ascorbate peroxidase, APX) has been shown to enhance tolerance to different stress conditions [327,328].

In terms of copy number, many plants (*Arabidopsis thaliana*, *Hordeum vulgare* etc.) contain single cytosolic CSD gene, whereas others (*Oryza sativa*, *Gossypium hirsutum* etc.) contains more than one, due to duplication events in the genome [143,146]. Different types of duplication events that occur during the course of evolution are responsible for genetic rearrangements in multiple ways (**Fig. 3.4.1)** [329]. The whole genome duplication (WGD) events is generally rare but allows large inter/intra chromosomal exchanges leading to increase in copy number, diversification in regulation/function of genes, formation of new genes/gene families [329–331].

Of around 65 % of duplicated genes in plants, large proportion is attributed to WGD events [329,332,333]. Syntenic analysis in model monocot and dicot plants have revealed that more than 50-60 % genes are paralogous in nature [329,334,335]. In rice genome, the two loci coding for cytosolic CSDs, LOC_Os03g22810 (OsCSD1) and LOC_Os07g46990 (OsCSD4), have also originated due to a block gene

duplication event between chromosome 3 and chromosome 7 (PLAZA database; https://bioinformatics.psb. ugent.be/plaza/) [143].

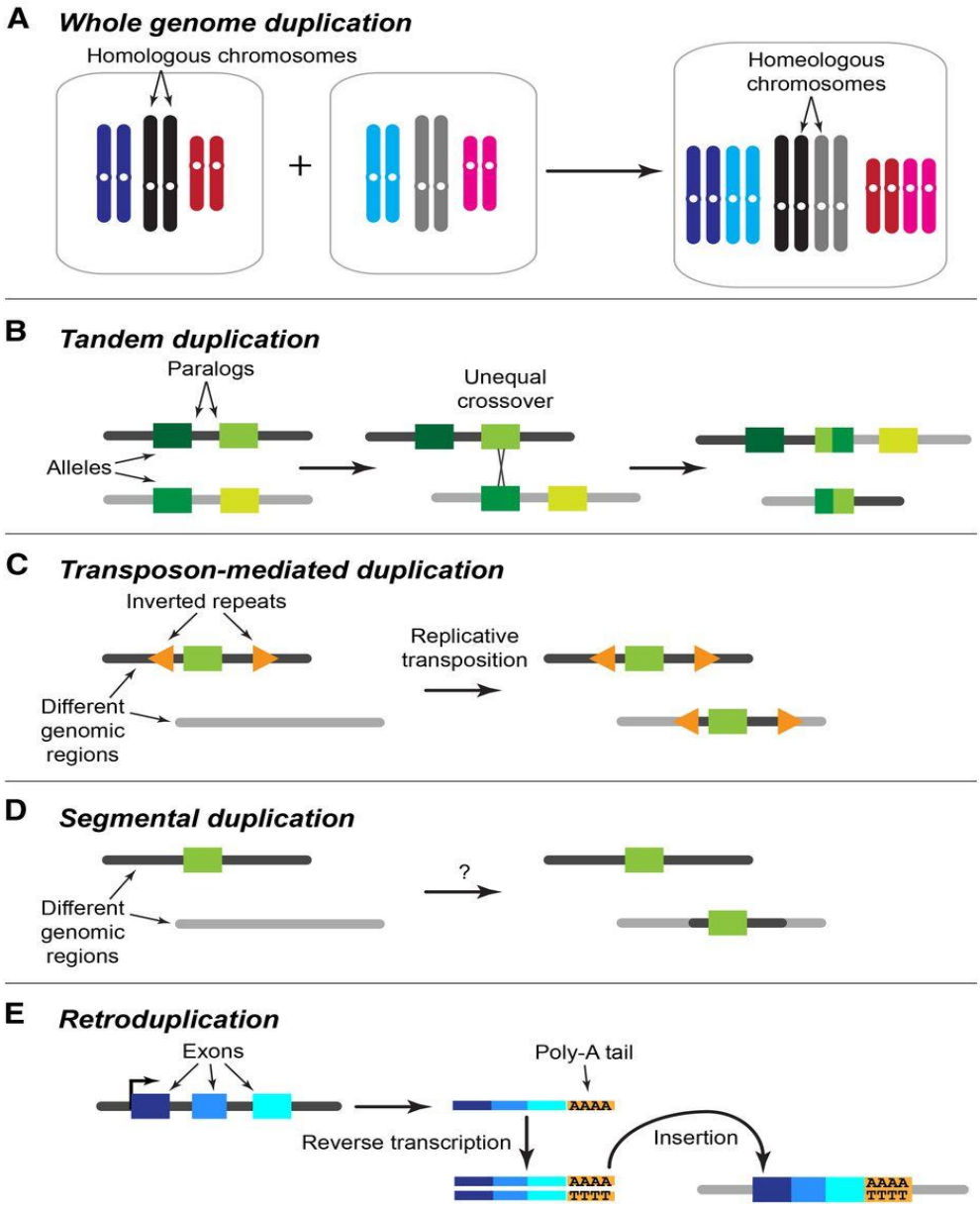

Fig. 3.4.1. Different types of gene duplication mechanisms in genomes. Adapted from Panchy et al. 2016 [329]

The RGAP-MSU database predicted gene structure of the two cytosolic CSDs show considerable heterogeneity in length and organization of UTRs, exons and

introns (http://rice.plantbiology.msu.edu/). Additionally, two splice variants are predicted for OsCSD4, with variations in 5′-UTR region (**Fig. 3.1.2**). Differential responsiveness of the two cytosolic CSD genes at transcript level (**Section 3.1, Fig. 3.1.7**) to abiotic stresses indicates variations in the up-stream regulatory elements. Similar observations were also reported in a study on rice APX and CSDs [228,288]. This chapter includes results of comprehensive *in silico* and functional analysis of two cytosolic rice CSDs (OsCSD1 and OsCSD) to understand the impact of post-duplication divergence on the two genes.

Results

3.4.2. Gene structure analysis showed heterogeneity in the two cytosolic CSDs

The loci coding for the two rice cytosolic CSDs are present on chromosome 3 (LOC_Os03g22810, OsCSD1) and chromosome 7 (Os07g46990, OsCSD4). The RGAP-MSU database (release 7) predicted gene structure showed heterogeneity in length, exon/intron/UTR organization, and coding region of the two genes (http://rice.plantbiology.msu.edu/). OsCSD1 gene (5422 bp long) contains ten exons (E1-E10), nine introns (I1-I9) and a single UTR at 3′-end, with 813 bp long CDS (**Fig 3.4.2A**). On the other hand, OsCSD4 gene is considerably smaller (2119 bp) with eight exons (E1-E8), seven introns (I1-I7), UTRs at 5′- and 3′- ends, with a 459 bp long CDS (**Fig 3.4.2B**). OsCSD1 and OsCSD4 genes are predicted to code for 270 aa and 152 aa long polypeptides. Comparative sequence analysis showed N-terminal length heterogeneity due to extra 118 aa in OsCSD1, encoded by E1-E3 and a small

region of E4. Primers were designed for full-length cDNA (FL-cDNA) amplification, cloning and over-expression of the two proteins in *E. coli* system.

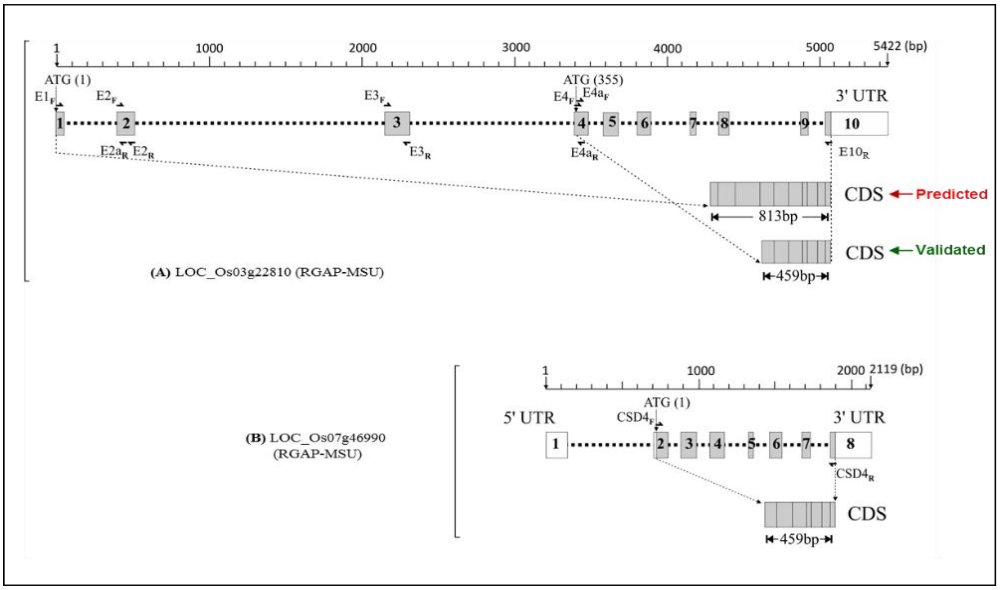

Fig. 3.4.2. Schematic overview of RGAP-MSU predicted gene structures of two rice cytosolic Cu/Zn SOD genes. (A) Organization of locus LOC_Os03g22810 (OsCSD1 gene) **(B)** Organization of locus LOC_Os07g46990 (OsCSD4 gene). Exons (numbered grey boxes), untranslated regions/UTRs (white boxes), introns (dashed lines) and positions of primers, 'ATG' codons are shown in the figure. The CDS region of OsCSD1 and OsCSD4 are also shown after joining the exons. Scale on the top indicates the length in base pairs (bp).

3.4.3. PCR analysis of full-length CSD/exons indicate inconsistency in RGAP-MSU predicted OsCSD1 gene organization

3.4.3.1. PCR amplification of full-length cDNAs of OsCSD1 and OsCSD4

RGAP-MSU predicted OsCSD1 full-length cDNA (813 bp) could not be PCR amplified using primers ($E1_F$ and $E10_R$, **Table 2.5**), whereas OsCSD4 FL-cDNA was successfully amplified using primers (OsCSD4-F and OsCSD4-R, **Table 2.5**) (**Fig.**

3.4.3A). Multiple attempts to amplify OsCSD1 FL-cDNAs did not yield the predicted 813 bp product from different lots of cDNA, however few other cDNAs (length: >1 kb) of other genes could be successfully amplified. In another approach, use of additional primers in combination with end primers ($E1_F$ and $E4a_R$; $E4_F$ and $E10_R$, **Table 2.6**), to amplify two smaller overlapping fragments (to be joined later), did not yielded the product from exon1 to exon3 and partial E4 region, whereas region from exon4 to exon10 (470 bp) was amplified (**Fig. 3.4.3B**).

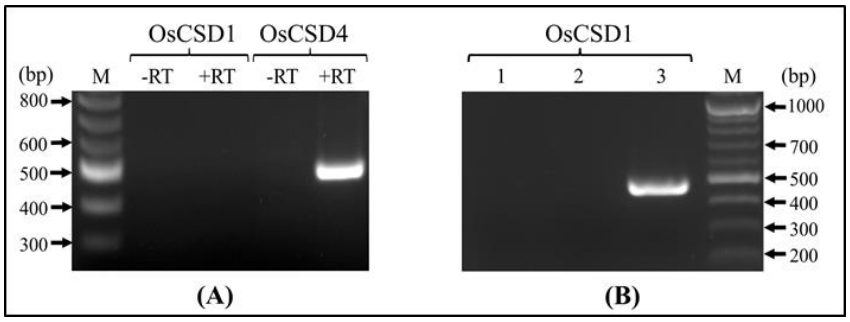

Fig. 3.4.3. **PCR amplification of full-length cDNAs of rice cytosolic CSDs. (A)** PCR amplification of full-length cDNA of OsCSD1 and OsCSD4 from rice cDNA from −RT and +RT samples using end primers. **(B)** PCR amplification of different OsCSD1 regions from total rice cDNA using different primer combinations. Lane 1; $E1_F$-$E10_R$ primers, lane 2; $E1_F$-$E4a_R$ primers, lane 3; $E4_F$-$E10_R$ primers. Lane M; represents DNA Mw markers (in bp).

OsCSD1 PCR primers were also assessed for amplification using genomic DNA template. Forward primers designed in exon1 ($E1_F$), exon2 ($E2_F$), exon3 ($E3_F$), and exon4 ($E4_F$) in combination with $E10_R$ (**Table 2.6)** yielded expected sized products (E1-E10; 5060 bp; E2-E10:4667 bp; E3-E10: 2916 bp, and E4-E10: 1663 bp) indicating that the primers and PCR conditions used in cDNA amplification were fine (**Fig. 3.4.4A**). Further, presence of individual exons/combination (in case of smaller

exons) was investigated in genomic DNA and cDNA. Genomic DNA template yielded expected sized products (**Fig. 3.4.4B, lane 1**; E1-E2: 459 bp, **lane 2**; E2: 113 bp, **lane 3**, E3: 172 bp and **lane 4**; E4-E10: 1663 bp) in PCR with different primer combinations viz. ($E1_F$ and $E2a_R$; $E2_F$ and $E2_R$; $E3_F$ and $E3_R$; $E4_F$ and $E10_R$, **Table 2.6**), whereas only E4-E10 region (470 bp) fragment was amplified from the cDNA template (**lane 4, Fig. 3.4.4B**). Collectively, these results suggested that OsCSD1 protein coding region (as per RGAP-MSU database predicted gene model) seems smaller than 813 bp, and exon1, exon2, and certain region of exon3 may not be even part of the mature transcript.

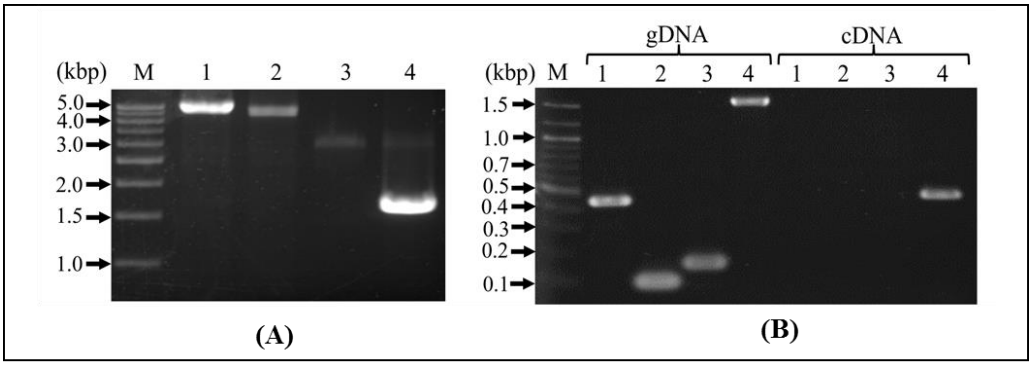

Fig. 3.4.4. PCR based validation of RGAP-MSU predicted OsCSD1 gene structure using rice genomic DNA and cDNA. (A) PCR amplification of different regions of OsCSD1 from rice genomic DNA using different primer combinations. Lane 1; E1-E10 ($E1_F$-$E10_R$), lane 2; E2-E10 ($E2_F$-$E10_R$), lane 3; E3-E10 ($E3_F$-$E10_R$) and E4-E10 ($E4_F$-$E10_R$) **(B)** PCR amplification of different exons/exon combinations using rice genomic DNA (gDNA) and cDNA as template and different primer combinations. Lane 1; E1-E2 ($E1_F$-$E2a_R$), lane 2; E2 ($E2_F$ and $E2_R$), lane 3; E3 ($E3_F$-$E10_R$) and E4 ($E4a_F$-$E10_R$). Lane M indicates 500 bp DNA ladder (Fig. 3.4.4. A) and 100 bp ladder (Fig. 3.4.4. B).

3.4.3.2. *In silico* analysis of the OsCSD1 ORF:

In silico analysis of 1-354 bp of 5´-end of the 813 bp OsCSD1 CDS (predicted protein coding region) using different tools/online databases further confirmed the results of the PCR based analysis detailed above. NCBI-Blast did not showed similarity (in 1- 210 bp region) with any EST in GenBank database (**Fig. 3.4.5A**) and CDD-Blast did not detect any domain in the N-terminal 118 amino acid region (**Fig. 3.4.5B**). Further, analysis at RGAP-MSU database also showed that no probes have been designed/utilized from E1-E4 region in different transcriptomics approaches viz. SAGE, Agilent or Affymetrix arrays (**Fig. 3.4.5C**). These results show that the RGAP-MSU predicted OsCSD1 gene organization is inconsistent as the predicted exon1, exon2 and exon3 do not correspond to protein coding regions, and exon1, exon2 are not even part of the transcript.

3.4.3.3. PCR based fine mapping indicates that partial exon3 region contributes to the 5′-UTR

Exon3 region was further examined by RT-PCR analysis using a series of overlapping forward primers ($E3a_F$, $E3b_F$, $E3c_F$, $E3d_F$, $E3e_F$, $E3g_F$, $E3h_F$) in combination with the reverse primer, $E10_R$ (**Fig. 3.4.6**). Expected size products were detected only until region corresponding to primer $E3b_F$ indicating that complete exon3 is not part of OsCSD1 transcript (**lane 4, Fig. 3.4.6**), as also observed previously (**lane 3, cDNA panel, Fig. 3.4.4**). Interestingly, upstream to primer $E3e_F$, the PCR efficiency reduced considerably (**compare lanes 5-7 and 8-12, Fig. 3.4.6**) indicating lower levels of the longer transcript. Collectively, these above-mentioned findings suggest that the RGAP-MSU predicted organization of OsCSD1 gene (LOC_Os03g22810) may needs to be revised.

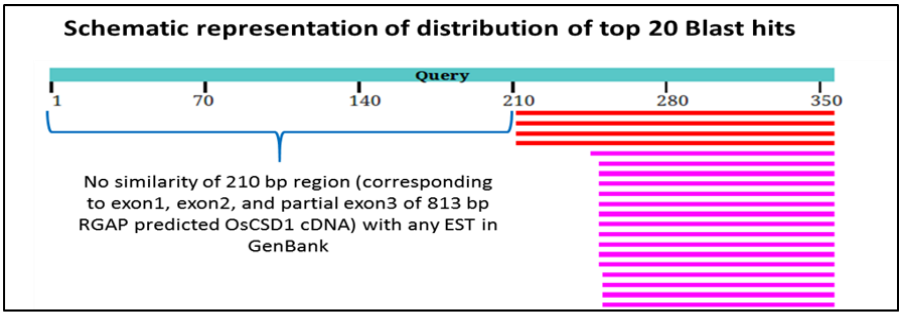

(A)

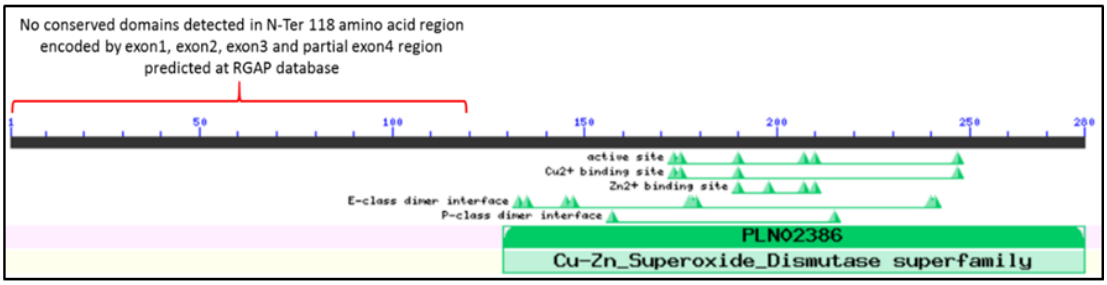

(B)

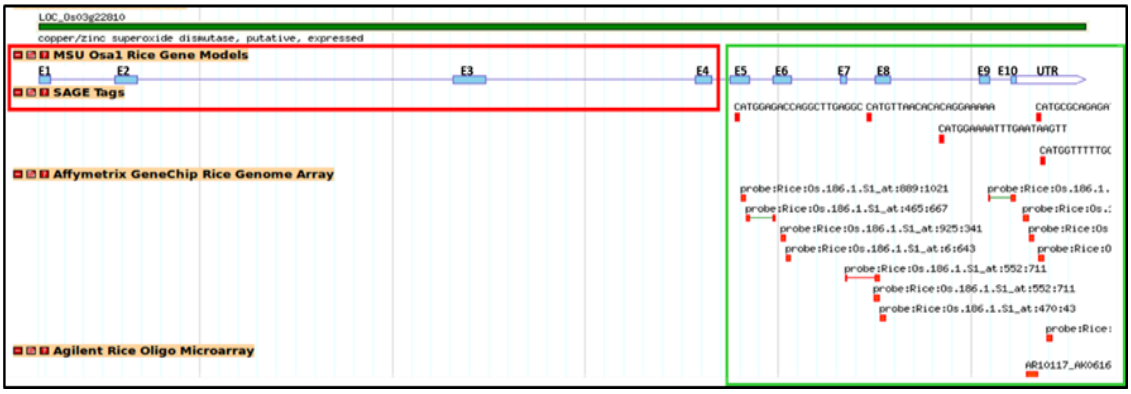

(C)

Fig. 3.4.5. ***In silico*** **analysis of cDNA region/encoded amino acid sequence of the region corresponding to exon1-exon3 of RGAP predicted OsCSD1 gene structure**. **(A)** Blastn top hits of the OsCSD1 RGAP-MSU predicted 1-354 bp cDNA region (of total 813 bp) corresponding to exon1 to exon3. **(B)** Conserved domain analysis of RGAP-MSU predicted 270 aa OsCSD1 protein at CDD-Blast server of NCBI. **(C)** Schematic representation of location of SAGE Tags and microarray probes (Affymetrix and Agilent) along the length of OsCSD1 gene structure.

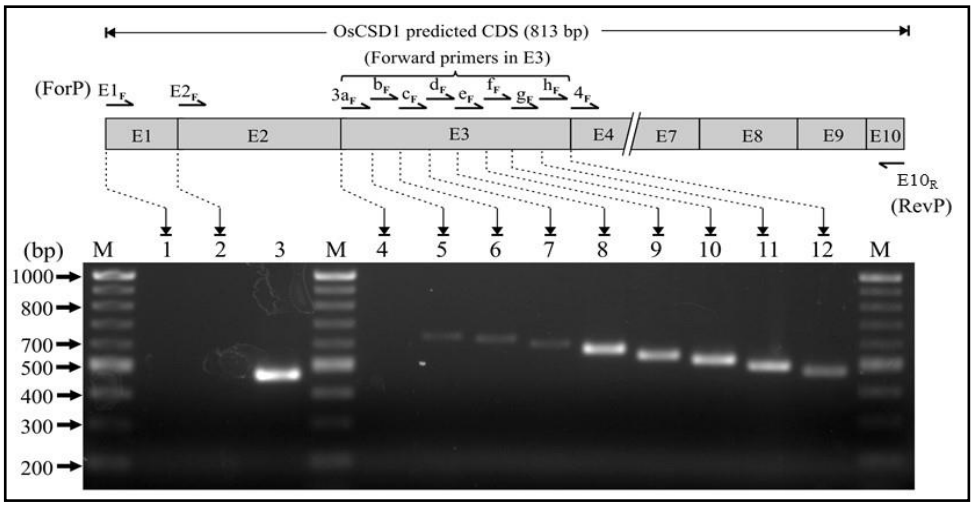

Fig. 3.4.6. PCR analysis based fine mapping of exon3 region from rice cDNA using different combinations of primers. Lane 1; $E1_F$ and $E10_R$, lane 2; $E2_F$ and $E10_R$, lane 3; $E4_F$ and $E10_R$; lane 4; $E3a_F$ and $E10_R$, lane 5; $E3b_F$ and $E10_R$, lane 6; $E3c_F$ and $E10_R$, lane 7; $E3d_F$ and $E10_R$, lane 8; $E3b_F$ and $E10_R$, lane 9; $E3e_F$ and $E10_R$, lane 10; $E3g_F$ and $E10_R$, lane 11; $E3h_F$ and $E10_R$, lane12; $E4_F$ and $E10_R$. RGAP-MSU predicted OsCSD1 CDS is shown along with exons (E1-E10) and positions of different forward and reverse primers. Lanes of the corresponding PCR products are shown by arrows on top of each lane. Lane M showed 100 bp DNA ladder.

Hence, the OsCSD1 coding region starts from the 'ATG' present at position 355 (not position 1) of the predicted CDS (**Fig. 3.4.2A**). This makes the length of validated OsCSD1 CDS (459 bp) and protein (152 aa) same as that of OsCSD4 (**Fig. 3.4.2A and 3.4.2B**). The validated CDS of OsCSD1 showed consistency with predicted gene structure at another rice database, RAP-DB (**Fig. 3.4.7**). The cloning primers to amplify the 459 bp validated OsCSD1 CDS were redesigned for cDNA amplification, cloning and overexpression of recombinant protein, for comparative analysis with OsCSD4, the second cytosolic CSD.

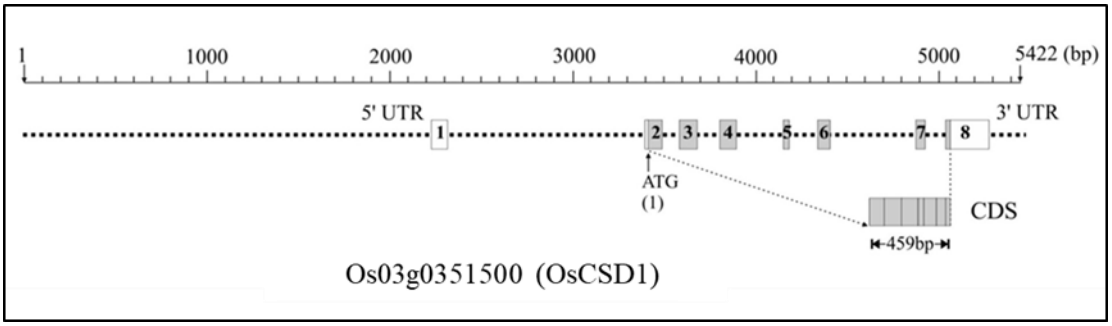

Fig. 3.4.7. Schematic overview of RAP-DB predicted gene structure of OsCSD1 rice cytosolic Cu/Zn SOD gene. Organization of locus Os03g03g0351500 (OsCSD1 gene); Exons (numbered grey boxes), untranslated regions/UTRs (white boxes), and introns (dashed lines), are shown in the figure. The CDS region of OsCSD1 is shown after joining the exons. Scale on the top indicates the length in base pairs (bp).

3.4.4. Two rice cytosolic CSDs originated due to a block duplication event

Rice genome has undergone several chromosomal duplication events involving large fragments [329]. Duplication event between chromosome 3 and 7 also contain the loci coding for LOC_Os03g22810 (OsCSD1) and LOC_Os07g46990 (OsCSD4) genes (**Fig. 3.4.8A**). Analysis of three more monocot species (*Oryza brachyantha*, *Setaria italica* and *Zea mays*) and four dicots (*Manihot esculanta*, *Coffea canephora*, *Daucus carota* and *Brassica oleracea*) showed evidence of block duplication events involving CSD loci (**Fig. 3.4.8**). On the contrary, many other plants viz. *Arabidopsis thaliana, Solanum tuberosum, Solanum lycopersicum* etc. showed a single cytosolic CSD. The post-duplication divergence is also evident in the heterogeneity in gene (and intron) structure of the two rice CSDs genes (**Fig. 3.4.2A and 3.4.2B**). The variations also seem to have affected their regulation as evident in different transcripts

levels in tissues and responsiveness to abiotic stresses (**Section 3.1, Fig. 3.1.7A and 3.1.7B**). Both the genes were analyzed by *in silico tools* and wet lab experiments for more insights.

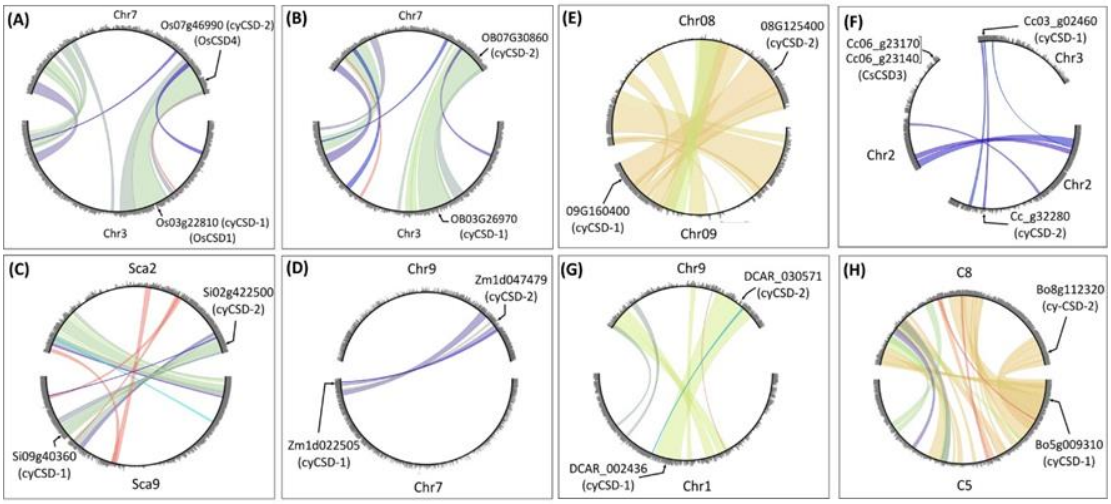

Fig. 3.4.8. Schematic representation of duplication events leading to multiple cytosolic CSDs in monocots and dicots. Analysis was done using PLAZA monocots and dicots web resources (version 4.5)**.** Monocot species: **(A)** *Oryza sativa*, **(B)** *Oryza brachyantha*, **(C)** *Setaria italica*, **(D)** *Zea mays*. Dicot species: **(E)** *Manihot esculanta*, **(F)** *Coffea canefora*, **(G)** *Daucus carota*, **(H)** *Brassica oleracea*. In each species, only the chromosomes involved in duplication events are shown. Colored bands showed the regions involved in the inter-chromosomal exchanges, while arrows indicate the location of the cytosolic CSDs.

3.4.5. OsCSD1 and OsCSD4 genes showed heterogeneity in the promoter structure and cis-regulatory elements

For *in silico* analysis of promoter elements, upstream regions of OsCSD1 (-5,409 bp) and OsCSD4 (-1108 bp) was analyzed at PlantPAN 3.0 and PlantCARE

web resources. Considerable variations were observed in the upstream regulatory regions of two genes. Two CpG islands (CpG1: 1106 bp and CpG2: 918 bp) were identified in upstream region of OsCSD1 compared to a single (790 bp) CpG island in OsCSD4 (**Figure 3.4.9A**). Sequence comparison revealed higher similarity between the OsCSD4-CpG with OsCSD1-CpG2 than OsCpG1 (**Fig. 3.4.9.A**). Four highly conserved motifs (length: 12-23 bp, sequence identity: 92-100 %) were identified in the upstream region of the two genes, while a tandem repetitive motif (length: 14 bp, copy number: 2.7) was specifically present in OsCSD1-CpG2 island (**Fig. 3.4.9A**). Analysis at PlantCARE revealed considerable variation in *cis*- elements present in the two cytosolic CSD genes with ~50% less *cis*-elements in upstream region of OsCSD4 than OsCSD1 (**Fig. 3.4.9B**).

Twenty-eight *cis*-elements (light response, auxin response, MYB binding, anoxic specific response, gibberellin response etc.) were present in OsCSD1, while three with no assigned role were specific to OsCSD4. Certain motifs (abscisic acid, anaerobic induction, methyl jasmonate, defense and stress response, and certain light responsive motifs) showed higher copy number in OsCSD1 (**Fig. 3.4.9B**). Some motifs were also common to the two genes such as, MYB and ATBP-1 binding sites and response elements for light, gibberellin, low-temperature, salicylic acid etc.

3.4.6. Amplification and cloning of two cytosolic CSDs

Validated FL-cDNAs of OsCSD1 and OsCSD4 (both 459 bp) were successfully PCR amplified using *Pwo* DNA polymerase and primers (OsCSD1; OsCSD1-F and OsCSD1-R, OsCSD4; OsCSD4-F and OsCSD4-R) containing NdeI and EcoRI sites for cloning (**Fig. 3.4.10**). The PCR products were restriction digested,

cloned into pET28a(+) and transformed into *E. coli* TOP10 cells. Positive clones were confirmed by colony PCR, restriction digestion and finally by sequencing. Sequences of OsCSD1 and OsCSD4 cDNA were submitted to the GenBank (Accession numbers; OsCSD1: MW091043 and OsCSD4: MW091044). Hereafter, the pET28a(+)

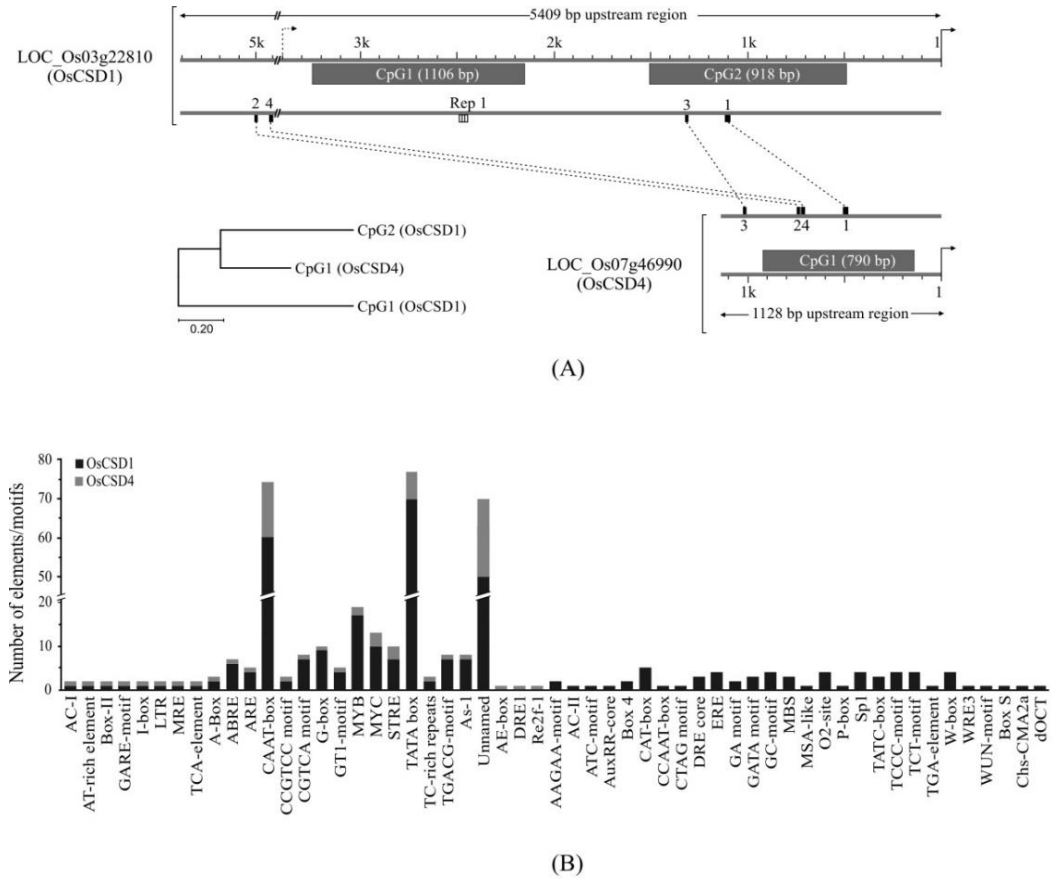

Fig. 3.4.9. *In silico* analysis of the promoter region of OsCSD1 and OsCSD4 gene. **(A)** Analysis of CpG islands in upstream region of OsCSD1 and OsCSD4 genes at PlantPAN 3.0 server. Positions of four conserved motifs (1, 2, 3 and 4) and one repetitive motif (Rep1) is indicated. Dendrogram showed the divergence between the CpG islands of OsCSD1 and OsCSD4. **(B)** Relative abundance of cis-regulatory elements in upstream regions of OsCSD1 and OsCSD4 genes as analyzed at PlantCARE database.

constructs carrying OsCSD1 and OsCSD4 cDNA will be referred as pET28a-OsCSD1 and pET28a-OsCSD4 respectively.

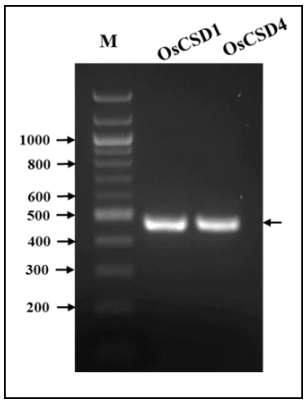

Fig. 3.4.10. PCR amplification of OsCSD1 and OsCSD4 cDNA. Lane OsCSD1 and OsCSD4 represent the PCR amplified cDNA of OsCSD1 and OsCSD4 respectively. Lane M corresponds to 100 bp DNA ladder.

3.4.7. OsCSD1 and OsCSD4 showed similarity to cytosolic Cu/Zn SODs

The CSD sequences (peroxisomal, chloroplastic and cytosolic) from several monocot and dicot plant species were retrieved from NCBI-GenBank (https://www.ncbi.nlm.nih.gov/genbank/) and PLAZA database (https://bioinformatics.psb.ugent.be/plaza/). Multiple sequence alignment identified the conserved and variable regions among CSDs from different species as well as between multiple intra-genomic cytosolic CSDs. Phylogenetic analysis placed the various CSDs into three clusters, I (cytosolic), II (chloroplastic), and III (peroxisomal) (**Fig. 3.1.1**). Both OsCSD1 and OsCSD4 were placed in the monocot specific sub-cluster of cluster I. Although the two OsCSDs were duplicated genes, they showed distinct divergence due to sequence heterogeneity. Sequence divergence between

duplicated cytosolic CSDs originated due to block duplication events was also evident in some species like *Z. mays* (**Section 3.1, Fig. 3.1.1**). Sequence analysis of the two OsCSDs (OsCSD1 and OsCSD4) from genotype NSICRc106 showed 100% identity to corresponding sequences of Nipponbare genotype.

3.4.8. Functionally important residues are conserved in two OsCSDs

Both OsCSD1 and OsCSD4 code for 152 aa polypeptides with minor variation in theoretical Mw/pI values (OsCSD1: 15.27 kDa, 5.71 and OsCSD4: 15.08 kDa, 5.92). The two OsCSDs showed 88.15 % identity due to variations at 18 positions distributed across the length of protein (**Fig. 3.4.11**). Functionally important amino acid residues such as involved in coordination with Cu^{2+} (His-45, His-47, His-62 and His-119) and Zn^{2+} (His-62, His-70, His-79, Aps-82), and disulfide bond formation (Cys-66 and Cys-145) were identical (**Fig 3.4.11**). Two of the 11 amino acids predicted to important for surface interactions were changed (H19F and T29S) in OsCSD4. However, the substituted amino acids were of similar physicochemical nature and predicted (CDD analysis) to be capable of surface interactions.

Although, the remaining 16 amino acid changes did not affect important residues; their impact on other characteristics was investigated. Effect of these variations on secondary structure of both rice cytosolic and few other reported CSDs was analyzed at Chou and Fasman Secondary Structure Prediction server (CFSSP). Result showed that of the four α-helix rich regions (#1-#4) two are substantially affected, resulting in enhanced β-sheet content in OsCSD4 (**Fig. 3.4.12**).

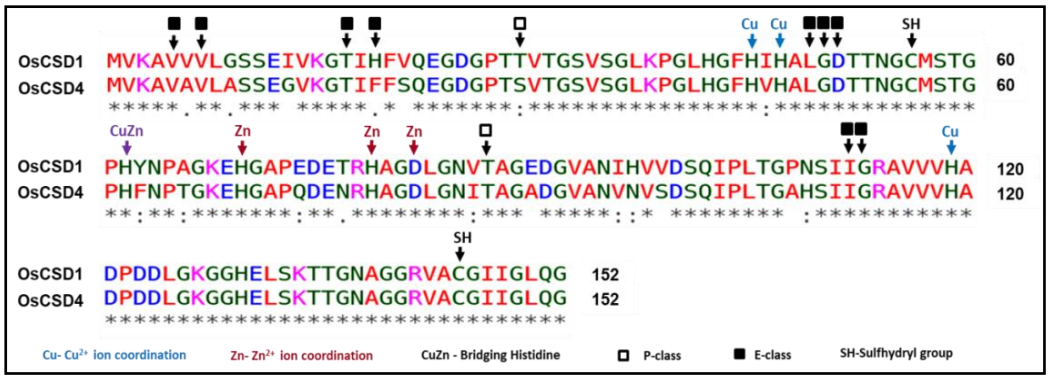

Fig. 3.4.11. Sequence and domain analysis of cytosolic CSDs, OsCSD1 and OsCSD4. Domain analysis was performed at Conserved Domain Database at NCBI (CDD-NCBI). The sequences were aligned with ClustalX software. Conserved residues are indicated with '*' and other important residues are indicated with arrows with suitable symbols, Cu^{2+} and Zn^{2+} coordination (Cu and Zn), subunit interaction residues (E-class '■' and P-Class '□' interaction), intra-subunit disulfide bond formation (SH).

3.4.9. Overexpression and purification of recombinant OsCSD1 and OsCSD4 proteins

The recombinant rice OsCSD1 and OsCSD4 were overexpressed in *E. coli* SHuffle T7 Express cells. Recombinant plasmids pET28a-OsCSD1 and pET28a-OsCSD4 were transformed into SHuffle T7 Express strain and protein was overexpressed at optimized conditions. Denaturing PAGE analysis showed that both the proteins were successfully overexpressed, and were present in soluble fraction (**Fig. 3.4.13A and 3.4.13B**). The proteins showed minor variation in the protein size (OsCSD1: ~21 kDa and OsCSD4: ~20 kDa, inclusive of His-tag), which might be due to amino acid variations. Both the recombinant proteins were purified to near homogeneity using Ni-NTA affinity chromatography followed by Gel-filtration

chromatography for further biochemical and biophysical characterization.

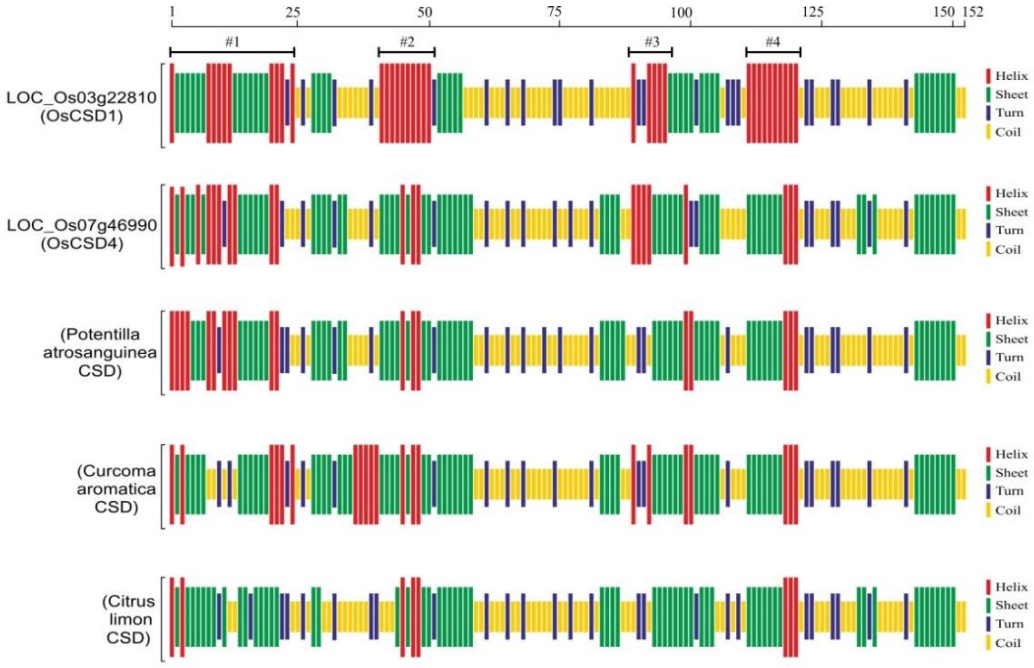

Fig. 3.4.12. ***In silico*** **secondary structure prediction of the cytosolic CSDs from different plants.** The scale on top, shows length of the CSD proteins. Different secondary structure elements are shown by different colors, and the major regions affected due to sequence variations are indicated with '#'.

3.4.10. Biochemical and biophysical characterization of two rice cytosolic OsCSDs

Recombinant OsCSD1 and OsCSD4 were analyzed for biochemical and biophysical characteristics, to study the nature and extent of effects, if any, due to amino acid variations.

3.4.10.1. Rice cytosolic OsCSD1 and OsCSD4 exists as homodimeric protein

Recombinant OsCSD1 and OsCSD4 were analyzed by gel-filtration to see the effect of two amino acid substitutions (H19F and T29S) on subunit interactions and oligomeric status of the proteins. Both the proteins eluted as single absorbance peak

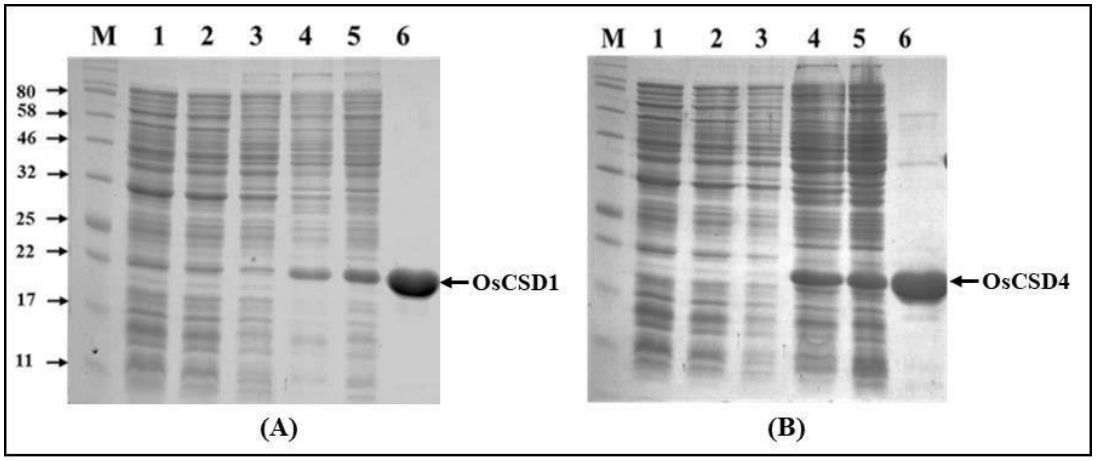

Fig. 3.4.13. Overexpression and purification of OsCSD1 and OsCSD4 from *E. coli* SHuffle T7 Express cells. Total proteins were isolated from different fractions of SHuffle T7 Express cells expressing **(A)** OsCSD1 **(B)** OsCSD4. Lane 1-2; Uninduced and induced cells containing empty pET28a(+), lane 3-4; Uninduced and induced cells containing pET28a-OsCSD1 or pET28a-OsCSD4, lane 5; Soluble fraction; lane 6; Ni-NTA affinity purified fraction. Lane M indicates protein Mw standard (in kDa).

(A_{230nm}) of ~43 kDa and ~36.0 kDa (**Fig. 3.4.14A and 3.4.14B**). Analysis of gel-filtration purified OsCSD1 and OsCSD4 on denaturing PAGE of showed subunit Mw of ~21 kDa and ~20 kDa as observed previously (**Fig. 3.4.13)**. These results confirmed that both OsCSDs exist as homodimers in the native state.

3.4.10.2. OsCSD4 showed higher specific activity than OsCSD1

SOD activity of the two OsCSDs was determined by NBT reduction assay as mentioned in **section 2.2.18.1**. Both the proteins were found to be enzymatically active, however OsCSD4 showed ~2-fold higher specific activity (OsCSD4; 4317 ±337 U mg^{-1} ml^{-1}) than the OsCSD1 (2402 ±171 U mg^{-1} ml^{-1}) (**Fig. 3.4.15**).

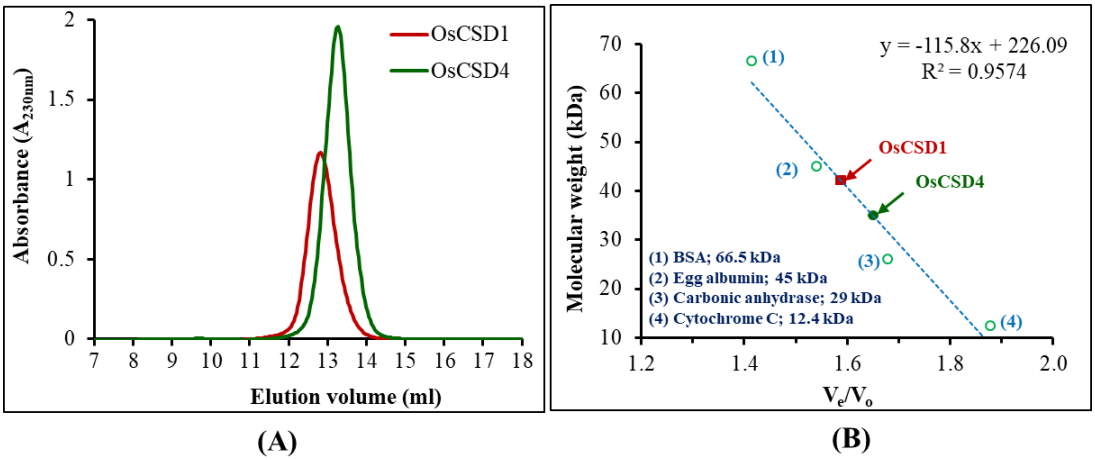

Fig. 3.4.14. Analysis of oligomeric status of OsCSD1 and OsCSD4. (A) OsCSD1 and OsCSD4 proteins were subjected to Gel-filtration chromatography on Superdex 75 30/100 GL column. Proteins were monitored at absorbance (A_{230nm}). **(B)** Column was calibrated with protein Mw standards. The calibration curve between Mw (kDa) vs V_e/V_o (V_e; elution volume and V_o; void volume) was plotted to estimate the native Mw of the proteins. Arrows indicates the positions of OsCSD1 and OsCSD4 protein.

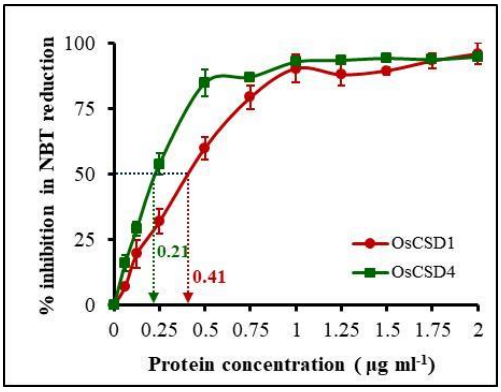

Fig. 3.4.15. Estimation of SOD activity of OsCSD1 and OsCSD4 by NBT reduction assay. Increasing protein concentration (0-2 µg ml^{-1}) was taken and SOD activity was measured as detailed in **section 2.2.18.1.** Vertical arrow represents protein concentration for 50 % inhibition of NBT reduction (equivalent to 1 U of SOD activity). Data are represented as mean ± SD of three independent replicates.

3.4.10.3. Two OsCSDs showed similar sensitivity to SOD inhibitors

The OsCSD1 and OsCSD4 were analyzed for relative sensitivity to SOD inhibitors (DDC, NaN_3 and H_2O_2) in terms of effect on SOD activity. DDC (a Cu^{2+} chelator) inhibited the SOD activity of both OsCSD1 and OsCSD4 in a concentration dependent (IC_{50}; ~0.52 mM) manner with complete inhibition at 2 mM (**Fig. 3.4.16A**). The two proteins were not affected by NaN_3 (**Fig. 3.4.16B**), and exhibited minor variation in sensitivity towards H_2O_2 (IC_{50} value: 0.4 mM and 0.6 mM) (**Fig. 3.4.16C**).

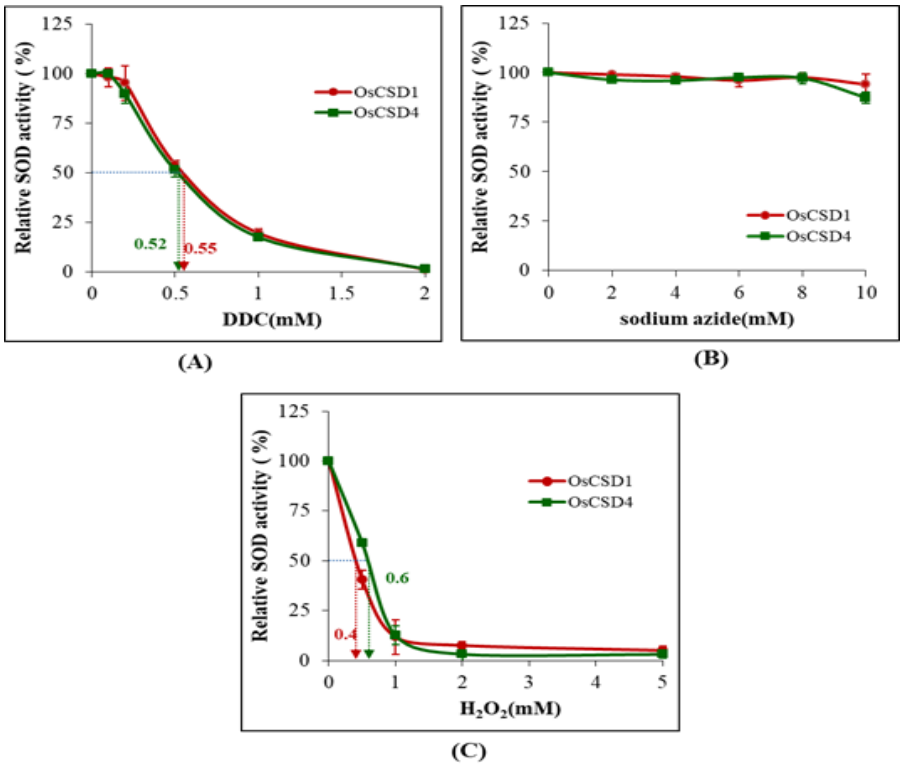

Fig. 3.4.16. Effect of SOD inhibitors on SOD activity of OsCSD1 and OsCSD4. 1 U equivalent of OsCSD1 and OsCSD4 was pre-incubated for 1 h with different SOD inhibitors and SOD activity was estimated. **(A)** DDC (0-2 mM), **(B)** NaN_3 (0-10 mM), **(C)** H_2O_2 (0-5 mM). Data was represented as relative SOD activity (%) considering activity with no inhibitor as 100 %. Vertical arrow indicates IC_{50} values. Data are represented as mean ± SD of three independent replicates.

These results showed the both the proteins show inhibitor characteristics typical of Cu/Zn SODs.

3.4.10.4. OsCSD4 is more tolerant to pH changes than OsCSD1

Effect pH on activity and stability of the OsCSD1 and OsCSD3 was analyzed by pre-incubating the proteins in different pH buffers. Both the proteins showed same pH optima (pH 9.0); however, OsCSD1 showed loss in activity rapidly above pH 9.0, with a complete loss at pH 10.0 and beyond. On the contrary, OsCSD4 showed comparatively higher activity at most pH values below and beyond optimum pH and lost activity at pH 10.8. (**Fig. 3.4.17A**).

The two proteins also showed differential stability to change in pH. OsCSD4 was relatively more stable to change in pH with no significant loss in the activity even after 48 h pre-incubation in different buffers (pH 5 and above). Likewise, OsCSD1 also showed tolerance to change in pH (5-10), however activity was lost on longer incubation times at higher pH (>10.0). OsCSD1 retained ~65 % and ~40 % SOD activity at pH 10.5 and 10.8, which further dropped to ~50 % and ~10 % respectively at 48 h pre-incubation. At pH 4.0, both the proteins showed no SOD activity (**Fig. 3.4.17B**).

3.4.10.5. OsCSD4 is structurally more thermostable than OsCSD1

Effect of temperature on SOD activity was determined by pre-incubating two OsCSDs at different temperature (30-80 °C), followed by SOD activity assay. Both the proteins showed comparable tolerance to thermal inactivation with no loss in the activity till 50 °C, retained ~20 % SOD activity at 65 ºC, with similar $T_{1/2}$ values (OsCSD4: 62.2 °C; OsCSD1: 63.5 °C)

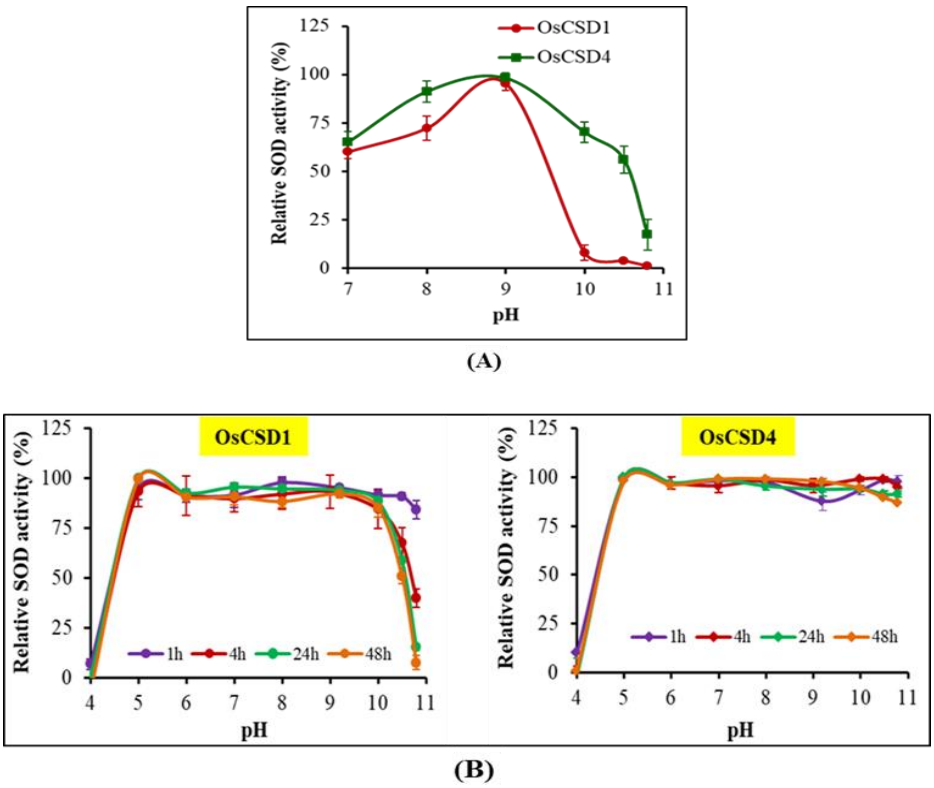

Fig. 3.4.17. Effect of pH on activity and stability of OsCSD1 and OsCSD4. 1 U equivalent amount of OsCSD1 and OsCSD4 was taken for pre-incubation in different buffers for up to 48 h. SOD activity was measured as detailed in **section 2.2.18.2. (A)** Effect of pH on SOD activity. Relative SOD activity was estimated by considering maximum activity as 100 %. **(B)** Effect of pH on stability of OsCSD1 and OsCSD4. Relative SOD activity was measured considering activity at 0 h as 100 %. Data are represented as mean ± SD of three independent replicates.

(**Fig. 3.4.18A**). Effect of temperature on structural stability of the proteins was evaluated in terms of protein unfolding/melting temperature (Tm) by Differential Scanning Fluorimetry (DSF), based on measurement of SYPRO Orange fluorescence (excitation: 465 nm and emission: 580 nm) as a function of temperature, showed that

OsCSD4 (Tm: 78.2 °C) is structurally more stable than OsCSD1 (Tm: 72.0 °C) (**Fig. 3.4.18B**).

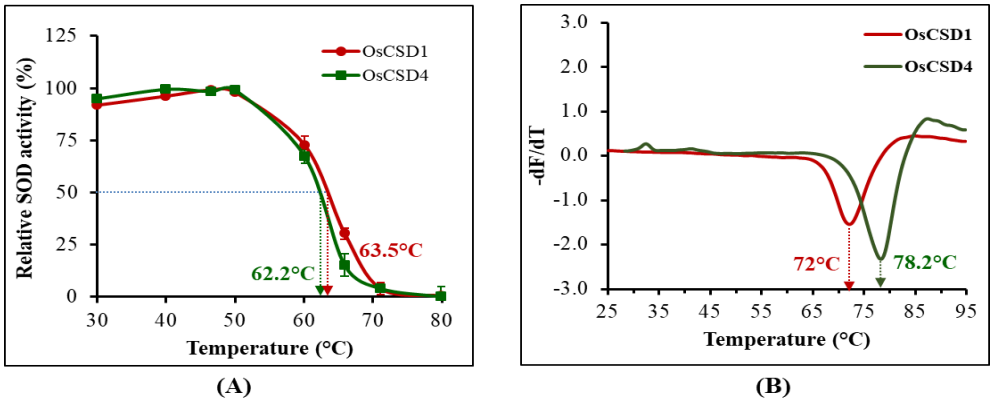

Fig. 3.4.18. Effect of temperature on stability of OsCSD1 and OsCSD4. (A) Thermal-inactivation assay: 1 U equivalent protein was pre-incubated at different temperatures (30–80°C) for 1 h, and assayed for residual SOD activity. Relative SOD activity was estimated by considering activity at 0 h time-point as 100 %. Vertical lines indicate $T_{1/2}$ (°C) of proteins. **(B)** DSF analysis for structural stability: Structural stability of the proteins was determined by Differential Scanning Fluorimetry (DSF). Fluorescence of SYPRO Orange was monitored as a function of temperature and used to generate first derivative curve for estimation of unfolding/melting temperature (Tm) of the proteins. Data are represented as mean ± SD of three independent replicates.

3.4.10.6. The rice cytosolic OsCSDs also exhibits peroxidase activity

The Cu/Zn SODs are often reported to exhibit bicarbonate dependent peroxidase activity due to formation of carbonate radical ($CO_3^{\cdot -}$) from HCO_3^-/SOD/ H_2O_2 system and oxidization of DCFH into DCF [261]. Peroxidase activity of OsCSD1 and OsCSD4 was measured by monitoring the oxidation of DCFH into DCF, in presence of bicarbonate as described in **Section 2.2.18.5** of materials and methods.

Analysis showed that both cytosolic OsCSDs exhibits bicarbonate dependent peroxidase activity, however, OsCSD4 showed higher peroxidase activity than OsCSD1 and OsCSD3, the peroxisomal CSD (**Fig. 3.4.19**).

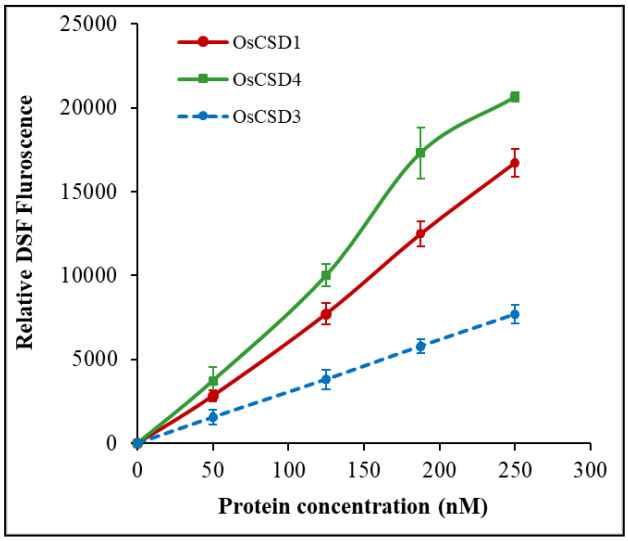

Fig. 3.4.19. Analysis of bicarbonate dependent peroxidase activity of rice cytosolic (OsCSD1, OsCSD4) and peroxisomal CSD (OsCSD3). Increasing protein concentration (0-250 nM) was taken and peroxidase activity of the proteins were monitored by measuring DCF fluorescence (excitation: 480 nm; emission: 524 nm). Data are represented as mean ± SD of three independent replicates.

3.4.11. Discussion

The cytosolic CSDs are important in regulating plant responses to different stresses by neutralizing the excess ROS levels in cytosol [156,325,328]. The protective role is also evident from overexpression studies of cytosolic CSDs in different plants resulting into tolerance to stress conditions [156,325,326]. The cytosolic CSDs have been very well characterized in different plant systems, however the regulation and functional heterogeneity among multi-copy genes originated due to

duplication events has not been addressed sufficiently. During the course of evolution, monocots as well as dicots plants has undergone several types of genome rearrangements, including whole genome duplication (WGD), and block and tandem duplications [329]. Rice genome has also undergone several duplication events, which resulted in many paralogs genes and functional redundancy [329]. The two cytosolic CSDs (OsCSD1 and OsCSD4) in rice are outcome of an inter-chromosomal block duplication between chromosome 3 and 7 [143]. Such duplication events have also been reported in some other monocots and dicots plant species [146,165,336]. Analysis of the duplication events involving CSDs in few monocots and dicots species revealed different outcomes possibly due to sequence divergence subsequent to the duplication. For example, in duplication events in few plants (*Brassica rapa, Daucus Carota, Glycine max*) resulted in duplicated CSDs with few variations (0-9 aa), whereas some other species (*Oryza sativa, Setaria italica, Sorghum bicolor*) showed 16-42 aa variations in the duplicated CSD copies. In rice, OsCSD1 and OsCSD4 genes accumulated variations in the length and sequence of the upstream regulatory elements leading to differential response to different conditions as seen in the present and previous studies [227,228]. Change in promoter size resulted in reduction in length of one CpG island and loss of the other in OsCSD4. This may contribute to their differential response as CpG islands serve as important regulatory sites, and are sensitive to modifications by DNA methyl transferases (this may alter the gene/promoter activity), indicating important roles in regulation of gene function [171,337]. In *Arabidopsis* and rice high prevalence of CpG islands were found to be associated with several genes, responsive to diverse conditions [171,338]. Differences in presence/absence/copy number of *cis*-elements also indicate differential gene

responses of the two genes in different environmental and developmental signals. The OsCSD1 and OsCSD4 were shown to be differentially responsive to ABA, light and stress conditions indicating their role in growth, development and stress adaptation [148,227,288].

The present study also identified predicted gene structure anomaly in one of the rice CSD gene. *In silico* analysis and experimental validation of OsCSD1 gene structure indicated inconsistency in the RGAP-MSU predicted gene structure. Results showed that OsCSD1 protein coding region seems considerably smaller than the predicted and is equal to OsCSD4 coding region, in length. While exon1, 2 and 3 are not contributing towards the protein coding region, exon3 contribute partially to the 5′-UTR region. The validated OsCSD1 gene structure looks more similar to the organization predicted at RAP-DB, another rice database (**Fig. 3.4.7**). Hence, RGAP-MSU predicted OsCSD1 gene structure needs to be updated, as it is also integrated with many other databases/web resources for comparative genome analysis.

Phylogenetic analysis also revealed that the two OsCSDs are substantially divergent as also observed for duplicated CSDs in Maize (**Fig. 3.1.1**). The two CSDs showed polypeptide of same length (152 aa) but with variations at 18 sites (2 involved in subunit interactions). Previous studies have shown that substitutions in residues involved in subunit interactions can affect protein properties [135,260,339]. In papaya, a single amino acid change affected the subunit interactions in cytosolic CSD [135], whereas mutation in *Ipomoea carnea* CSD resulted into dissociation of dimer [260]. Despite two variations at subunit interaction residues, the two rice CSDs, showed homodimeric interactions. Some plant cytosolic CSDs are reported to exist as equilibrium of dimeric and monomeric forms, where the dimeric form is more active

and thermostable and is suggested to be due to subunit interactions [135,260,306]. No monomeric form was observed in two rice CSDs, however the variations did affect some important characteristics. Gel filtration also indicated that the OsCSD4 is slightly more compactly folded than OsCSD1, which might be due to certain amino acids variations [340].

OsCSD4 was structurally more stable to thermal denaturation (at par with peroxisomal OsCSD3) than OsCSD1. The amino acid variations seems to enhance the proportion of β-sheet content of OsCSD4 compared to OsCSD1, which is known to contribute towards higher structural stability [312]. Comparison of secondary structures of few other reportedly thermostable CSDs *Potentilla atrosanguinea* [312], *Curcuma aromatica* [341] and *Citrus limon* [306] showed high β-sheet content (**Fig. 3.4.12**). OsCSD4 also exhibited higher specific activity, tolerance to pH changes, as reported for SODs of some plants [306], as well as displayed higher peroxidase (bicarbonate depended) activity too [260].

Collectively, the results show that two cytosolic Cu/Zn SODs (CSDs) in rice originated due to a duplication event have diverged with slightly different regulatory and protein characteristics, and may provide advantage to rice to tackle different environmental stress conditions.

CHAPTER 4

DISCUSSION

Discussion:

Exposure to adverse environmental conditions negatively impact every aspect of plant physiology. Plants use a variety of mechanisms (compatible solutes, chaperone proteins, phytohormone-induced changes, post-translation modifications, ion/water channels and stress responsive transcription factors, antioxidants etc.) to mitigate stress induced damage [342]. Many of these mechanisms are well worked out in plants, however they seldom work alone, and the overall stress response is collective outcome of interplay of multiple mechanisms. However, this scenario is becoming more complex with emergence of additional/novel stress responsive mechanisms. The present work investigates alternative splicing (AS), in regulation and functioning of rice Cu/Zn SODs (CSDs) at RNA/protein level. Additionally, impact of sequence divergence on expression and properties of two duplicated CSDs was also evaluated.

Alternative splicing (AS), a fundamental eukaryotic mechanism, generates multiple transcripts and/or protein isoforms from a single intron containing gene [174]. Its importance in cellular functioning is evident from the fact that majority of eukaryotic genes undergo AS in normal conditions, and the AS pattern is also modulated under diverse conditions [196,274]. AS events results in different outcomes such as, enhancement of transcriptome/proteome diversity, regulation of gene expression, establishment of stress-memory etc. [218]. RNAseq studies have shown predominance of AS events in organisms, and its dynamics in different conditions [286,287].

The AS is modulated/affected by both intrinsic (phytohormones) and extrinsic (environmental factors) stimuli [343–346]. Splicing is carried out by spliceosome, a

complex ribonucleoprotein (RNP) machinery [192], and it involves splice junction recognition proteins [347]. Changes in the AS pattern is modulated by alterations in the expression of splice site recognition protein, such as SR proteins [199,346]. Furthermore, the SR genes also undergo AS, which may affect the splice site recognition pattern [192] . Apart from understanding the splicing mechanism *per se*, it is also important to understand the impact of AS-mediated changes on the regulation and functioning of individual genes. This thesis deals with the analysis of AS of four rice Cu/Zn SODs. A total of nine Cu/Zn SODs transcripts (constitutive and alternative) and eight encoded protein isoforms were analyzed in the study. Transcript level analysis, compared stability of SVs and their expression in different rice tissues and abiotic stress conditions. More emphasis was to study the impact of missing/additional/alternative domains on the characteristics of different SV isoforms.

Alternative splicing operates on pre-existing transcripts and alters the relative levels of constitutive/alternative transcripts for regulation at RNA and/or protein level. In the present study, AS of rice CSDs showed tissue-specificity and modulation of pattern by stress-specific conditions. AS is known to affect transcript levels of several genes in plants and animals [189,272,348]. In *Arabidopsis*, several physiological processes (circadian rhythm, flowering etc.) are regulated by AS [272,274,349]. Circadian rhythm regulators CCA1 (circadian clock associated1) and PPR7 (pseudo response regulator 7) undergo AS to generate PTC (premature termination codon) containing transcripts [350,351]. Modulation of splicing of CCA1 and PPR7 by different factors provides a rapid and dynamic way to regulate functional protein levels [352]. AS of different SOD types have also been reported in plants (*O. sativa, A. thaliana, P. trichocarpa, G. max*) [226,245–248].

Among the two rice Fe SOD SVs (OsFe-SODa and OsFe-SODb), OsFe-SODb is generated by AS-IR event and exhibits tissue-, genotype-, and stress (light and temperature)-specific pattern, and both were found to be functionally active [245]. A similar study on Populus CSDs (homolog of rice OsCSD3) identified two SVs with expression patterns differences in cells/tissues [247]. AS of chloroplastic CSD from *Glycine max* generates an IR event-mediated alternative transcript with altered expression by Cu content of the cell [246]. These studies show that AS regulate the transcript levels of Fe- and Cu/Zn SODs in response to physiological/environmental cues. Present study investigated SVs of cytosolic (OsCSD1, OsCSD4), chloroplastic (OsCSD2) and peroxisomal (OsCSD3) Cu/Zn SODs (CSDs) in rice tissues, and in response to salinity, PEG and oxidative stress. Abundance pattern of CSD SVs shows that AS *per se* is differentially regulated in rice tissues, and is also modulated by abiotic stresses.

Splicing is a complex but precise mechanism regulated by multiple factors. For example, post-translation modifications mediated modulation and stress-induced changes in SR protein/isoform levels affects spliceosome composition (and/or function) and influence splicing pattern [353,354]. Together, such factors influence AS-mediated impact on physiological functions and stress responses. All OsCSD SVs showed expression in all rice (NSICRc106 genotype) tissues; however, their relative levels were different. Furthermore, certain CSD splice variants exhibited altered stabilities suggesting that such AS-mediated changes are also affecting CSD transcript/protein levels as per the cellular requirements. In animals, AS is known to generates PTC containing transcripts that are preferentially targeted for degradation by NMD pathway [355], however, it is not a predominant mechanism in plants [274].

Rice CSDs, particularly OsCS3, showed differential response to salinity, PEG and oxidative stress indicating stress induced AS events alters the relative levels of CSD SVs. Such variations in splicing pattern suggests involvement of either stress-specific splicing factors or modulation of activity/composition of spliceosomes [216,356].

Overall, the rice CSD SVs seems to be physiologically relevant as they are present in control conditions, and also show distinct tissue-specific patterns. Moreover, these are also responsive to different abiotic stress conditions. CSDs, being important antioxidant enzymes, are responsive to a variety of stress conditions that impose oxidative stress to the cell [143,165]. Additionally, CSDs are equally important for maintenance of intricate and physiologically relevant cellular ROS balance [88,91]. Like many stress responsive genes, CSD expression is also driven by specific *cis*-elements present in the promoter regions [165,166,288]. Furthermore, CSDs are also under negative regulation of miR398 in control and stress conditions [150,239–241]. Present study adds another dimension to the intricate regulation of CSDs, where AS seems to be involved in modulation of transcript levels of CSDs, in response to development and environmental cues.

Alternative splicing alters the relative levels of transcripts leading to changes in level of constitutive protein isoforms. Second important function of AS is to generate multiple transcripts with UTR and/or exon region variations for functional diversification of genes or enhanced transcriptome/proteome diversity [357]. In plants, AS is known to alter activity, interaction, stability of protein isoforms involved in mechanisms like hormone signaling, flowering and abiotic/biotic stress responses [174,190,358]. For example, *Arabidopsis* FLM (flowering locus M) gene (code for MADS-box TF) undergo temperature dependent AS-MEE event to generate β and δ

isoforms [211,359]. Both interacts with SVP (short vegetative phase) protein, but β isoform further interacts with DNA to suppresses flowering. Ambient temperature alters the AS and modulates the β/δ ratio to promote flowering [211,212]. AS generates an alternative isoform of JAZ protein (negative regulator of jasmonic acid signaling) and alters jasmonic acid signaling [207]. Alternative isoform lacks Jas domain, which is crucial for ubiquitin-mediated proteasomal degradation of the protein [360]. Its overexpression affects anthesis and results into male sterile plants [208]. Auxin biosynthesis gene YUCCA4 undergoes tissue-specific AS (5′ ASS event) to produce a cytosolic isoform (expressed in all tissues), and an alternative ER membrane localized (flower specific) isoform important for intra-cellular auxin level in flowers [210].

Among SODs also there are reports of AS-mediated functional diversification of protein isoforms. While in rice the two Fe SOD isoforms (FeSODa and FeSODb) were found to be enzymatically active despite C-terminal length heterogeneity [245]. However, AS at 3′ end of *Arabidopsis* Fe SOD (AtFSD3, chloroplastic) generates two isoforms (FSD3 and FSD3S) with similar SOD activity, but different localization (FSD3: nucleoid; FSD3S: stroma and chloroplastic membrane) and role in chloroplast [248]. AS-mediated introduction of PTC in Soybean chloroplastic CSD (GmCSD2) results in a truncated isoform, however both isoforms are enzymatically active [246].

In the present study, AS of four CSDs generates five alternative splice variants, of which four showed variations in coding region that results in different types of heterogeneity in the encoded proteins. AS generated OsCSD2-SV2 isoform of chloroplastic CSD showed loss of four amino acids, whereas three peroxisomal CSD (OsCSD3) isoforms (SV2, SV3 and SV4) showed considerable length and/or

sequence variations in encoded proteins. AS mediated removal of 4 amino acids (GPTT) in OsCSD2-SV2 isoform of rice chloroplastic CSD affected several characteristics (specific activity, thermostability, pH stability, sensitivity to H_2O_2) except the homo-dimeric status of the isoform. This suggest that the loss of these amino acids is affecting the overall structure/conformation of the protein isoform. However, it may be important for AS-mediated regulation of activity of chloroplastic CSD in rice. Hence, it will be important to study the impact of heteromeric subunit interaction of this isoform with the constitutive isoform. On the contrary, AS-mediated removal of large coding regions that contained amino acid residues involved in metal cofactor binding (Cu^{2+} and Zn^{2+}), disulfide bond formation, surface interactions in OsCSD3, rendered the three alternative isoforms inactive for the SOD function. However, such apparently non-functional isoforms may serve as additional controls for modulation (downregulation) of SOD activity by either channeling these towards degradation or by generating less efficient heteromeric configuration with reduced activity [212,361]. However, existence of both these possibilities will need further experimental support.

Hence, alternative splicing mechanism is likely to be involved (combination with other mechanisms) in modulation of the rice CSD levels at RNA and/or protein levels. Regulation of SODs in coordination with other antioxidant enzymes is crucial for maintenance of physiologically relevant ROS ($O_2^{\cdot -}/H_2O_2$) levels and scavenging of excess ROS in the cell [55,88]. A gradient of $O_2^{\cdot -}/H_2O_2$ seems to be important for cell proliferation/differentiation in *Arabidopsis* [88,91,362]. Since CSDs are localized to different sub-cellular compartments, AS-mediated generation of alternative isoforms may also be involved in organelle specific redox signaling, adjustment of

retrograde signal for gene expression [68,81,293]. Recently, a novel function associated with an AS-generated alternative AtFSD3S isoform in *Arabidopsis* was reported. AtFSD3S interacts with plastid encoded RNA polymerase (PEP) and PEP-associated proteins (PAP), and negatively regulates photosynthesis and chloroplast development [248]. AS also modifies the presence/absence of important signals/regions and alters sub-cellular localizations protein isoforms [210]. These examples and other studies show that AS can generate isoforms with altogether novel functions other than constitutive isoform [357]. The alternative isoforms of SODs in rice, *Arabidopsis* and other plants, with alterations in domains may also be involved in other functions, which needs to be carefully investigated. Hence, alternative transcript/protein isoforms of ~60 to >90% genes among different eukaryotes advocates a thorough analysis for identification and assessment of associated novel functions to understand their precise role in cellular functioning.

The types of AS events (ES, IR, MEE, 3′ ASS) shown by rice CSDs are different than homologs in *Arabidopsis*, Populus and Soybean that showed differences in type of AS events and number of SVs. For instance, OsCSD2 undergoes 3′ ASS event, while Soybean GmCSD2 show IR event. Rice CSD3 (peroxisomal) generates four SVs corresponding genes in Populus and *Arabidopsis* (TAIR; https://www.arabidopsis.org/index.jsp) generates two SVs [226,247]. These differences indicate that splicing events of CSDs are not conserved across the different species [247], and different plants may utilize AS to regulate the functioning of same gene by different means.

One more aspect of this study involved analysis of two cytosolic CSDs in rice. Several plants (e.g., *Arabidopsis*) have a single cytosolic CSD; while many others

species (e.g., rice) contain more than one cytosolic CSD, originated as a consequence of duplication events (https://bioinformatics.psb.ugent.be/plaza/). Genome-wide analysis of SODs in different plants have shown evidence of segmental duplication resulting into multiple isozymes [279,336,363]. However, the impact of the duplication event and subsequent sequence divergence, if any, on the structure/function of SODs has not been addressed in-depth, in most cases. The OsCSD1 and OsCSD4, have originated due to a block duplication event between chromosome 3 and 7 of rice [143]. Gene duplication events may allow sequence divergence affecting regulatory or coding region of duplicated genes with impact on responsiveness and functionality [333,364]. Present and previous studies showed that the two cytosolic OsCSDs responds differentially to abiotic stresses suggesting heterogeneity in upstream regulatory elements [227,228,288]. The two OsCSD genes were analyzed in this study to understand the impact of duplication event. RGAP-MSU predicted OsCSD1 annotation showed some inconsistency in the gene structure. As many online database servers/tools utilize the predicted gene models, updates in gene structure will be important to avoid errors during comparative analysis across genomes. Differences in the promoter region (CpG islands and presence/absence and copy number of *cis*-regulatory elements) indicate post-duplication divergence resulted in differential response of genes. Coding region divergence mediated changes in amino acid resulted in better properties of OsCSD4 (structural stability, high enzyme activity, ability to tolerate pH changes) than OsCSD1. Gene duplication analysis in few monocot and dicot species showed different extent of divergence in cytosolic CSDs in coding region suggesting divergence of protein sequence/structure. Results showed that the two rice cytosolic CSDs originated by GD event are regulated

differentially under different conditions, and the two proteins with different characteristics might be beneficial to plant under unfavourable conditions. Overall, the study highlights the importance of alternative splicing of peroxisomal, chloroplastic and cytosolic Cu/Zn SODs type at RNA level, and the impact of changes at protein level. Additionally, the impact of duplication event in regulation and functioning of two cytosolic CSDs was also analyzed. Collectively, the two mechanisms contribute towards regulation and functioning of rice CSDs, and further analysis may also provide more insights into other roles of isoforms lacking SOD function. Certain CSDs with remarkable properties were identified that may be useful for biotechnological applications, and collectively the information may be useful for devising strategies for stress tolerance enhancement of plants.

BIBLIOGRAPHY

1. Cramer GR, Urano K, Delrot S, Pezzotti M, Shinozaki K. Effects of abiotic stress on plants: A systems biology perspective. BMC Plant Biology. BioMed Central; 2011. pp. 1–14. doi:10.1186/1471-2229-11-163
2. Singh G. Climate Change and Sustainable Management of Salinity in Agriculture. Res Med Eng Sci. 2018;6. doi:10.31031/rmes.2018.06.000635
3. Praveen B, Sharma P. Climate Change and its impacts on Indian agriculture: An Econometric analysis. J Public Aff. 2020;20: 1–6. doi:10.1002/pa.1972
4. Alexieva V, Sergiev I, Mapelli S, Karanov E. The effect of drought and ultraviolet radiation on growth and stress markers in pea and wheat. Plant, Cell Environ. 2001;24: 1337–1344. doi:10.1046/j.1365-3040.2001.00778.x
5. Lamaoui M, Jemo M, Datla R, Bekkaoui F. Heat and drought stresses in crops and approaches for their mitigation. Front Chem. 2018;6: 1–14. doi:10.3389/fchem.2018.00026
6. Fahad S, Adnan M, Noor M, Arif M, Alam M, Khan IA, et al. Major Constraints for Global Rice Production. Advances in Rice Research for Abiotic Stress Tolerance. Elsevier Inc.; 2019. doi:10.1016/b978-0-12-814332-2.00001-0
7. Thu TTP, Yasui H, Yamakawa T. Effects of salt stress on plant growth characteristics and mineral content in diverse rice genotypes. Soil Sci Plant Nutr. 2017;63: 1–10. doi:10.1080/00380768.2017.1323672
8. Lobell DB, Schlenker W, Costa-Roberts J. Climate trends and global crop production since 1980. Science (80-). 2011;333: 616–620. doi:10.1126/science.1204531
9. Zhao C, Liu B, Piao S, Wang X, Lobell DB, Huang Y, et al. Temperature increase reduces global yields of major crops in four independent estimates. Proc

Natl Acad Sci U S A. 2017;114: 9326–9331. doi:10.1073/pnas.1701762114

10. Wheeler T, Von Braun J. Climate change impacts on global food security. Science. American Association for the Advancement of Science; 2013. pp. 508–513. doi:10.1126/science.1239402
11. Hatfield JL, Boote KJ, Kimball BA, Ziska LH, Izaurralde RC, Ort D, et al. Climate impacts on agriculture: Implications for crop production. Agron J. 2011;103: 351–370. doi:10.2134/agronj2010.0303
12. Ray DK, Ramankutty N, Mueller ND, West PC, Foley JA. Recent patterns of crop yield growth and stagnation. Nat Commun. 2012;3: 1293. doi:10.1038/ncomms2296
13. Fukagawa NK, Ziska LH. Rice: importance for global nutrition. J Nutr Sci Vitaminol (Tokyo). 2019;65: S2–S3. doi:10.3177/jnsv.65.S2
14. Ashikari M, Ma JF. Exploring the power of plants to overcome environmental stresses. Rice. 2015;8: 12284. doi:10.1186/s12284-014-0037-y
15. Mohd Hanafiah N, Mispan MS, Lim PE, Baisakh N, Cheng A. The 21st Century Agriculture: When Rice Research Draws Attention to Climate Variability and How Weedy Rice and Underutilized Grains Come in Handy. Plants. 2020;9: 365. doi:10.3390/plants9030365
16. Jackson SA. Rice: The First Crop Genome. Rice. Springer New York LLC; 2016. p. 14. doi:10.1186/s12284-016-0087-4
17. Zhang Q. Strategies for developing Green Super Rice. Proc Natl Acad Sci U S A. 2007;104: 16402–16409. doi:10.1073/pnas.0708013104
18. Maiti RK, Satya P. Research advances in major cereal crops for adaptation to abiotic stresses. GM crops & food. Taylor & Francis; 2014. pp. 259–279.

doi:10.4161/21645698.2014.947861

19. Arif M, Jan T, Riaz M, Fahad S, Arif MS, Shakoor MB, et al. Advances in Rice Research for Abiotic Stress Tolerance. Advances in Rice Research for Abiotic Stress Tolerance. Elsevier Inc.; 2019. doi:10.1016/b978-0-12-814332-2.00029-0
20. Lesk C, Rowhani P, Ramankutty N. Influence of extreme weather disasters on global crop production. Nature. 2016;529: 84–87. doi:10.1038/nature16467
21. Kapoor D, Bhardwaj S, Landi M, Sharma A, Ramakrishnan M, Sharma A. The Impact of Drought in Plant Metabolism: How to Exploit Tolerance Mechanisms to Increase Crop Production. Appl Sci. 2020;10: 5692. doi:10.3390/app10165692
22. Shah K, Chaturvedi V, Gupta S. Climate Change and Abiotic Stress-Induced Oxidative Burst in Rice. Advances in Rice Research for Abiotic Stress Tolerance. Elsevier; 2019. pp. 505–535. doi:10.1016/b978-0-12-814332-2.00025-3
23. Hu Y, Schmidhalter U. Drought and salinity: A comparison of their effects on mineral nutrition of plants. Journal of Plant Nutrition and Soil Science. John Wiley & Sons, Ltd; 2005. pp. 541–549. doi:10.1002/jpln.200420516
24. Kapoor D, Singh S, Kumar V, Romero R, Prasad R, Singh J. Antioxidant enzymes regulation in plants in reference to reactive oxygen species (ROS) and reactive nitrogen species (RNS). Plant Gene. 2019;19. doi:10.1016/j.plgene.2019.100182
25. Gommers C. Keep Cool and Open Up: Temperature-Induced Stomatal Opening. Plant Physiol. 2020;182: 1188–1189. doi:10.1104/pp.20.00158
26. Gill SS, Tuteja N. Reactive oxygen species and antioxidant machinery in abiotic

stress tolerance in crop plants. Plant Physiology and Biochemistry. 2010. pp. 909–930. doi:10.1016/j.plaphy.2010.08.016

27. Takagi D, Takumi S, Hashiguchi M, Sejima T, Miyake C. Superoxide and singlet oxygen produced within the thylakoid membranes both cause photosystem I photoinhibition. Plant Physiol. 2016;171: 1626–1634. doi:10.1104/pp.16.00246

28. Sewelam N, Kazan K, Schenk PM. Global plant stress signaling: Reactive oxygen species at the cross-road. Frontiers in Plant Science. Frontiers Media S.A.; 2016. doi:10.3389/fpls.2016.00187

29. Balazadeh S, Jaspert N, Arif M, Mueller-Roeber B, Maurino VG. Expression of ROS-responsive genes and transcription factors after metabolic formation of H_2O_2 in chloroplasts. Front Plant Sci. 2012;3. doi:10.3389/fpls.2012.00234

30. Gupta P, Yadav C, Singla-Pareek SL, Pareek A. Recent Advancements in Developing Salinity Tolerant Rice. Advances in Rice Research for Abiotic Stress Tolerance. Elsevier; 2019. pp. 87–112. doi:10.1016/b978-0-12-814332-2.00005-8

31. Shahid MA, Sarkhosh A, Khan N, Balal RM, Ali S, Rossi L, et al. Insights into the physiological and biochemical impacts of salt stress on plant growth and development. Agronomy. MDPI AG; 2020. doi:10.3390/agronomy10070938

32. Miller G, Suzuki N, Ciftci-Yilmaz S, Mittler R. Reactive oxygen species homeostasis and signalling during drought and salinity stresses. Plant, Cell Environ. 2010;33: 453–467. doi:10.1111/j.1365-3040.2009.02041.x

33. Kumar Yadav S. c INRA. Agron Sustain Dev. 2010;30: 515–527. doi:10.1051/agro/2009050ï

34. Hasanuzzaman M, Nahar K, Alam MM, Roychowdhury R, Fujita M. Physiological, biochemical, and molecular mechanisms of heat stress tolerance in plants. International Journal of Molecular Sciences. Multidisciplinary Digital Publishing Institute (MDPI); 2013. pp. 9643–9684. doi:10.3390/ijms14059643

35. Hatfield JL, Prueger JH. Temperature extremes: Effect on plant growth and development. Weather Clim Extrem. 2015;10: 4–10. doi:10.1016/j.wace.2015.08.001

36. Suzuki N, Mittler R. Reactive oxygen species and temperature stresses: A delicate balance between signaling and destruction. Physiologia Plantarum. John Wiley & Sons, Ltd; 2006. pp. 45–51. doi:10.1111/j.0031-9317.2005.00582.x

37. Huang M, Guo Z. Responses of antioxidative system to chilling stress in two rice cultivars differing in sensitivity. Biol Plant. 2005;49: 81–84. doi:10.1007/s00000-005-1084-3

38. Saropulos AS, Drennan DSH. Ultrastructural alterations in mesophyll and bundle sheath chloroplasts of two maize cultivars in response to chilling at high irradiance. Biol Plant. 2007;51: 690–698. doi:10.1007/s10535-007-0144-3

39. Allen DJ, Ort DR. Impacts of chilling temperatures on photosynthesis in warm-climate plants. Trends in Plant Science. 2001. pp. 36–42. doi:10.1016/S1360-1385(00)01808-2

40. Liu X, Zhou Y, Xiao J, Bao F. Effects of chilling on the structure, function and development of chloroplasts. Frontiers in Plant Science. Frontiers Media S.A.; 2018. p. 1715. doi:10.3389/fpls.2018.01715

41. Shahid M, Pourrut B, Dumat C, Nadeem M, Aslam M, Pinelli E. Heavy-metal-induced reactive oxygen species: Phytotoxicity and physicochemical changes in

plants. Reviews of Environmental Contamination and Toxicology. Springer New York LLC; 2014. pp. 1–44. doi:10.1007/978-3-319-06746-9_1

42. Tchounwou PB, Yedjou CG, Patlolla AK, Sutton DJ. Heavy metal toxicity and the environment. EXS. 2012. pp. 133–164. doi:10.1007/978-3-7643-8340-4_6

43. Maheshwari R, Dubey RS. Nickel-induced oxidative stress and the role of antioxidant defence in rice seedlings. Plant Growth Regul. 2009;59: 37–49. doi:10.1007/s10725-009-9386-8

44. Schützendübel A, Polle A. Plant responses to abiotic stresses: Heavy metal-induced oxidative stress and protection by mycorrhization. Journal of Experimental Botany. Oxford University Press; 2002. pp. 1351–1365. doi:10.1093/jxb/53.372.1351

45. Jan A, Azam M, Siddiqui K, Ali A, Choi I, Haq Q. Heavy Metals and Human Health: Mechanistic Insight into Toxicity and Counter Defense System of Antioxidants. Int J Mol Sci. 2015;16: 29592–29630. doi:10.3390/ijms161226183

46. Dutta S, Mitra M, Agarwal P, Mahapatra K, De S, Sett U, et al. Oxidative and genotoxic damages in plants in response to heavy metal stress and maintenance of genome stability. Plant Signaling and Behavior. Taylor and Francis Inc.; 2018. doi:10.1080/15592324.2018.1460048

47. Perfus-Barbeoch L, Leonhardt N, Vavasseur A, Forestier C. Heavy metal toxicity: Cadmium permeates through calcium channels and disturbs the plant water status. Plant J. 2002;32: 539–548. doi:10.1046/j.1365-313X.2002.01442.x

48. Czégény G, Mátai A, Hideg É. UV-B effects on leaves-Oxidative stress and acclimation in controlled environments. Plant Science. Elsevier Ireland Ltd; 2016. pp. 57–63. doi:10.1016/j.plantsci.2016.04.013

49. Jansen MAK, Gaba V, Greenberg BM. Higher plants and UV-B radiation: Balancing damage, repair and acclimation. Trends in Plant Science. Elsevier Ltd; 1998. pp. 131–135. doi:10.1016/S1360-1385(98)01215-1

50. Hideg É, Jansen MAK, Strid Å. UV-B exposure, ROS, and stress: Inseparable companions or loosely linked associates? Trends in Plant Science. 2013. pp. 107–115. doi:10.1016/j.tplants.2012.09.003

51. P. Sharma ABJRSDMP. Reactive oxygen species, oxidative damage, and antioxidative defense mechanism in plants under stressful conditions. J Bot. 2012;1: 1–26.

52. Choudhury FK, Rivero RM, Blumwald E, Mittler R. Reactive oxygen species, abiotic stress and stress combination. Plant J. 2017;90: 856–867. doi:10.1111/tpj.13299

53. Baxter A, Mittler R, Suzuki N. ROS as key players in plant stress signalling. Journal of Experimental Botany. Oxford University Press; 2014. pp. 1229–1240. doi:10.1093/jxb/ert375

54. Tripathy BC, Oelmüller R. Reactive oxygen species generation and signaling in plants. Plant Signal Behav. 2012;7. doi:10.4161/psb.22455

55. Mittler R. ROS Are Good. Trends in Plant Science. Elsevier Ltd; 2017. pp. 11–19. doi:10.1016/j.tplants.2016.08.002

56. Das K, Roychoudhury A. Reactive oxygen species (ROS) and response of antioxidants as ROS-scavengers during environmental stress in plants. Frontiers in Environmental Science. Frontiers Media S.A.; 2014. p. 53. doi:10.3389/fenvs.2014.00053

57. Sessions AL, Doughty DM, Welander P V., Summons RE, Newman DK. The

Continuing Puzzle of the Great Oxidation Event. Current Biology. Elsevier; 2009. pp. R567–R574. doi:10.1016/j.cub.2009.05.054

58. Farooq MA, Niazi AK, Akhtar J, Saifullah, Farooq M, Souri Z, et al. Acquiring control: The evolution of ROS-Induced oxidative stress and redox signaling pathways in plant stress responses. Plant Physiology and Biochemistry. Elsevier Masson SAS; 2019. pp. 353–369. doi:10.1016/j.plaphy.2019.04.039

59. Waszczak C, Carmody M, Kangasjärvi J. Reactive Oxygen Species in Plant Signaling. Annual Review of Plant Biology. Annual Reviews Inc.; 2018. pp. 209–236. doi:10.1146/annurev-arplant-042817-040322

60. Sharma P, Jha AB, Dubey RS, Pessarakli M. Reactive Oxygen Species, Oxidative Damage, and Antioxidative Defense Mechanism in Plants under Stressful Conditions. J Bot. 2012;2012: 1–26. doi:10.1155/2012/217037

61. Janku M, Luhová L, Petrivalský M. On the origin and fate of reactive oxygen species in plant cell compartments. Antioxidants. MDPI AG; 2019. doi:10.3390/antiox8040105

62. Khorobrykh S, Havurinne V, Mattila H, Tyystjärvi E. Oxygen and ROS in photosynthesis. Plants. MDPI AG; 2020. p. 91. doi:10.3390/plants9010091

63. Triantaphylidès C, Krischke M, Hoeberichts FA, Ksas B, Gresser G, Havaux M, et al. Singlet oxygen is the major reactive oxygen species involved in photooxidative damage to plants. Plant Physiol. 2008;148: 960–968. doi:10.1104/pp.108.125690

64. Mittler R. Oxidative stress, antioxidants and stress tolerance. Trends in Plant Science. Elsevier; 2002. pp. 405–410. doi:10.1016/S1360-1385(02)02312-9

65. Del Río LA, Corpas FJ, Sandalio LM, Palma JM, Gómez M, Barroso JB.

Reactive oxygen species, antioxidant systems and nitric oxide in peroxisomes. J Exp Bot. 2002;53: 1255–1272. doi:10.1093/jxb/53.372.1255

66. Corpas FJ, González-Gordo S, Palma JM. Plant Peroxisomes: A Factory of Reactive Species. Front Plant Sci. 2020;11: 853. doi:10.3389/fpls.2020.00853

67. Kohli SK, Khanna K, Bhardwaj R, Abd Allah EF, Ahmad P, Corpas FJ. Assessment of subcellular ROS and NO metabolism in higher plants: Multifunctional signaling molecules. Antioxidants. MDPI AG; 2019. p. 641. doi:10.3390/antiox8120641

68. Shapiguzov A, Vainonen JP, Wrzaczek M, Kangasjärvi J. ROS-talk - how the apoplast, the chloroplast, and the nucleus get the message through. Frontiers in Plant Science. Frontiers Research Foundation; 2012. p. 292. doi:10.3389/fpls.2012.00292

69. Farvardin A, González-hernández AI, Llorens E, García-agustín P, Scalschi L, Vicedo B. The apoplast: A key player in plant survival. Antioxidants. MDPI AG; 2020. pp. 1–26. doi:10.3390/antiox9070604

70. Podgórska A, Burian M, Szal B. Extra-cellular but extra-ordinarily important for cells: Apoplastic reactive oxygen species metabolism. Frontiers in Plant Science. Frontiers Media S.A.; 2017. doi:10.3389/fpls.2017.01353

71. Jajic I, Sarna T, Strzalka K. Senescence, stress, and reactive oxygen species. Plants. MDPI AG; 2015. pp. 393–411. doi:10.3390/plants4030393

72. Bienert GP, Møller ALB, Kristiansen KA, Schulz A, Møller IM, Schjoerring JK, et al. Specific aquaporins facilitate the diffusion of hydrogen peroxide across membranes. J Biol Chem. 2007;282: 1183–1192. doi:10.1074/jbc.M603761200

73. Hawkins BJ, Madesh M, Kirkpatrick CJ, Fisher AB. Superoxide flux in

endothelial cells via the chloride channel-3 mediates intracellular signaling. Mol Biol Cell. 2007;18: 2002–2012. doi:10.1091/mbc.E06-09-0830

74. Mackova K, Misak A, Tomaskova Z. Lifting the Fog over Mitochondrial Chloride Channels. Ion Channels in Health and Sickness. InTech; 2018. doi:10.5772/intechopen.76419

75. Mhamdi A, Van Breusegem F. Reactive oxygen species in plant development. Dev. 2018;145. doi:10.1242/dev.164376

76. Suzuki N, Koussevitzky S, Mittler R, Miller G. ROS and redox signalling in the response of plants to abiotic stress. Plant, Cell and Environment. John Wiley & Sons, Ltd; 2012. pp. 259–270. doi:10.1111/j.1365-3040.2011.02336.x

77. Cadet J, Douki T, Gasparutto D, Ravanat JL. Oxidative damage to DNA: Formation, measurement and biochemical features. Mutation Research - Fundamental and Molecular Mechanisms of Mutagenesis. Elsevier; 2003. pp. 5–23. doi:10.1016/j.mrfmmm.2003.09.001

78. Dröge W. Free radicals in the physiological control of cell function. Physiological Reviews. American Physiological Society; 2002. pp. 47–95. doi:10.1152/physrev.00018.2001

79. Buffenstein R, Edrey YH, Yang T, Mele J. The oxidative stress theory of aging: Embattled or invincible? Insights from non-traditional model organisms. Age. Springer; 2008. pp. 99–109. doi:10.1007/s11357-008-9058-z

80. Choudhury S, Panda P, Sahoo L, Panda SK. Reactive oxygen species signaling in plants under abiotic stress. Plant Signal Behav. 2013;8. doi:10.4161/psb.23681

81. Peleg-Grossman S, Melamed-Book N, Cohen G, Levine A. Cytoplasmic H_2O_2

prevents translocation of NPR1 to the nucleus and inhibits the induction of PR genes in Arabidopsis. Plant Signal Behav. 2010;5. doi:10.4161/psb.5.11.13209

82. Gupta R, Luan S. Redox control of protein tyrosine phosphatases and mitogen-activated protein kinases in plants. Plant Physiol. 2003;132: 1149–1152. doi:10.1104/pp.103.020792

83. Dogra V, Rochaix JD, Kim C. Singlet oxygen-triggered chloroplast-to-nucleus retrograde signalling pathways: An emerging perspective. Plant Cell and Environment. Blackwell Publishing Ltd; 2018. pp. 1727–1738. doi:10.1111/pce.13332

84. Gechev TS, Van Breusegem F, Stone JM, Denev I, Laloi C. Reactive oxygen species as signals that modulate plant stress responses and programmed cell death. BioEssays. 2006;28: 1091–1101. doi:10.1002/bies.20493

85. Fang X, Zhao G, Zhang S, Li Y, Gu H, Li Y, et al. Chloroplast-to-Nucleus Signaling Regulates MicroRNA Biogenesis in Arabidopsis. Dev Cell. 2019;48: 371-382.e4. doi:10.1016/j.devcel.2018.11.046

86. Choudhary A, Kumar A, Kaur N. ROS and oxidative burst: Roots in plant development. Plant Divers. 2020;42: 33–43. doi:10.1016/j.pld.2019.10.002

87. Jeevan Kumar SP, Rajendra Prasad S, Banerjee R, Thammineni C. Seed birth to death: Dual functions of reactive oxygen species in seed physiology. Ann Bot. 2015;116: 663–668. doi:10.1093/aob/mcv098

88. Schmidt R, Schippers JHM. ROS-mediated redox signaling during cell differentiation in plants. Biochim Biophys Acta - Gen Subj. 2015;1850: 1497–1508. doi:10.1016/j.bbagen.2014.12.020

89. Schippers JHM, Foyer CH, van Dongen JT. Redox regulation in shoot growth,

SAM maintenance and flowering. Curr Opin Plant Biol. 2016;29: 121–128. doi:10.1016/j.pbi.2015.11.009

90. Mangano S, Juárez SPD, Estevez JM. ROS regulation of polar growth in plant cells. Plant Physiol. 2016;171: 1593–1605. doi:10.1104/pp.16.00191

91. Zeng J, Dong Z, Wu H, Tian Z, Zhao Z. Redox regulation of plant stem cell fate. EMBO J. 2017;36: 2844–2855. doi:10.15252/embj.201695955

92. Singh R, Singh S, Parihar P, Mishra RK, Tripathi DK, Singh VP, et al. Reactive oxygen species (ROS): Beneficial companions of plants' developmental processes. Front Plant Sci. 2016;7: 1–19. doi:10.3389/fpls.2016.01299

93. Yi J, Moon S, Lee YS, Zhu L, Liang W, Zhang D, et al. Defective tapetum cell death 1 (DTC1) regulates ROS levels by binding to metallothionein during tapetum degeneration. Plant Physiol. 2016;170: 1611–1623. doi:10.1104/pp.15.01561

94. Natesan SKA, Sullivan JA, Gray JC. Stromules: A characteristic cell-specific feature of plastid morphology. Journal of Experimental Botany. 2005. pp. 787–797. doi:10.1093/jxb/eri088

95. Caplan JL, Kumar AS, Park E, Padmanabhan MS, Hoban K, Modla S, et al. Chloroplast Stromules Function during Innate Immunity. Dev Cell. 2015;34: 45–57. doi:10.1016/j.devcel.2015.05.011

96. Brunkard JO, Runkel AM, Zambryski PC. Chloroplasts extend stromules independently and in response to internal redox signals. Proc Natl Acad Sci U S A. 2015;112: 10044–10049. doi:10.1073/pnas.1511570112

97. Hanson MR, Hines KM. Stromules: Probing formation and function. Plant Physiology. American Society of Plant Biologists; 2018. pp. 128–137.

doi:10.1104/pp.17.01287

98. Mittler R, Vanderauwera S, Suzuki N, Miller G, Tognetti VB, Vandepoele K, et al. ROS signaling: The new wave? Trends Plant Sci. 2011;16: 300–309. doi:10.1016/j.tplants.2011.03.007

99. Bindschedler L V., Dewdney J, Blee KA, Stone JM, Asai T, Plotnikov J, et al. Peroxidase-dependent apoplastic oxidative burst in Arabidopsis required for pathogen resistance. Plant J. 2006;47: 851–863. doi:10.1111/j.1365-313X.2006.02837.x

100. Lambeth JD. NOX enzymes and the biology of reactive oxygen. Nature Reviews Immunology. Nature Publishing Group; 2004. pp. 181–189. doi:10.1038/nri1312

101. Qi J, Wang J, Gong Z, Zhou JM. Apoplastic ROS signaling in plant immunity. Current Opinion in Plant Biology. Elsevier Ltd; 2017. pp. 92–100. doi:10.1016/j.pbi.2017.04.022

102. Nomura H, Komori T, Uemura S, Kanda Y, Shimotani K, Nakai K, et al. Chloroplast-mediated activation of plant immune signalling in Arabidopsis. Nat Commun. 2012;3. doi:10.1038/ncomms1926

103. Torres MA, Dangl JL, Jones JDG. Arabidopsis gp91phox homologues Atrbohd and Atrbohf are required for accumulation of reactive oxygen intermediates in the plant defense response. Proc Natl Acad Sci U S A. 2002;99: 517–522. doi:10.1073/pnas.012452499

104. Torres MA, Dangl JL. Functions of the respiratory burst oxidase in biotic interactions, abiotic stress and development. Current Opinion in Plant Biology. 2005. pp. 397–403. doi:10.1016/j.pbi.2005.05.014

105. Suzuki N, Miller G, Morales J, Shulaev V, Torres MA, Mittler R. Respiratory

burst oxidases: The engines of ROS signaling. Current Opinion in Plant Biology. 2011. pp. 691–699. doi:10.1016/j.pbi.2011.07.014

106. Czarnocka W, Karpiński S. Friend or foe? Reactive oxygen species production, scavenging and signaling in plant response to environmental stresses. Free Radical Biology and Medicine. Elsevier Inc.; 2018. pp. 4–20. doi:10.1016/j.freeradbiomed.2018.01.011

107. Foyer CH, Noctor G. Stress-triggered redox signalling: What's in pROSpect? Plant Cell and Environment. Blackwell Publishing Ltd; 2016. pp. 951–964. doi:10.1111/pce.12621

108. Kaludercic N, Deshwal S, Di Lisa F. Reactive oxygen species and redox compartmentalization. Front Physiol. 2014;5 JUL. doi:10.3389/fphys.2014.00285

109. Akter S, Huang J, Waszczak C, Jacques S, Gevaert K, Breusegem F Van, et al. Cysteines under ROS attack in plants: a proteomics view. J Exp Bot. 2015;66: 2935–2944. doi:10.1093/jxb/erv044

110. Fritsche S, Wang X, Jung C. Recent Advances in our Understanding of Tocopherol Biosynthesis in Plants: An Overview of Key Genes, Functions, and Breeding of Vitamin E Improved Crops. Antioxidants. 2017;6: 99. doi:10.3390/antiox6040099

111. Chan Z, Song C-P, Kim Y, Yokawa K. Ros Regulation During Plant Abiotic Stress Responses. 2007. doi:10.3389/978-2-88945-054-1

112. Ighodaro OM, Akinloye OA. First line defence antioxidants-superoxide dismutase (SOD), catalase (CAT) and glutathione peroxidase (GPX): Their fundamental role in the entire antioxidant defence grid. Alexandria J Med.

2018;54: 287–293. doi:10.1016/j.ajme.2017.09.001

113. Sheng Y, Abreu IA, Cabelli DE, Maroney MJ, Miller AF, Teixeira M, et al. Superoxide dismutases and superoxide reductases. Chemical Reviews. American Chemical Society; 2014. pp. 3854–3918. doi:10.1021/cr4005296

114. Zhang Z, Xu Y, Xie Z, Li X, He Z-H, Peng X-X. Association-Dissociation of Glycolate Oxidase with Catalase in Rice: A Potential Switch to Modulate Intracellular H_2O_2 Levels. Mol Plant. 2016;9: 737–748. doi:10.1016/j.molp.2016.02.002

115. Rizhsky L, Liang H, Mittler R. The water-water cycle is essential for chloroplast protection in the absence of stress. J Biol Chem. 2003;278: 38921–38925. doi:10.1074/jbc.M304987200

116. Alscher RG. Role of superoxide dismutases (SODs) in controlling oxidative stress in plants. J Exp Bot. 2002;53: 1331–1341. doi:10.1093/jexbot/53.372.1331

117. Perry JJP, Shin DS, Getzoff ED, Tainer JA. The structural biochemistry of the superoxide dismutases. Biochimica et Biophysica Acta - Proteins and Proteomics. Elsevier; 2010. pp. 245–262. doi:10.1016/j.bbapap.2009.11.004

118. Miller AF. Superoxide dismutases: Ancient enzymes and new insights. FEBS Letters. 2012. pp. 585–595. doi:10.1016/j.febslet.2011.10.048

119. Martin W, Rujan T, Richly E, Hansen A, Cornelsen S, Lins T, et al. Evolutionary analysis of Arabidopsis, cyanobacterial, and chloroplast genomes reveals plastid phylogeny and thousands of cyanobacterial genes in the nucleus. Proc Natl Acad Sci U S A. 2002;99: 12246–12251. doi:10.1073/pnas.182432999

120. Case AJ. On the origin of superoxide dismutase: An evolutionary perspective of

superoxide-mediated redox signaling. Antioxidants. MDPI AG; 2017. doi:10.3390/antiox6040082

121. Wolfe-Simon F, Grzebyk D, Schofield O, Falkowski PG. The role and evolution of superoxide dismutases in algae. Journal of Phycology. 2005. pp. 453–465. doi:10.1111/j.1529-8817.2005.00086.x

122. Rodríguez-Serrano M, Romero-Puertas MC, Pastori GM, Corpas FJ, Sandalio LM, Del Río LA, et al. Peroxisomal membrane manganese superoxide dismutase: Characterization of the isozyme from watermelon (Citrullus lanatus Schrad.) cotyledons. J Exp Bot. 2007;58: 2417–2427. doi:10.1093/jxb/erm095

123. Shiraya T, Mori T, Maruyama T, Sasaki M, Takamatsu T, Oikawa K, et al. Golgi/plastid-type manganese superoxide dismutase involved in heat-stress tolerance during grain filling of rice. Plant Biotechnol J. 2015;13: 1251–1263. doi:10.1111/pbi.12314

124. Whittaker JW. The irony of manganese superoxide dismutase. Biochemical Society Transactions. Portland Press Ltd; 2003. pp. 1318–1321. doi:10.1042/bst0311318

125. Hunter T, Bonetta R, Sacco A, Vella M, Sultana PM, Trinh CH, et al. A Single Mutation is Sufficient to Modify the Metal Selectivity and Specificity of a Eukaryotic Manganese Superoxide Dismutase to Encompass Iron. Chem - A Eur J. 2018;24: 5303–5308. doi:10.1002/chem.201704655

126. Wuerges J, Lee JW, Yim YI, Yim HS, Kang SO, Carugo KD. Crystal structure of nickel-containing superoxide dismutase reveals another type of active site. Proc Natl Acad Sci U S A. 2004;101: 8569–8574. doi:10.1073/pnas.0308514101

127. Bowler C, Camp W Van, Montagu M Van, Inzé D. Superoxide Dismutase in

Plants. CRC Crit Rev Plant Sci. 1994;13: 199–218. doi:10.1080/07352689409701914

128. Spagnolo L, Töro I, D'Orazio M, O'Neil P, Pedersen JZ, Carugo O, et al. Unique features of the sodC-encoded superoxide dismutase from Mycobacterium tuberculosis, a fully functional copper-containing enzyme lacking zinc in the active site. J Biol Chem. 2004;279: 33447–33455. doi:10.1074/jbc.M404699200

129. Gleason JE, Galaleldeen A, Peterson RL, Taylor AB, Holloway SP, Waninger-Saroni J, et al. Candida albicans SOD5 represents the prototype of an unprecedented class of Cu-only superoxide dismutases required for pathogen defense. Proc Natl Acad Sci U S A. 2014;111: 5866–5871. doi:10.1073/pnas.1400137111

130. Frohner IE, Bourgeois C, Yatsyk K, Majer O, Kuchler K. Candida albicans cell surface superoxide dismutases degrade host-derived reactive oxygen species to escape innate immune surveillance. Mol Microbiol. 2009;71: 240–252. doi:10.1111/j.1365-2958.2008.06528.x

131. Robinett NG, Peterson RL, Culotta VC. Eukaryotic copper-only superoxide dismutases (SODs): A new class of SOD enzymes and SOD-like protein domains. Journal of Biological Chemistry. American Society for Biochemistry and Molecular Biology Inc.; 2018. pp. 4636–4643. doi:10.1074/jbc.TM117.000182

132. Robinett NG, Culbertson EM, Peterson RL, Sanchez H, Andes DR, Nett JE, et al. Exploiting the vulnerable active site of a copper-only superoxide dismutase to disrupt fungal pathogenesis. J Biol Chem. 2019;294: 2700–2713.

doi:10.1074/jbc.RA118.007095

133. Pilon M, Ravet K, Tapken W. The biogenesis and physiological function of chloroplast superoxide dismutases. Biochimica et Biophysica Acta - Bioenergetics. 2011. pp. 989–998. doi:10.1016/j.bbabio.2010.11.002

134. Gill SS, Anjum NA, Gill R, Yadav S, Hasanuzzaman M, Fujita M, et al. Superoxide dismutase—mentor of abiotic stress tolerance in crop plants. Environmental Science and Pollution Research. Springer Verlag; 2015. pp. 10375–10394. doi:10.1007/s11356-015-4532-5

135. Lin CT, Kuo TJ, Shaw JF, Kao MC. Characterization of the dimer-monomer equilibrium of the papaya copper/zinc superoxide dismutase and its equilibrium shift by a single amino acid mutation. J Agric Food Chem. 1999;47: 2944–2949. doi:10.1021/jf981355t

136. Tuteja N, Mishra P, Yadav S, Tajrishi M, Baral S, Sabat SC. Heterologous expression and biochemical characterization of a highly active and stable chloroplastic CuZn-superoxide dismutase from Pisum sativum. BMC Biotechnol. 2015;15. doi:10.1186/s12896-015-0117-0

137. Sundaram S, Khanna S, Khanna-Chopra R. Purification and characterization of thermostable monomeric chloroplastic Cu/Zn superoxide dismutase from Chenopodium murale. Physiol Mol Biol Plants. 2009;15: 199–209. doi:10.1007/s12298-009-0024-8

138. Gottfredsen RH, Larsen UG, Enghild JJ, Petersen S V. Hydrogen peroxide induce modifications of human extracellular superoxide dismutase that results in enzyme inhibition. Redox Biol. 2013;1: 24–31. doi:10.1016/j.redox.2012.12.004

139. Dehury B, Sarma K, Sarmah R, Sahu J, Sahoo S, Sahu M, et al. In silico

analyses of superoxide dismutases (SODs) of rice (Oryza sativa L.). J Plant Biochem Biotechnol. 2013;22: 150–156. doi:10.1007/s13562-012-0121-6

140. Kumar A, Randhawa V, Acharya V, Singh K, Kumar S. Amino acids flanking the central core of Cu,Zn superoxide dismutase are important in retaining enzyme activity after autoclaving. J Biomol Struct Dyn. 2016;34: 475–485. doi:10.1080/07391102.2015.1049551

141. Bafana A, Dutt S, Kumar S, Ahuja PS. Superoxide dismutase: An industrial perspective. Critical Reviews in Biotechnology. 2011. pp. 65–76. doi:10.3109/07388551.2010.490937

142. Takahashi MA, Asada K. Superoxide anion permeability of phospholipid membranes and chloroplast thylakoids. Arch Biochem Biophys. 1983;226: 558–566. doi:10.1016/0003-9861(83)90325-9

143. Yadav S, Gill SS, Passricha N, Gill R, Badhwar P, Anjum NA, et al. Genome-wide analysis and transcriptional expression pattern-assessment of superoxide dismutase (SOD) in rice and Arabidopsis under abiotic stresses. Plant Gene. 2019;17. doi:10.1016/j.plgene.2018.10.001

144. Soydam Aydin S, Büyük I, Aras S. Relationships among lipid peroxidation, SOD enzyme activity, and SOD gene expression profile in Lycopersicum esculentum L. exposed to cold stress. Genet Mol Res. 2013;12: 3220–3229. doi:10.4238/2013.August.29.6

145. Zhou Y, Hu L, Wu H, Jiang L, Liu S. Genome-Wide Identification and Transcriptional Expression Analysis of Cucumber Superoxide Dismutase (SOD) Family in Response to Various Abiotic Stresses. Int J Genomics. 2017;2017. doi:10.1155/2017/7243973

146. Wang W, Zhang X, Deng F, Yuan R, Shen F. Genome-wide characterization and expression analyses of superoxide dismutase (SOD) genes in Gossypium hirsutum. BMC Genomics. 2017;18: 1–25. doi:10.1186/s12864-017-3768-5

147. Vighi IL, Benitez LC, Amaral MN, Moraes GP, Auler PA, Rodrigues GS, et al. Functional characterization of the antioxidant enzymes in rice plants exposed to salinity stress. Biol Plant. 2017;61: 540–550. doi:10.1007/s10535-017-0727-6

148. Sakamoto A, Okumura T, Kaminaka H, Sumi K, Tanaka K. Structure and differential response to abscisic acid of two promoters for the cytosolic copper/zinc- superoxide dismutase genes, SodCcl and SodCc2, in rice protoplasts. FEBS Lett. 1995;358: 62–66. doi:10.1016/0014-5793(94)01396-I

149. Gallie DR, Chen Z. Chloroplast-localized iron superoxide dismutases FSD2 and FSD3 are functionally distinct in Arabidopsis. PLoS One. 2019;14. doi:10.1371/journal.pone.0220078

150. Sunkar R, Kapoor A, Zhu JK. Posttranscriptional induction of two Cu/Zn superoxide dismutase genes in Arabidopsis is mediated by downregulation of miR398 and important for oxidative stress tolerance. Plant Cell. 2006;18: 2051–2065. doi:10.1105/tpc.106.041673

151. Guan Q, Liao X, He M, Li X, Wang Z, Ma H, et al. Tolerance analysis of chloroplast OsCu/Zn-SOD overexpressing rice under NaCl and NaHCO3 stress. PLoS One. 2017;12. doi:10.1371/journal.pone.0186052

152. Jing X, Hou P, Lu Y, Deng S, Li N, Zhao R, et al. Overexpression of copper/zinc superoxide dismutase from mangrove Kandelia candel in tobacco enhances salinity tolerance by the reduction of reactive oxygen species in chloroplast. Front Plant Sci. 2015;6: 1–13. doi:10.3389/fpls.2015.00023

153. Pitcher LH, Zilinskas BA. Overexpression of copper/zinc superoxide dismutase in the cytosol of transgenic tobacco confers partial resistance to ozone-induced foliar necrosis. Plant Physiol. 1996;110: 583–588. doi:10.1104/pp.110.2.583

154. Li Z, Han X, Song X, Zhang Y, Jiang J, Han Q, et al. Overexpressing the Sedum alfredii Cu/Zn superoxide dismutase increased resistance to oxidative stress in Transgenic Arabidopsis. Front Plant Sci. 2017;8: 1010. doi:10.3389/fpls.2017.01010

155. Zhang H, Lin C, Gu L. Light Regulation of Alternative Pre-mRNA Splicing in Plants. Photochemistry and Photobiology. Blackwell Publishing Inc.; 2017. pp. 159–165. doi:10.1111/php.12680

156. Prashanth SR, Sadhasivam V, Parida A. Over expression of cytosolic copper/zinc superoxide dismutase from a mangrove plant Avicennia marina in indica Rice var Pusa Basmati-1 confers abiotic stress tolerance. Transgenic Res. 2008;17: 281–291. doi:10.1007/s11248-007-9099-6

157. Wang Y, Branicky R, Noë A, Hekimi S. Superoxide dismutases: Dual roles in controlling ROS damage and regulating ROS signaling. Journal of Cell Biology. Rockefeller University Press; 2018. pp. 1915–1928. doi:10.1083/jcb.201708007

158. Mhamdi A, Van Breusegem F. Reactive oxygen species in plant development. Dev. 2018;145. doi:10.1242/dev.164376

159. Tsang CK wa., Liu Y, Thomas J, Zhang Y, Zheng XFS. Superoxide dismutase 1 acts as a nuclear transcription factor to regulate oxidative stress resistance. Nat Commun. 2014;5: 3446. doi:10.1038/ncomms4446

160. Holzmeister C, Gaupels F, Geerlof A, Sarioglu H, Sattler M, Durner J, et al. Differential inhibition of Arabidopsis superoxide dismutases by peroxynitrite-

mediated tyrosine nitration. J Exp Bot. 2015;66: 989–999. doi:10.1093/jxb/eru458

161. Youssef N, Budd A, Bielawski JP. Introduction to genome biology and diversity. Methods in Molecular Biology. Humana Press Inc.; 2019. pp. 3–31. doi:10.1007/978-1-4939-9074-0_1

162. Nath P, Sane VA, Sane AP, Trivedi PK. Plant Gene Expression, Regulation of. Encyclopedia of Molecular Cell Biology and Molecular Medicine. Weinheim, Germany: Wiley-VCH Verlag GmbH & Co. KGaA; 2006. doi:10.1002/3527600906.mcb.200400154

163. Baulcombe DC, Dean C. Epigenetic regulation in plant responses to the environment. Cold Spring Harb Perspect Biol. 2014;6. doi:10.1101/cshperspect.a019471

164. Wei JW, Huang K, Yang C, Kang CS. Non-coding RNAs as regulators in epigenetics (Review). Oncol Rep. 2017;37: 3–9. doi:10.3892/or.2016.5236

165. Verma D, Lakhanpal N, Singh K. Genome-wide identification and characterization of abiotic-stress responsive SOD (superoxide dismutase) gene family in Brassica juncea and B. rapa. BMC Genomics. 2019;20. doi:10.1186/s12864-019-5593-5

166. Hu X, Hao C, Cheng ZM, Zhong Y. Genome-wide identification, characterization, and expression analysis of the grapevine superoxide dismutase (SOD) family. Int J Genomics. 2019;2019. doi:10.1155/2019/7350414

167. Law JA, Jacobsen SE. Establishing, maintaining and modifying DNA methylation patterns in plants and animals. Nature Reviews Genetics. 2010. pp. 204–220. doi:10.1038/nrg2719

168. Boyko A, Blevins T, Yao Y, Golubov A, Bilichak A, Ilnytskyy Y, et al. Transgenerational adaptation of Arabidopsis to stress requires DNA methylation and the function of dicer-like proteins. PLoS One. 2010;5. doi:10.1371/journal.pone.0009514

169. Niederhuth CE, Schmitz RJ. Covering your bases: Inheritance of DNA methylation in plant genomes. Molecular Plant. Oxford University Press; 2014. pp. 472–480. doi:10.1093/mp/sst165

170. Ojolo SP, Cao S, Priyadarshani SVGN, Li W, Yan M, Aslam M, et al. Regulation of plant growth and development: a review from a chromatin remodeling perspective. Frontiers in Plant Science. Frontiers Media S.A.; 2018. p. 1232. doi:10.3389/fpls.2018.01232

171. Ashikawa I. Gene-associated CpG islands in plants as revealed by analyses of genomic sequences. Plant J. 2001;26: 617–625. doi:10.1046/j.1365-313X.2001.01062.x

172. Saze H, Scheid OM, Paszkowski J. Maintenance of CpG methylation is essential for epigenetic inheritance during plant gametogenesis. Nat Genet. 2003;34: 65–69. doi:10.1038/ng1138

173. Finnegan EJ, Peacock WJ, Dennis ES. Reduced DNA methylation in Arabidopsis thaliana results in abnormal plant development. Proc Natl Acad Sci U S A. 1996;93: 8449–8454. doi:10.1073/pnas.93.16.8449

174. Chaudhary S, Khokhar W, Jabre I, Reddy ASN, Byrne LJ, Wilson CM, et al. Alternative splicing and protein diversity: Plants versus animals. Frontiers in Plant Science. Frontiers Media S.A.; 2019. doi:10.3389/fpls.2019.00708

175. Karousis ED, Nasif S, Mühlemann O. Nonsense-mediated mRNA decay: novel

mechanistic insights and biological impact. Wiley Interdiscip Rev RNA. 2016;7: 661–682. doi:10.1002/wrna.1357

176. Hashiguchi A, Komatsu S. Posttranslational Modifications and Plant–Environment Interaction. Methods in Enzymology. Academic Press Inc.; 2017. pp. 97–113. doi:10.1016/bs.mie.2016.09.030

177. Zhang Y, Zeng L. Crosstalk between Ubiquitination and Other Post-translational Protein Modifications in Plant Immunity. Plant Commun. 2020;1: 100041. doi:10.1016/j.xplc.2020.100041

178. Millar AH, Heazlewood JL, Giglione C, Holdsworth MJ, Bachmair A, Schulze WX. The Scope, Functions, and Dynamics of Posttranslational Protein Modifications. Annu Rev Plant Biol. 2019;70: 119–151. doi:10.1146/annurev-arplant-050718-100211

179. Guerra D, Crosatti C, Khoshro HH, Mastrangelo AM, Mica E, Mazzucotelli E. Post-transcriptional and post-translational regulations of drought and heat response in plants: A spider's web of mechanisms. Frontiers in Plant Science. Frontiers Research Foundation; 2015. doi:10.3389/fpls.2015.00057

180. Wang J, Meng X, Dobrovolskaya OB, Orlov YL, Chen M. Non-coding RNAs and Their Roles in Stress Response in Plants Wang J et al / miRNA and lncRNA in Plant Stress Response. Genomics, Proteomics and Bioinformatics. Beijing Genomics Institute; 2017. pp. 301–312. doi:10.1016/j.gpb.2017.01.007

181. Shang X, Cao Y, Ma L. Alternative splicing in plant genes: A means of regulating the environmental fitness of plants. International Journal of Molecular Sciences. MDPI AG; 2017. p. 432. doi:10.3390/ijms18020432

182. Liu SR, Zhou JJ, Hu CG, Wei CL, Zhang JZ. MicroRNA-mediated gene

silencing in plant defense and viral counter-defense. Frontiers in Microbiology. Frontiers Media S.A.; 2017. p. 1801. doi:10.3389/fmicb.2017.01801

183. Floris M, Mahgoub H, Lanet E, Robaglia C, Menand B. Post-transcriptional Regulation of Gene Expression in Plants during Abiotic Stress. Int J Mol Sci. 2009;10: 3168–3185. Available: http://arxiv.org/abs/1006.4113
184. Leoni G, Tramontano A. A structural view of microRNA-target recognition. Nucleic Acids Res. 2016;44: e82–e82. doi:10.1093/nar/gkw043
185. Brousse C, Liu Q, Beauclair L, Deremetz A, Axtell MJ, Bouché N. A non-canonical plant microRNA target site. Nucleic Acids Res. 2014;42: 5270–5279. doi:10.1093/nar/gku157
186. Shin C, Nam JW, Farh KKH, Chiang HR, Shkumatava A, Bartel DP. Expanding the microRNA targeting code: functional sites with centered pairing. Mol Cell. 2010;38: 789–802. doi:10.1016/j.molcel.2010.06.005
187. Lee Y, Rio DC. Mechanisms and regulation of alternative Pre-mRNA splicing. Annual Review of Biochemistry. Annual Reviews Inc.; 2015. pp. 291–323. doi:10.1146/annurev-biochem-060614-034316
188. Irimia M, Roy SW. Origin of spliceosomal introns and alternative splicing. Cold Spring Harb Perspect Biol. 2014;6. doi:10.1101/cshperspect.a016071
189. Boutz PL, Bhutkar A, Sharp PA. Detained introns are a novel, widespread class of post-transcriptionally spliced introns. Genes Dev. 2015;29: 63–80. doi:10.1101/gad.247361.114
190. Reddy ASN, Marquez Y, Kalyna M, Barta A. Complexity of the alternative splicing landscape in plants. Plant Cell. 2013. pp. 3657–3683. doi:10.1105/tpc.113.117523

191. Marquez Y, Brown JWS, Simpson C, Barta A, Kalyna M. Transcriptome survey reveals increased complexity of the alternative splicing landscape in Arabidopsis. Genome Res. 2012;22: 1184–1195. doi:10.1101/gr.134106.111

192. Reddy ASN. Alternative splicing of pre-messenger RNAs in plants in the genomic era. Annual Review of Plant Biology. 2007. pp. 267–294. doi:10.1146/annurev.arplant.58.032806.103754

193. Chen W, Moore MJ. Spliceosomes. Current Biology. Cell Press; 2015. pp. R181–R183. doi:10.1016/j.cub.2014.11.059

194. Staiger D, Brown JWS. Alternative splicing at the intersection of biological timing, development, and stress responses. Plant Cell. 2013. pp. 3640–3656. doi:10.1105/tpc.113.113803

195. Romero PR, Zaidi S, Fang YY, Uversky VN, Radivojac P, Oldfield CJ, et al. Alternative splicing in concert with protein intrinsic disorder enables increased functional diversity in multicellular organisms. Proc Natl Acad Sci U S A. 2006;103: 8390–8395. doi:10.1073/pnas.0507916103

196. Syed NH, Kalyna M, Marquez Y, Barta A, Brown JWS. Alternative splicing in plants - coming of age. Trends in Plant Science. 2012. pp. 616–623. doi:10.1016/j.tplants.2012.06.001

197. Sanyal RP, Misra HS, Saini A. Heat-stress priming and alternative splicing-linked memory. J Exp Bot. 2018;69: 2431–2434. doi:10.1093/jxb/ery111

198. Meyer K, Koester T, Staiger D. Pre-mRNA splicing in plants: In vivo functions of RNA-binding proteins implicated in the splicing process. Biomolecules. MDPI AG; 2015. pp. 1717–1740. doi:10.3390/biom5031717

199. Zhang P, Deng H, Xiao FM, Liu YS. Alterations of alternative splicing patterns

of Ser/Arg-Rich (SR) genes in response to hormones and stresses treatments in different ecotypes of rice (Oryza sativa). J Integr Agric. 2013;12: 737–748. doi:10.1016/S2095-3119(13)60260-9

200. McGlincy NJ, Smith CWJ. Alternative splicing resulting in nonsense-mediated mRNA decay: what is the meaning of nonsense? Trends in Biochemical Sciences. 2008. pp. 385–393. doi:10.1016/j.tibs.2008.06.001
201. Reddy ASN, Shad Ali G. Plant serine/arginine-rich proteins: Roles in precursor messenger RNA splicing, plant development, and stress responses. Wiley Interdisciplinary Reviews: RNA. 2011. pp. 875–889. doi:10.1002/wrna.98
202. Shaul O. Unique Aspects of Plant Nonsense-Mediated mRNA Decay. Trends in Plant Science. Elsevier Ltd; 2015. pp. 767–779. doi:10.1016/j.tplants.2015.08.011
203. Swarup R, Crespi M, Bennett MJ. Developmental Cell Previews One Gene, Many Proteins: Mapping Cell-Specific Alternative Splicing in Plants. 2016 [cited 10 Sep 2020]. doi:10.1016/j.devcel.2016.11.002
204. Laloum T, Martín G, Duque P. Alternative Splicing Control of Abiotic Stress Responses. Trends in Plant Science. Elsevier Ltd; 2018. pp. 140–150. doi:10.1016/j.tplants.2017.09.019
205. Nimeth BA, Riegler S, Kalyna M. Alternative Splicing and DNA Damage Response in Plants. Front Plant Sci. 2020;11: 1–9. doi:10.3389/fpls.2020.00091
206. Kamiya Y. Plant Hormones: Versatile Regulators of Plant Growth and Development. Annu Rev Plant Biol. 2010;61: annurev.arplant.61.031110.100001. doi:10.1146/annurev.arplant.61.031110.100001

207. Mach J. Alternative splicing produces a JAZ protein that is not broken down in response to jasmonic acid. Plant Cell. American Society of Plant Biologists; 2009. p. 14. doi:10.1105/tpc.108.210111

208. Moreno JE, Shyu C, Campos ML, Patel LC, Chung HS, Yao J, et al. Negative feedback control of jasmonate signaling by an alternative splice variant of JAZ10. Plant Physiol. 2013;162: 1006–1017. doi:10.1104/pp.113.218164

209. Cao X, Yang H, Shang C, Ma S, Liu L, Cheng J. The roles of auxin biosynthesis YUCCA gene family in plants. International Journal of Molecular Sciences. MDPI AG; 2019. doi:10.3390/ijms20246343

210. Kriechbaumer V, Wang P, Hawes C, Abell BM. Alternative splicing of the auxin biosynthesis gene YUCCA4 determines its subcellular compartmentation. Plant J. 2012;70: 292–302. doi:10.1111/j.1365-313X.2011.04866.x

211. Lee JH, Ryu HS, Chung KS, Posé D, Kim S, Schmid M, et al. Regulation of temperature-responsive flowering by MADS-box transcription factor repressors. Science (80-). 2013;342: 628–632. doi:10.1126/science.1241097

212. Posé D, Verhage L, Ott F, Yant L, Mathieu J, Angenent GC, et al. Temperature-dependent regulation of flowering by antagonistic FLM variants. Nature. 2013;503: 414–417. doi:10.1038/nature12633

213. Jeong HL, Seong JY, Soo HP, Hwang I, Jong SL, Ji HA. Role of SVP in the control of flowering time by ambient temperature in Arabidopsis. Genes Dev. 2007;21: 397–402. doi:10.1101/gad.1518407

214. Bedre R, Irigoyen S, Petrillo E, Mandadi KK. New era in plant alternative splicing analysis enabled by advances in high-throughput sequencing (HTS) technologies. Front Plant Sci. 2019;10: 1–5. doi:10.3389/fpls.2019.00740

215. Zhang XC, Gassmann W. Alternative splicing and mRNA levels of the disease resistance gene RPS4 are induced during defense responses. Plant Physiol. 2007;145: 1577–1587. doi:10.1104/pp.107.108720

216. Zhang W, Du B, Liu D, Qi X. Splicing factor SR34b mutation reduces cadmium tolerance in Arabidopsis by regulating iron-regulated transporter 1 gene. Biochem Biophys Res Commun. 2014;455: 312–317. doi:10.1016/j.bbrc.2014.11.017

217. Gu J, Xia Z, Luo Y, Jiang X, Qian B, Xie H, et al. Spliceosomal protein U1A is involved in alternative splicing and salt stress tolerance in Arabidopsis thaliana. Nucleic Acids Res. 2018;46: 1777–1792. doi:10.1093/nar/gkx1229

218. Ling Y, Serrano N, Gao G, Atia M, Mokhtar M, Woo YH, et al. Thermopriming triggers splicing memory in Arabidopsis. J Exp Bot. 2018;69: 2659–2675. doi:10.1093/jxb/ery062

219. Conrath U, Beckers GJM, Langenbach CJG, Jaskiewicz MR. Priming for Enhanced Defense. Annual Review of Phytopathology. Annual Reviews Inc.; 2015. pp. 97–119. doi:10.1146/annurev-phyto-080614-120132

220. Sanyal RP, Misra HS, Saini A. Heat-stress priming and alternative splicing-linked memory. J Exp Bot. 2018;69. doi:10.1093/jxb/ery111

221. Yan K, Liu P, Wu CA, Yang GD, Xu R, Guo QH, et al. Stress-Induced Alternative Splicing Provides a Mechanism for the Regulation of MicroRNA Processing in Arabidopsis thaliana. Mol Cell. 2012;48: 521–531. doi:10.1016/j.molcel.2012.08.032

222. Zhou HL, Luo G, Wise JA, Lou H. Regulation of alternative splicing by local histone modifications: Potential roles for RNA-guided mechanisms. Nucleic

Acids Res. 2014;42: 701–713. doi:10.1093/nar/gkt875

223. Szweykowska-Kulinska Z, Jarmolowski A, Vazquez F. The crosstalk between plant microRNA biogenesis factors and the spliceosome. Plant Signal Behav. 2013;8. doi:10.4161/psb.26955

224. Bardou F, Ariel F, Simpson CG, Romero-Barrios N, Laporte P, Balzergue S, et al. Long Noncoding RNA Modulates Alternative Splicing Regulators in Arabidopsis. Dev Cell. 2014;30: 166–176. doi:10.1016/j.devcel.2014.06.017

225. Ueda Y, Uehara N, Sasaki H, Kobayashi K, Yamakawa T. Impacts of acute ozone stress on superoxide dismutase (SOD) expression and reactive oxygen species (ROS) formation in rice leaves. Plant Physiol Biochem. 2013;70: 396–402. doi:10.1016/j.plaphy.2013.06.009

226. Xia L, Zou D, Sang J, Xu X, Yin H, Li M, et al. Rice Expression Database (RED): An integrated RNA-Seq-derived gene expression database for rice. J Genet Genomics. 2017;44: 235–241. doi:10.1016/j.jgg.2017.05.003

227. Kaminaka H, Morita S, Tokumoto M, Masumura T, Tanaka K. Differential gene expressions of rice superoxide dismutase isoforms to oxidative and environmental stresses. Free Radical Research. Harwood Academic Publishers GmbH; 1999. doi:10.1080/10715769900301541

228. Morita S, Nakatani S, Koshiba T, Masumura T, Ogihara Y, Tanaka K. Differential Expression of Two Cytosolic Ascorbate Peroxidases and Two Superoxide Dismutase Genes in Response to Abiotic Stress in Rice. Rice Sci. 2011;18: 157–166. doi:10.1016/S1672-6308(11)60023-1

229. Xing Y, Chen WH, Jia W, Zhang J. Mitogen-activated protein kinase kinase 5 (MKK5)-mediated signalling cascade regulates expression of iron superoxide

dismutase gene in Arabidopsis under salinity stress. J Exp Bot. 2015;66: 5971–5981. doi:10.1093/jxb/erv305

230. Xing Y, Cao Q, Zhang Q, Qin L, Jia W, Zhang J. MKK5 regulates high light-induced gene expression of Cu/Zn superoxide dismutase 1 and 2 in arabidopsis. Plant Cell Physiol. 2013;54: 1217–1227. doi:10.1093/pcp/pct072
231. Boyd SD, Ullrich MS, Skopp A, Winkler DD. Copper Sources for Sod1 Activation. Antioxidants (Basel, Switzerland). 2020;9: 1–14. doi:10.3390/antiox9060500
232. Culotta VC, Yang M, O'Halloran T V. Activation of superoxide dismutases: Putting the metal to the pedal. Biochimica et Biophysica Acta - Molecular Cell Research. 2006. pp. 747–758. doi:10.1016/j.bbamcr.2006.05.003
233. Banci L, Bertini I, Ciofi-Baffoni S. Copper trafficking in biology: An NMR approach. HFSP J. 2009;3: 165–175. doi:10.2976/1.3078306
234. Luchinat E, Barbieri L, Banci L. A molecular chaperone activity of CCS restores the maturation of SOD1 fALS mutants. Sci Rep. 2017;7: 1–8. doi:10.1038/s41598-017-17815-y
235. Furukawa Y, Torres AS, O'Halloran T V. Oxygen-induced maturation of SOD1: A key role for disulfide formation by the copper chaperone CCS. EMBO J. 2004;23: 2872–2881. doi:10.1038/sj.emboj.7600276
236. Jensen LT, Culotta VC. Activation of CuZn superoxide dismutases from Caenorhabditis elegans does not require the copper chaperone CCS. J Biol Chem. 2005;280: 41373–41379. doi:10.1074/jbc.M509142200
237. Leitch JM, Jensen LT, Bouldin SD, Outten CE, Hart PJ, Culotta VC. Activation of Cu,Zn-superoxide dismutase in the absence of oxygen and the copper

chaperone CCS. J Biol Chem. 2009;284: 21863–21871. doi:10.1074/jbc.M109.000489

238. Huang CH, Kuo WY, Weiss C, Jinn TL. Copper chaperone-dependent and -independent activation of three copper-zinc superoxide dismutase homologs localized in different cellular compartments in Arabidopsis. Plant Physiol. 2012;158: 737–746. doi:10.1104/pp.111.190223
239. Lu Y, Feng Z, Bian L, Xie H, Liang J. miR398 regulation in rice of the responses to abiotic and biotic stresses depends on CSD1 and CSD2 expression. Funct Plant Biol. 2011;38: 44. doi:10.1071/fp10178
240. Li YF, Zheng Y, Addo-Quaye C, Zhang L, Saini A, Jagadeeswaran G, et al. Transcriptome-wide identification of microRNA targets in rice. Plant J. 2010;62: 742–759. doi:10.1111/j.1365-313X.2010.04187.x
241. Jagadeeswaran G, Saini A, Sunkar R. Biotic and abiotic stress down-regulate miR398 expression in Arabidopsis. Planta. 2009;229: 1009–1014. doi:10.1007/s00425-009-0889-3
242. Sunkar R, Li YF, Jagadeeswaran G. Functions of microRNAs in plant stress responses. Trends in Plant Science. 2012. pp. 196–203. doi:10.1016/j.tplants.2012.01.010
243. Zhu C, Ding Y, Liu H. MiR398 and plant stress responses. Physiol Plant. 2011;143: 1–9. doi:10.1111/j.1399-3054.2011.01477.x
244. Schulten A, Bytomski L, Quintana J, Bernal M, Krämer U. Do Arabidopsis Squamosa promoter binding Protein-Like genes act together in plant acclimation to copper or zinc deficiency? Plant direct. 2019;3: e00150. doi:10.1002/pld3.150
245. Feng W, Hongbin W, Bing L, Jinfa W. Cloning and characterization of a novel

splicing isoform of the iron-superoxide dismutase gene in rice (Oryza sativa L.). Plant Cell Rep. 2006;24: 734–742. doi:10.1007/s00299-005-0030-4

246. Sagasti S, Bernal M, Sancho D, Del Castillo MB, Picorel R. Regulation of the chloroplastic copper chaperone (CCS) and cuprozinc superoxide dismutase (CSD2) by alternative splicing and copper excess in glycine max. Funct Plant Biol. 2014;41: 144–155. doi:10.1071/FP13134

247. Srivastava V, Srivastava MK, Chibani K, Nilsson R, Rouhier N, Melzer M, et al. Alternative splicing studies of the reactive oxygen species gene network in populus reveal two isoforms of high-isoelectric-point superoxide dismutase 1[c][w]. Plant Physiol. 2009;149: 1848–1859. doi:10.1104/pp.108.133371

248. Lee S, Joung YH, Kim JK, Do Choi Y, Jang G. An isoform of the plastid RNA polymerase-associated protein FSD3 negatively regulates chloroplast development. BMC Plant Biol. 2019;19: 524. doi:10.1186/s12870-019-2128-9

249. Cherepanov PP, Wackernagel W. Gene disruption in Escherichia coli: TcR and KmR cassettes with the option of Flp-catalyzed excision of the antibiotic-resistance determinant. Gene. 1995;158: 9–14. doi:10.1016/0378-1119(95)00193-A

250. Thompson JD, Gibson TJ, Plewniak F, Jeanmougin F, Higgins DG. The CLUSTAL X windows interface: Flexible strategies for multiple sequence alignment aided by quality analysis tools. Nucleic Acids Res. 1997;25: 4876–4882. doi:10.1093/nar/25.24.4876

251. Hall TA. BIOEDIT: a user-friendly biological sequence alignment editor and analysis program for Windows 95/98/ NT. Nucleic Acids Symp Ser. 1999;41: 95–98.

252. Tamura K, Dudley J, Nei M, Kumar S. MEGA4: Molecular Evolutionary Genetics Analysis (MEGA) software version 4.0. Mol Biol Evol. 2007;24: 1596–1599. doi:10.1093/molbev/msm092

253. Liu W, Xie Y, Ma J, Luo X, Nie P, Zuo Z, et al. IBS: An illustrator for the presentation and visualization of biological sequences. Bioinformatics. 2015;31: 3359–3361. doi:10.1093/bioinformatics/btv362

254. Holtorf H, Schöb H, Kunz C, Waldvogel R, Meins F. Stochastic and nonstochastic post-transcriptional silencing of chitinase and β-1,3-glucanase genes involves increased RNA turnover-possible role for ribosome-independent RNA degradation. Plant Cell. 1999;11: 471–483. doi:10.1105/tpc.11.3.471

255. Livak KJ, Schmittgen TD. Analysis of relative gene expression data using real-time quantitative PCR and the 2-ΔΔCT method. Methods. 2001;25: 402–408. doi:10.1006/meth.2001.1262

256. Bradford MM. A rapid and sensitive method for the quantitation of microgram quantities of protein utilizing the principle of protein-dye binding. Anal Biochem. 1976;72: 248–254. doi:10.1016/0003-2697(76)90527-3

257. He F. BCA (Bicinchoninic Acid) Protein Assay. BIO-PROTOCOL. 2011;1. doi:10.21769/bioprotoc.44

258. Chen JR, Liao CW, Mao SJT, Chen TH, Weng CN. A simple technique for the simultaneous determination of molecular weight and activity of superoxide dismutase using SDS-PAGE. J Biochem Biophys Methods. 2001;47: 233–237. doi:10.1016/S0165-022X(00)00162-7

259. Ewing JF, Janero DR. Microplate superoxide dismutase assay employing a nonenzymatic superoxide generator. Anal Biochem. 1995;232: 243–248.

doi:10.1006/abio.1995.0014

260. Mishra P, Dixit A, Ray M, Sabat SC. Mechanistic study of CuZn-SOD from Ipomoea carnea mutated at dimer interface: Enhancement of peroxidase activity upon monomerization. Biochimie. 2014;97: 181–193. doi:10.1016/j.biochi.2013.10.014

261. Zhang H, Joseph J, Gurney M, Becker D, Kalyanaraman B. Bicarbonate enhances peroxidase activity of Cu,Zn-superoxide dismutase: Role of carbonate anion radical and scavenging of carbonate anion radical by metalloporphyrin antioxidant enzyme mimetics. J Biol Chem. 2002;277: 1013–1020. doi:10.1074/jbc.M108585200

262. Baba T, Ara T, Hasegawa M, Takai Y, Okumura Y, Baba M, et al. Construction of Escherichia coli K-12 in-frame, single-gene knockout mutants: The Keio collection. Mol Syst Biol. 2006;2. doi:10.1038/msb4100050

263. Narita L, Peng S. Construction of Catalase Double Knockout Escherichia coli Strain for Isogenic Strain Comparison Studies of the Role of Catalase. J Exp Microbiol Immunol. 2012. Available: http://www.bioinformatics.nl/cgi-

264. Thomason LC, Costantino N, Court DL. E. coli Genome Manipulation by P1 Transduction . Current Protocols in Molecular Biology. John Wiley & Sons, Inc.; 2007. pp. 1.17.1-1.17.8. doi:10.1002/0471142727.mb0117s79

265. Goulielmos GN, Arhontaki K, Eliopoulos E, Tserpistali K, Tsakas S, Loukas M. Drosophila Cu,Zn superoxide dismutase gene confers resistance to paraquat in Escherichia coli. Biochem Biophys Res Commun. 2003;308: 433–438. doi:10.1016/S0006-291X(03)01422-0

266. Panat NA, Maurya DK, Ghaskadbi SS, Sandur SK. Troxerutin, a plant flavonoid,

protects cells against oxidative stress-induced cell death through radical scavenging mechanism. Food Chem. 2016;194: 32–45. doi:10.1016/j.foodchem.2015.07.078

267. Ben Rejeb I, Pastor V, Mauch-Mani B. Plant responses to simultaneous biotic and abiotic stress: Molecular mechanisms. Plants. MDPI AG; 2014. pp. 458–475. doi:10.3390/plants3040458

268. Haak DC, Fukao T, Grene R, Hua Z, Ivanov R, Perrella G, et al. Multilevel regulation of abiotic stress responses in plants. Frontiers in Plant Science. Frontiers Media S.A.; 2017. p. 1564. doi:10.3389/fpls.2017.01564

269. Petrillo E, Herz MAG, Barta A, Kalyna M, Kornblihtt AR. Let there be light: Regulation of gene expression in plants. RNA Biology. Landes Bioscience; 2014. pp. 1215–1220. doi:10.4161/15476286.2014.972852

270. Meyer P. Epigenetic variation and environmental change. Journal of Experimental Botany. Oxford University Press; 2015. pp. 3541–3548. doi:10.1093/jxb/eru502

271. Dhar MK, Vishal P, Sharma R, Kaul S. Epigenetic Dynamics: Role of Epimarks and Underlying Machinery in Plants Exposed to Abiotic Stress. International Journal of Genomics. Hindawi Limited; 2014. doi:10.1155/2014/187146

272. Filichkin SA, Mockler TC. Unproductive alternative splicing and nonsense mRNAs: A widespread phenomenon among plant circadian clock genes. Biol Direct. 2012;7. doi:10.1186/1745-6150-7-20

273. Devarie-Baez NO, Lopez EIS, Furdui CM. Biological chemistry and functionality of protein sulfenic acids and related thiol modifications. Free Radic Res. 2016;50: 172–194. doi:10.3109/10715762.2015.1090571

274. Kalyna M, Simpson CG, Syed NH, Lewandowska D, Marquez Y, Kusenda B, et al. Alternative splicing and nonsense-mediated decay modulate expression of important regulatory genes in Arabidopsis. Nucleic Acids Res. 2012;40: 2454–2469. doi:10.1093/nar/gkr932

275. Ito Y, Hirochika H, Kurata N. Organ-specific alternative transcripts of KNOX family class 2 homeobox genes of rice. Gene. 2002;288: 41–47. doi:10.1016/S0378-1119(02)00460-2

276. Barbazuk WB, Fu Y, McGinnis KM. Genome-wide analyses of alternative splicing in plants: Opportunities and challenges. Genome Research. 2008. pp. 1382–1391. doi:10.1101/gr.053678.106

277. Freese NH, Estrada AR, Blakley IC, Duan J, Loraine AE. Many rice genes are differentially spliced between roots and shoots but cytokinin has minimal effect on splicing. Plant Direct. 2019;3: e00136. doi:10.1002/pld3.136

278. Nath K, Kumar S, Poudyal RS, Yang YN, Timilsina R, Park YS, et al. Developmental stage-dependent differential gene expression of superoxide dismutase isoenzymes and their localization and physical interaction network in rice (Oryza sativa L.). Genes and Genomics. 2014;36: 45–55. doi:10.1007/s13258-013-0138-9

279. Zhang J, Li B, Yang Y, Hu W, Chen F, Xie L, et al. Genome-wide characterization and expression profiles of the superoxide dismutase gene family in Gossypium. Int J Genomics. 2016;2016. doi:10.1155/2016/8740901

280. Biswal AK, Kohli A. Cereal flag leaf adaptations for grain yield under drought: Knowledge status and gaps. Molecular Breeding. Springer; 2013. pp. 749–766. doi:10.1007/s11032-013-9847-7

281. Filichkin S, Priest HD, Megraw M, Mockler TC. Alternative splicing in plants: Directing traffic at the crossroads of adaptation and environmental stress. Current Opinion in Plant Biology. Elsevier Ltd; 2015. pp. 125–135. doi:10.1016/j.pbi.2015.02.008

282. Mockenhaupt S, Makeyev E V. Non-coding functions of alternative pre-mRNA splicing in development. Semin Cell Dev Biol. 2015;47–48: 32–39. doi:10.1016/j.semcdb.2015.10.018

283. Wang HF, Feng L, Niu DK. Relationship between mRNA stability and intron presence. Biochem Biophys Res Commun. 2007;354: 203–208. doi:10.1016/j.bbrc.2006.12.184

284. Dugas D V., Bartel B. Sucrose induction of Arabidopsis miR398 represses two Cu/Zn superoxide dismutases. Plant Mol Biol. 2008;67: 403–417. doi:10.1007/s11103-008-9329-1

285. Islam F, Ali B, Wang J, Farooq MA, Gill RA, Ali S, et al. Combined herbicide and saline stress differentially modulates hormonal regulation and antioxidant defense system in Oryza sativa cultivars. Plant Physiol Biochem. 2016;107: 82–95. doi:10.1016/j.plaphy.2016.05.027

286. Filichkin SA, Hamilton M, Dharmawardhana PD, Singh SK, Sullivan C, Ben-Hur A, et al. Abiotic Stresses Modulate Landscape of Poplar Transcriptome via Alternative Splicing, Differential Intron Retention, and Isoform Ratio Switching. Front Plant Sci. 2018;9: 5. doi:10.3389/fpls.2018.00005

287. Liu Z, Qin J, Tian X, Xu S, Wang Y, Li H, et al. Global profiling of alternative splicing landscape responsive to drought, heat and their combination in wheat (*Triticum aestivum* L.). Plant Biotechnol J. 2018;16: 714–726.

doi:10.1111/pbi.12822

288. Tsukamoto S, Morita S, Hirano E, Yokoi H, Masumura T, Tanaka K. A novel cis-element that is responsive to oxidative stress regulates three antioxidant defense genes in rice. Plant Physiol. 2005;137: 317–327. doi:10.1104/pp.104.045658

289. Tsang EWT, Bowler C, Hérouart D, Van Camp W, Villarroel R, Genetello C, et al. Differential regulation of superoxide dismutases in plants exposed to environmental stress. Plant Cell. 1991;3: 783–792. doi:10.1105/tpc.3.8.783

290. Schrader M, Fahimi HD. The peroxisome: Still a mysterious organelle. Histochemistry and Cell Biology. Springer; 2008. pp. 421–440. doi:10.1007/s00418-008-0396-9

291. Kaur N, Reumann S, Hu J. Peroxisome Biogenesis and Function. Arab B. 2009;7: e0123. doi:10.1199/tab.0123

292. Smith JJ, Aitchison JD. Peroxisomes take shape. Nature Reviews Molecular Cell Biology. NIH Public Access; 2013. pp. 803–817. doi:10.1038/nrm3700

293. Sewelam N, Jaspert N, Van Der Kelen K, Tognetti VB, Schmitz J, Frerigmann H, et al. Spatial H_2O_2 signaling specificity: H_2O_2 from chloroplasts and peroxisomes modulates the plant transcriptome differentially. Mol Plant. 2014;7: 1191–1210. doi:10.1093/mp/ssu070

294. Agrawal G, Subramani S. De novo peroxisome biogenesis: Evolving concepts and conundrums. Biochimica et Biophysica Acta - Molecular Cell Research. Elsevier B.V.; 2016. pp. 892–901. doi:10.1016/j.bbamcr.2015.09.014

295. Corpas FJ, del Río LA, Palma JM. Impact of nitric oxide (NO) on the ROS metabolism of peroxisomes. Plants. 2019;8. doi:10.3390/plants8020037

296. Begara-Morales JC, Sánchez-Calvo B, Chaki M, Valderrama R, Mata-Pérez C, Padilla MN, et al. Antioxidant Systems are Regulated by Nitric Oxide-Mediated Post-translational Modifications (NO-PTMs). Front Plant Sci. 2016;7. doi:10.3389/fpls.2016.00152

297. Molassiotis A, Fotopoulos V. Oxidative and nitrosative signaling in plants: Two branches in the same tree? Plant Signaling and Behavior. 2011. pp. 210–214. doi:10.4161/psb.6.2.14878

298. Sandalio LM, Romero-Puertas MC. Peroxisomes sense and respond to environmental cues by regulating ROS and RNS signalling networks. Annals of Botany. Oxford University Press; 2015. pp. 475–485. doi:10.1093/aob/mcv074

299. Sandalio LM, Palma JM, Del Rio LA. Localization of manganese superoxide dismutase in peroxisomes isolated from Pisum sativum L. Plant Sci. 1987;51: 1–8. doi:10.1016/0168-9452(87)90213-5

300. del Río LA, Lyon DS, Olah I, Glick B, Salin ML. Immunocytochemical evidence for a peroxisomal localization of manganese superoxide dismutase in leaf protoplasts from a higher plant. Planta. 1983;158: 216–224. doi:10.1007/BF01075257

301. Corpas FJ, Fernández-Ocaña A, Carreras A, Valderrama R, Luque F, Esteban FJ, et al. The expression of different superoxide dismutase forms is cell-type dependent in olive (Olea europaea L.) leaves. Plant Cell Physiol. 2006;47: 984–994. doi:10.1093/pcp/pcj071

302. Droillard MJ, Paulin A. Isozymes of superoxide dismutase in mitochondria and peroxisomes isolated from petals of carnation (Dianthus caryophyllus) during senescence. Plant Physiol. 1990;94: 1187–1192. doi:10.1104/pp.94.3.1187

303. Bueno P, Del Río LA. Purification and properties of glyoxysomal cuprozinc superoxide dismutase from watermelon cotyledons (Citrullus vulgaris Schrad). Plant Physiol. 1992;98: 331–336. doi:10.1104/pp.98.1.331

304. Bueno P, Varela J, Gimenez-Gallego G, Del Rio LA. Peroxisomal copper, zinc superoxide dismutase. Characterization of the isoenzyme from watermelon cotyledons. Plant Physiol. 1995;108: 1151–1160. doi:10.1104/pp.108.3.1151

305. Mahanty S, Kaul T, Pandey P, Reddy RA, Mallikarjuna G, Reddy CS, et al. Biochemical and molecular analyses of copper-zinc superoxide dismutase from a C 4 plant Pennisetum glaucum reveals an adaptive role in response to oxidative stress. Gene. 2012;505: 309–317. doi:10.1016/j.gene.2012.06.001

306. Lin MW, Lin MT, Lin CT. Copper/zinc-superoxide dismutase from lemon cDNA and enzyme stability. J Agric Food Chem. 2002;50: 7264–7270. doi:10.1021/jf0207070

307. Mishra P, Satpati S, Baral SK, Dixit A, Sabat SC. S95C substitution in CuZn-SOD of: Ipomoea carnea: Impact on the structure, function and stability. Mol Biosyst. 2016;12: 3017–3031. doi:10.1039/c6mb00458j

308. Shen J, Zeng Y, Zhuang X, Sun L, Yao X, Pimpl P, et al. Organelle pH in the arabidopsis endomembrane system. Mol Plant. 2013;6: 1419–1437. doi:10.1093/mp/sst079

309. Kaur N, Hu J. Defining the plant peroxisomal proteome: From arabidopsis to rice. Front Plant Sci. 2011;2: 1–20. doi:10.3389/fpls.2011.00103

310. Chen N, Teng X-L, Xiao X-G. Subcellular Localization of a Plant Catalase-Phenol Oxidase, AcCATPO, from Amaranthus and Identification of a Non-canonical Peroxisome Targeting Signal. Front Plant Sci. 2017;8: 1345.

doi:10.3389/fpls.2017.01345

311. Bowler C, Van Montagu M, Inzé D. Superoxide dismutase and stress tolerance. Annu Rev Plant Physiol Plant Mol Biol. 1992;43: 83–116. doi:10.1146/annurev.pp.43.060192.000503

312. Kumar A, Dutt S, Bagler G, Ahuja PS, Kumar S. Engineering a thermo-stable superoxide dismutase functional at sub-zero to >50°C, which also tolerates autoclaving. Sci Rep. 2012;2. doi:10.1038/srep00387

313. Li HY, Zhao Y, Cao Y, Wang WN, Zhao DQ. Purification and characterization of a superoxide dismutase from Panax ginseng. Biomed Chromatogr. 2010;24: 1203–1207. doi:10.1002/bmc.1428

314. Ellerby LM, Cabelli DE, Graden JA, Valentine JS. Copper-zinc superoxide dismutase: Why not pH-dependent? J Am Chem Soc. 1996;118: 6556–6561. doi:10.1021/ja953845x

315. Exposito-Rodriguez M, Laissue PP, Yvon-Durocher G, Smirnoff N, Mullineaux PM. Photosynthesis-dependent H_2O_2 transfer from chloroplasts to nuclei provides a high-light signalling mechanism. Nat Commun. 2017;8. doi:10.1038/s41467-017-00074-w

316. Imlay JA. Iron-sulphur clusters and the problem with oxygen. Molecular Microbiology. John Wiley & Sons, Ltd; 2006. pp. 1073–1082. doi:10.1111/j.1365-2958.2006.05028.x

317. Liochev S, Fridovich I. Superoxide and Iron: Partners in Crime. IUBMB Life. 1999;48: 157–161. doi:10.1080/713803492

318. Imlay JA. Cellular defenses against superoxide and hydrogen peroxide. Annual Review of Biochemistry. 2008. pp. 755–776.

doi:10.1146/annurev.biochem.77.061606.161055

319. Cohu CM, Abdel-Ghany SE, Gogolin Reynolds KA, Onofrio AM, Bodecker JR, Kimbrel JA, et al. Copper delivery by the copper chaperone for chloroplast and cytosolic copper/zinc-superoxide dismutases: Regulation and unexpected phenotypes in an arabidopsis mutant. Mol Plant. 2009;2: 1336–1350. doi:10.1093/mp/ssp084

320. Jing X, Hou P, Lu Y, Deng S, Li N, Zhao R, et al. Overexpression of copper/zinc superoxide dismutase from mangrove Kandelia candel in tobacco enhances salinity tolerance by the reduction of reactive oxygen species in chloroplast. Front Plant Sci. 2015;6: 1–13. doi:10.3389/fpls.2015.00023

321. Gupta AS, Heinen JL, Holaday AS, Burke JJ, Allen RD. Increased resistance to oxidative stress in transgenic plants that overexpress chloroplastic Cu/Zn superoxide dismutase. Proc Natl Acad Sci U S A. 1993;90: 1629–1633. doi:10.1073/pnas.90.4.1629

322. Lin CT, Lin MT, Chen YT, Shaw JF. Subunit interaction enhances enzyme activity and stability of sweet potato cytosolic Cu/Zn-superoxide dismutase purified by a His-tagged recombinant protein method. Plant Mol Biol. 1995;28: 303–311. doi:10.1007/BF00020249

323. Sanyal RP, Samant A, Prashar V, Misra HS, Saini A. Biochemical and functional characterization of OsCSD3, a novel CuZn superoxide dismutase from rice. Biochem J. 2018;475: 3105–3121. doi:10.1042/BCJ20180516

324. Moran JF, James EK, Rubio MC, Sarath G, Klucas R V., Becana M. Functional Characterization and Expression of a Cytosolic Iron-Superoxide Dismutase from Cowpea Root Nodules. Plant Physiol. 2003;133: 773–782.

doi:10.1104/pp.103.023010

325. Perl A, Perl-Treves R, Galili S, Aviv D, Shalgi E, Malkin S, et al. Enhanced oxidative-stress defense in transgenic potato expressing tomato Cu,Zn superoxide dismutases. Theor Appl Genet. 1993;85: 568–576. doi:10.1007/BF00220915

326. Negi NP, Shrivastava DC, Sharma V, Sarin NB. Overexpression of CuZnSOD from Arachis hypogaea alleviates salinity and drought stress in tobacco. Plant Cell Rep. 2015;34: 1109–1126. doi:10.1007/s00299-015-1770-4

327. Lu F, Liang X, Lu H, Li Q, Chen Q, Zhang P, et al. Overproduction of superoxide dismutase and catalase confers cassava resistance to Tetranychus cinnabarinus. Sci Rep. 2017;7: 1–13. doi:10.1038/srep40179

328. Lightfoot DJ, Mcgrann GRD, Able AJ. The role of a cytosolic superoxide dismutase in barley-pathogen interactions. Mol Plant Pathol. 2017;18: 323–335. doi:10.1111/mpp.12399

329. Panchy N, Lehti-Shiu M, Shiu SH. Evolution of gene duplication in plants. Plant Physiol. 2016;171: 2294–2316. doi:10.1104/pp.16.00523

330. Eckardt NA. Grass genome evolution. Plant Cell. American Society of Plant Biologists; 2008. pp. 3–4. doi:10.1105/tpc.108.058586

331. Salse J, Bolot S, Throude M, Jouffe V, Piegu B, Quraishi UM, et al. Identification and characterization of shared duplications between rice and wheat provide new insight into grass genome evolution. Plant Cell. 2008;20: 11–24. doi:10.1105/tpc.107.056309

332. Fischer I, Dainat J, Ranwez V, Glémin S, Dufayard JF, Chantret N. Impact of recurrent gene duplication on adaptation of plant genomes. BMC Plant Biol.

2014;14: 151. doi:10.1186/1471-2229-14-151

333. Kondrashov FA. Gene duplication as a mechanism of genomic adaptation to a changing environment. Proceedings of the Royal Society B: Biological Sciences. Royal Society; 2012. pp. 5048–5057. doi:10.1098/rspb.2012.1108

334. Stein JC, Yu Y, Copetti D, Zwickl DJ, Zhang L, Zhang C, et al. Genomes of 13 domesticated and wild rice relatives highlight genetic conservation, turnover and innovation across the genus Oryza. Nat Genet. 2018;50: 285–296. doi:10.1038/s41588-018-0040-0

335. Yu J, Wang J, Lin W, Li S, Li H, Zhou J, et al. The Genomes of Oryza sativa: A History of Duplications. Bennetzen J, editor. PLoS Biol. 2005;3: e38. doi:10.1371/journal.pbio.0030038

336. Jiang W, Yang L, He Y, Zhang H, Li W, Chen H, et al. Genome-wide identification and transcriptional expression analysis of superoxide dismutase (SOD) family in wheat (Triticum aestivum). PeerJ. 2019;2019: e8062–e8062. doi:10.7717/peerj.8062

337. Banerjee A, Roychoudhury A. Epigenetic regulation during salinity and drought stress in plants: Histone modifications and DNA methylation. Plant Gene. 2017;11: 199–204. doi:10.1016/j.plgene.2017.05.011

338. Ashikawa I, Numa H, Sakata K. Segmental distribution of genes harboring a CpG island-like region on rice chromosomes. Mol Genet Genomics. 2006;275: 18–25. doi:10.1007/s00438-005-0060-1

339. Carlsson LM, Marklund SL, Edlund T. The rat extracellular superoxide dismutase dimer is converted to a tetramer by the exchange of a single amino acid. Proc Natl Acad Sci U S A. 1996;93: 5219–5222.

doi:10.1073/pnas.93.11.5219

340. Chakravarty D, Bihani SC, Banerjee M, Ballal A. Novel molecular insights into the anti-oxidative stress response and structure–function of a salt-inducible cyanobacterial Mn-catalase. Plant Cell Environ. 2019;42: 2508–2521. doi:10.1111/pce.13563

341. Kumar A, Kaachra A, Bhardwaj S, Kumar S. Copper, zinc superoxide dismutase of Curcuma aromatica is a kinetically stable protein. Process Biochem. 2014;49: 1288–1296. doi:10.1016/j.procbio.2014.04.010

342. Challa S, Neelapu NRR. Genome-Wide Association Studies (GWAS) for Abiotic Stress Tolerance in Plants. Biochemical, Physiological and Molecular Avenues for Combating Abiotic Stress in Plants. Elsevier; 2018. pp. 135–150. doi:10.1016/B978-0-12-813066-7.00009-7

343. Mancini E, Sanchez SE, Romanowski A, Schlaen RG, Sanchez-Lamas M, Cerdán PD, et al. Acute Effects of Light on Alternative Splicing in Light-Grown Plants. Photochemistry and Photobiology. Blackwell Publishing Inc.; 2016. pp. 126–133. doi:10.1111/php.12550

344. Shikata H, Hanada K, Ushijima T, Nakashima M, Suzuki Y, Matsushita T. Phytochrome controls alternative splicing to mediate light responses in Arabidopsis. Proc Natl Acad Sci U S A. 2014;111: 18781–18786. doi:10.1073/pnas.1407147112

345. Godoy Herz MA, Kornblihtt AR. Alternative splicing and transcription elongation in plants. Frontiers in Plant Science. Frontiers Media S.A.; 2019. doi:10.3389/fpls.2019.00309

346. Palusa SG, Ali GS, Reddy ASN. Alternative splicing of pre-mRNAs of

Arabidopsis serine/arginine-rich proteins: Regulation by hormones and stresses. Plant J. 2007;49: 1091–1107. doi:10.1111/j.1365-313X.2006.03020.x

347. Chen SY, Li C, Jia X, Lai SJ. Sequence and evolutionary features for the alternatively spliced exons of eukaryotic genes. International Journal of Molecular Sciences. 2019. doi:10.3390/ijms20153834

348. Palusa SG, Reddy ASN. Extensive coupling of alternative splicing of pre-mRNAs of serine/arginine (SR) genes with nonsense-mediated decay. New Phytol. 2010;185: 83–89. doi:10.1111/j.1469-8137.2009.03065.x

349. Sureshkumar S, Dent C, Seleznev A, Tasset C, Balasubramanian S. Nonsense-mediated mRNA decay modulates FLM-dependent thermosensory flowering response in Arabidopsis. Nat Plants. 2016;2. doi:10.1038/NPLANTS.2016.55

350. Mateos JL, de Leone MJ, Torchio J, Reichel M, Staiger D. Beyond transcription: Fine-tuning of circadian timekeeping by post-transcriptional regulation. Genes. MDPI AG; 2018. doi:10.3390/genes9120616

351. McClung CR. The plant circadian oscillator. Biology. MDPI AG; 2019. doi:10.3390/biology8010014

352. Bartok O, Kyriacou CP, Levine J, Sehgal A, Kadener S. Adaptation of molecular circadian clockwork to environmental changes: a role for alternative splicing and miRNAs. Proc R Soc B Biol Sci. 2013;280: 20130011. doi:10.1098/rspb.2013.0011

353. McKay SL, Johnson TL. A bird's-eye view of post-translational modifications in the spliceosome and their roles in spliceosome dynamics. Molecular BioSystems. 2010. pp. 2093–2102. doi:10.1039/c002828b

354. Marondedze C, Thomas L, Lilley KS, Gehring C. Drought Stress Causes

Specific Changes to the Spliceosome and Stress Granule Components. Front Mol Biosci. 2020;6. doi:10.3389/fmolb.2019.00163

355. de Lima Morais DA, Harrison PM. Large-Scale Evidence for Conservation of NMD Candidature Across Mammals. Stajich JE, editor. PLoS One. 2010;5: e11695. doi:10.1371/journal.pone.0011695

356. Muthusamy M, Yoon EK, Kim JA, Jeong MJ, Lee SI. Brassica rapa sr45a regulates drought tolerance via the alternative splicing of target genes. Genes (Basel). 2020;11. doi:10.3390/genes11020182

357. Hiller M, Huse K, Platzer M, Backofen R. Creation and disruption of protein features by alternative splicing -- a novel mechanism to modulate function. Genome Biol. 2005;6: R58. doi:10.1186/gb-2005-6-7-r58

358. Wei H, Lou Q, Xu K, Yan M, Xia H, Ma X, et al. Alternative splicing complexity contributes to genetic improvement of drought resistance in the rice maintainer HuHan2B. Sci Rep. 2017;7: 1–13. doi:10.1038/s41598-017-12020-3

359. Capovilla G, Symeonidi E, Wu R, Schmid M. Contribution of major FLM isoforms to temperature-dependent flowering in Arabidopsis thaliana. J Exp Bot. 2017;68: 5117–5127. doi:10.1093/jxb/erx328

360. Browse J. Jasmonate passes muster: A receptor and targets for the defense hormone. Annu Rev Plant Biol. 2009;60: 183–205. doi:10.1146/annurev.arplant.043008.092007

361. Gagete AP, Riera M, Franco L, Rodrigo MI. Functional analysis of the isoforms of an ABI3-like factor of Pisum sativum generated by alternative splicing. J Exp Bot. 2009;60: 1703–1714. doi:10.1093/jxb/erp038

362. Tsukagoshi H, Busch W, Benfey PN. Transcriptional regulation of ROS controls

transition from proliferation to differentiation in the root. Cell. 2010;143: 606–616. doi:10.1016/j.cell.2010.10.020

363. Feng K, Yu J, Cheng Y, Ruan M, Wang R, Ye Q, et al. The SOD gene family in tomato: Identification, phylogenetic relationships, and expression patterns. Front Plant Sci. 2016;7. doi:10.3389/fpls.2016.01279

364. Xu G, Guo C, Shan H, Kong H. Divergence of duplicate genes in exon-intron structure. Proc Natl Acad Sci U S A. 2012;109: 1187–1192. doi:10.1073/pnas.1109047109

APPENDIX

JOURNAL PUBLICATIONS

Biochemical Journal (2018) **475** 3105–3121
https://doi.org/10.1042/BCJ20180516

PORTLAND PRESS

Research Article

Biochemical and functional characterization of OsCSD3, a novel CuZn superoxide dismutase from rice

Ravi Prakash Sanyal[1,2], Amol Samant[1], Vishal Prashar[3], Hari Sharan Misra[1,2] and Ajay Saini[1,2]

[1]Molecular Biology Division, Bhabha Atomic Research Centre, Trombay, Mumbai, Maharashtra, India; [2]Homi Bhabha National Institute, Anushaktinagar, Trombay, Mumbai, Maharashtra, India; [3]Radiation Biology and Health Sciences Division, Bhabha Atomic Research Centre, Trombay, Mumbai, Maharashtra, India

Correspondence: Ajay Saini (ajays@barc.gov.in)

Superoxide dismutases (SODs, EC 1.15.1.1) belong to an important group of antioxidant metalloenzymes. Multiple SODs exist for scavenging of reactive oxygen species (ROS) in different cellular compartments to maintain an intricate ROS balance. The present study deals with molecular and biochemical characterization of CuZn SOD encoded by LOC_Os03g11960 (referred to as OsCSD3), which is the least studied among the four rice isozymes. The OsCSD3 showed higher similarity to peroxisomal SODs in plants. The OsCSD3 transcript was up-regulated in response to salinity, drought, and oxidative stress. Full-length cDNA encoding OsCSD3 was cloned and expressed in *Escherichia coli* and analyzed for spectral characteristics. UV (ultraviolet)–visible spectroscopic analysis showed evidences of *d–d* transitions, while circular dichroism analysis indicated high β-sheet content in the protein. The OsCSD3 existed as homodimer (~36 kDa) with both Cu^{2+} and Zn^{2+} metal cofactors and was substantially active over a wide pH range (7.0–10.8), with optimum pH of 9.0. The enzyme was sensitive to diethyldithiocarbamate but insensitive to sodium azide, which are the characteristics features of CuZn SODs. The enzyme also exhibited bicarbonate-dependent peroxidase activity. Unlike several other known CuZn SODs, OsCSD3 showed higher tolerance to hydrogen peroxide and thermal inactivation. Heterologous overexpression of OsCSD3 enhanced tolerance of *E. coli sod* double-knockout (Δ*sodA* Δ*sodB*) mutant and wild-type strain against methyl viologen-induced oxidative stress, indicating the *in vivo* function of this enzyme. The results show that the locus LOC_Os03g11960 of rice encodes a functional CuZn SOD with biochemical characteristics similar to the peroxisomal isozymes.

Introduction

Abiotic stress conditions are detrimental to all living organisms, and plants being sessile are more prone to stress-induced damage [1]. An important aspect of most stress conditions is reactive oxygen species (ROS)-mediated cellular damage. ROS such as superoxide radical ($O_2^{\cdot-}$), hydrogen peroxide (H_2O_2) and hydroxyl radical ($^{\cdot}OH$) are cellular metabolic byproducts and physiologically important; however, when their levels are elevated (e.g. in stress conditions), it leads to 'oxidative stress' [2]. Cellular ROS homeostasis is important and maintained by several enzymatic and non-enzymatic antioxidant mechanisms [2]. Unlike other ROS, the $O_2^{\cdot-}$ radical predominantly contributes towards oxidative stress in an indirect manner. It spontaneously dismutates to H_2O_2 that subsequently generates highly reactive $^{\cdot}OH$ radical in Fe^{2+}-mediated Fenton reaction [3]. Both H_2O_2 and $^{\cdot}OH$ radical are detrimental to several cellular components namely membrane lipids, nucleic acids and proteins [4]. Therefore, $O_2^{\cdot-}$ scavenging is important and constitutes the very first line of defense, where superoxide dismutases (EC 1.15.1.1) play a crucial role in reducing $O_2^{\cdot-}$ and $^{\cdot}OH$ levels [5–7]. Superoxide dismutases efficiently catalyze the disproportionation of $O_2^{\cdot-}$ by increasing the rate constant of the spontaneous dismutation by >1000-fold [3]. Based on the metal cofactors, SODs are categorized into four types: CuZn, Mn, Fe, and Ni SOD. Plants contain only three SOD types localized to cytosol (CuZn

Received: 6 July 2018
Revised: 31 August 2018
Accepted: 3 September 2018

Accepted Manuscript online: 4 September 2018
Version of Record published: 12 October 2018

Biochemical Journal (2018) 475 3105–3121
https://doi.org/10.1042/BCJ20180516

SOD), chloroplast (CuZn SOD and Fe SOD), mitochondria (Mn SOD), and peroxisomes (CuZn SOD and Mn SOD) [6,8,9]. CuZn SODs (also referred to as CSDs) are reported to be the most abundant isozymes in plants [6]. CuZn SODs generally exist as homodimers containing non-covalently linked Cu^{2+} and Zn^{2+} ions in each subunit [5]; however, the homo-tetrameric [10] and monomeric forms [11] have also been reported. While Cu^{2+} is important for the catalytic activity of the enzyme, Zn^{2+} is involved in its dimerization and structural stabilization [12,13]. Hydrophobic interactions between the subunits do not contribute towards enzyme activity as the monomers are also catalytically active [12,14]. Although the various CuZn SOD isozymes show sequence heterogeneity, structural and functional important residues and secondary structure elements are highly conserved [13].

The CuZn SOD isozymes have been studied and characterized in a variety of plants [7,14–21]. Furthermore, the role of SODs in protection against oxidative stress including overexpression for enhanced stress tolerance in transgenic plants has also been studied [7,20,22–27]. However, recent reports on certain CuZn SODs from plants have provided new information about their unusual stability [15,28], specific activity [15], and biochemical/biophysical characteristics of mono- and dimeric forms [14]. Such beneficial characteristics of enzymes are often desirable for agricultural or industrial applications [15,28]. Therefore, analyses of uncharacterized/putative isozymes would provide information of their biochemical/biophysical characteristics *vis-à-vis* other known SODs, and new insights into their role in stress responses.

Rice has four CuZn SODs encoded by different genomic loci: OsCSD1 (LOC_Os03g22810, cytosolic), OsCSD2 (LOC_Os08g44770, chloroplastic), OsCSD3 (LOC_Os03g11960), and OsCSD4 (LOC_Os07g46990, cytosolic). Most previous studies have been focused primarily on OsCSD1 and OsCSD2 isozymes [11,18,29]. Information available on OsCSD3 include limited transcript expression data under certain abiotic stresses [21,30–32]. Therefore, functional characterization of OsCSD3 protein, its characteristics *vis-à-vis* other CSD isozymes, and association with stress tolerance in rice would be worth exploring.

Here, we present the first report on the functional characterization of OsCSD3 encoded by LOC_Os03g11960 locus (Figure 1) in the rice genome. We demonstrated that this gene was up-regulated in response to multiple abiotic stresses. Recombinant protein purified from *Escherichia coli* was found to be a homodimeric CuZn SOD enzyme, active over a broad pH range and relatively more tolerant to H_2O_2 and thermal inactivation. Interestingly, the OsCSD3 also exhibited bicarbonate-dependent peroxidase activity. More importantly, this enzyme showed significant protection against oxidative stress in both wild-type and *sod* double-knockout (Δ*sodA* Δ*sodB*) mutant strains of *E. coli*. Thus, the rice OsCSD3 is a functional CuZn SOD with peroxisomal features.

Experimental

Plant material and experimental conditions

Rice genotype NSICRc106 (salt tolerant) used in this study was obtained from International Rice Research Institute (IRRI, Philippines). Rice seedlings were grown hydroponically in Hoagland media (Himedia, India) in MLR-351H plant growth chamber (Sanyo, Japan) under a 14 h light and 10 h dark period. Following growth conditions used: light intensity: 150 μmol m^{-2} s^{-1} (photon flux density), temperature: 28 ± 1°C (light period) and 26 ± 1°C (dark period) and humidity: 65%. For stress treatment, the 6-day-old rice seedlings were subjected to salinity (150 mM sodium chloride, NaCl), drought (15% polyethylene glycol, PEG), and oxidative stress (10 μM methyl viologen, MV). Shoot tissue was collected at different time-points from control and stressed seedlings, frozen in liquid nitrogen, and stored at −70°C until further use. Chemicals and reagents used (if not specifically mentioned) were from Sigma–Aldrich (U.S.A.), and common molecular biology protocols were followed as per Sambrook and Russel [33].

RNA isolation, full-length cDNA isolation and cloning

Total RNA was isolated from rice shoot tissue by the Trizol (Invitrogen, U.S.A.) method and assessed for quality and quantity. RNA preparation was treated with DNase I (Roche Diagnostics, Germany) to remove DNA contamination and it was subsequently heat-inactivated. Total RNA (10 μg) was reverse transcribed using SuperScript II reverse transcriptase (Invitrogen, U.S.A.) and a mixture of anchored oligo$(dT)_{35}$ and random nonamers (dN_9) (New England Biolabs, U.S.A.) as per the protocol recommended by the manufacturer. The quantity of complementary DNA (cDNA) was estimated on a UV-1800 spectrophotometer (Shimadzu, Japan) and used for quantitative real-time PCR analysis.

Biochemical Journal (2018) **475** 3105–3121
https://doi.org/10.1042/BCJ20180516

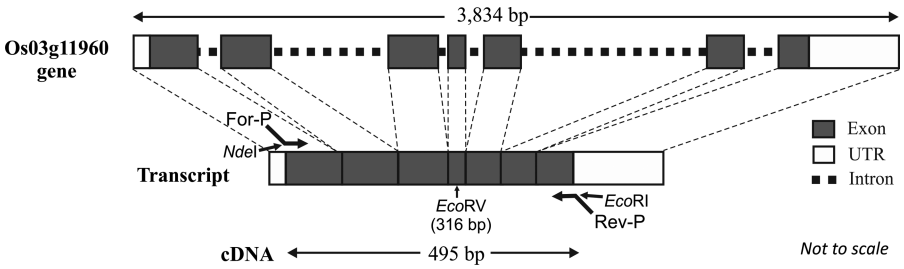

Figure 1. Schematic diagram of the rice Os03g11960 CuZn superoxide dismutase gene.
Length of the gene and cDNA, organization of exons and introns, location of the oligonucleotide primers used for cDNA amplification, and position of restriction enzyme sites used for cloning and restriction analysis are indicated.

Full-length OsCSD3 cDNA was PCR amplified using a forward (Os11960-ForP: 5′-GGGAATTCCATATGA TGGCAGGGAAAGCCGGCGGCC-3′) and a reverse (Os11960-RevP: 5′-CGGAATTCTTAAACTGCAGA TCGAAGTCCAATGATAC-3′) primer (Figure 1) designed using the sequence available at the Rice Genome Annotation Project website (http://rice.plantbiology.msu.edu) [34]. Underlined bases indicate the sites for restriction enzymes in the forward (*Nde*I) and reverse (*Eco*RI) primers for cloning compatibility in pET28a(+) vector (Novagen, U.S.A.). PCR was carried out using *Pwo* DNA polymerase (Roche Diagnostics, Germany) on a Mastercycler Gradient PCR machine (Eppendorf, Germany) using following conditions: initial denaturation at 94°C (5 min), 35 cycles of 94°C for 1 min, 60°C for 1 min, 72°C for 1.5 min, and final extension at 72°C (5 min).

The PCR product was purified, double-digested with *Nde*I and *Eco*RI, and ligated to pET28a(+) linearized with the same enzymes. The ligation mixture was transformed into *E. coli* (DH5α) cells and transformants were selected on LB agar containing kanamycin (25 μg ml^{-1}). Transformants were screened by colony PCR for the presence of insert (Os03g11960 cDNA), and also confirmed by restriction analysis of plasmid. The full-length cDNA product and insert from the recombinant plasmid (referred to as pET28a(+)-OsCSD3) of the two clones was sequenced and submitted to the GenBank database (accession numbers: KF953542, KF953543). One of these (KF953542) was used for heterologous expression of rice OsCSD3 in *E. coli* BL-21(DE3) strain. The rice cDNA was also cloned in pMAL-c5x plasmid (New England Biolabs, U.S.A.) using the same restriction enzymes (*Nde*I and *Eco*RI) for protein expression and stress tolerance studies in *E. coli sod*A *sod*B double mutant.

Quantitative RT-PCR analysis

Quantitative RT-PCR analysis for comparative transcript abundance of four rice CuZn SODs was carried out using the following sets of primers: (1) OsCSD3 (ForP: 5′-CAACGGCTGCAACTCTACCGGGCC-3′ and RevP: 5′- GGTCCTTTATGAAGATATCTGCAACAC-3′), (2) OsCSD1 (ForP: 5′-GCATGTCAACTGGGCCACACTACA-3′ and RevP: 5′-CATGGATATTAGCAACACCATCTTC-3′), OsCSD2 (ForP: 5′-TGGGTGCATATCAACAGGACC ACA-3′ and RevP: 5′-GGTTGCCTCAGCTACACCTTCAGC-3′), and OsCSD4 (ForP: 5′-CATGTCAACTGG ACCACACTTCAA-3′ and RevP: 5′-ATTGACATTAGCAACACCATCTGC-3′). Wherever possible, primers were designed at the exon–exon junctions with amplicon size <200 bp. Primer specificity was assessed by the Primer-BLAST program available at the National Centre for Biotechnology Information (NCBI) website (http://www.ncbi.nlm.nih.gov/tools/primer-blast).

Quantitative RT-PCR analysis was carried out on a Master cycler ep realplex PCR instrument (Eppendorf, Germany) using SYBR Green Jumpstart *Taq* Ready mix (Sigma–Aldrich, U.S.A.) following the recommended protocol. Following thermal cycling conditions were used: 94°C (2 min), 45 cycles of 94°C (10 s), 60°C (15 s) and 68°C (20 s). Specificity of the PCR amplification was assessed by melting curve analysis as well as on 2.0% agarose gel. Relative transcript abundance was estimated by Schmittgen and Livak [35] using Actin-2 (LOC_Os10g36650) as a reference gene (ForP: 5′-CTAGTGGACGTACTACTGGTATTG-3′ and RevP: 5′-GATC CCTACCAGCAAGATCAAGAC-3′) and validated by using a second reference gene, GAPDH (LOC_Os08g03290) (ForP: 5′-GTGACAGCAGGTCGAGCATCTTCG-3′; RevP: 5′-GTCGATGACACGGTTGCTGTAACC-3′). Analysis was carried out using two independent biological replicates, where 8–10 rice seedlings were pooled for RNA extraction in each sample. All the PCRs were run in triplicates and appropriate controls including the no

Biochemical Journal (2018) 475 3105–3121
https://doi.org/10.1042/BCJ20180516

template control were included for each set of analysis. Statistical analysis of the qPCR data in control and treated samples was carried out by Student's *t*-test and the differences were considered significant only when the $P < 0.05$.

Construction of *E. coli sod* double-knockout (Δ*sodA* Δ*sodB*) mutant strain

Single-gene *sodA* and *sodB* knockouts of *E. coli* (BW25113) were obtained from Keio collection [36]. The mutants contained removable (FLP recombinase-mediated) kanamycin resistance gene (KanR) cassette in place of the *sod* gene(s). Plasmid pCP20 that features temperature-sensitive origin of replication, a heat-inducible Flp-recombinase, and an ampicillin resistance gene (AmpR) as selection marker was used for removal of KanR cassette. *E. coli sod* double-knockout (Δ*sodA* Δ*sodB*) strain was generated using the FLP-FRT recombination system as per the protocol described by Narita and Peng [37] with minor modifications. Briefly, *E. coli sodA* mutant containing KanR cassette (in place of *sodA* gene) was transformed with pCP20 plasmid, followed by selection on LB agar ampicillin plates at 30°C. Few positive cells were grown at 43°C in LB media, serially diluted, and plated on LB agar plates for Flp recombinase-mediated removal of KanR cassette, and curing of pCP20 plasmid. Loss of KanR and AmpR was confirmed by patching clones on LB agar plates containing no or appropriate antibiotics. These *sodA* cells were designated as *sodA*-KanS (S: sensitive). *E. coli sodB* mutant was transduced with P1 phage, and the lysate was used to transduce the *E. coli sodA*-KanS cells as per the standard protocol. The transformed cells were selected on LB agar kanamycin plates to identify *sodA sodB* double-knockout mutants.

Oxidative stress tolerance in *E. coli sod* double-knockout (Δ*sodA* Δ*sodB*) mutant and wild-type strains

Effect of MV-induced oxidative stress on growth of *E. coli sod* double-knockout mutant (Δ*sodA* Δ*sodB*) and wild-type BL-21(DE3) strains was carried out as per Goulielmos et al. [38]. Briefly, *E. coli* double-mutant cells containing either pMAL-c5x (control vector) or pMAL-c5x-OsCSD3 were grown at 37°C in LB medium containing kanamycin (25 μg ml^{-1}) and ampicillin (50 μg ml^{-1}). Cultures were diluted (1 : 100) in LB–Kan–Amp media supplemented with 0.2 mM $CuCl_2$ and $ZnCl_2$, grown further until absorbance ($A_{600\ nm}$) reached ∼0.2, and induced with 0.5 mM isopropyl β-D-thiogalactopyranoside (IPTG) for 4 h, for expression of recombinant OsCSD3 in *E. coli*. The cultures were again normalized to absorbance ($A_{600\ nm}$) ∼0.2, treated with different concentrations (0.0–0.025 mM) of MV in the presence of 0.5 mM IPTG, for 20 h at 25°C, and growth was measured at regular intervals. The cultures were also diluted serially in 0.85% saline and analyzed by spot test (10 μl of respective dilutions were spotted) on LB agar plate containing both kanamycin (25 μg ml^{-1}) and ampicillin (50 μg ml^{-1}). Oxidative stress tolerance was also analyzed in wild-type *E. coli* strains, BL-21(DE3) containing pET28a(+) (control vector), or pET28a(+)-OsCSD3. Transformed *E. coli* cells were induced with 0.1 mM IPTG for 16 h at 20°C and normalized to absorbance ($A_{600\ nm}$) ∼0.2. These cells were treated with different concentrations (0.0–0.2 mM) of MV and absorbance ($A_{600\ nm}$) was measured at regular interval. Additionally, the cultures were serially diluted in saline and analyzed by spot test (10 μl of respective dilutions were spotted) on LB agar plate containing kanamycin (50 μg ml^{-1}). The experiment was repeated three times in triplicates. Statistical analysis was carried out by Student's *t*-test and the differences were considered significant only when $P < 0.05$.

Lipid peroxidation analysis

Lipid peroxidation was determined by Panat et al. [39] with minor modifications. The assay is based on quantification of malondialdehyde (MDA), an end product of lipid peroxidation that reacts with 2-thiobarbituric acid (TBA) to produce a red colored adduct. Briefly, *E. coli* cells were harvested, washed (twice) with phosphate buffer saline (PBS, pH 7.4), resuspended in 300 μl of PBS, and lysed by sonication in a Branson Digital Sonifier 450 (Branson Ultrasonics Corporation, U.S.A.) using the following settings: amplitude: 35%, ON time 2 s, OFF time 2 s, processing time 5 min. The samples were kept on ice (4°C) during the sonication. Sample volume of 300 μl was mixed with 900 μl of TBA reagent (0.375% TBA, 0.25 M HCl, 15% trichloroacetic acid and 6 mM Na_2EDTA) and incubated at 95°C for 30 min. Samples were cooled to room temperature and centrifuged at 13 680×***g*** for 20 min at 4°C. MDA equivalents were estimated in the supernatant by measuring the fluorescence (excitation/emission: 530/590 nm) on a multi-well-plate reader (Infinite M200, Tecan, U.K.). The

experiment was repeated three times in triplicates. The lipid peroxidation was expressed as μmoles of MDA equivalents mg^{-1} protein using 1,1,3,3-tetramethoxypropane (TMP) as a standard.

Bioinformatic studies

The plant CuZn SODs (cytosolic, peroxisomal and chloroplastic) similar to the rice OsCSD3 protein were identified by the Basic Local Alignment Search Tool, BLASTP [40], and sequences from 9 monocots and 12 dicots (Supplementary Table S1) were retrieved from the GenBank database at the NCBI website (http://www.ncbi.nlm.nih.gov). Parameters like molecular weight (Mw) and theoretical isoelectric point (pI) of the sequences were estimated by the 'Compute pI/Mw tool' at the ExPASy web site (http://web.expasy.org/compute_pi/). Multiple sequence alignment was done by ClustalX software [41] using default gap opening and gap extension penalties and edited by BioEdit Software [42]. Sequence divergence and genetic relationships were inferred using the Molecular Evolutionary Genetic Analysis software (MEGA version 4) [43]. Phylogenetic analysis was done by the neighbor-joining [44] method and statistical analysis was performed by the bootstrap method [45].

The molecular model of the rice OsCSD3 was generated using the SWISS-MODEL [46] work space (http://swissmodel.expasy.org/workspace) using a dimeric target sequence of rice SOD, and *Solanum lycopersicum* CuZn SOD crystal structure (PDB ID: 3PU7) as the template. Template structure included both Cu^{2+} and Zn^{2+} cofactors. Structural superposition of the model onto the template was carried out using the molecular modeling software O [47]. Figures of the molecular models were rendered using computer program PyMOL [48].

Purification of recombinant protein

E. coli BL-21(DE3) cells containing the recombinant plasmid pET28a(+)-OsCSD3 were grown overnight at 37°C in LB medium with kanamycin (25 μg ml^{-1}) and diluted to 1 : 100 in the fresh LB-Kan medium supplemented with 0.2 mM $CuCl_2$ and $ZnCl_2$. Cells in mid-log phase were induced with 0.1 mM IPTG at 20°C, harvested after 16 h by centrifugation (4500×***g***, 10 min), resuspended in the resuspension buffer (50 mM potassium phosphate; 100 mM potassium chloride, KCl; and 1 mM phenylmethanesulfonyl fluoride, PMSF, pH 8.0), and lysed by sonication with following settings: amplitude: 35%, ON time 2 s, OFF time 2 s, processing time 15 min (repeated twice). The samples were kept on ice (4°C) during the sonication. Supernatant and pellet fractions were separated by centrifugation (10 000×***g***, 20 min, 4°C), resolved on 15% SDS–PAGE, and stained with Coomassie Blue R-250 (Sigma, U.S.A.). The recombinant rice protein was purified from the supernatant fraction obtained from a total of 4.0 gFW^{-1} (gram fresh weight) of IPTG-induced *E. coli* cells. Affinity purification was carried out using 0.5 ml Ni-NTA affinity resin (Qiagen, Germany) as per the recommended protocol and analyzed on 15% SDS–PAGE. The purified protein was dialyzed against resuspension buffer using 2 kDa MWCO dialysis tube (Sigma–Aldrich, U.S.A.) and concentrated using 3 kDa MWCO centrifugal columns (Vivaspin, GE Healthcare, U.S.A.). Protein samples were quantitated by the Bradford method [49] using bovine serum albumin (BSA) as a standard.

Determination of metal content in the protein

Copper and zinc content of the protein was estimated on a VG PQExCell Inductively Coupled Plasma-Mass Spectrometer (ICP-MS) instrument (VG Elemental, U.K.). Briefly, recombinant protein (1 mg) was dialyzed against deionized water using 2 kDa MWCO dialysis tubing (Sigma–Aldrich, U.S.A.). The protein sample (in a silica crucible) was charred at 500°C in a blast furnace and the inorganic ash was resuspended with 1% supra-pure nitric acid solution for ICP-MS analysis. The metal content was expressed as the number of Cu^{2+} and Zn^{2+} ions per protein subunit.

Biophysical studies

The native molecular weight of the recombinant OsCSD3 was determined by gel filtration chromatography on a Superdex™ 75 10/300 GL chromatography column (GE Healthcare) preequilibrated with potassium phosphate buffer (10 mM potassium phosphate; 100 mM KCl, pH 8.0). The column was precalibrated with following standard proteins, BSA (66.5 kDa), chicken egg albumin (45 kDa), carbonic anhydrase (29 kDa), and cytochrome *C* (12.4 kDa). The native molecular weight was estimated by plotting a calibration curve of the log of molecular weight of the standard proteins versus their respective V_e/V_o values (V_e: elution volume, V_o: void volume). The molecular weight of the monomeric subunit was determined by 15% SDS–PAGE using prestained protein molecular weight standard (New England Biolabs, U.S.A.). A standard curve of the log of molecular

Biochemical Journal (2018) 475 3105–3121
https://doi.org/10.1042/BCJ20180516

weight of the standard proteins versus their R_f values (R_f: migration distance of the protein/migration distance of the dye front) was used for estimating the subunit molecular weight.

Spectrophotometric characteristics of the recombinant OsCSD3 were analyzed at room temperature (25°C) on a double-beam UV-1800 spectrophotometer (Shimadzu, Japan). Absorbance spectra of protein (1 mg ml^{-1}) in potassium phosphate buffer (10 mM, pH 8.0) containing KCl (10 mM) were recorded between wavelengths of 200 and 800 nm. Circular dichroism (CD) analysis was carried out on a Jasco J-815 CD spectropolarimeter (Jasco, Japan) at 20°C, using protein sample (concentration: 0.15 mg ml^{-1}) in potassium phosphate buffer (10 mM, pH 8.0) containing KCl (10 mM). CD spectra was recorded between wavelengths 190–260 nm using a quartz cuvette (path length: 0.2 cm) with the following settings: scan speed: 20 nm min^{-1}, data integration time: 2 s, data pitch: 0.1 nm, and band width: 1.0 nm. The measurements from five scans were averaged and corrected for the sample buffer. Protein concentration estimated by the Bradford method [49] was used to determine the molar ellipticity.

Biochemical assays

In solution, SOD activity of OsCSD3 was determined by the nitro blue tetrazolium (NBT) reduction assay in a multi-well-plate assay [50]. In brief, purified protein (0–2 μg) was incubated in 200 μl assay volume containing sodium phosphate buffer (50 mM, pH 7.8), reduced nicotinamide adenine dinucleotide (NADH, 78 μM), NBT (50 μM), and EDTA (0.1 mM). Reaction was initiated by the addition of phenazine methosulfate (final concentration: 3.3 μM) and absorbance ($A_{560\ nm}$) was measured for 5 min on a multi-well-plate reader (Infinite M200, Tecan, U.K.). The biochemical assays were carried out using 1 U of the protein. One unit (1 U) of SOD activity is defined as the amount of protein required to inhibit the NBT reduction by 50%.

The effect of pH was measured in two ways (1: assaying enzyme at different pH and 2: incubation of enzyme at a pH followed by activity measurement at different incubation time) using the following buffers: sodium phosphate (pH 7.0–8.0), Tris–HCl (pH 7.0–9.0), and sodium bicarbonate (pH 9.0–10.8). Effect of temperature on the stability on the protein was evaluated as described earlier [7] with minor modification. For instance, the recombinant protein was preincubated in 50 mM sodium phosphate buffer (pH 7.8) at different temperatures (25, 37, 45, 50, 60, and 70°C) before the aliquots were taken for activity measurement. For measuring the effect of inhibitors like diethyldithiocarbamate (DDC), sodium azide (NaN_3), and hydrogen peroxide (H_2O_2), the protein (5 U) was preincubated with increasing concentration of DDC (0.0–2.0 mM), NaN_3 (0.0–10.0 mM), and H_2O_2, (0.0–10.0 mM) for 30 min. Enzyme activity was measured as described above.

In-gel SOD activity assay of OsCSD3 was carried out on non-denaturing as well SDS polyacrylamide gel as described by Chen et al. [51]. Protein samples were analyzed by electrophoresis on 15% SDS–PAGE [10% for non-denaturing polyacrylamide gel electrophoresis (PAGE) gels]. The gel was rinsed in distilled water for 15 min (thrice) and incubated in 'solution A' (50 mM sodium phosphate buffer, pH 8.0 + 28 μM riboflavin + 28 mM tetramethylethylenediamine) for 30 min. Then, 'solution B' (50 mM sodium phosphate buffer, pH 8.0 + 1 mM NBT) was added and the gel was exposed to light (20 min) for color development and photographed on the gel-documentation system (Syngene, U.K.).

Bicarbonate-dependent peroxidase activity of OsCSD3 was determined by monitoring oxidation of dichlorodihydrofluorescein (DCFH) to 2′,7′-dichlorofluorescein (DCF) as per Zhang et al. [52]. In brief, assay was carried out at 25°C in potassium phosphate buffer (100 mM, pH 7.4) containing 0.1 mM diethylenetriaminepentaacetic acid (DTPA), 50 μM DCFH, 25 mM sodium bicarbonate ($NaHCO_3$), and increasing amount (0–10 μg) of protein. The reaction was initiated by the addition of H_2O_2 (1 mM) and fluorescence signal (emission: 524 nm; excitation: 480 nm) of the product DCF was monitored for 5 min. The analysis was carried out on a multi-well-plate reader instrument (Infinite M200, Tecan, U.K.). The formation of DCF was also monitored by recording the absorbance spectra on a UV-1800 spectrophotometer (Shimadzu, Japan).

Results

Rice OsCSD3 CuZn SOD is up-regulated in response to abiotic stresses

Quantitative RT-PCR analysis estimated the basal transcript levels of four CuZn SOD isozymes in rice seedlings. Transcripts of OsCSD1 and OsCSD2 showed higher abundance and collectively represented >50% of the total CuZn SOD transcript (Figure 2A). The OsCSD3 transcript was ∼20% of the total transcript (Figure 2A). The rice CuZn SODs were up-regulated in response to abiotic stress conditions with minor variations in expression pattern. OsCSD3 showed >1.5-fold to 2.5-fold up-regulation under salinity, drought and oxidative

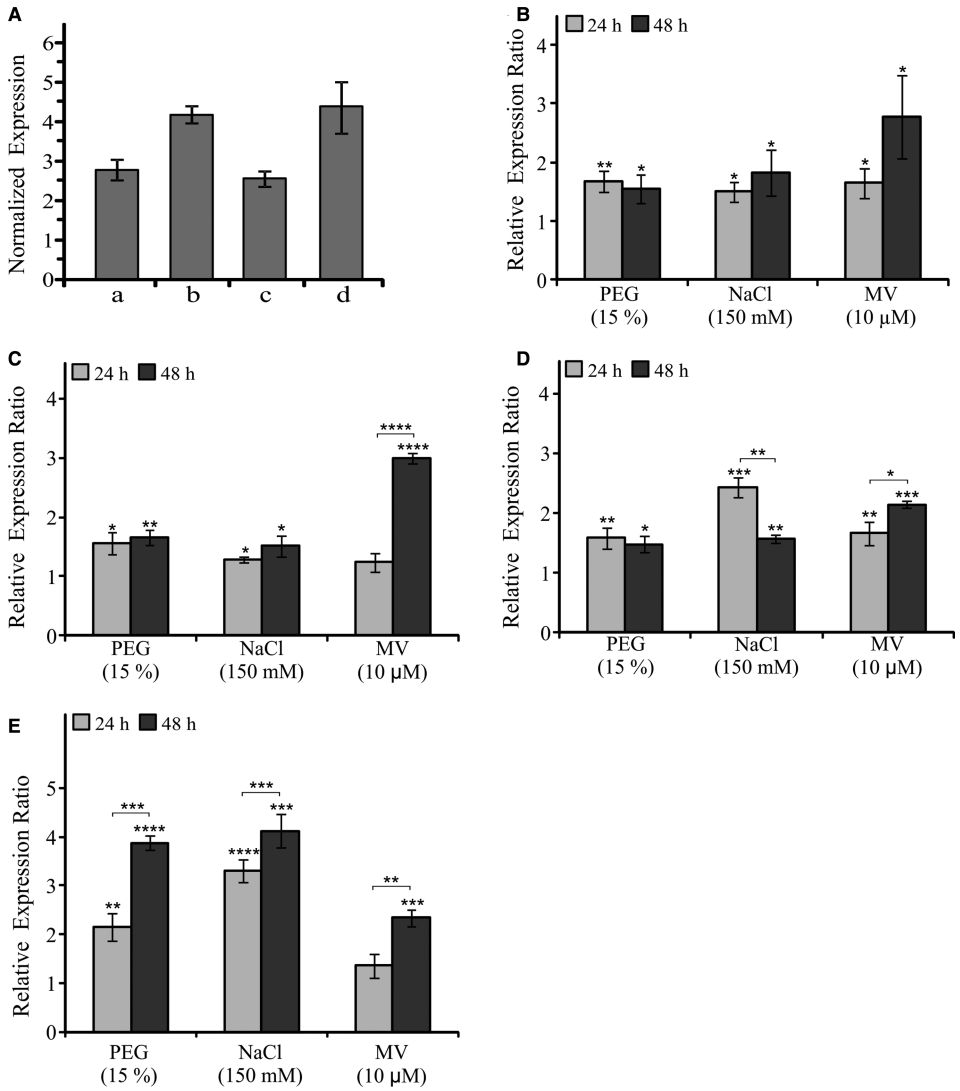

Figure 2. Quantitative RT-PCR analysis of rice CuZn SODs.

(**A**) relative abundance of transcripts of four CuZn SODs in 6-day-old control seedlings: (a) OsCSD3, (b) OsCSD1, (c) OsCSD4, and (d) OsCSD2. (**B**–**E**) Relative transcript levels of four CuZn SODs in rice seedlings subjected to polyethylene glycol (15%), sodium chloride (150 mM), and MV (10 µM) at 24 and 48 h after stress treatment: (**B**) OsCSD3, (**C**) OsCSD1, (**D**) OsCSD2, and (**E**) OsCSD4. Transcript levels were normalized as per Schmittgen and Livak [35] using actin as a reference gene. The experiment was carried out with two independent biological replicates (each sample had three technical replicates). Data are represented as normalized transcript level ± SD. Statistical analysis was carried out by Student's *t*-test, and significant differences between transcript levels in control and treated samples and/or between two time-points (24 and 48 h of a stress treatment) are indicated by $^{*}P < 0.05$, $^{**}P < 0.01$, $^{***}P < 0.001$ and $^{****}P < 0.0001$.

stress (Figure 2B). OsCSD1 overall showed a similar pattern with enhanced transcript levels at 48 h under oxidative stress (Figure 2C). OsCSD2 transcript level were ∼1.5-fold up-regulated, except at 24 h (>2-fold) time-point under salt stress and ∼2-fold at 48 h in response to oxidative stress (Figure 2D). OsCSD4 showed higher up-regulation than other three isozymes under drought and salt stress (Figure 2E).

OsCSD3 showed high similarity to peroxisomal CuZn SODs

The OsCSD3 cDNA was successfully PCR amplified (Supplementary Figure S1) cloned, sequenced, and submitted to GenBank (accession numbers: KF953542 and KF953543). The NSICRc106 OsCSD3 polypeptide

Biochemical Journal (2018) 475 3105–3121
https://doi.org/10.1042/BCJ20180516

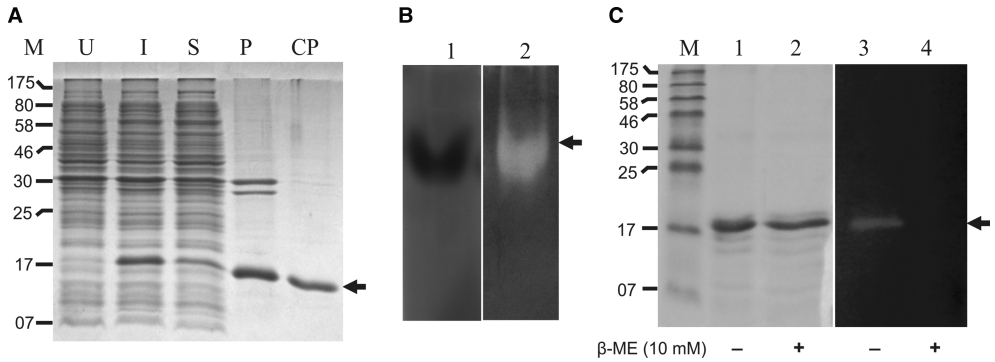

Figure 3. Overexpression, purification, and in-gel activity analysis of recombinant OsCSD3.

Arrow indicates the position of OsCSD3 protein. (**A**) Analysis of total protein isolated from different fractions on 15% SDS–PAGE; lane U: uninduced BL-21(DE3) pET28a(+)-OsCSD3 cells; lane I: BL-21(DE3) pET28a(+)-OsCSD3 cells induced with 0.1 mM IPTG; lane S: supernatant fraction; lane P: pellet fraction; lane CP: Ni-NTA affinity column purified protein; lane M: protein molecular weight standards in kilodaltons (kDa). Twenty-five (25 μg) protein was loaded on lanes U, I, and S and 10 and 5 μg of protein was loaded on lanes P and CP, respectively. (**B**) In-gel SOD activity of OsCSD3 on 10% non-denaturing PAGE. Equal amount (10 μg) of protein was loaded per lane and after the run the gel was divided into two halves, one was stained with Coomassie Blue (lane 1) and the other was used for activity staining (lane 2) as per Chen et al. [51]. (**C**) In-gel SOD activity assay of OsCSD3 on 15% SDS–PAGE in the presence and absence of 10 mM β-mercaptoethanol (β-ME). Equal amount (10 μg) of protein was loaded per lane and after the run gel was divided into two halves, one was stained with Coomassie Blue (left panel) and the other was used for activity staining (right panel) as per Chen et al. [51]. Lanes 1 and 3 contain untreated OsCSD3; lanes 2 and 4 OsCSD3 treated with β-ME; lane M: protein molecular weight standards in kilodaltons (kDa).

contained 164 amino acid residues with a predicted molecular weight of 16.5 kDa. The protein sequence showed 99.3% identity with Nipponbare OsCSD3 sequence with single variation at 151 position (A151T). The OsCSD3 showed both length and sequence heterogeneity with CuZn SOD isozymes from other plants (Supplementary Figure S2). Comparison of OsCSD3 with rice cytosolic CuZn SODs (OsCSD1 and OsCSD4) showed heterogeneity at ∼37% sites and length variation at N-terminal region (Supplementary Figure S2).

The multiple sequence alignment of CuZn SOD sequences from 9 monocots and 12 dicots (Supplementary Table S1) identified conserved and variable regions (Supplementary Figure S2). Phylogenetic analysis placed the SODs into three clusters: I (cytosolic), II (chloroplastic), and III (peroxisomal) supported by high bootstrap values, where monocot and dicot sequences showed distinct divergence (Supplementary Figure S3). The OsCSD3 CuZn SOD was placed in the monocot specific sub-cluster within cluster III. This cluster also included AtCSD3 from *Arabidopsis thaliana* (known to localize in peroxisomes) [9] and high isoelectric point SODs (*PthipI-SODC1* and *Pthip-SODC2*) from *Populus* [53]. CuZn SODs in peroxisomal cluster III exhibited higher divergence (*p*-distance: 0.239) than the cytosolic (p-distance: 0.149) and chloroplastic isozymes (*p*-distance: 0.224). The theoretical pI of CuZn SODs including OsCSD3 protein (pI: 6.82) in this cluster were generally higher than cluster I and II sequences, in both monocots (6.38–7.19) and dicots (6.22–7.87). Sequence comparison of monocot and dicot CuZn SODs from peroxisomal cluster III revealed high conservation of important residues involved in coordination with Cu^{2+} (His-55, His-57, His-72, and His-129) and Zn^{2+}(His-72, His-80, His-89 and Aps-92), disulfide bond formation (Cys-66 and Cys-155) and surface interactions (Supplementary Figure S4). Sequence heterogeneity was more predominant towards N-terminal than C-terminal or middle region of the CuZn SODs (Supplementary Figure S4). Despite overall similarity to peroxisomal isozymes, the characteristic peroxisomal targeting signals could not be detected in OsCSD3.

Recombinant OsCSD3 is a homodimer and contains Cu^{2+} and Zn^{2+} cofactors

Rice OsCSD3, cloned in pET28a(+), was overexpressed in *E. coli* BL-21(DE3) as described in Experimental section. Recombinant protein (∼18 kDa) was expressed in cells containing pET28a(+)-OsCSD3 plasmid (lane I, Figure 3A) and was not seen in uninduced cells (lane U, Figure 3A). The yield of the recombinant OsCSD3 was ∼0.6 mg gFW^{-1} of IPTG-induced *E. coli* cells. In-gel SOD activity assay on non-denaturing PAGE showed

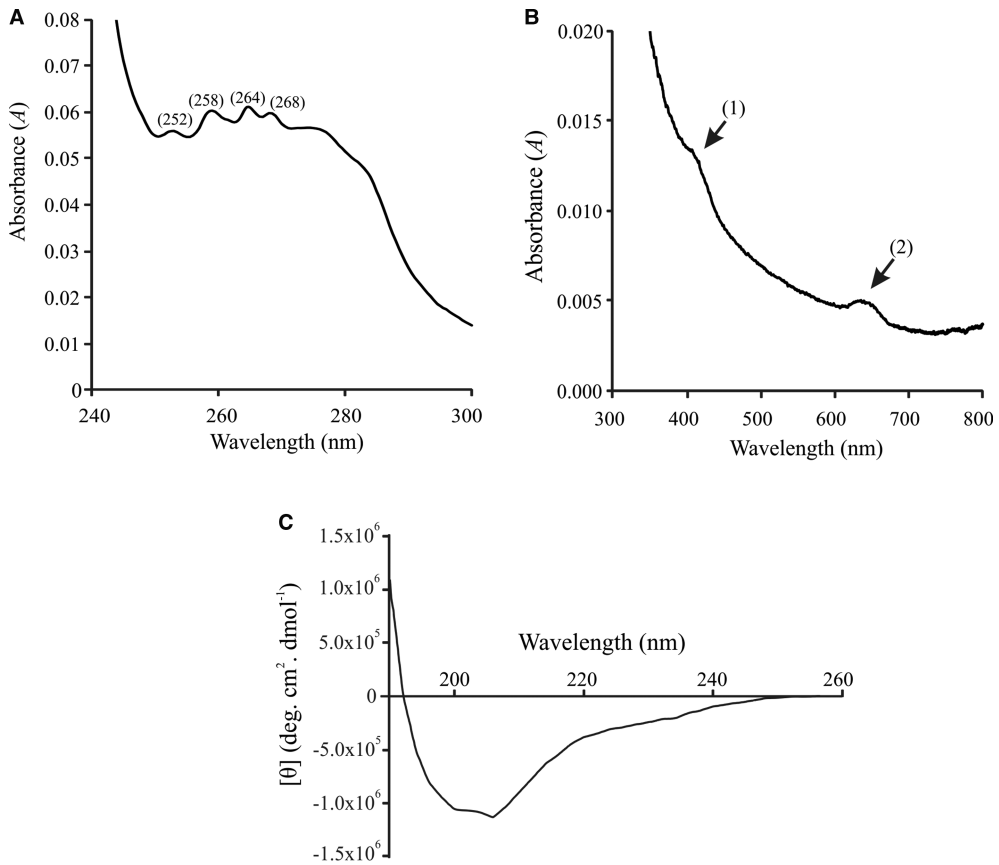

Figure 4. UV–visible and CD spectroscopy analysis of OsCSD3.

(**A**) UV absorption spectra of the protein in 240–300 nm wavelength range: small peaks characteristic of aromatic amino acids in the protein (Phe and Tyr) are indicated. (**B**) Optical absorption spectra in the 300–800 nm wavelength range: electronic transitions indicative of ligand-to-metal interaction (1) and *d–d* electronic transition for Cu^{2+}coordination (2) are indicated. (**C**) CD spectra were recorded on a Jasco J-815 CD spectropolarimeter using following parameters: wavelength range: 190–260 nm, quartz cuvette with 0.2 cm path length, scan speed: 20 nm min^{-1}, data integration time: 2 s, data pitch: 0.1 nm, band width: 1.0 nm.

that recombinant OsCSD3 is enzymatically active (lane 2, Figure 3B). The SOD activity of OsCSD3 was lost upon treatment with 10 mM β-mercaptoethanol (lane 4, Figure 3C), suggesting the importance of disulfide bond in the functionality of this protein. These results showed that LOC_Os03g11960 locus in the rice genome contains a coding sequence that expressed to SOD of expected molecular weight (18.7 kDa: 16.5 kDa, OsCSD3 and 2.2 kDa from pET28a(+) plasmid) in *E. coli*. Gel-filtration chromatography analysis showed that protein elutes as a single peak, corresponding to a molecular mass of ∼36 kDa (Supplementary Figure S5). Since the estimated size of the subunit was ∼18 kDa (Figure 3C), the OsCSD3 is suggested to be a homodimer in native form. ICP-MS analysis confirmed the presence of both Cu^{2+} and Zn^{2+} metal cofactors at concentration of 0.905 ± 0.18 and 0.945 ± 0.16 per protein subunit. Collectively, these results show that the rice protein is a CuZn SOD.

Recombinant OsCSD3 showed spectral signatures of a functional structure of CuZn SOD

The OsCSD3 isozyme contained a single tyrosine residue (Tyr-37) and six phenylalanines (at positions 29, 30, 54, 59, 73, and 107) and no tryptophan. The UV (ultraviolet) absorption spectra showed specific peaks associated with these aromatic amino acid residues in the protein (Figure 4A). The spectra in the visible region showed evidence of electronic transitions in two regions: (a) ∼620–680 nm, indicative of *d–d* electronic transition for Cu^{2+} coordination and (b) ∼380–410 nm, attributed to ligand-to-metal interaction between imidazole

Biochemical Journal (2018) 475 3105–3121
https://doi.org/10.1042/BCJ20180516

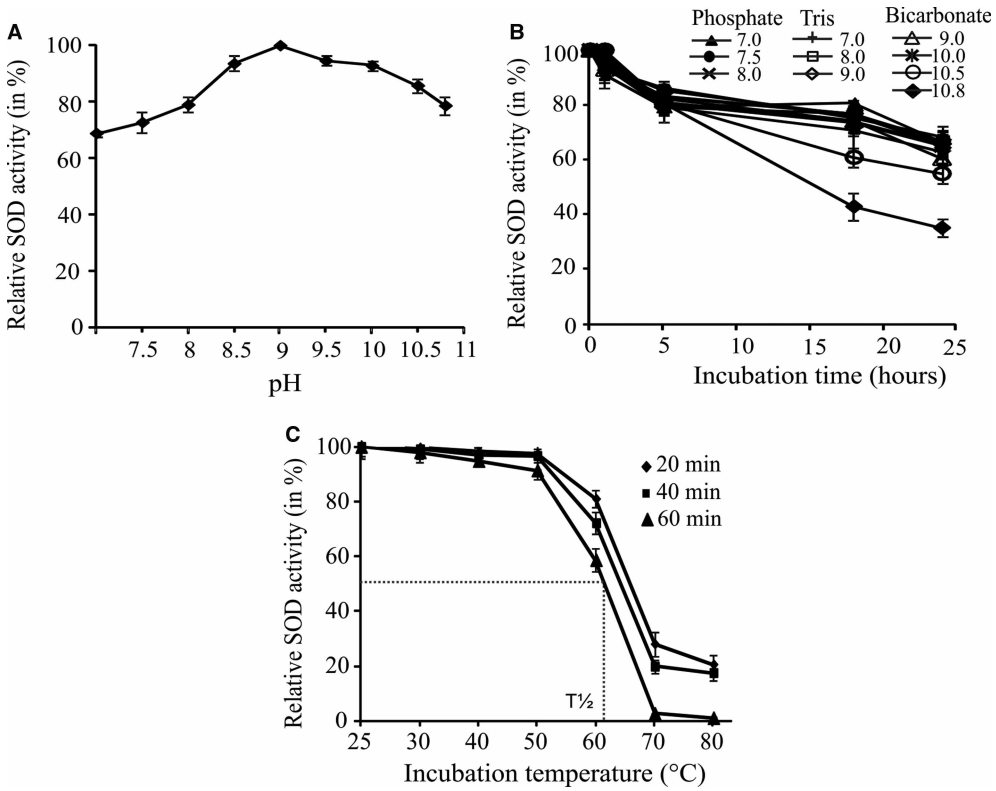

Figure 5. Biochemical characteristics of OsCSD3.

One unit (1 U) of purified protein was used for biochemical assays and data are represented as mean ± SD of three independent replicates. (**A**) Effect of pH on the activity: SOD activity of the protein was assayed at different pH using phosphate (pH 7.0–8.0), Tris–Cl (pH 7.0–9.0), and bicarbonate (pH 9.0–10.8) buffers. Relative SOD activity was estimated by considering maximum activity as 100%. (**B**) Effect of pH on stability: Protein was incubated in different buffers (pH range 7.0–10.8). Aliquots were removed at 1, 5, 18 and 24 h and assayed for SOD activity. Relative SOD activity was estimated by considering activity at 0 h time-point (before preincubation) as 100%. (**C**) Effect of temperature: protein was incubated at different temperatures (20–80°C). Aliquots were removed at 20, 40 and 60 min and assayed for SOD activity. Relative SOD activity was estimated by considering activity at 0 h time-point (before preincubation) as 100%. The SOD activity was also plotted as a function of temperature. Dotted line indicates *T*½ value (temperature at which 50% of enzyme activity was lost).

ring of the histidine (His-62) and Cu^{2+} (Figure 4B). CD spectroscopic analysis revealed higher β-sheet and low α-helix content in the rice protein (Figure 4C). These results indicated that the OsCSD3 has all the spectral signatures that qualify it to be a CuZn SOD.

OsCSD3 is a CuZn SOD with higher tolerance to thermal inactivation and H_2O_2

Purified OsCSD3 showed a specific activity of 4500 ± 500 U mg^{-1} protein (Supplementary Figure S6). The enzyme showed maximum activity at pH 9.0; however, it was active over a broad pH range (7.0–10.8) with 60–80% residual activity (Figure 5A). Stability of OsCSD3 was comparable from pH 7.0 to 10.0, and 40–60% loss in activity was observed beyond pH 10.0 within 18 h of incubation (Figure 5B). OsCSD3 showed tolerance to thermal inactivation with no substantial loss of activity at 50°C and a *T*½ value (temperature at which 50% of activity is lost) of 62°C (Figure 5C). The rice SOD retained 20% activity even on 40 min preincubation at 80°C.

OsCSD3 showed a differential response to SOD-specific inhibitors. SOD activity of OsCSD3 was inhibited by DDC (a CuZn SOD-specific inhibitor) in a concentration-dependent manner (IC_{50} 0.5 mM), with complete inhibition at 2 mM (Figure 6). The OsCSD3 was relatively insensitive to H_2O_2 as it exhibited an IC_{50} (H_2O_2) value of ∼7.6 mM (Figure 6). OsCSD3 activity remained unaffected by sodium azide (NaN_3) (Figure 6).

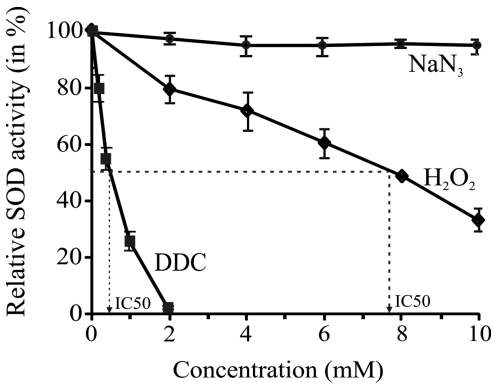

Figure 6. Effect of SOD inhibitors on OsSCD3 activity.

Inhibition profiles of OsCSD3 after treatment with DDC (0.0–2.0 mM), hydrogen peroxide (H_2O_2, 0.0–10.0 mM), and sodium azide (NaN_3 0.0–10.0 mM). Relative SOD activity was estimated by considering activity at 0 h time-point (before preincubation) as 100%. Vertical arrows indicate IC_{50} values for DDC (0.5 mM) and H_2O_2 (~7.6 mM). Data are represented as mean ± SD of three independent replicates.

OsCSD3 also exhibited bicarbonate-dependent peroxidase activity as assessed by enzyme-mediated oxidation of DCFH to DCF (Supplementary Figure S7A,B).

OsCSD3 enhanced oxidative stress tolerance of *E. coli sod* double mutant and wild type

The ability of rice OsCSD3 to protect *E. coli* cells from MV-mediated oxidative stress was investigated. Growth of wild-type BL-21(DE3) cells containing pET28a(+) or pET28a(+)-OsCSD3 was evaluated in the presence of increasing MV concentration. Overexpression of OsCSD3 enhanced the tolerance to MV-mediated oxidative stress (up to 0.2 mM MV) in the wild-type BL-21(DE3) cells (Figure 7A,C). However, the wild-type cells contain inherent SOD isozymes SODA and SODB which constitutes ~97% SOD activity in the cell. To evaluate the protection conferred solely by OsCSD3, a *sod* double-knockout (Δ*sodA* Δ*sodB*) mutant was generated (detailed in Experimental section), and loss of both SODA and SODB activities was confirmed by the in-gel SOD assay (Supplementary Figure S8A). *E. coli sodA sodB* double mutant showed high sensitivity to MV treatment (Supplementary Figure S8B) than the *sodA* (Supplementary Figure S8C) and *sodB* single mutants (Supplementary Figure S8D).

The pET28a(+)-OsCSD3 plasmid construct was compatible for heterologous expression in *E. coli* BL-21 (DE3) host, but not suitable for *sod* double mutant (Δ*sodA* Δ*sodB*) as it lacked T7 RNA polymerase-dependent overexpression, and contained selection marker (kanamycin) similar to pET28a(+). Hence, plasmid vector pMAL-c5x [containing maltose-binding protein (MBP) tag] that was suitable for T7 RNA polymerase-independent expression and contained an ampicillin selection marker was used. Additionally, the presence of N-terminal MBP tag kept the recombinant OsCSD3 in the soluble form. For functional analysis in *E. coli* double mutant, plasmid pMAL-c5x-OsCSD3 was transformed into *sod* double mutant and activity of the OsCSD3 was confirmed (Supplementary Figure S8E). Growth of *sod* double-knockout mutant containing pMAL-c5x or pMAL-c5x-OsCSD3 was evaluated in the presence of increasing MV concentration. The double mutant showed enhanced tolerance at 10 μM MV (Figure 7B,D). The *sod* double mutant was also evaluated for oxidative stress-induced lipid peroxidation. MV treatment resulted in increased lipid peroxidation in the *sodA sodB* double mutant. However, the cells expressing OsCSD3 showed reduced lipid peroxidation compared with the control (Figure 8). This indicates that the OsCSD3 is able to protect the *E. coli* cells from the MV-mediated oxidative damage.

Homology model shows structural features conserved in OsCSD3

The homology model of OsCSD3 was generated using the crystal structure of *S. lycopersicum* CuZn SOD (PDB ID: 3PU7) as a template (Figure 9). The two sequences showed 64% identity (*E*-value of 2.26834×10^{-39}; Supplementary Figure S9) in the template identification module of Swiss model workspace. The template structure, refined to 1.8 Å resolution, included both Cu and Zn cofactors. Homology model was a homodimer

Biochemical Journal (2018) **475** 3105–3121
https://doi.org/10.1042/BCJ20180516

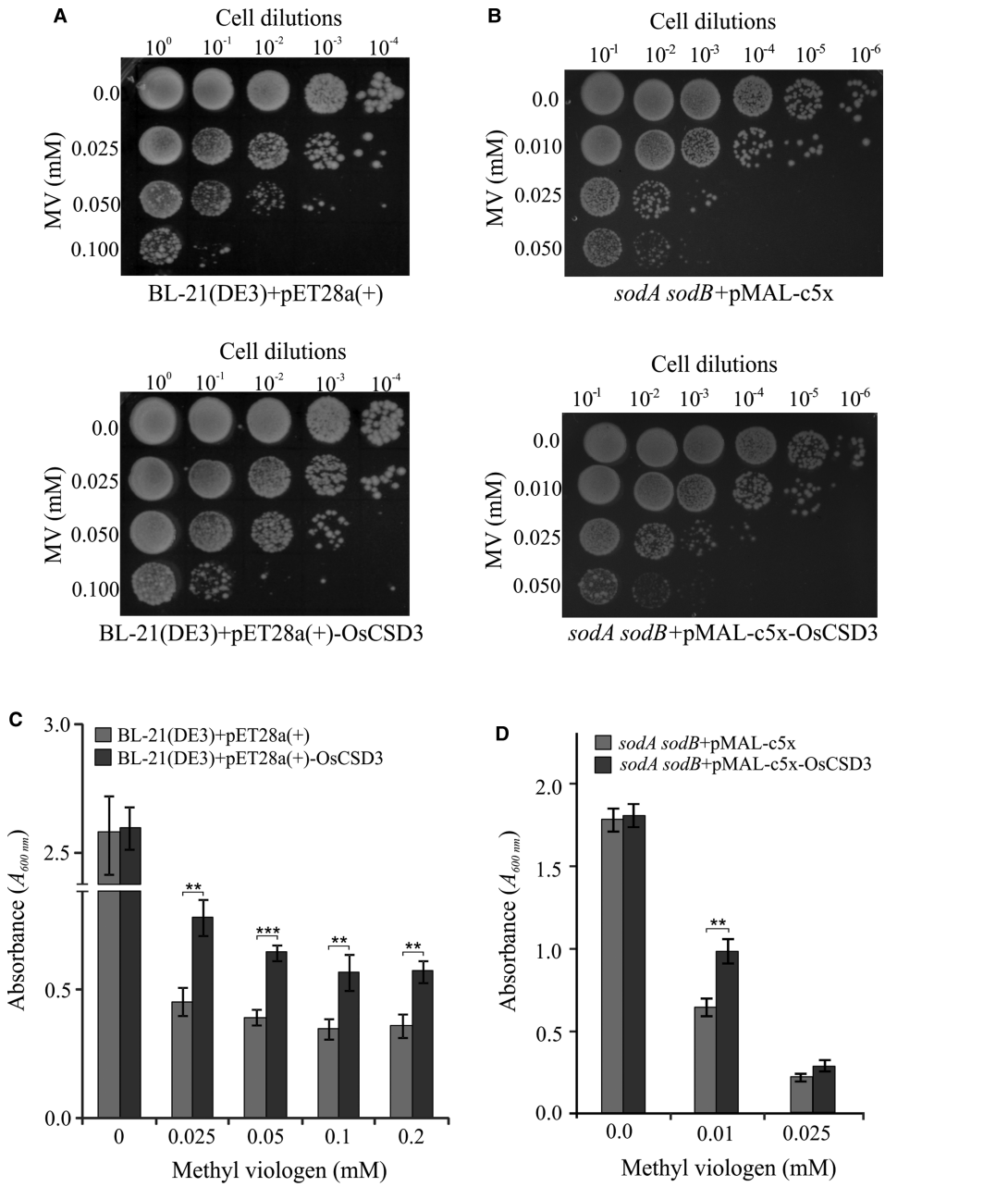

Figure 7. Analysis of oxidative stress tolerance of *E. coli* BL-21(DE3) wild-type and *sod* double-knockout (Δ*sodA* Δ*sodB*) mutant cells containing empty vector or recombinant vector expressing rice OsCSD3.

(**A**) Spot assay of *E. coli* BL-21(DE3) wild-type cells containing pET28a(+) or pET28a(+)-OsCSD3 treated with MV (0.0–0.100 mM). (**B**) Spot assay of *E. coli sod* double mutant containing pMAL-c5x or pMAL-c5x-OsCSD3 treated with MV (0.0–0.050 mM). (**C**) Comparison of growth of *E. coli* BL-21(DE3) wild-type cells containing empty vector (pET28a(+) or pET28a (+)-OsCSD3) in LB media containing IPTG (0.100 mM) and MV (0.0–0.200 mM), by measuring absorbance ($A_{600\ nm}$). The experiment was repeated three times and data are represented as mean absorbance ($A_{600\ nm}$) ± SD of three replicates. Statistical analysis was carried out by Student's *t*-test, and significant differences are indicated by $^{**}P < 0.01$, $^{***}P < 0.001$. (**D**) Comparison of growth of *E. coli sod* double-mutant cells containing empty vector (pMAL-c5x) or pMAL-c5x-OsCSD3 in LB media containing IPTG (0.5 mM) and MV (0.0–0.025 mM), by measuring absorbance ($A_{600\ nm}$). The experiment was repeated three times and data are represented as mean absorbance ($A_{600\ nm}$) ± SD of three independent replicates. Statistical analysis was carried out by Student's *t*-test, and significant differences are indicated by $^{**}P < 0.01$.

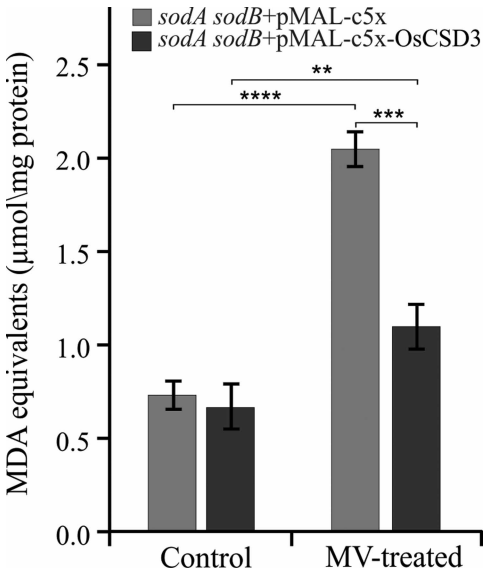

Figure 8. Analysis of lipid peroxidation in *E. coli sod* double-mutant (*ΔsodA ΔsodB*) cells containing empty vector (pMAL-c5x) or pMAL-c5x-OsCSD3 grown in control (no MV) and MV-treated (10 µM MV) conditions.

Lipid peroxidation was determined in terms of MDA as per Panat et al. [39] and expressed as µmoles of MDA equivalents mg^{-1} protein using TMP as a standard. The experiment was repeated three times and data are represented as mean MDA equivalents ± SD of three independent replicates. Statistical analysis was carried out by Student's *t*-test, and significant differences are indicated by $^{**}P < 0.01$, $^{***}P < 0.001$ and $^{****}P < 0.0001$.

covering the residue range 19–160 with QMEA-*N*-score 4 and QMEAN4-*Z*-score of 0.782 and −0.21, respectively [54], and showed the Greek key β-barrel structural core typical of CuZn SODs. The alpha carbons of residues 19–31, 37–160 of both the chains of the model were superposed onto the corresponding residues of

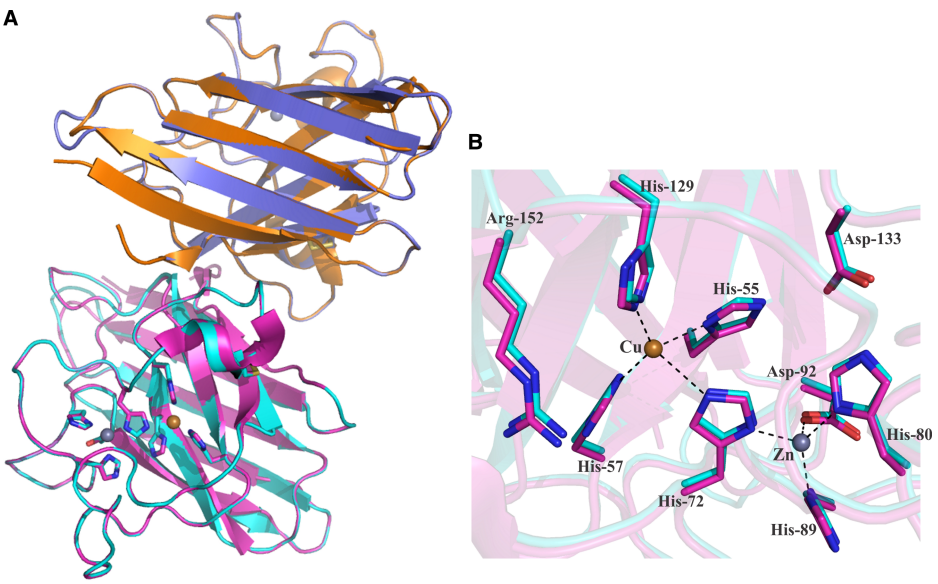

Figure 9. Homology model of 3D structure of OsCSD3 generated using SWISS-MODEL work space.

(**A**) Predicted homology model (shown as homodimer) of rice OsCSD3 superimposed with the template CuZn SOD structure (PDB ID: 3PU7) from *S. lycopersicum*. Two chains of the dimer are shown in cyan and slate color in case of the rice model while those are shown in magenta and orange color in case of the template. (**B**) Enlarged view of the active site region showing histidine and aspartate residues involved in the Cu and Zn coordination. Rice protein residues are shown in cyan carbons, whereas template residues are shown in magenta carbons.

Biochemical Journal (2018) 475 3105–3121
https://doi.org/10.1042/BCJ20180516

the template, thus omitting a beta turn where there is an insertion of a proline residue in case of rice model (Figure 9A). Structural superposition showed that the positions of active site residues (His-55, His-57, His-72, His-129, His-80, His-89 and Asp-92 involved in coordination with the metal cofactors (Cu and Zn), cysteines (Cys-66 and Cys-155) involved in intra-subunit disulfide bond), and catalytically important second-sphere residues (Asp-133 and Arg-152) were highly conserved. The two structures superposed to a *root-mean-square deviation* (*RMSD*) of 0.08 Å. After the superposition, active site of the model could very well accommodate both the metal cofactors (Cu and Zn) from the template (Figure 9B).

Discussion

Oxidative stress mediated by ROS is minimized by coordinated action of multiple antioxidant enzymes in plants [2,6]. Since superoxide radical $O_2^{\cdot-}$ participates in generation of several ROS and RNS (reactive nitrogen species), its dismutation catalyzed by SOD reduces their levels [3,55]. Multiple CuZn SOD isozymes dismutate the membrane impermeable $O_2^{\cdot-}$ to minimize the oxidative stress in organelles actively involved in oxidative metabolism [6,8,56]. Despite importance of peroxisomes in oxidative metabolism [57], the peroxisome-specific SOD isozymes have been relatively less studied.

The present study involves functional characterization of a putative CuZn SOD encoded by LOC_Os03g11960 in the rice. We present evidence to suggest that rice OsCSD3 showed sequence, structural and biochemical characteristics similar to peroxisomal SODs in plants. Different SODs contribute towards antioxidant activity at different physiological stages [16] and stress conditions [25,27,30,32,58,59]. Isozymes specific to subcellular compartments are important for ROS homoeostasis within and for ROS signaling between the organelles [55]. Changes in SOD activity at one location may affect gradient of H_2O_2 (also a signaling molecule) leading to modulation of redox-sensitive pathways [55]. Therefore, for a better insight into dynamics of oxidative stress management at cellular level, it is necessary to understand role of each isozyme.

Among the four rice CuZn SODs, the chloroplastic isozyme was analyzed for tissue-specific expression pattern [29], while the cytosolic isozyme was expressed in *E. coli* to study certain enzyme characteristics [18]. A rice Fe-SOD was also analyzed for stress responsiveness at transcript level [60]. However, these SODs have not been characterized in detail for biochemical/biophysical properties. Similarly, OsCSD3 has not been studied thoroughly, except few reports on effect of anoxia [32], salinity [30], ozone [21] and gamma radiation [31] on OsCSD3 transcript levels. Stress responsiveness of this locus under drought and oxidative (observed in this study) indicates this to be a general abiotic stress responsive gene.

The rice OsCSD3 showed homodimeric subunit organization, metal cofactor composition (1 $Cu^{2+}$and 1 Zn^{2+} per subunit) and predicted structural features similar to other plant CuZn SODs [7,12,14]. *In silico* analysis showed the presence of single intra-subunit disulfide bond between Cys66 and Cys165, which seems crucial for the functional conformation of OsCSD3 protein. Additional biochemical evidences confirmed that OsCSD3 is indeed a CuZn type of isozyme that also exhibits bicarbonate-dependent peroxidase activity reported in some other plant CuZn SOD isozymes [14,15].

Despite high conservation in structurally and functionally important residues, certain sequence variations affecting important characteristics (stability, oligomerization dynamics, specific activity) have been reported in some SOD isozymes [7,14,15,28]. Such characteristics have potential for biotechnological applications of the proteins [14,15,28]. The OsCSD3 showed remarkable properties (wide pH range, thermal stability, higher H_2O_2 and tolerance) that might qualify this protein to be a stress tolerant enzyme. These features may be attributed to variations specific to this isozyme.

Among various CuZn SOD isozymes, peroxisomal types are generally reported to be more thermostable [7,17,61]. The thermostability of OsCSD3 was comparable to the peroxisomal isozymes. It retained >80% SOD activity at alkaline pH, generally not observed for CuZn SODs [15,18,62], suggesting that the enzyme is more tolerant to pH-induced changes on subunit interactions, and Cu^{2+} leaching that may affect stability/activity [14,15,56]. At 4–5 mM concentration, H_2O_2 mediated by oxidation of metal (Cu^{2+}) coordinating amino acid residues causes irreversible inactivation of most CuZn SODs [7,14,15,17,63]. Higher H_2O_2 tolerance (~30% activity at 10 mM) of OsCSD3 further corroborates its peroxisomal nature. As peroxisomes contain higher H_2O_2 levels, the isozymes localized in this organelle are suggested to have adapted for higher H_2O_2 levels [17]. The alkaline pH optima and higher H_2O_2 tolerance of OsCSD3 seem suitable for functioning in the alkaline environment of plant peroxisomes [64]. Despite overall sequence similarity to peroxisomal SODs, the OsCSD3 lacked typical C-terminal peroxisomal signal peptide [57]. Furthermore, its N-terminal region could not be modeled due to lack of good similarity with the template (Supplementary Figure S9). It may be speculated that

this enzyme has additional N-terminal region and the possibility of its involvement in an alternative targeting mechanism of this protein cannot be ruled out.

In addition to generation of H_2O_2 and $^{\cdot}OH$ radical, the $O_2^{\cdot-}$, in a membrane permeable protonated form ($HO_2^{\cdot}$), can also initiate lipid peroxidation and damage cellular membranes [3]. Oxidative stress-mediated damage resulting into cellular toxicity and cell death can be minimized by scavenging of $O_2^{\cdot-}$. OsCSD3-mediated enhanced tolerance of wild-type and *sod* double-mutant *E. coli* cells subjected to MV (a redox-cycling agent for $O_2^{\cdot-}$ generation) demonstrated the *in vivo* $O_2^{\cdot-}$ scavenging function of this enzyme, resulting into reduced oxidative damage including lipid peroxidation. However, OsCSD3 alone was not sufficient to confer tolerance to higher levels of oxidative stress in *E. coli sod* double mutant lacking SODA and SODB. The *in vivo* $O_2^{\cdot-}$ scavenging capability of other SOD isozymes in *E. coli* cells has also been previously demonstrated [7,38].

This study comprises the first report on the expression and characterization of the CuZn SOD encoded by LOC_Os03g11960 in rice genome. The locus is responsive to multiple abiotic stresses and codes for a functional homodimeric, CuZn SOD. It also exhibits peroxidase activity and is capable of conferring protection against oxidative stress as demonstrated in *E. coli*. Overall sequence similarity, several structural, biochemical features suggest it to be a peroxisomal isozyme. The peroxisomal SODs are relatively less studied in plants; however, these are important component of antioxidant system in normal physiology and stress conditions [8,65] and contribute to ∼18% of total SOD activity [66]. The rice OsCSD3, with higher thermal stability and tolerance to H_2O_2, may serve as a better candidate for abiotic stress tolerance enhancement in plants. Furthermore, experimental validation of its cellular localization may provide insights into involvement of non-canonical targeting sequences/mechanisms in rice, which contains a high diversity of potential PTS sequences [57].

Abbreviations

AmpR, ampicillin resistance gene; BSA, bovine serum albumin; CD, circular dichroism; cDNA, complementary DNA; CSD, CuZn superoxide dismutase; DCF, dichlorofluorescein; DCFH, dichlorodihydrofluorescein; DDC, diethyl dithiocarbamate; H_2O_2, hydrogen peroxide; ICP-MS, inductively coupled plasma-mass spectrometer; IPTG, isopropyl β-D-thiogalactopyranoside; KanR, kanamycin resistance gene; MBP, maltose binding protein; MDA, malondialdehyde; MV, methyl viologen; Mw, molecular weight; NaN_3, sodium azide; NBT, nitroblue-tetrazolium; PAGE, polyacrylamide gel electrophoresis; PBS, phosphate buffer saline; pI, isoelectric point; *RMSD*, *root-mean-square deviation*; ROS, reactive oxygen species; SODs, superoxide dismutases; TBA, thiobarbuteric acid; TEMED, tetramethylethylenediamine; UV, ultraviolet.

Author Contribution

R.P.S. planned and executed experiments, analyzed results and wrote paper. A.S. (Amol) conducted experiments and analyzed results. V.P. conducted bioinformatic studies and results analysis. H.S.M. analyzed results and wrote the paper.

A.S. (Ajay) is a principal investigator, conceived idea, conducted experiments, analyzed results, wrote the paper and communicated.

Funding

The present study was supported by the institutional funding of Bhabha Atomic Research Centre, Mumbai, India. No separate funding was obtained from any other National/International funding body for the present study.

Acknowledgements

We thank Dr S. Chattopadhyay and Dr N. Jawali for the encouragement and support during this study, and Dr Sheetal Uppal, MBD, BARC for suggestions and comments. The authors are thankful to the International Rice Research Institute (IRRI), Philippines for providing the rice seed material used in this study.

Competing Interests

The Authors declare that there are no competing interests associated with the manuscript.

References

1 Bray, E.A., Bailey-Serres, J. and Weretilnyk, E. (2000) Responses to abiotic stresses. In *Biochemistry and Molecular Biology of Plants* (Gruissem, W., Buchannan, B. and Jones, R., eds), pp. 1158–1249, American Society of Plant Physiologists, Rockville, MD

2 Gill, S.S. and Tuteja, N. (2010) Reactive oxygen species and antioxidant machinery in abiotic stress tolerance in crop plants. *Plant Physiol. Biochem.* **48**, 909–930 https://doi.org/10.1016/j.plaphy.2010.08.016

Biochemical Journal (2018) **475** 3105–3121
https://doi.org/10.1042/BCJ20180516

3 Satomi, M., Muller, F. and Beckman, K.B. (2008) The basics of oxidative biochemistry. Aging medicine. In *Oxidative Stress in Aging: From Model Systems to Human Diseases* (Miwa, S., Beckman, K.B. and Muller, F.L., eds), Humana Press, Totowa, NJ
4 Bowler, C., van Montague, M. and Inzé, D. (1992) Superoxide dismutase and stress tolerance. *Annu. Rev. Plant Physiol. Plant Mol. Biol.* **43**, 83–116 https://doi.org/10.1146/annurev.pp.43.060192.000503
5 Fridovich, I. (1995) Superoxide radical and superoxide dismutases. *Annu. Rev. Biochem.* **64**, 97–112 https://doi.org/10.1146/annurev.bi.64.070195.000525
6 Alscher, R.G., Erturk, N. and Heath, L.S. (2002) Role of superoxide dismutases in controlling oxidative stress in plants. *J. Exp. Bot.* **53**, 331–1341 https://doi.org/10.1093/jexbot/53.372.1331
7 Mahanty, S., Kaul, T., Pandey, P., Reddy, R.A., Mallikarjuna, G., Reddy, C.S. et al. (2012) Biochemical and molecular analyses of copper-zinc superoxide dismutase from a C_4 plant *Pennisetum glaucum*reveals an adaptive role in response to oxidative stress. *Gene* **505**, 309–317 https://doi.org/10.1016/j.gene.2012.06.001
8 Kliebenstein, D.J., Monde, R.A. and Last, R.L. (1998) Superoxide dismutase in *Arabidopsis*: an eclectic enzyme family with disparate regulation and protein localization. *Plant Physiol.* **118**, 637–650 https://doi.org/10.1104/pp.118.2.637
9 Huang, C.-H., Kuo, W.-Y., Weiss, C. and Jinn, T.-L. (2012) Copper chaperone-dependent and independent activation of three copper-zinc superoxide dismutase homologs localized in different cellular compartments in *Arabidopsis*. *Plant Physiol.* **158**, 737–746 https://doi.org/10.1104/pp.111.190223
10 Bordo, D., Djinovic, K. and Bolognesi, M. (1994) Conserved patterns in the Cu–Zn superoxide dismutase family. *J. Mol. Biol.* **238**, 366–386 https://doi.org/10.1006/jmbi.1994.1298
11 Kanematsu, S. and Asada, K. (1989) CuZn-superoxide dismutase in rice: occurrence of an active, monomeric enzyme and two types of isozyme in leaf and non-photosynthetic tissues. *Plant Cell Physiol.* **30**, 381–391 https://doi.org/10.1093/oxfordjournals.pcp.a077753
12 Pelmenschikov, V. and Siegbahn, P.E. (2005) Copper-zinc superoxide dismutase: theoretical insights into the catalytic mechanism. *Inorg. Chem.* **44**, 3311–3320 https://doi.org/10.1021/ic050018g
13 Li, H.-T., Jiao, M., Chen, J. and Liang, Y. (2010) Roles of zinc and copper in modulating the oxidative refolding of bovine copper, zinc superoxide dismutase. *Acta Biochim. Biophys. Sin.* **42**, 183–194 https://doi.org/10.1093/abbs/gmq005
14 Mishra, P., Dixit, A., Ray, M. and Sabat, S.C. (2014) Mechanistic study of CuZn-SOD from *Ipomoea carnea* mutated at dimer interface: enhancement of peroxidase activity upon monomerization. *Biochimie* **97**, 181e193 https://doi.org/10.1016/j.biochi.2013.10.014
15 Tuteja, N., Mishra, P., Yadav, S., Tajrishi, M., Baral, S. and Sabat, S.C. (2015) Heterologous expression and biochemical characterization of a highly active and stable chloroplastic CuZn-superoxide dismutase from *Pisum sativum*. *BMC Biotechnol.* **15**, 3 https://doi.org/10.1186/s12896-015-0117-0
16 Pan, S.-M. and Yau, Y.-Y. (1991) The isozymes of superoxide dismutase in rice. *Bot. Bull. Acad. Sin.* **32**, 253–258
17 Bueno, P., Varela, J., Gimeénez-Gallego, G. and del Río, L.A. (1995) Peroxisomal copper, zinc superoxide dismutases: characterization of the isoenzyme from watermelon cotyledons. *Plant Physiol.* **108**, 1151–1160 https://doi.org/10.1104/pp.108.3.1151
18 Pan, S.M., Hwang, G.B. and Liu, H.C. (1999) Over-expression and characterization of copper/zinc-superoxide dismutase from rice in *Escherichia coli*. *Bot. Bull. Acad. Sin.* **40**, 275–281
19 Kernodle, S.P. and Scandalios, J.G. (2001) Structural organization, regulation and enzyme expression of the chloroplastic superoxide dismutase Sod1 gene in maize. *Arch. Biochem. Biophys.* **391**, 137–147 https://doi.org/10.1006/abbi.2001.2397
20 Dong, C., Zheng, X., Li, G., Zhu, H., Zhou, M. and Hu, Z. (2011) Molecular cloning and expression of two cytosolic copper-zinc superoxide dismutases genes from *Nelumbo nucifera*. *Appl. Biochem. Biotechnol.* **163**, 679–691 https://doi.org/10.1007/s12010-010-9074-1
21 Ueda, Y., Uehara, N., Sasaki, H., Kobayashi, K. and Yamakawa, T. (2013) Impacts of acute ozone stress on superoxide dismutase (SOD) expression and reactive oxygen species (ROS) formation in rice. *Plant Physiol. Biochem.* **70**, 396–402 https://doi.org/10.1016/j.plaphy.2013.06.009
22 Sen Gupta, A., Heinen, J.L., Holaday, A.S., Burke, J.J. and Allen, R.D. (1993) Increased resistance to oxidative stress in transgenic plants that overexpress chloroplastic Cu/Zn superoxide dismutase. *Proc. Natl Acad. Sci. U.S.A.* **90**, 1629–1633 https://doi.org/10.1073/pnas.90.4.1629
23 Camp, W.V., Willekens, H., Bowler, C., Montagu, M.V., Inzé, D., Reupold-Popp, P. et al. (1994) Elevated levels of superoxide dismutase protect transgenic plants against ozone damage. *BioTechnology* **12**, 165–168 https://doi.org/10.1038/nbt0294-165
24 Arisi, A.M., Cornic, G., Jouanin, L. and Foyer, C.H. (1998) Overexpression of iron superoxide dismutuase in transformed poplar modifies the regulation of photosynthesis at low CO_2 partial pressures or following exposure to the prooxidant herbicide methyl viologen. *Plant Physiol.* **117**, 565–574 https://doi.org/10.1104/pp.117.2.565
25 Raghavan, P.S., Sadhasivam, V. and Parida, A.K. (2007) Overexpression of cytosolic copper/zinc superoxide dismutase from a mangrove plant *Avicennia marina* in *indica* rice var Pusa Basmati-1 confers abiotic stress tolerance. *Transgenic Res.* **17**, 281–291 https://doi.org/10.1007/s11248-007-9099-6
26 Lee, J.P., Kim, S.H., Bang, J.W., Lee, H.S., Kwak, S.S. and Kwon, S.Y. (2007) Enhanced tolerance to oxidative stress in transgenic tobacco plants expressing three antioxidant enzymes in chloroplasts. *Plant Cell Rep.* **26**, 591–598 https://doi.org/10.1007/s00299-006-0253-z
27 Faize, M., Burgos, L., Faize, L., Petri, C., Barba-Espin, G., Diaz-Vivancos, P. et al. (2012) Modulation of tobacco bacterial disease resistance using cytosolic ascorbate peroxidase and Cu, Zn-superoxide dismutase. *Plant Pathol.* **61**, 858–866 https://doi.org/10.1111/j.1365-3059.2011.02570.x
28 Kumar, A., Dutt, S., Bagler, G., Ahuja, P.S. and Kumar, S. (2012) Engineering a thermo-stable superoxide dismutase functional at sub-zero to >50°C, which also tolerates autoclaving. *Sci. Rep.* **2**, 387 https://doi.org/10.1038/srep00387
29 Kaminaka, H., Morita, S., Yokoi, H., Masumura, T. and Tanaka, K. (1997) Molecular cloning and characterization of a cDNA for plastidic copper/zinc-superoxide dismutase in rice (*Oryza sativa* L.). *Plant Cell Physiol.* **38**, 65–69 https://doi.org/10.1093/oxfordjournals.pcp.a029086
30 Senadheera, P., Tirimanne, S. and Maathuis, F.J.M. (2012) Long term salinity stress reveals cultivar specific differences in root oxidative stress response. *Rice Sci.* **19**, 36–43 https://doi.org/10.1016/S1672-6308(12)60018-3
31 Kim, S.H., Song, M., Lee, K.J., Hwang, S.G., Jang, C.S., Kim, J.B. et al. (2012) Genome-wide transcriptome profiling of ROS scavenging and signal transduction pathways in rice (*Oryza sativa* L.) in response to different types of ionizing radiation. *Mol. Biol. Rep.* **39**, 11231–11248 https://doi.org/10.1007/s11033-012-2034-9
32 Lasanthi-Kudahettige, R., Leonardo, M., Loreti, E., Gonzali, S., Licausi, F., Novi, G. et al. (2007) Transcript profiling of the anoxic rice coleoptile. *Plant Physiol.* **144**, 218–231 https://doi.org/10.1104/pp.106.093997
33 Sambrook, J. and Russell, D.W. (2001) *Molecular Cloning: A Laboratory Manual*, 3rd edn, Cold Spring Harbor Laboratory Press, New York
34 Kawahara, Y., de la Bastide, M., Hamilton, J.P., Kanamori, H., Mccombie, W.R., Ouyang, S. et al. (2013) Improvement of the *Oryza sativa* Nipponbare reference genome using next generation sequence and optical map data. *Rice* **6**, 4 https://doi.org/10.1186/1939-8433-6-4

35 Schmittgen, T.D. and Livak, K. (2008) Analyzing real-time PCR data by the comparative C(T) method. *Nat. Protoc.* **3**, 1101–1108 https://doi.org/10.1038/nprot.2008.73
36 Baba, T., Ara, T., Hasegawa, M., Takai, Y., Okumura, Y., Baba, M. et al. (2006) Construction of *Escherichia coli* K-12 in-frame, single-gene knockout mutants: the Keio collection. *Mol. Syst. Biol.* **2**, 2006.0008 https://doi.org/10.1038/msb4100050
37 Narita, L. and Peng, S. (2012) Construction of catalase double knockout *Escherichia coli* strain for isogenic strain comparison studies of the role of catalase. *J. Exp. Microbiol. Immunol.* **16**, 123–128
38 Goulielmos, G.N., Arhontaki, K., Eliopoulos, K., Tserpistali, K., Tsakas, S. and Loukas, M. (2003) *Drosophila* Cu,Zn superoxide dismutase gene confers resistance to paraquat in *Escherichia coli*. *Biochem. Biophys. Res. Commun.* **308**, 433–438 https://doi.org/10.1016/S0006-291X(03)01422-0
39 Panat, N.A., Maurya, D.K., Ghaskadbi, S.S. and Sandur, S.K. (2016) Troxerutin, a plant flavonoid, protects cells against oxidative stress-induced cell death through radical scavenging mechanism. *Food Chem.* **194**, 32–45 https://doi.org/10.1016/j.foodchem.2015.07.078
40 Altschul, S.F., Madden, T.L., Schäffer, A.A., Zhang, J., Zhang, Z., Miller, W. et al. (1997) Gapped BLAST and PSI-BLAST: a new generation of protein database search programs. *Nucleic Acids Res.* **25**, 3389–3402 https://doi.org/10.1093/nar/25.17.3389
41 Thompson, J.D., Gibson, T.J., Plewniak, F., Jeanmougin, F. and Higgins, D.G. (1997) The ClustalX Windows interface: flexible strategies for multiple sequence alignment aided by quality analysis tools. *Nucleic Acids Res.* **24**, 4876–4882 https://doi.org/10.1093/nar/25.24.4876
42 Hall, T.A. (1999) Bioedit: a user-friendly sequence alignment editor and analysis program for Windows 95/98/NT. *Nucleic Acids Symp. Ser.* **41**, 95–98
43 Tamura, K., Dudley, J., Nei, M. and Kumar, S. (2007) MEGA4: molecular evolutionary genetics analysis (MEGA) software version 4.0. *Mol. Biol. Evol.* **24**, 1596–1599 https://doi.org/10.1093/molbev/msm092
44 Saitou, N. and Nei, M. (1987) The neighbor-joining method: a new method for reconstructing phylogenetic trees. *Mol. Biol. Evol.* **4**, 406–425 PMID:3447015
45 Felsenstein, J. (1985) Confidence limits of phylogenies: an approach using bootstrap. *Evolution* **39**, 783–791 https://doi.org/10.1111/j.1558-5646.1985.tb00420.x
46 Biasini, M., Bienert, S., Waterhouse, A., Arnold, K., Studer, G., Schmidt, T. et al. (2014) SWISS-MODEL: modelling protein tertiary and quaternary structure using evolutionary information. *Nucleic Acids Res.* **42**, W252–W258 https://doi.org/10.1093/nar/gku340
47 Jones, T.A., Zou, J.Y., Cowan, S.W. and Kjeldgaard, M. (1991) Improved methods for building protein models in electron density maps and the location of errors in these models. *Acta Crystallogr. A Found. Crystallogr.* **47**, 110–119 https://doi.org/10.1107/S0108767390010224
48 DeLano, W.L. (2002) *The PyMOL Molecular Graphics System*, DeLano Scientific, San Carlos, CA
49 Bradford, M.M. (1976) A simple and sensitive method for the quantification of microgram quantities of protein utilizing the principle of protein-dye binding. *Anal. Biochem.* **72**, 248–254 https://doi.org/10.1016/0003-2697(76)90527-3
50 Ewing, J.F. and Janero, D.R. (1995) Microplate superoxide dismutase assay employing a non enzymatic superoxide generator. *Anal. Biochem.* **232**, 243–248 https://doi.org/10.1006/abio.1995.0014
51 Chen, J.R., Liao, C.-W., Mao, S.J.T., Chen, T.-H. and Weng, C.-N. (2001) A simple technique for the simultaneous determination of molecular weight and activity of superoxide dismutase using SDS-PAGE. *J. Biochem. Biophys. Methods* **47**, 233–237 https://doi.org/10.1016/S0165-022X(00)00162-7
52 Zhang, H., Joseph, J., Gurney, M., Becker, D. and Kalyanaraman, B. (2002) Bicarbonate enhances peroxidase activity of Cu,Zn-superoxide dismutase. *J. Biol. Chem.* **277**, 1013–1020 https://doi.org/10.1074/jbc.M108585200
53 Srivastava, V., Srivastava, M.K., Chibani, K., Nilsson, R., Rouhier, N., Melzer, M. et al. (2009) Alternative splicing studies of the reactive oxygen species gene network in Populus reveal two isoforms of high isoelectric point superoxide dismutase. *Plant Physiol.* **49**, 1848–1859 https://doi.org/10.1104/pp.108.133371
54 Benkert, P., Biasini, M. and Schwede, T. (2011) Toward the estimation of the absolute quality of individual protein structure models. *Bioinformatics* **27**, 343–350 https://doi.org/10.1093/bioinformatics/btq662
55 Wang, Y., Branicky, R., Noë, A. and Hekimi, S. (2018) Superoxide dismutases: dual roles in controlling ROS damage and regulating ROS signaling. *J. Cell Biol.* **217**, 1915–1928 https://doi.org/10.1083/jcb.201708007
56 Takahashi, M.A. and Asada, K. (1983) Superoxide anion permeability of phospholipid membranes and chloroplast thylakoids. *Arch. Biochem. Biophys.* **226**, 558–566 https://doi.org/10.1016/0003-9861(83)90325-9
57 Kaur, N. and Hu, J. (2011) Defining the plant peroxisomal proteome: from *Arabidopsis* to rice. *Front. Plant. Sci.* **2**, 103 https://doi.org/10.3389/fpls.2011.00103
58 Hernández-Nistal, J., Dopico, B. and Labrador, E. (2002) Cold and salt stress regulates the expression and activity of a chickpea cytosolic Cu/Zn superoxide dismutase. *Plant Sci.* **163**, 507–514 https://doi.org/10.1016/S0168-9452(02)00153-X
59 Sakamoto, A., Ohsuga, H. and Tanaka, K. (1992) Nucleotide sequences of two cDNA clones encoding different Cu/Zn-superoxide dismutases expressed in developing rice seed (*Oryza sativa* L.). *Plant Mol. Biol.* **19**, 323–327 https://doi.org/10.1007/BF00027355
60 Feng, W., Hongbin, W., Bing, L. and Jinfa, W. (2006) Cloning and characterization of a novel splicing isoforms of the iron-superoxide dismutase gene in rice (*Oryza sativa* L.). *Plant Cell Rep.* **24**, 734–742 https://doi.org/10.1007/s00299-005-0030-4
61 Padiglia, A., Medda, R., Cruciani, E., Lorrai, A. and Floris, G. (1996) Purification and properties of *Oryza sativa* Cu-Zn superoxide dismutase. *Prep. Biochem. Biotechnol.* **26**, 135–142 https://doi.org/10.1080/10826069608000059
62 Lin, M.W., Lin, M.T. and Lin, C.T. (2002) Copper/zinc-superoxide dismutase from lemon cDNA and enzyme stability. *J. Agric. Food Chem.* **50**, 7264–7270 https://doi.org/10.1021/jf0207070
63 Sampson, J.B. and Beckman, J.S. (2001) Hydrogen peroxide damages the zinc-binding site of zinc-deficient Cu, Zn superoxide dismutase. *Arch. Biochem. Biophys.* **392**, 8–13 https://doi.org/10.1006/abbi.2001.2418
64 Shen, J., Zeng, Y., Zhuang, X., Sun, L., Yao, X., Pimpl, P. et al. (2013) Organelle pH in the *Arabidopsis* endomembrane system. *Mol. Plant.* **6**, 1419–1437 https://doi.org/10.1093/mp/sst079
65 Swidzinski, J.A., Sweetlove, L.J. and Leaver, C.J. (2002) A custom microarray analysis of gene expression during programmed cell death in *Arabidopsis thaliana*. *Plant J.* **30**, 431–446 https://doi.org/10.1046/j.1365-313X.2002.01301.x
66 Sandalio, L.M. and del Río, L.A. (1987) Localization of superoxide dismutase in glyoxysomes from *Citrullus vulgaris*. Functional implications in cellular metabolism. *J. Plant Physiol.* **127**, 395–409 https://doi.org/10.1016/S0176-1617(87)80248-1

Thesis Highlight

Name of the Student: Ravi Prakash Sanyal

Name of the CI/OCC: BARC, Mumbai **Enrolment No.: LIFE01201404001**

Thesis Title: Molecular and Biochemical Characterization of Cu/Zn Superoxide Dismutase Splice Variants of Rice (*Oryza sativa*)

Discipline: Life Sciences **Sub-Area of Discipline: Plant Molecular Biology**

Date of viva voce: 25/03/2021

Alternative splicing (AS) has emerged as a key molecular mechanism in plants to regulate diverse array of physiological processes as well as response to stress conditions. AS generate more than one transcript/protein isoform from single gene and can control the levels, activity/function in multiple ways. Superoxide dismutases (SODs), are important antioxidant enzymes that provide protection against reactive oxygen species (ROS) mediated cellular damage. In rice, the seven SOD genes undergo AS and generate fourteen splice variants (SVs), with maximum of nine from four Cu/Zn SODs (CSDs). In this study, AS of rice Cu/Zn SODs (OsCSDs) were analyzed at both RNA and protein level to understand their significance in regulation and functioning of Cu/Zn SODs.

At transcript level, AS affected the OsCSD transcript abundance in different rice tissues and in response to abiotic stresses. AS also affected the transcript stability of some of the OsCSD splice variants. Collectively, AS mediated modulation in the OsCSD transcript level might be important for fine tuning the cellular CSD transcript/protein levels in response to various environmental perturbations.

At protein level, AS mediated alterations (major/minor) in the amino acid sequence of the alternative splice variants affected the important characteristics of rice peroxisomal CSD (OsCSD3) and chloroplastic CSD (OsCSD2). AS-mediated large variations in the three OsCSD3-SV isoforms (SV2, SV3 and SV4), significantly affected the SOD function. Out of four SV isoforms, only OsCSD3-SV1 (constitutive SV) was enzymatically active, whereas other three alternative isoforms (OsCSD3-SV2, -SV3 and -SV4) were rendered enzymatic inactive. On contrary, two splice variant isoforms of chloroplastic CSD (OsCSD2-SV1 and -SV2) with minor variation in four amino acid region (GPTT), were functionally active. However alternative isoform (OsCSD2-SV2) lacking four amino acids exhibited substantial differences in protein properties (activity, structural stability etc.) compared to the constitutive isoform (OsCSD2-SV1). Such AS imparted variations in OsCSD-SV isoforms may be crucial for dynamic regulation of enzyme activity as per cellular requirements in different situations.

In addition, two rice cytosolic CSDs (OsCSD1 and OsCSD4), originated due to a block duplication showed variations in the regulatory region of the gene and protein characteristics. The cytosolic OsCSDs, showed differential response to abiotic stress conditions. At protein level, the proteins showed variations at 18 sites and seems important for better protein properties (high enzyme activity, tolerance to pH change and structural stability) of OsCSD4 than OsCSD1.

In summary, this study indicates that alternative splicing is involved in regulation and functioning of rice Cu/Zn SODs at both RNA and protein levels. In addition, a gene duplication event resulting in two cytosolic CSDs was found to be important for regulation and functioning of the two gene.